



NTNU – Trondheim
Norwegian University of
Science and Technology

Analysis of the Deformation Behavior at the Underground Caverns of Neelum Jhelum HPP, Pakistan

Magni Larsen Vestad

Geotechnology

Submission date: June 2014

Supervisor: Krishna Kanta Panthi, IGB

Norwegian University of Science and Technology
Department of Geology and Mineral Resources Engineering



Your ref.: MS/N16T25/IGB/MVKKP

Date: 06.01.2014

TGB4930 INGGEOL/BERGMEK - MSc thesis
for
Eng. geo. student Magni Larsen Vestad

**ANALYSIS ON THE DEFORMATION BEHAVIOUR AT THE UNDERGROUND
POWERHOUSE CAVERNS OF NEELUM JHELUM HPP, PAKISTAN**

Background

The 969 MW run-of-the-river Neelum Jhelum Hydropower Project (NJHPP) is under construction and is planned to be completed in 2016. The project comprises many underground structures like headrace tunnel, pressure shaft, tailrace tunnel, access tunnel and underground caverns. Most of the underground structures are located in the lower part of the Himalaya, mainly Siwalik and lower part of lesser Himalayan rock formation consisting young sedimentary formation to medium aged meta-sediments. Underground excavation through these formations always poses serious challenges regarding stability. Due to weak quality rock mass in these young formations large deformations may occur even in relatively low overburden.

During last semester the candidate has carried out project work in collecting engineering geological data and information of the project, presented deformations records measured at the powerhouse cavern and analysed recorded deformations using empirical and semi-empirical approaches.

MSc thesis task

This MSc thesis will continue to analyse recorded deformations (squeezing condition) of the Powerhouse cavern of NJHPP more extensively using both analytical and numerical approach and shall fulfil following MSc thesis task.

- Review existing theory on the stability issues in tunnelling and large underground caverns.
- Briefly describe Neelum Jhelum HPP, comment on the engineering geological investigations carried out during planning (if possible).

- Review overall engineering geological conditions, used rock support principles and used tunnel excavation methods for waterway system.
- Document the major excavation challenges.
- Discuss overall engineering geological conditions of the Power house cavern.
- Evaluate the methods for analysis of squeezing in large scale caverns.
- Carry out 2D Numerical analysis of the underground powerhouse caverns.
- Compare and discuss analysis results from empirical, se-analytical, analytical and numerical approaches.

Relevant computer software packages

Candidate shall use *roc-science package* and other relevant computer software for the master study.

Background information for the study

- Relevant information about the project such as reports, maps, information and data received from Multiconsult.
- The information provided by the professor about rock engineering and hydropower.
- Scientific papers, reports and books related to the Himalayan geology and tunnelling.
- Scientific papers and books related to international tunnelling and rock engineering cases.
- Literatures in rock engineering, rock support principles, rock mechanics and tunnelling.

Cooperating partner

Multiconsult is the co-operating partner. Relevant project information, geological and engineering geological investigation reports shall be received from Multiconsult, Oslo. **Mr. Asbjørn Halvorsen** will be the contact person for this project work at Multiconsult.

The project work is to start on January 13, 2014 and to be completed by June 10, 2014.

The Norwegian University of Science and Technology (NTNU)
Department of Geology and Mineral Resources Engineering

January 06, 2014



Dr. Krishna K. Panthi

Associate Professor of geological engineering, main supervisor

FOREWORD

This master thesis titled “**Analysis of the deformation behavior at the underground caverns of Neelum Jhelum HPP, Pakistan**” is submitted to the Department of Geology and Mineral Resources Engineering, as the final requirement for fulfillment of Master of Science in Engineering Geology and Rock Mechanics (2009-2014).

The main focus for the thesis is the evaluation of methods for analysis of squeezing in large scale caverns. The methods were evaluated based on their ability to recreate the deformations measured in the powerhouse cavern at the Neelum Jhelum HPP in Pakistan. Thorough evaluation of the geological conditions and deformation characteristics of the cavern was essential for the correct input and interpretation of the results for the analysis. Applied methods include empirical, semi-empirical, analytical and numerical methods. The information about NJHPP was supplied by Multiconsult AS (Norplan AS).

Magni Larsen Vestad

NTNU, Trondheim

June 2014

ACKNOWLEDGMENTS

I would like to express my gratitude to my main supervisor Krishna Kanta Panthi. During this last year of project and thesis work he has offered the guidance, good discussions and encouragement that made this thesis come together. Furthermore, I would like to thank Pawan Kumar Shrestha for wise input and discussion on the CCM analysis.

I would also like to thank the employees at the Department for Dams and Underground Constructions at Multiconsult AS. The idea and motivation behind this thesis arose as a product of the wish for a common project that would fulfill their interest as well as mine. I am thankful to Asbjørn Halvorsen for making the project possible. Finally, special thanks go to Hui Lu, for supplying most of the material for the thesis, and for offering some of his personal experiences and work with the project.

ABSTRACT

Many risks and challenges are associated with large scale underground projects. Stability issues are typically related to high stresses around the opening. Excavations will change the existing stress regime in the ground, inducing tangential stresses around the periphery of the underground opening. Failure of the rock mass will occur if induced stresses exceed the strength of the rock mass. In weak and deformable rocks, the process of failure may present as plastic deformation, better known as *squeezing*. Squeezing can be described as the time-dependent inward movement of the rock material towards the opening when subjected to tangential stress (Panthi, 2006).

The squeezing phenomenon was reviewed in relation to the deformations measured in the powerhouse cavern at the Neelum Jhelum HPP (NJHPP) in Pakistan. The cavern is constructed in fractured sandstone with the intercalation of thin to thick layers of locally sheared siltstone and mudstone. The mean overburden in the cavern is 430 m. Since constructions began in 2011, the deformations have been monitored progressively with convergence lines and extensometers. The highest deformation is seen for the middle sections, with up to 282 mm convergence of the walls.

The objective of this study involves an evaluation of available methods for prediction and assessment of squeezing in large scale caverns. The deformation characteristics for the Neelum Jhelum HPP cavern are essential input for the analysis. Proper knowledge on the ground conditions and influencing factors are essential for a well-founded evaluation of the methods. In this study, five methods are selected for the assessment of squeezing for five sections in the cavern. The empirical method by Goel (1994) and the Q-system are used for prediction of the occurrence of squeezing, along with the semi-analytical method by Hoek and Marinos (2000) without support pressure. Analysis of squeezing and required support pressure is investigated using Hoek and Marinos with support and with the CCM by Carranza-Torres and Fairhurst (2000). Extensive plastic analysis using the 2D finite element program *Phase²* is included. Calibration of the stress conditions and rock mass deformability are an essential part of the numerical analysis.

The deformation data reveal a complex interplay of internal and external factors influencing on the behavior of the rock mass. Weak and fractured rock mass combined with relatively high overburden is the main cause for the high degree of squeezing. However, the variation in measured deformation is believed to be caused by changing external factors. The two major influencing events accelerating the deformation was the excavation of the bulleted gate niches in the downstream wall (4 niches), and the excavation down to the bottom floor level. The intersecting and potentially water bearing shear zone may be the reason for the highest deformations observed for the middle sections.

The deformation characteristics of a tunnel are less influenced by external factors, relative to the complexity involving a powerhouse cavern. The methods applied typically only consider stress conditions and rock mass quality and strength, and most have been developed for circular tunnels. The analysis of the deformations in the NJHPP cavern indicate that for a powerhouse cavern the complex excavation layout, large dimensions and excavation progress are major influencing factors. The effects of these are not properly considered by any of the selected methods. Consequently, special considerations are necessary for the analysis of squeezing in large caverns.

SAMMENDRAG

Betydelig risiko og utfordring er knyttet til store anlegg i fjell. Høye bergspenninger rundt åpningen er den hyppigste årsaken til stabilitetsproblemer. Byggingen av en tunnel eller berghall medfører at det eksisterende spenningsregimet i grunnen endres, slik at tangentielle spenninger induseres rundt åpningens periferi. Bergmassen vil gå i brudd om de induserte spenningene er høyere enn styrken til berget. I myke bergarter vil dette typisk skje i form av plastisk deformasjon, også kjent som *squeezing* (skviseberg). Enkelt forklart er squeezing prosessen der berget beveger seg inn mot åpningen når det utsettes for tangentielle spenninger (Panthi, 2006).

Skviseberg er i denne oppgaven undersøkt i forbindelse med et vannkraftprosjekt i Pakistan, Neelum Jhelum HPP (NJHPP). I kraftstasjonshallen er det observert store deformasjoner i vegger og heng, hvilket har skapt betydelige utfordringer for byggingen. Geologien er preget av oppsprukket sandstein, med lokalt forekommende sterkt oppsprukket siltstein og leirstein med varierende tykkelse. Gjennomsnittlig bergoverdekning i hallen er 430 m. Konvergens og ekstensometermålinger har pågått kontinuerlig siden byggingen begynte i 2011. Deformasjoner opptil 282 mm er målt for de midtre seksjonene i hallen.

Et sentralt mål med denne oppgaven er å evaluere tilgjengelige metoder for å kunne anslå omfang og grad av skvising for store fjellhaller. Tolkningen av de målte deformasjonene og grunnforholdene ved NJHPP er derfor essensiell informasjon for å kunne gjøre en velbegrunnet analyse. Forekomst og omfang av skviseberg er i dette studiet evaluert ved anvendelse av fem ulike metoder, utført for fem utvalgte snitt i kraftstasjonshallen. En empirisk metode av Goel (1994) og Q-systemet er brukt for å anslå grad av skvising, samt den semi-analytiske metoden av Hoek og Marinos (2000) uten sikringstrykk. CCM og metoden av Hoek og Marinos (2000) inkludert sikringstrykk er benyttet for analyse av skvising og nødvendig sikringstrykk. Omfattende plastisk og elastisk analyse er utført med *Phase²*, et 2D numerisk modellerings program. Kalibrering av spenninger og bergets deformasjonsegenskaper er en sentral del av denne analysen.

Deformasjonsdataene indikerer at det er et komplekst samspill mellom indre og ytre faktorer, som sammen påvirker bergets respons. Dårlig bergkvalitet kombinert med høy overdekning er hovedårsaken til de store deformasjonene. Ulikt omfang indikerer likevel at deformasjonene er påvirket av skiftende lokale forutsetninger. Akselerasjon i konvergensmålingene er korrelert til to signifikante hendelser; byggingen av 4 nisjer i veggen nedstrøms, og sprengningen ned til endelig gulvnivå. En mulig vannførende svakhetsone er også observert i veggen midt i hallen, og kan være en medvirkende årsak til at de høyeste deformasjonene er målt i dette området.

Sammenlignet med en kompleks kraftstasjonshall, kan bergets respons i en tunnel sies å være mindre påvirket av skiftende ytre faktorer. De anvendte metodene i denne oppgaven tar typisk kun hensyn til spenningsforhold og styrken til bergmassen, og de fleste er utviklet med tanke på sirkulære tunneler. Observasjoner i kraftstasjonshallen ved NJHPP indikerer at forhold som fjellhallens komplekse design, store dimensjoner og drivemåte har stor betydning for de målte deformasjonene. Disse effektene blir i liten grad tatt hensyn til i de utvalgte metodene. Med andre ord vil det være nødvendig med omfattende hensyn for analyse av skvising i store fjellhaller.

Contents

Foreword	i
Acknowledgments	iii
Abstract	v
Contents	ix
List of Figures	xiii
List of Tables	xvii
List of Abbreviations	xix
1. INTRODUCTION	1
1.1. BACKGROUND	1
1.2. OBJECTIVE AND SCOPE	1
1.3. METHODOLOGY OF THE STUDY	2
1.4. LIMITATIONS OF THE STUDY	3
2. ROCK AND ROCK MASS PROPERTIES	5
2.1. INTRODUCTION	5
2.2. ROCK MASS STRUCTURES	6
2.2.1. Bedding- or foliation planes	6
2.2.2. Jointing of rock mass	6
2.2.3. Weakness zones and faults	6
2.3. ROCK MASS STRENGTH AND DEFORMABILITY	8
2.3.1. Factors influencing rock mass strength	8
2.3.2. Failure criteria	11
2.3.3. Estimation of rock mass strength	14
2.3.4. Estimation of rock mass deformability	15
3. STRESS INDUCED INSTABILITIES	17
3.1. IN-SITU ROCK STRESSES	17
3.1.1. Initial stress conditions	17
3.1.2. Distribution of stresses around an excavation	19
3.2. STRESS INDUCED INSTABILITIES	21
3.2.1. Problems related to tensile stress	21
3.2.2. Problems induced by high compressive stress	21
3.3. THE SQUEEZING PHENOMENON	22
3.3.1. Instantaneous squeezing	22
3.3.2. Secondary squeezing (creep)	23
3.3.3. Factors influencing squeezing	25

3.3.4.	Time-dependency and the face-effect	26
3.4.	CONSIDERATIONS FOR LARGE SCALE CAVERNS	27
3.5.	MEASURING AND MONITORING DEFORMATIONS	29
3.5.1.	Convergence measurements	29
3.5.2.	Extensometer measurements	29
3.5.3.	Load cell and pressure cell measurements	30
3.5.4.	Concluding remarks on deformation measurements	30
4.	THE CASE: NEELUM JHEMUM HPP, PAKISTAN	31
4.1.	PROJECT DESCRIPTION	31
4.1.1.	General	31
4.1.2.	Project location	32
4.1.3.	Project layout features	33
4.1.4.	Powerhouse complex design	34
4.2.	GEOLOGICAL AND ENGINEERING GEOLOGICAL CONDITIONS	36
4.2.1.	Regional geology	36
4.2.2.	Geologic and tectonic conditions in the project area	37
4.2.3.	Geological investigations	39
4.2.4.	Rock units classified in the project area	40
4.2.5.	Geology along the headrace tunnel	40
4.2.6.	Geology of the powerhouse complex	41
4.3.	ROCK MASS CONDITIONS OF THE POWERHOUSE COMPLEX	42
4.3.1.	Intact rock properties	42
4.3.2.	Discontinuities	43
4.3.3.	Rock mass properties	44
4.3.4.	Rock mass classification	44
4.4.	INSTALLED SUPPORT	45
4.5.	DEFORMATION IN THE POWERHOUSE CAVERN	47
4.5.1.	Overview of available deformation data	47
4.5.2.	Analysis of measured deformation in the cavern	49
4.5.3.	Correlation between convergence and extensometer data	50
4.5.4.	Concluding remarks	52
5.	REVIEW ON SQUEEZING ANALYSIS	53
5.1.	INTRODUCTION	53
5.2.	EMPIRICAL AND SEMI-ANALYTICAL METHODS	53
5.2.1.	Q-method	53
5.2.2.	Goel (1994) approach	55
5.2.3.	Hoek and Marinos (2000) approach	56
5.3.	ANALYTICAL METHOD	58
5.3.1.	Convergence-Confinement Method (CCM)	59

5.3.2.	Limitations of CCM	66
5.4.	NUMERICAL ANALYSIS	69
5.4.1.	General	69
5.4.2.	The Phase ² program	70
5.4.3.	Input parameters for the model in Phase ²	70
5.4.4.	Interpretation of results	73
5.5.	CONCLUDING REMARKS ON SQUEEZING ANALYSIS	73
6.	SQUEEZING ANALYSIS	75
6.1.	GENERAL	75
6.2.	INPUT DATA	77
6.2.1.	Selected sections for the analysis	77
6.2.2.	Estimation of rock mass quality	77
6.2.3.	Estimation of rock mass parameters	78
6.2.4.	Estimation of support	78
6.2.5.	Summary of input parameters for selected section	79
6.3.	PREDICTION OF SQUEEZING	80
6.3.1.	Prediction of squeezing using empirical methods	80
6.3.2.	Discussion of applicability of the empirical methods	80
6.4.	ANALYSIS OF SQUEEZING	81
6.4.1.	Hoek and Marinos (2000) with support pressure	81
6.4.2.	CCM: Longitudinal displacement profiles	82
6.4.3.	CCM: Comparison to measured deformation	85
6.4.4.	CCM: Ground and support interaction	86
6.4.5.	Discussion of the applicability of the CCM to cavern analysis	88
6.5.	NUMERICAL MODELING	90
6.5.1.	Construction of the models in Phase ²	90
6.5.2.	Model input	91
6.5.3.	Calibration of models	93
6.5.4.	Elastic analysis	96
6.5.5.	Plastic analysis	97
6.5.6.	Discussion of the applicability of 2D numerical modeling	101
6.6.	DISCUSSION ON SQUEEZING ANALYSIS FOR A CAVERN	103
7.	CONCLUSIONS AND RECOMMENDATIONS	105
7.1.	CONCLUSIONS	105
7.2.	RECOMMENDATIONS	107
	Bibliography	109

APPENDICES	113
A. STANDARD CHARTS AND FIGURES	115
A.1. Hoek and Brown constant m_i (Hoek and Marinos, 2000b)	115
A.2. Determination of GSI (Hoek and Marinos, 2000b)	116
A.3. Disturbance factor D (Hoek et al., 2002)	117
A.4. Description of ratings for input parameters for Q-system (Barton, 2002) .	118
A.5. Q-system support charts (NGI, 2013)	120
A.6. Rock Mass Rating system (RMR) (Bieniawski, 1989)	121
A.7. Relationship between Q-value and RMR (Panthi, 2006)	122
B. NJHPP DEFORMATION PLOTS	123
B.1. Convergence plots (NJC, 2013a)	123
B.2. Extensometer plots	126
B.3. Convergence plotted based on rock type anchoring	128
C. DETAILED CALCULATIONS AND RESULT	129
C.1. Prediction by Goel (1994) and Q-method	129
C.2. Hoek and Marinos (2000) calculations	130
C.3. CCM: GRC and LDP	131
C.4. SCC calculations	137
C.5. Estimation of stress	139
D. PHASE2 MODELING RESULTS	141
D.1. Calibration plots	141
D.2. Elastic analysis	142
D.3. Plastic analysis	147
E. PROJECT RELATED DOCUMENTS AND DRAWINGS	153
E.1. RQD frequency distribution in borehole cores below 60m (NJC, 2011a) .	153
E.2. Geological surface maps and profiles	153
E.3. Technical drawings	153

List of Figures

2.1. Factors influencing on tunnel stability (Panthi, 2006)	5
2.2. Schematic of the primary geometrical properties of discontinuities in rocks (Hudson and Harrison, 2000)	7
2.3. Types of faults and weakness zones (Panthi, 2006)	7
2.4. Influence of specimen size on the strength of intact rock (Hoek, 2007c)	8
2.5. Uniaxial compressive strength at different angle of schistosity plane (Panthi, 2006)	9
2.6. Compressive strength of rocks (left) and strength reduction in percentage (right) as a function of weathering grade (Panthi, 2006)	11
2.7. The Mohr-Coulomb failure criterion with tension cutoff (Hudson and Harrison, 2000)	12
2.8. Left: Selection of failure criteria according to rock mass condition. Right: Relationship between major and minor principle stresses for Hoek-Brown and equivalent Mohr-Coulomb criteria. Modified from Hoek (2007c)	14
3.1. Plot of a) vertical stress against depth below surface, and b) variation in ratio of average horizontal stress to vertical stress with depth below surface (Carranza-Torres and Fairhurst, 2000)	18
3.2. Stress map of western region of the Himalayas, with project location (World Stress Map, 2008)	19
3.3. Left: Stress trajectories around an circular opening. Right: Tangential and radial stress distribution in elastic and non elastic conditions. (Panthi, 2006)	20
3.4. Illustration of squeezing in a circular tunnel (Panthi, 2006)	23
3.5. Strain-time curve for creep, with the three characteristic stages (Goodman, 1989)	24
3.6. Creep in relation to the complete stress-strain curve (Goodman, 1989)	24
3.7. Pattern of deformation in the rock mass surrounding an advancing tunnel (Hoek, 2007e)	27
3.8. Numerical stability analysis of horseshoe shaped cavern (left), and elliptically shaped caverns (right). (Hoek, 2007a)	28
3.9. Typical convergence monitoring program (Panthi, 2013a)	29
4.1. Neelum Jhelum HPP organization	31
4.2. Google earth image of project area	32
4.3. Project location	33
4.4. Project layout features (not in scale) (Norplan A/S, 2013a)	34
4.5. Layout of the powerhouse area. Modified from Norplan A/S (2013a)	35

4.6. Dimensions of the powerhouse cavern and transformer hall. (Norplan A/S, 2013a)	35
4.7. Downstream wall of powerhouse cavern (NJC, 2013b)	36
4.8. Regional tectonic map of North Pakistan and adjoining areas. NJHPP lies right south of Balakot (Khan et al., 2010)	37
4.9. Block diagram of the Himalaya giving different litho-tectonic units (Deo-ja et al., 1991)	38
4.10. The Hazara-Kashmir syntaxis. The Murre fault is also known as the Main Boundary Thrust. Modified from Calkins et al. (1975)	39
4.11. Profile along headrace tunnel	41
4.12. Face location at Muzaffarabad fault and Jhelum crossing	41
4.13. Geological long wall mapping of the powerhouse cavern (NJC, 2011b)	42
4.14. Installed support zone A, cross section. NJC (2011b)	45
4.15. Shotcrete support. From NJC (2011b)	46
4.16. (a) Squeezing in pillar wall. (b) Concrete jacket installed for niche pillar. Photos by Norplan A/S (2013b).	47
4.17. Overview of measuring stations in the powerhouse cavern (NJC, 2013a)	48
4.18. a) Cross-sectional view of the measuring points. Blue lines represent convergence measurements, red dots are the extensometer points. b) Illustration of installed extensometers	48
4.19. Summary of all measured deformation along the cavern	49
4.20. Convergence over time for chainage 0+065	50
4.21. Extensometer data for chainage 0+032	51
4.22. Extensometers at el. 610, for section 0+032, 0+085 and 0+127	51
5.1. Goel's approach for predicting squeezing by rock mass number (N).	55
5.2. Tunnel convergence against ratio of rock mass strength to in-situ stress, found by Hoek and Marinos (2000).	56
5.3. Suggested classification of severity of squeezing, proposed by Hoek and Marinos (2000a).	57
5.4. a) A cylindrical tunnel of radius R driven in the rock mass. b) Cross-section of the rock mass at section A-A'. c) Cross-section of the circular support installed at section A-A' (Carranza-Torres and Fairhurst, 2000).	59
5.5. Loading of the support at section A-A' due to progressive advance of the tunnel face (Carranza-Torres and Fairhurst, 2000)	60
5.6. Schematic representation of Longitudinal Deformation Profile (LDP), Ground Reaction Curve (GRC) and Support Characteristics Curve (SCC) (Carranza-Torres and Fairhurst, 2000)	61

5.7. Representation of sections of a) concrete/shotcrete rings and b) ungrouted mechanical-anchored bolts (Hoek, 2007e)	65
5.8. a) A circular cavity in a Mohr-Coulomb material subjected to a uniform internal pressure and unequal far-field stresses. b) Limiting values of stress ratio k_{lim} as a function of scaled mean stress σ_0/σ_{ci} and friction angle ϕ (Carranza-Torres and Fairhurst, 2000)	68
5.9. Illustration of residual Young's modulus	72
6.1. Overview of performed analysis	75
6.2. Selected sections for the analysis	76
6.3. Deformation by Hoek and Marinos compared to measured deformation	82
6.4. Original LDP and improved LDP for the 5 sections	83
6.5. Improved LDPs for variation in rock type	84
6.6. Improved LDPs with variation to applied stress	84
6.7. Total deformation from CCM compared to measured deformation	85
6.8. Deformation at correct distance from the end-walls	86
6.9. GRC for all sections with applied mean stress	87
6.10. GRC and SCC for section 0+085, for support installed 5m behind face	87
6.11. Support characteristics curves for all installed support types	89
6.12. Realistic shape of SCC	90
6.13. Example model 0+085	91
6.14. Example of the model for section 0+085 with installed support	92
6.15. Graph for calibration results of model 0+085	94
6.16. Strength factor for model 0+085	96
6.17. Total deformation for unsupported plastic analysis for section 0+085	97
6.18. Total deformation for plastic analysis with installed support for section 0+085	98
6.19. Wall convergence for plastic analysis with and without support compared to measured deformations	99
6.20. Deformation in pillar between powerhouse and transformer chamber for section 0+085	99
6.21. Illustration of stages for section 0+085	100
6.22. Total displacement for excavation in stages for section 0+085	101

List of Tables

2.1. Weathering classification according to ISRM, 1978 (Panthi, 2006)	10
2.2. Empirical formulas for estimation of rock mass strength. After Panthi (2006)	15
2.3. Empirical formulas for the estimation of rock mass deformation modulus	16
4.1. Type of Himalayan rocks and their geomorphic units (Panthi, 2006) . . .	38
4.2. Rock units classified in the project area. Summarized from NJC (2011a) .	40
4.3. Summary of intact rock properties from laboratory testing	43
4.4. Estimation of rock properties with Roc-Lab	44
4.5. Rock mass classification per chainage (NJC, 2011a)	44
4.6. Summary of installed support	46
5.1. Squeezing condition according to Q-system (based on Barton, 2002) . . .	54
5.2. Geotechnical issues and suggested support types for the 5 classes of squeezing severity Hoek and Marinos (2000a).	58
6.1. Estimation for rock mass quality ratings	78
6.2. Estimated rock mass strength and deformability	78
6.3. Support properties	79
6.4. Summary of input parameters for each section	79
6.5. Squeezing prediction according to Geol (1994), Q-method and Hoek and Marinos (2000a)	80
6.6. Model input for <i>Phase</i> ² analysis	92
6.7. Model results for 0+085 compared to measured deformations	94
6.8. Model results for 0+127 compared to measured deformations	95
6.9. Model results for 0+032 compared to measured deformations	95

List of Abbreviations

σ_0	Far-field stress	[MPa]
σ_1	Major principal stress	[MPa]
σ_3	Minor principal stress	[MPa]
$\sigma_{\theta max}$	Maximum tangential stress	[MPa]
$\sigma_{\theta min}$	Minimal tangential stress	[MPa]
σ_{cm}	Rock mass strength	[MPa]
p_i^{cr}	Critical internal pressure	[MPa]
p_o	In-situ stress	[MPa]
u_r	Radial displacement	[mm]
CCM	Convergence Confinement Method	
GRC	Ground Reaction Curve	
LDP	Longitudinal Deformation Profile	
MBT	Main Boundary Thrust	
MF	Muzaffarabad Fault	
N	Rock Mass Number	
NGI	Norwegian Geotechnical Institute	
NJC	Neelum Jhelum Consultants	
NJHPP	Neelum Jhelum Hydropower Project	
RQD	Rock Quality Designation	
SCC	Support Characteristics Curve	
SRF	Strength Reduction Factor	
TBM	Tunnel Boring Machine	
WAPDA	Water and Power Development Authority	

1. INTRODUCTION

1.1. BACKGROUND

Sufficient and affordable energy supply is an essential key to development for any nation. For countries in the Himalayan region, the high mountains and many rivers naturally facilitate hydropower development. Pakistan has in recent years focused to increase the utilization of renewable energy sources, with the Neelum-Jhelum Hydropower project (NJHPP) as one of the greatest new contributions. This run-of-the-river project will have an installed capacity of 969 MW, and is scheduled to be finalized in 2016. The project will contribute with 5.15 billion units of low-cost electricity to the national grid (WAPDA, 2013).

For larger hydropower projects the topography typically dictates the layout of the facilities. High tectonic activity and risk of landslides contribute to the alternative of an underground design for the main waterway and powerhouse structures. As was the case for NJHPP, where most of the facilities are located underground. Challenges related to high overburdens and weak and jointed rock mass have been experienced along the head-race tunnel and in the powerhouse complex. Experiences from previous projects in the Himalayan region have shown that the tectonized and young formations typically show plastic behavior, even for small overburdens (Shrestha, 2006; Panthi, 2006). Severe stability problems due to “squeezing” behavior are not uncommon for the region, and have also been experienced in the powerhouse cavern at NJHPP.

The large dimensions necessary for underground powerhouse caverns contribute to the deformation behavior of the rock mass. A reliable prediction of the extent of squeezing is therefore essential for adequate design of the cavern layout, construction procedure and support. Available methods for analysis of squeezing today are typically developed for tunnels, and there is less knowledge about the appropriate choice of analysis for large scale caverns.

The main cause for instability in the NJHPP powerhouse cavern is squeezing deformation. Since constructions commenced in 2011, the convergence of the cavern roof and walls have been progressively monitored during excavation. This makes for a potentially rare opportunity to evaluate the deformation characteristics of a powerhouse cavern, as well as to evaluate available methods for prediction and assessment of squeezing in large scale caverns. The focus of this thesis is therefore to evaluate the applicability of five selected methods for analysis of squeezing, based on comparison to the measured deformations at the NJHPP cavern.

1.2. OBJECTIVE AND SCOPE

Main objectives for the study:

- Evaluate and interpret the measured deformations in the powerhouse cavern at Neelum Jhelum HHP
- Apply empirical, analytical and numerical methods for the assessment of cavern deformation

- Evaluate the applicability of the methods for deformation analysis with regard to large scale caverns

The scope of the project involve:

- Review existing theory for stress-induced instabilities in rock, with particular focus on squeezing
- Review theory related to constructions of large scale caverns in weak rock
- Briefly describe the Neelum Jhelum HPP, including geologic conditions, installed rock support, excavation methods and major challenges for the project
- Document and discuss the engineering geological conditions and installed support in the powerhouse cavern
- Review theory on existing methods for analysis of rock deformation
- Deformation analysis using 4 different empirical and analytical methods, and 2D numerical modeling using *Phase²*
- Compare and discuss the results of the analysis to the measured deformations

1.3. METHODOLOGY OF THE STUDY

The following methodology has been applied during the study:

1. Literature review:

- a) Study of existing theory on rock mass properties and stress-induced instabilities in weak rock
- b) Special considerations for constructions of large scale caverns
- c) Review of available methods for deformation analysis

2. Study of the Neelum Jhelum HPP:

- a) Overview of the project layout, with particular focus on the headrace tunnel and powerhouse complex
- b) Evaluate engineering geological conditions and rock mass properties for the powerhouse area
- c) Evaluate and interpret measured deformations in the powerhouse cavern, with respect to excavation progress, geology, cavern layout and measuring location

3. Deformation analysis:

Rock mass parameters and stress conditions were estimated with empirical formulas and by calibration to the measured deformations using *Phase²*. The following methods of analysis were applied:

- Empirical methods: Q-method and Geol's approach
- Semi-analytical method by Hoek and Marinos (2000)

1.4 LIMITATIONS OF THE STUDY

- Analytical method: Convergence-Confinement method by Carranza-Torres and Fairhurst (2000)
- 2D numerical modeling using *Phase²* (Rocscience software)

4. Comparison of results and evaluation of methods:

The results from the analysis were compared to the measured deformations in the cavern. The applicability of the methods with regard to deformation analysis in large scale caverns was assessed. The evaluation was based on the accordance with measured deformations, and compared with limitations and assumptions for each method.

1.4. LIMITATIONS OF THE STUDY

The main challenge for the study was to establish reliable input for the analysis. With considerations for personal safety it was not advised to conduct a field visit. No firsthand information was therefore available for the study. All information and understanding of the projects complexity had to be found through desk study of project drawings, photos, deformation measurements and in conversations with Norplan A/S. This limited the type of available geological data, and the author's ability to evaluate the quality of the existing material.

The analysis was limited to only include detailed evaluation and assessment of the conditions in the powerhouse cavern. Norplan A/S is working as a one of 5 consultants in a joint venture, and the project has been divided based on areas of expertise and for logistical reasons. The employees available at the offices in Norway have mainly worked with the powerhouse cavern and surrounding areas. Getting information for the remaining parts of the project was therefore difficult, and limited this study to only consider the powerhouse cavern.

2. ROCK AND ROCK MASS PROPERTIES

2.1. INTRODUCTION

Rocks are naturally occurring solid aggregates of one or more minerals. Different minerals have different physical properties, naturally affecting the physical and mechanical properties of the rock. Main physical properties of a rock include density, porosity, wave velocity, heat transfer and expansion. However, a discussion of the rocks specific properties is less important for the understanding of the actual behavior of the ground. In this context, the mechanical properties of the rock mass as a whole will be of more relevance.

Rock mass is 'rock penetrated by discontinuities', i.e the structural material which is being excavated (Nilsen and Palmström, 2000). The rock mass is a heterogeneous medium, characterized by two main features: 1) rock mass quality and 2) the mechanical processes acting on the rock mass (Panthi, 2006). These two are highly interlinked, and are key functions to the stability of an underground excavation (Fig.2.1). The rock mass quality depends on rock mass strength, deformability, anisotropy, presence of discontinuities and weathering. The mechanical processes influencing tunnel stability are mainly rock stresses and groundwater. Additionally the "non-ground" related factors like size, shape and orientation of the excavation will influence on total tunnel stability.

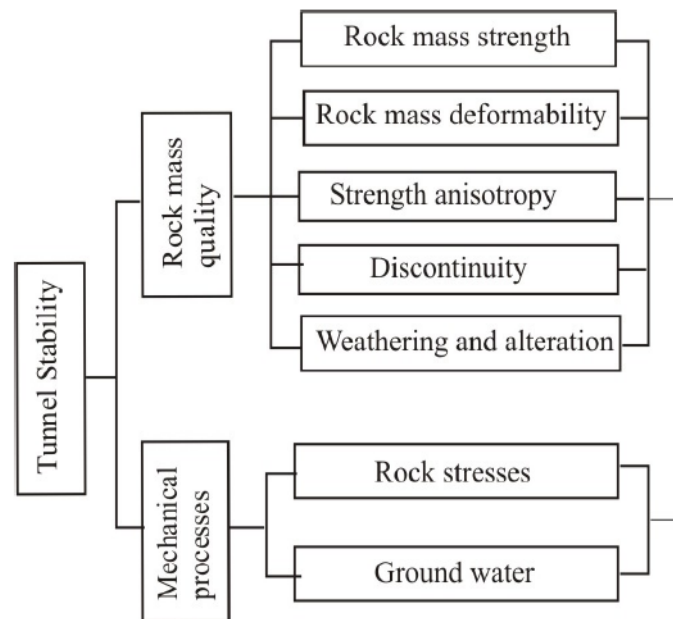


Figure 2.1.: Factors influencing on tunnel stability (Panthi, 2006)

This chapter will give a brief introduction to some of the factors influencing on rock mass quality, which should be know to perform an evaluation of the stability of an underground excavation. Common rock engineering principles for estimation and assessment of rock mass quality will be presented. Rock stresses and the mechanical processes leading to failure will be further discussed in the proceeding chapter.

2.2. ROCK MASS STRUCTURES

A rock mass is per definition penetrated by discontinuities; structural or geological features which change the homogeneity of the rock mass. A discontinuity is the general term for any mechanical discontinuity in the rock mass having zero or close to zero tensile strength (Nilsen and Palmström, 2000). It's a wide collective term for most types of joints, bedding planes, foliation planes, weakness zones and fault zones. In an engineering context, the discontinuities can be the single most important factor governing the mechanical properties of the rock mass.

2.2.1. Bedding- or foliation planes

Rock mass structures caused by the formation of the rock itself is often referred to as *bedding planes* in sedimentary rocks, and *foliation planes* in metamorphic rocks. Bedding planes divide the rock into layers called beds or strata, and are highly persistent features. The thickness of the beds may range from a centimeter to several meters, and may contain parting material or different grain sizes. Foliation planes are repetitive layer in metamorphic rocks, and may range from a few millimeters to over a meter in thickness. In bedding planes, and especially foliation planes, there is often a preferred orientation of particles causing directional differences (anisotropy) in mechanical properties. This is particularly seen for metamorphic rocks containing much platy (sheet) minerals, e.g. micaceous and chloritic schists (Nilsen and Palmström, 2000).

2.2.2. Jointing of rock mass

Joints, or fractures, are the most common structural features in a rock mass. A group of parallel joints is called a joint set, and joint sets intersect to form a joint system. Random joints or individual joints may also occur. Most joints are typically a result of tectonic activity, but also originate from chemical or physical forces or during the formation of the rock. Joints parallel to the bedding or foliation formed during formation of the rock, are typically called bedding or foliation joints respectively. In general, joints are defined based on origin (e.g. exfoliation joints, sheeting joints, tectonic joints etc.), or by size and composition (e.g. crack, fracture, seam etc.) (Nilsen and Palmström, 2000).

In an engineering context, the joint characteristics are of major importance as they influencing the mechanical properties of the rock mass. Fig.2.2 summarize the main characteristics of joints that should be identified during field mapping. Dip and dip direction should be presented and considered when planning the orientation of the underground structure, usually by a joint rosette and/or stereographic projection. The joints delineate blocks, and the block size is an extremely important parameter in rock mass behavior as it may explain most scale effects (Nilsen and Palmström, 2000). Further, the roughness, waviness, presence of potential alteration or infill in the joint walls could be of major importance for the stability of the excavation.

2.2.3. Weakness zones and faults

There are two major groups of weakness zones; those formed by tectonic activity, or those formed by other processes (Nilsen and Palmström, 2000). Faults are tectonically formed minor to major structures in the rock mass, and are identified by the occurrence of shear displacement (Fig.2.3). Minor faults normally range in thickness from a decimeter to a

2.2 ROCK MASS STRUCTURES

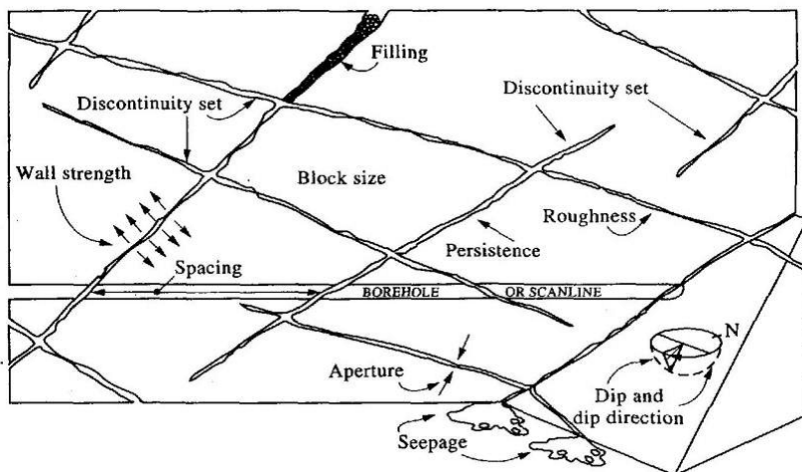


Figure 2.2.: Schematic of the primary geometrical properties of discontinuities in rocks (Hudson and Harrison, 2000)

meter, while major faults range from several meters to hundreds of meters. A weakness zone may be beds or layers of particularly weak rock in a series of sedimentary or metamorphic rocks (Nilsen and Thiedemann, 1993). Weakness zones and faults form patterns in the surface, or lineaments, and may be identified by inspection of areal photos or maps, or during field mapping.

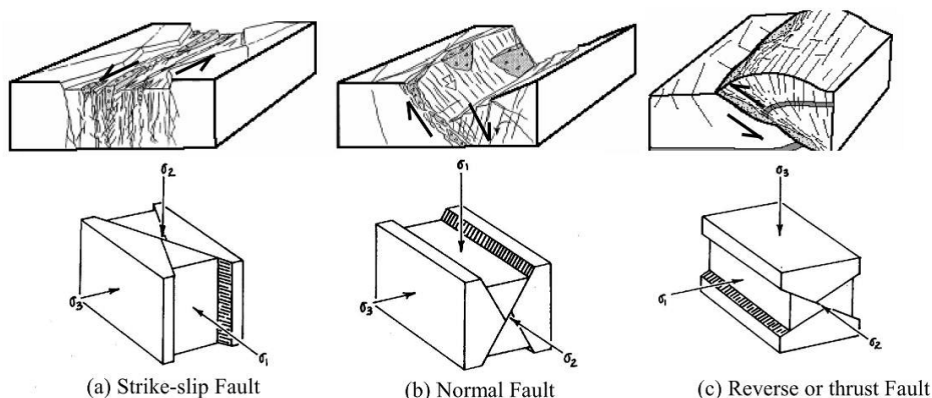


Figure 2.3.: Types of faults and weakness zones (Panthi, 2006)

Faults and crushed zones may vary greatly in composition, from mostly becciated or crushed to highly weathered or altered rock material. The filling is called *gauge material*. Its composition of rock fragments may be similar to the host rock, or new material may have been deposited or formed over time. Weathering, hydrothermal activity and alterations may have a significant impact on the composition and properties of the zone (Nilsen and Palmström, 2000). Some minerals may be altered to form clay minerals. The properties of these minerals may be crucial to the stability of the tunnels, especially swelling clay minerals like smectite and montmorillonite. These minerals will in contact with water experience a substantial increase in volume, and may exert a devastating pressure on the installed support.

2.3. ROCK MASS STRENGTH AND DEFORMABILITY

Rock strength and elastic properties play a major role in all aspects of rock engineering. Determination of the strength for the intact rock (σ_{ci}) is done by laboratory testing or field tests. The *rock mass strength* (σ_{rm}) is typically estimated by empirical relationships. Common intact rock strength tests include uniaxial compressive test, triaxial strength test and the point load test. Methods for field estimation have also been developed, but are only good as a firsthand estimate. No tests were performed especially for this study, although results from previous tests have been used. The reader will in either case be referred to other sources for theory on rock strength testing.

2.3.1. Factors influencing rock mass strength

Most methods for estimating rock mass strength depends on the uniaxial compressive strength of the intact rock. The factors influencing the strength of intact rock are therefore just as important for the discussion of factors for rock mass strength. Some of the many factors will be discussed below.

The scale effect

An intact rock test specimen is usually strong and close to homogeneous with few discontinuities. The specimen does not represent the strength and deformability of the rock mass; there is a considerable *scale effect*. The more discontinuous features in the rock mass, the more size dependance should be expected. Crystalline unweathered rocks have

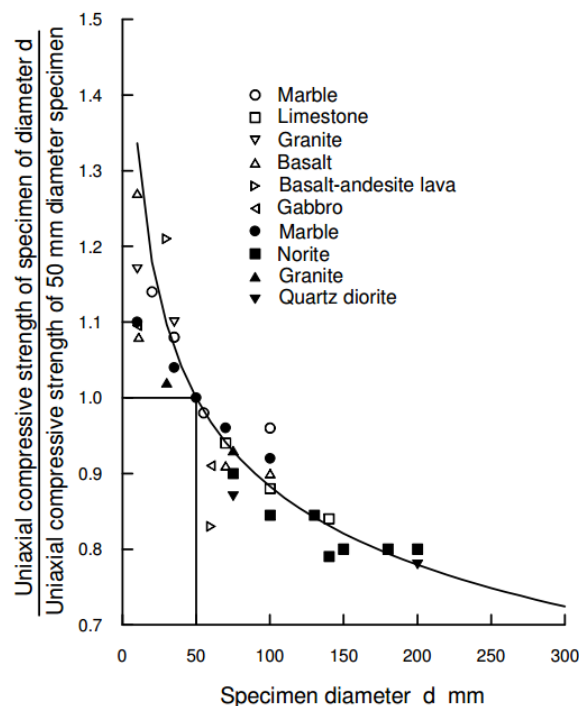


Figure 2.4.: Influence of specimen size on the strength of intact rock (Hoek, 2007c)

small size effect. Highly schistose, foliated and deformed rocks of sedimentary and metamorphic origin like shale, slate, phyllite and schist have considerable size and directional

2.3 ROCK MASS STRENGTH AND DEFORMABILITY

effect on their strength (Panthi, 2006). This is shown in Fig. 2.4, and it is seen that increasing the specimen diameter from 50 mm to 200 mm will reduce the intact rock strength by almost 25 percent.

The effect of anisotropy

Anisotropy in rocks is mainly caused by a preferred orientation of mineral grains and directional stress history. This is especially common in sedimentary and metamorphic rocks as a result of bedding, foliation and schistosity (Goodman, 1989). According to Panthi (2006) the Himalayan rocks often consist of thin bands of very weak and highly sheared rocks such as slate, phyllite and schists interlayered within the bands of relatively strong and brittle rocks such as gneisses, quartzite and dolomite. The layers of weak and schistose rocks lack sufficient bonding/friction and have reduced self-supporting capacity, and may result in severe stability problems while tunneling.

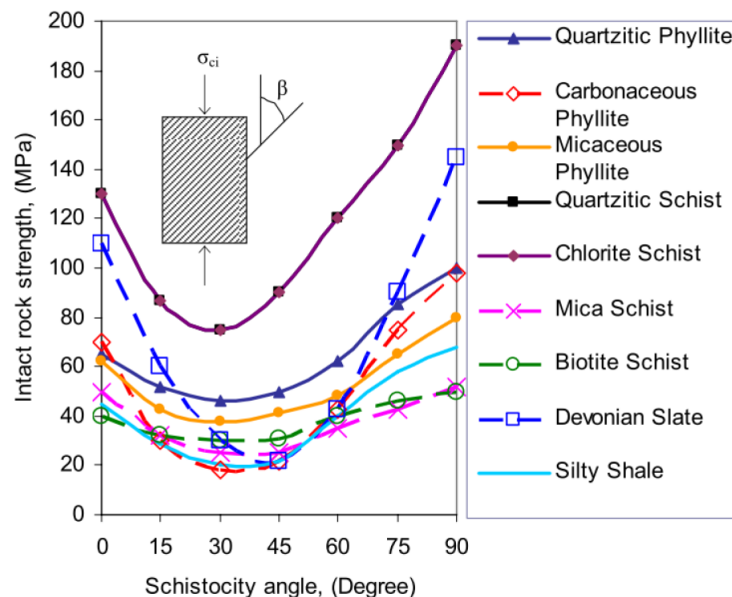


Figure 2.5.: Uniaxial compressive strength at different angle of schistosity plane (Panthi, 2006)

Fig. 2.5 illustrates the effect of anisotropy on uniaxial compressive strength. The diagram is based on research of different rocks in the Himalayas and other parts of the world. The data show that the strength of intact rocks is lowest when the schistosity plane is inclined at around 30 degrees from the direction of loading ($\beta = 30^\circ$). The strength is highest when the schistosity plane is perpendicular to the direction of loading ($\beta = 90^\circ$). Anisotropic rocks are commonly recommended to be tested perpendicular and normal to the schistosity plane. The test results may therefore give the false impression of strength characteristics (Panthi, 2006).

The effect of water

The occurrence of water has a considerable effect on rock mass strength, especially for highly schistose or porous rocks like sandstone and shale. Laboratory tests of moist sand-

stone and shale have shown a reduction in strength of 40% and 60% respectively, compared to dry strength (Nilsen and Palmström, 2000). The reduction in strength is due to the effect of pore and fissure water pressure, and can be reduced by drying the samples before testing. Other effects related to water in rocks can be swelling, slaking and desiccation (Palmström and Stille, 2010). These effects are more relevant in an engineering context for large scale excavations, and will not be discussed further in this section.

The effect of weathering and alteration

Rock weathering is the process of *disintegration* and *decomposition* of the rock material. The rock loses its coherence by mechanical disintegration or breakdown of the material. This causes opening or new formation of joints, opening of grain boundaries and fracturing of individual mineral grains (Nilsen and Palmström, 2000). Chemical decomposition involves rock decay accompanied by changes in chemical and mineralogical composition. This leads to discolorations, decomposition and alteration of silicate minerals to clay minerals and *leaching* or solution of calcite, anhydrite and salt minerals (Nilsen and Palmström, 2000). Generally, the weathering starts in the walls of the discontinuities and migrates to the rock material (Panthi, 2006).

Table 2.1.: Weathering classification according to ISRM, 1978 (Panthi, 2006)

Term	Description of rock mass conditions	Weathering grade
Fresh rock	No visible sign of rock material weathering; perhaps slight discolouration on major discontinuity surfaces.	I
Slightly weathered	Discolouration indicates weathering of rock material and discontinuity surfaces. All the rock material may be discoloured by weathering and may be some what weaker externally than in its fresh condition.	II
Moderately weathered	Less than half of the material is decomposed and/or disintegrated to a soil. Fresh or discoloured rock is present either as a continuous framework or as corestones.	III
Highly weathered	More than half of the rock material is decomposed and/or disintegrated to a soil. Fresh or discoloured rock is present either as a discontinuous framework or as corestones.	IV
Completely weathered	All rock material is decomposed and/or disintegrated to soil. The original mass structure is still largely intact.	V
Residual soil	All rock material is converted to soil. The mass structure and material fabric are destroyed. There is a large change in volume, but the soil has not been significantly transported.	VI

The degree of weathering is usually assessed by visual observations. Tab.2.1 show classification of weathering and alteration, as suggested by ISRM (1978). A more precise characterization would require analysis of thin sections in a microscope.

Weathering reduces the mechanical properties of the rock mass, such as strength, deformability, slaking durability and frictional resistance. Slaking durability is a measure

2.3 ROCK MASS STRENGTH AND DEFORMABILITY

of the rock's resistance against slaking (hydration/swelling) or disintegration when exposed to weathering processes (Nilsen and Palmström, 2000). A considerable increase in permeability may also be an effect of weathering (Panthi, 2006). According to Panthi (2006), Beavis (1985) and Gupta and Rao (2000) evaluated the weathering effect on rock mass properties such as porosity, density, tensile strength, uniaxial compression strength and elasticity modulus. They found that there is a considerable reducing effect, although there is variation in the degree of influence on uniaxial compressive strength (Fig.2.6).

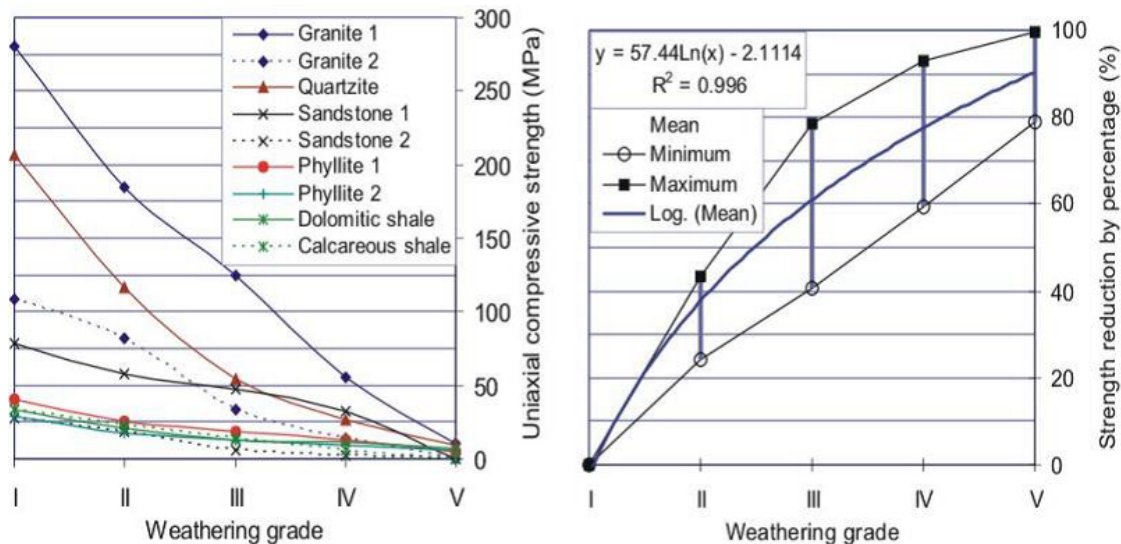


Figure 2.6.: Compressive strength of rocks (left) and strength reduction in percentage (right) as a function of weathering grade (Panthi, 2006)

2.3.2. Failure criteria

The term failure can be regarded as the 'loss of integrity' of the material, which in engineering is interpreted as the loss of the materials load carrying capacity. There has been developed a number of theories or criteria for the attempt to explain and predict when and where failure will occur in the rock mass. This has been done by assuming that the failure will occur due to a specific mechanism, when a specific mechanical property is exceeded (Myrvang, 2001). Further it is evaluated which principal stress condition will lead to such a failure. Among the classical theoretical failure criteria are the Tresca criterion (max. shear stress), Mohr-Coulomb (max effective shear stress), Drucker Prager criterion and Griffith's criterion (Myrvang, 2001). The theoretical criteria rarely reflect the true nature of the failure mechanism. Many have therefore tried to formulate empirical relationships, where the Hoek-Brown criterion is widely applied.

The failure criteria are valid for intact rock materials. As the stability in underground excavations will be strongly influenced by natural joints and cracks created by blasting, they are of limited importance to practical tunneling (Nilsen and Thiedemann, 1993). However, both the Mohr-Coulomb criterion and the Hoek-Brown criterion are commonly applied in rock engineering. They are used as basis in preliminary design calculations and in numerical modeling, and will therefore be further explained in the following.

2.3 ROCK MASS STRENGTH AND DEFORMABILITY

defining a tension cutoff; the Mohr-Coulomb line is extrapolated in the tensile region down to the point where the minor principal stress equals the uniaxial tensile strength (tension cutoff given by $\sigma_3 = -\sigma_t$) (Goodman, 1989).

The Hoek-Brown criterion

Hoek and Brown introduced their failure criterion as an attempt to provide input data for the analysis required for the design of underground excavations in hard rock (Hoek et al., 2002). The criterion is an empirical relation derived from a best-fit of strength data plotted in a principal stress space ($\sigma_1 - \sigma_3$) (Hudson and Harrison, 2000). The ratings of its constants have been adjusted numerous times, and lead to a modified criterion presented in several editions (Nilsen and Palmström, 2000; Hoek et al., 2002).

The original Hoek-Brown criterion is expressed in terms of the major and minor principal stresses at failure as:

$$\sigma'_1 = \sigma'_3 + \sigma_{ci} \left(m \frac{\sigma'_3}{\sigma_{ci}} + s \right)^{0.5} \quad (2.3)$$

where σ'_1 and σ'_3 are the major and minor effective principal stresses at failure, σ_{ci} is the uniaxial compressive strength of the intact material. m and s are empirical material constants, and represent the inherent properties of the jointing and rock characteristics ($s=1$ for intact rock) (Nilsen and Palmström, 2000). The rating of the constant m was later adjusted, and the ratio m_b/m_i was introduced by Wood (1991) and Hoek et.al (1992). Further adjustment of the criterion was done based on tangents of the principal stress plot (Mohr-envelope). From various practical situations, they found that the Mohr-envelope could be adjusted with a variable constant a instead of the square root term (Hoek, 1990). The generalized Hoek-Brown criterion was introduced:

$$\sigma'_1 = \sigma'_3 + \sigma_{ci} \left(m_b \frac{\sigma'_3}{\sigma_{ci}} + s \right)^a \quad (2.4)$$

where the material constants m_b , s and a are defined as:

$$m_b = m_i \exp \left(\frac{GSI - 100}{28 - 14D} \right) \quad (2.5)$$

$$s = \exp \left(\frac{GSI - 100}{9 - 3D} \right) \quad (2.6)$$

$$a = \frac{1}{2} + \frac{1}{6} \left(e^{-GSI/15} - e^{-20/3} \right) \quad (2.7)$$

where m_i is a material constant for intact rock and GSI is the Geological Strength Index. D is the disturbance factor, and depend upon the degree of disturbance of the rock mass by blasting and stress relaxation (0 for undisturbed masses). The determination of these are given in App. A.1-A.3.

Relationship between Hoek-Brown and Mohr-Coulomb failure criteria

Selection of failure criterion should be done based on the type of rock mass being investigated. Mohr-Coulomb is best fitted for situations with rock mass consisting of one or two joint sets; or when one of the discontinuity sets is significantly weaker than the others.

Hoek-Brown is best suited for intact rock, or for rock masses with a sufficient number of closely spaced discontinuities with similar characteristics. Then isotropic behavior involving failure on discontinuities can be assumed (Hoek, 2007c)(Fig.2.8).

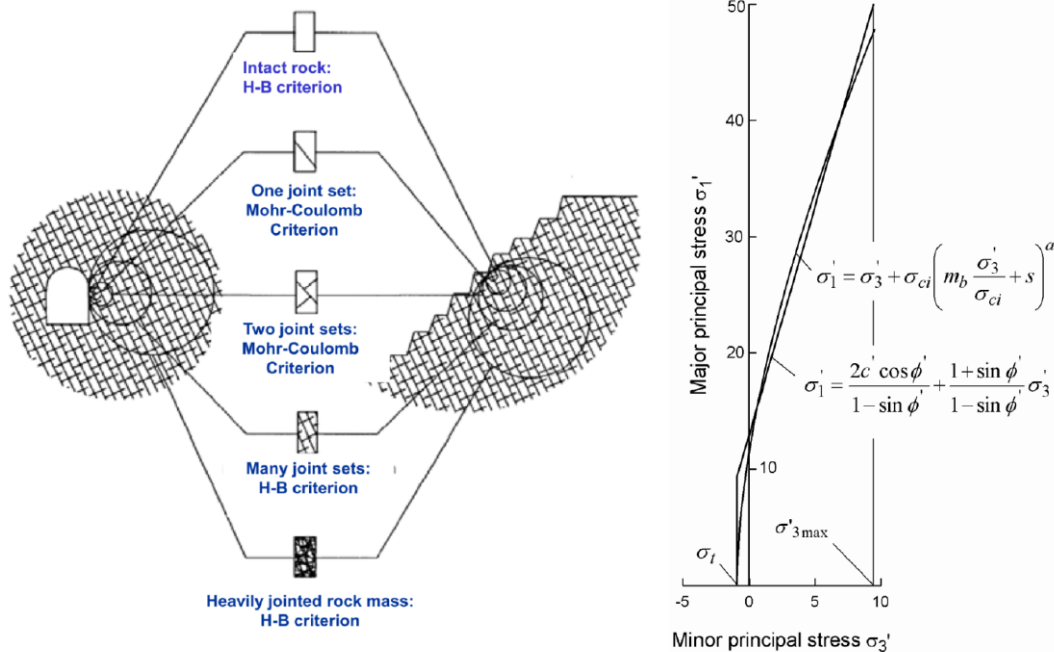


Figure 2.8.: Left: Selection of failure criteria according to rock mass condition. Right: Relationship between major and minor principle stresses for Hoek-Brown and equivalent Mohr-Coulomb criteria. Modified from Hoek (2007c)

Many geotechnical software programs are still written in terms of Mohr-Coulomb, and it may therefore be necessary to determine equivalent angles of friction and cohesive strengths for a rock mass and the stress range (Hoek, 2007c). This is done by fitting an average linear relationship to the curve defined by the original Hoek-Brown criterion for a range of principal stress values $\sigma_1 < \sigma_3 < \sigma_{3max}'$ (Fig.2.8 right). σ_{3max}' is the upper limit of confining stress for which the relationship between the Mohr-Coulomb and Hoek-Brown criteria is considered (Hoek, 2007c).

2.3.3. Estimation of rock mass strength

Rock mass strength and deformation is different from that of an intact rock specimen. An intact rock specimen is usually strong and homogeneous with few discontinuities, and can therefore not represent the strength and deformability of the total rock mass. As discussed above, there are several factors influencing the strength of intact rock, and by this the strength of the rock mass. Evaluation of strength of the rock mass will additionally include the influence of discontinuities, foliation or schistosity planes, and the orientation of these relative to the direction in which the strength is assessed (Panthi, 2006).

Rock mass strength is difficult to estimate in the field, or by laboratory testing, and many authors have therefore suggested empirical relationships for estimation of rock mass

2.3 ROCK MASS STRENGTH AND DEFORMABILITY

strength (σ_{cm}). Typically, the methods include intact rock strength (σ_{ci}) and a form of rock mass characterization parameter like Q-value or Rock Mass Rating (RMR).

Table 2.2.: Empirical formulas for estimation of rock mass strength. After Panthi (2006)

Proposed by	Empirical relationship
Bieniawski (1993)	$\sigma_{rm} = \sigma_{ci} \times \exp \left[\frac{RMR-100}{18.75} \right]$
Hoek et al. (2002)	$\sigma_{cm} = \sigma_{ci} \times s^a = \sigma_{ci} \times \left[\exp \frac{GSI-100}{9} \right]^a = \sigma_{ci} \times \left[\exp \frac{RMR-105}{9} \right]^a$
Barton (2002)	$\sigma_{cm} = 5\gamma \times \sigma_c^{1/3} = 5\gamma \times \left[\frac{\sigma_{ci}}{100} Q \right]^{1/3} = 5\gamma \times \left[\frac{\sigma_{ci}}{100} \times 10^{\frac{RMR-50}{15}} \right]^{1/3}$
Panthi (2006)	$\sigma_{cm} = \frac{\sigma_{ci}^{1.5}}{60}$

In Tab.2.2 σ_{cm} is the rock mass strength in MPa, σ_{ci} is the intact rock strength (uniaxial compressive strength) in MPa, RMR is the Rock Mass Rating by Bieniawski (see App. A.6), s and a are the Hoek-Brown material properties described in Sec.2.3.2. GSI is the Geological Strength Index (see App. A.2), γ is the rock density in t/m^3 . Q_c is the normalized rock mass quality, while Q is the rock mass quality rating, further described in Sec.5.2.1. The rock mass classification ratings are related as follows (Barton, 2002):

$$RMR = 15 \log Q + 50 \quad (2.8)$$

$$GSI = RMR - 5 \quad (2.9)$$

The methods relating both rock mass rating and intact rock strength have been found to have a weakness when evaluating weak, fractured and schistose rocks. The reduced strength of discontinuous rocks will be double accounted for; in the laboratory determination of σ_{ci} and in the determination of the rock mass rating (RMR, Q or GSI) (Hoek and Marinos, 2000a). The relation by Panthi (2006) is only dependent on one rock parameter, σ_{ci} . His relation is an empirical best-fit power function, based on plots of intact rock strength against the estimated rock mass strength using the 3 other relations in Tab.2.2 (Panthi, 2006). According to Panthi (2006) the relation may be used for highly schistose, foliated, thinly bedded and anisotropic rocks of metamorphic and sedimentary origin with low compression strength.

2.3.4. Estimation of rock mass deformability

Deformability of the intact rock is referred to as the Young's modulus or *modulus of elasticity* (E_{ci}), and is the ratio between applied stress and corresponding strain within the elasticity limit. Rock mass deformability or *modulus of deformation* (E_m) is defined as the ratio of stress to corresponding strain during loading of the rock mass, and includes both elastic and inelastic behavior (Panthi, 2006). A jointed rock mass does not behave elastically, and it is therefore necessary with the term *modulus of deformation* rather than modulus of *elasticity* (Bieniawski, 1989). As for rock mass strength, the deformability of the rock mass is lower than for the intact rock, and may be reduced down to 10% of the intact deformability (Panthi, 2006).

The modulus of deformation may be measured directly in the field (e.g. plate bearing, dilatometer test, flatjack test, hydraulic chamber etc.), but often provide values that differ considerably (Nilsen and Palmström, 2000). The tests are also considered time-consuming and costly. Many authors have therefore proposed empirical equations for estimating the modulus of deformation, where a selection is given in Tab.2.3.

Table 2.3.: Empirical formulas for the estimation of rock mass deformation modulus

<i>Proposed by</i>	<i>Empirical relationship</i>
Bieniawski (1989)	$E_m = 2RMR - 100$
Hoek et al. (2002)	$E_m = (1 - \frac{D}{2}) \sqrt{\frac{\sigma_{ci}}{100}} 10^{\left(\frac{GSI-10}{40}\right)}$
Barton (2002)	$E_m = 10 \times Q_c^{1/3} = 10 \times \left(\frac{Q \times \sigma_{ci}}{100}\right)^{1/3}$
Hoek and Diederichs (2006)	$E_m = E_{ci} \times \left(0.02 + \frac{1-D/2}{1+e^{((60+15D-GSI)/11)}}\right)$
Panthi (2006)	$E_m = \frac{1}{60} \times E_{ci} \times \sigma_{ci}^{0.5}$

In Tab.2.3, E_m is the modulus of deformation in GPa, E_{ci} is the modulus of elasticity in GPa, and D in the relation by Hoek et al. (2002) is the disturbance factor (see App. A.3). The other parameters are described in the previous section.

3. STRESS INDUCED INSTABILITIES

Rock stresses are the stresses (force per unit area) already existent in the rock mass, and makes the rock 'unique' in the sense that the material is pre-loaded. Creating an underground excavation will change the stress conditions in the rock mass surrounding the opening. The final stress state will be a result of the initial stress conditions and the stresses induced by the excavation. The stability of an underground excavation will depend on the rocks ability to sustain failure induced by the stresses around the opening. Since the final stress condition is dependent on the initial stresses, specification and determination of the pre-excavation stress state is a key component of any stability and design analysis.

3.1. IN-SITU ROCK STRESSES

3.1.1. Initial stress conditions

The stress conditions existent in the rock mass before an excavation is referred to as the in-situ stresses, virgin stresses or initial stresses. The initial stress conditions in a rock mass are a result of the following components (Nilsen and Palmström, 2000):

- *Gravitation stresses*: are the result of gravity alone.
- *Tectonic stresses*: are mainly caused by plate tectonics.
- *Topographic stresses*: occur when the surface is not horizontal, and the topography will have a considerable influence on rock stress situation.
- *Residual stresses*: are stresses locked into the rock material from earlier stages of its geologic history.

Much can be said about the origin, influence and determination of each of these components. However, in an engineering geologic context the magnitude and direction of the *principal stresses* are the most interesting stress related parameters. The stability of an underground excavation is usually assessed by evaluation of the major and minor principal stresses, which are defined as the major and minor normal stresses on a plane with no shear stress (Nilsen and Palmström, 2000). The gravitational and tectonic components of the in-situ stresses are generally regarded as the two most influencing stress components, and are easiest quantified.

Gravitational stresses

The gravitational stress is divided into a vertical and horizontal component. When the surface is horizontal, the vertical gravitational stress at a depth H (in meters) is given by:

$$\sigma_v = \sigma_z = \gamma H \quad (3.1)$$

where γ is the specific gravity of the rock in MN/m^3 . Fig.3.1a show a plot of measured vertical stresses against depth below surface, measured at different locations around the world. The figure shows that estimation by Eq. 3.1 is in fair agreement with the measurements, as 0.027 is the mean specific gravity of rocks. The magnitude of the total vertical stress may be identical with the magnitude of the gravitational vertical component (Nilsen and Palmström, 2000). However, considerable deviations may occur, especially at great

or shallow depths. Close to the surface, the deviation may be caused by the fact that most measuring tools are close to its limits for low stress magnitudes. For greater depths, abnormally high vertical stresses are often explained as being caused by residual stresses (Nilsen and Palmström, 2000).

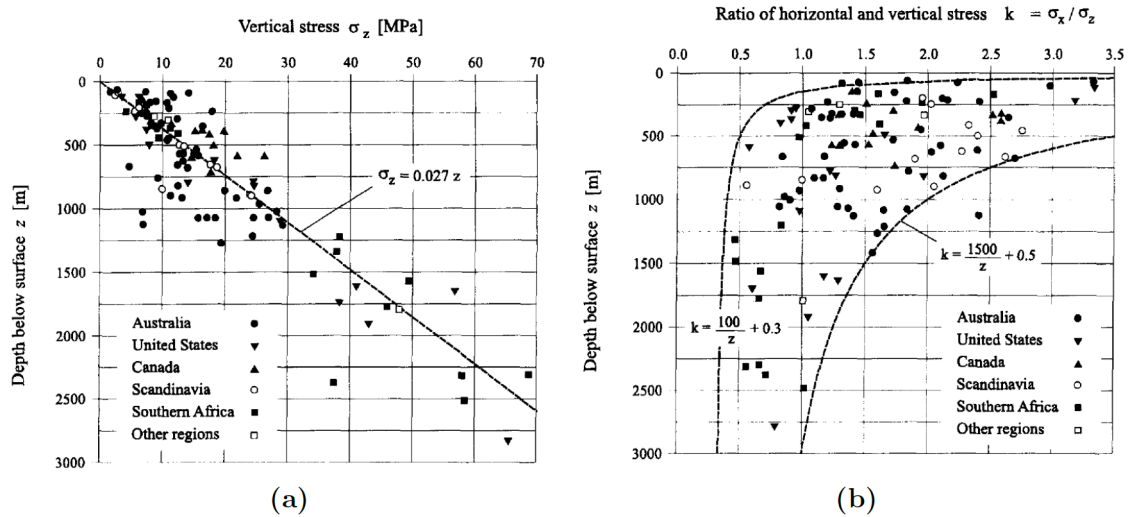


Figure 3.1.: Plot of a) vertical stress against depth below surface, and b) variation in ratio of average horizontal stress to vertical stress with depth below surface (Carranza-Torres and Fairhurst, 2000)

The total horizontal stress can be divided into a gravitational and a tectonic component (Panthi, 2006):

$$\sigma_h = \frac{\nu}{1-\nu} \gamma H + \sigma_{tec} \quad (3.2)$$

where the first term is the gravitationally dependent term. The vertical gravitational stress is assumed reduced by the ratio defined by the Poisson's ratio ν . Fig.3.1b show that the ratio (k) between horizontal and vertical in-situ stresses vary greatly with depth, and is assumed to vary between:

$$\frac{100}{H} + 0.3 < k < \frac{1500}{H} + 1.5 \quad (3.3)$$

Close to surface (depths less than 500m), the horizontal stresses are in many cases observed to be larger than the vertical stress. At depths larger than 1 km, the vertical and horizontal stresses tend to equalize, and the value of k will approach a constant value. This suggests that the magnitude of the average horizontal stress is to a great extent influenced by tectonic movements (Panthi, 2006).

Tectonic stresses

The main cause of tectonic stress is the plate tectonics; the drifting and tectonic activity along margins of the about 20 rigid plates that constitute the earth's crust (Nilsen and Palmström, 2000). The tectonic activity is responsible for earthquakes, volcanic activity, formation of the mountain chains etc. More importantly, the tectonic stresses are responsible for faulting and folding of the rock mass.

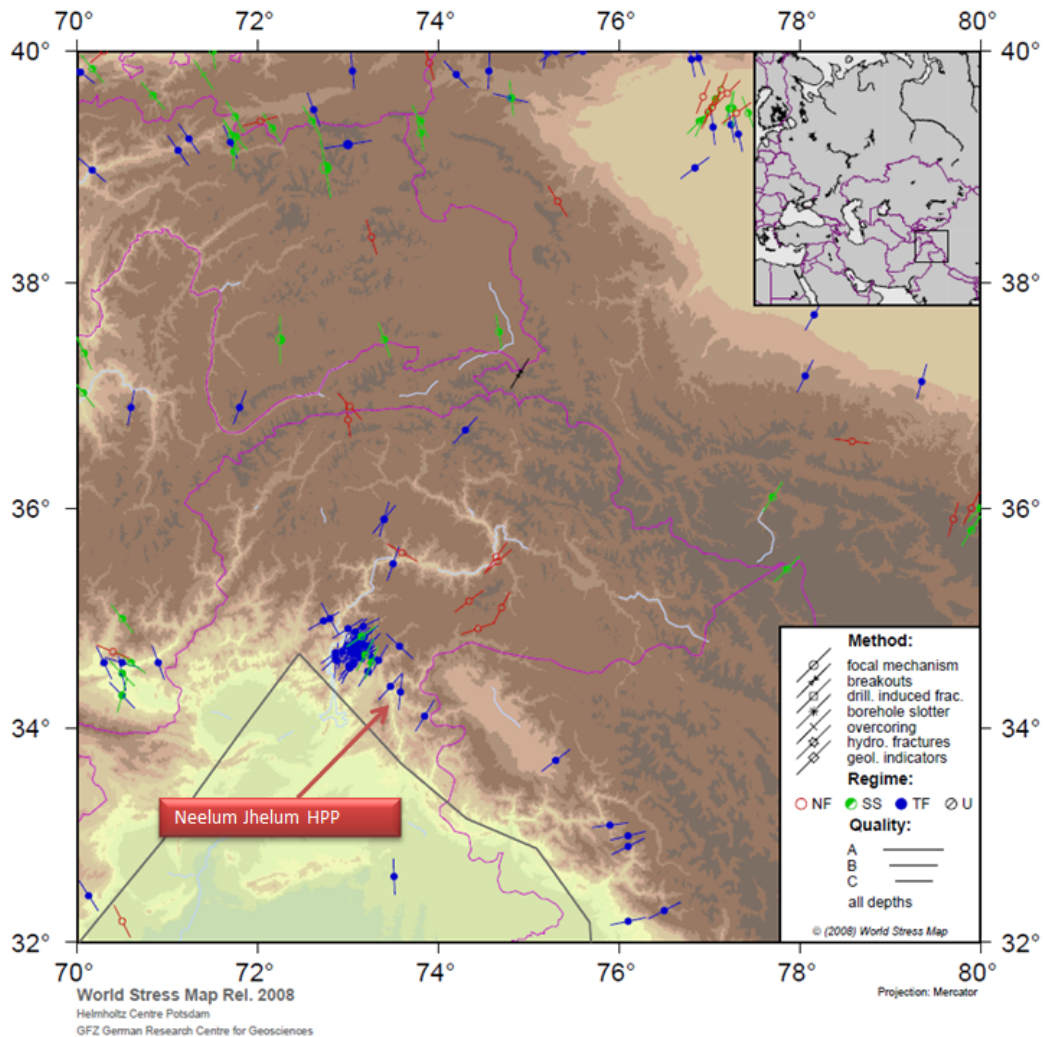


Figure 3.2.: Stress map of western region of the Himalayas, with project location (World Stress Map, 2008)

The tectonic processes have a considerable effect on the magnitude of the major tectonic principal stress in the Himalaya. In the southwest region of the Himalayas, where the Neelum Jhelum HPP project is located, the tectonic principal stresses are oriented horizontally with a Northeast-Southwest trend (Fig.3.2). The project is located relatively close to the plate boundary (black line in Fig.3.2), in an area with high seismic activity. An analysis of the stress derivations from earthquake focal mechanisms¹ in the vicinity of the project area indicates that the horizontal stress is oriented about N38°-42°E.

3.1.2. Distribution of stresses around an excavation

During and after excavation of an underground opening, the stresses in the rock mass will be redistributed around the periphery of the excavation. The load carried by the mass removed must be transferred to the remaining mass. The stresses induced by the

¹See the 'Guidelines' at www.world-stress-map.org for further explanation

excavation will depend on the magnitude and direction of the principal stresses and the geometry of the opening (Nilsen and Palmström, 2000).

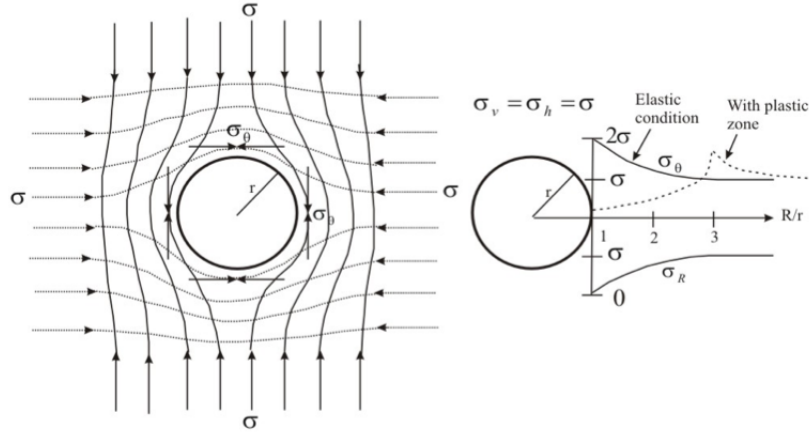


Figure 3.3.: Left: Stress trajectories around an circular opening. Right: Tangential and radial stress distribution in elastic and non elastic conditions. (Panthi, 2006)

Fig.3.3 illustrates how the redistribution of the stresses can be expressed around a circular opening, for an elastic material in isostatic stress conditions ($\sigma_h = \sigma_v = \sigma$). In elastic material the tangential stress (σ_θ) will be twice the principal stress (σ) at the wall of the opening, and the radial stress (σ_R) equal to zero. Moving away from the opening, the stresses will normalize as the ratio between radial distance (R) and opening radius (r) increases (Fig.3.3 right). Formally, this theory is known as the *Kirsch solution*:

$$\sigma_\theta = \sigma \left(1 + \frac{r^2}{R^2} \right) \quad (3.4)$$

$$\sigma_R = \sigma \left(1 - \frac{r^2}{R^2} \right) \quad (3.5)$$

For non-isostatic stress conditions, the Kirsch solution states that the maximum tangential stress ($\sigma_{\theta_{max}}$) will occur in the direction where the major principal stress (σ_1) is tangent to the contour. Likewise will the minimal tangential stress ($\sigma_{\theta_{min}}$) occur where the minor principal stress (σ_3) is tangent to the contour. According to the Kirsch solution, the magnitude of the tangential stresses are defined as:

$$\sigma_{\theta_{max}} = 3\sigma_1 - \sigma_3 \quad (3.6)$$

$$\sigma_{\theta_{min}} = 3\sigma_3 - \sigma_1 \quad (3.7)$$

The Kirsch solution is valid for a homogeneous, isotropic and elastic rock mass with widely spaced and tight joints (Panthi, 2006). For weak and anisotropic rocks, the tangential stresses will cause destruction and cracking of the material, resulting in a gradual reduction of the strength. A zone of broken rock will form around the opening, so called plastic zone, where the material loses its load carrying ability. In such rock masses, the maximum tangential stresses are moved further from the periphery of the opening, until

the elastic zone is reached (Panthi, 2006). This is illustrated by the dotted line to the right in Fig.3.3.

A non-circular opening will change the locational and magnitude of the tangential stresses. Sharp corners in particular, may strongly influence the magnitude; the sharper the corner, the higher the stress concentration in that corner will be (Nilsen and Palmström, 2000). The magnitude of the maximum tangential stress depends in theory on the shape of the excavation, and not its size. However, the zone of influence increases when the size increases. Consequently, the more masses are removed, the more stress is redistributed to the remaining masses (Myrvang, 2001).

3.2. STRESS INDUCED INSTABILITIES

When the tangential stress around the excavation exceeds the strength of the rock, the material will fail and cause instabilities in the underground opening. The problems are normally connected to the maximum tangential stress, causing compressive failure of the rock. However, if the minimum tangential stress is very low, this may cause tangential failure in the rock mass.

3.2.1. Problems related to tensile stress

Due to its discontinuous character, the rock mass has a low tolerance for tensile stress. Even a small tensile stress may cause radial failure. Tensile failure will occur if the minimal tangential stress (Eq. 3.7) exceeds the tangential strength of the rock mass. In most cases, tensile fracturing will not have much influence on rock stability in a tunnel. However, for high-pressure hydropower tunnels the presence of open fractures may increase the possibility of water leakage, causing a decrease in water-pressure (Nilsen and Palmström, 2000).

3.2.2. Problems induced by high compressive stress

Compressive failure of the rock mass will occur if the compressive tangential stress (Eq. 3.6) exceeds the compressive strength of the rock. Depending on the character of the rock, the failure usually takes the form of either: *i*) rock/burst spalling, or *ii*) squeezing or plastic deformation.

i) Rock burst/Rock spalling

Rock spalling is fracturing parallel to the tunnel contour induced by high compressive stresses, and typically occurs for strong brittle rocks. The fracturing process is often accompanied by loud noises and vibrations, and is then referred to as heavy spalling or rock burst. Rock burst or heavy spalling typically only occur for very high rock stresses, and are therefore most relevant for deep excavations. For moderate stress levels, the fracturing will result in loosening of thin rock slabs, referred to as rock slabbing or spalling (Nilsen and Palmström, 2000). Rock bursting may at times be quite violent and dramatic. In extreme cases the process can have the character of *popping* of large rock slabs with considerable force and speed. The activity is often most intensive in the vicinity of the face (10-20m behind face), and may therefore be a major threat to the safety of the workers if the appropriate support is not installed (Nilsen and Thiedemann, 1993).

The assessment of risk for rock burst or spalling is generally based on the ratio between the maximum tangential stress given by Eq. 3.6, and the rock mass strength (Sec.2.3.3). The analysis and risk assessment of rock burst/spalling is not an objective of this study, and will not be discussed further.

ii) Squeezing or plastic deformation

Weak and soft rocks will due to its plastic nature behave very differently when subjected to tangential stress. In such rocks, the potential problems will be *squeezing* deformation. In extreme cases reduction of the original tunnel diameter of several tens of centimeters due to squeezing may occur (Nilsen and Palmström, 2000). As this is the major cause of stability problems at the caverns of Neelum Jhelum HPP, analysis and risk assessment of the squeezing phenomena will be discussed in detail.

3.3. THE SQUEEZING PHENOMENON

The *squeezing phenomenon* was first described by the alpine geologist Heim in 1878, and have later been observed in tunnels and caverns in various geologic environments around the world (Shrestha, 2006). However, the definition of the actual term “squeezing” is often vaguely formulated. The International Society of Rock Mechanics (ISRM) have defined squeezing as time dependent large deformations around the tunnel, which essentially is associated with creep caused by exceeding a limiting shear stress (Shrestha, 2006). According to Panet (1996) squeezing also include the instantaneous convergence due to the advancement of the face. Simplified, squeezing can be described as the time-dependent inward movement of the rock material towards the tunnel when subjected to tangential stress (Panthi, 2013c). Squeezing is therefore a phenomena which may occur “instantaneously” or by creep, further explained in the following.

3.3.1. Instantaneous squeezing

As explained in Sec.3.1.2, the existing stress regime will be redistributed around the opening of an excavation. The load carried by the rock mass removed must be transferred to the surrounding rock, and will for elastic material be distributed as illustrated to the left in Fig.3.3. Weak rock such as shale, slate, phyllite and weakness/fracture zones, behave very differently from isotropic and strong rocks when subjected to high tangential stress. If the strength of the weak rock is less than the induced tangential stress around the periphery of the opening, micro-cracks will gradually start forming, mainly along the schistosity or foliation planes (Panthi, 2006). A visco-plastic zone of micro-fractured rock mass will start forming around the opening, and further move deeply into the rock mass (Fig.3.4). The induced maximum tangential stresses will be moved away from the opening, into the elastic material outside the plastic zone. As a result, a time-dependent inward movement of the rock material will take place, and the installed support will experience a gradual buildup of pressure (Panthi, 2006). This is illustrated by the dotted line in Fig.3.4, where r is the tunnel radius, R is the radius of plastic zone, and p_i is the support pressure.

This type of failure due to overstressing of the rock mass is usually referred to as *instantaneous squeezing*. The inward movement, squeezing of the rock mass, is usually highest in the areas of maximum tangential stress. However, if the minimal tangential stress is very low, it may also cause stability problems (Shrestha, 2006).

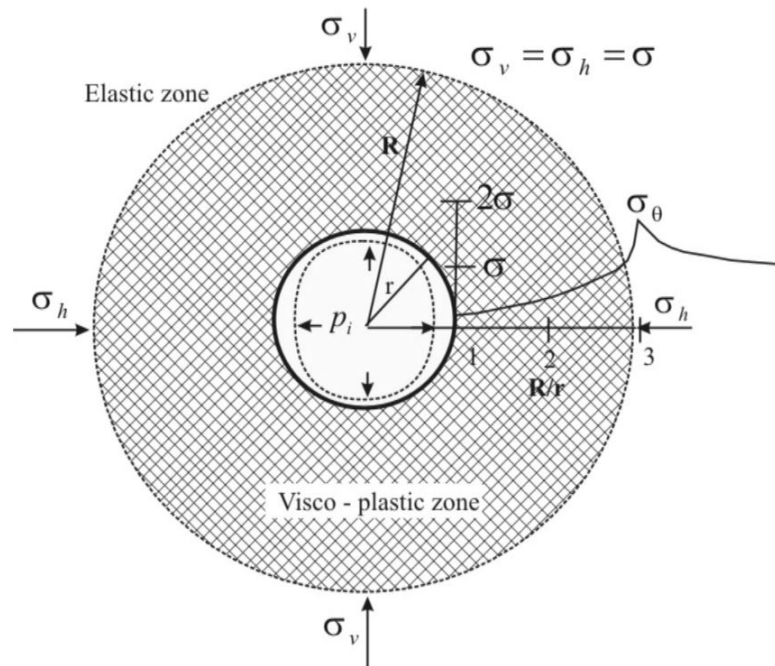


Figure 3.4.: Illustration of squeezing in a circular tunnel (Panthi, 2006)

3.3.2. Secondary squeezing (creep)

As defined by ISRM, time-dependent deformation (squeezing) is related to creep caused by exceeding a limiting shear stress (Shrestha, 2006). Materials that may not show much deformation right after the excavation could during constant stress over a long time experience increasing strain (deformation) which ultimately can lead to failure. This is called creep, and may continue for a long time before the material completely fails. Creep is important at low pressures only in a few rock types: shale, soft chalks and evaporite rocks (e.g. rock salts, gypsum and anhydrites) (Shrestha, 2006).

The creep process follows a characteristic development over time, as shown by the strain-time curve in Fig.3.5. From the time load is applied, the strain development is characterized by 3 phases; the primary-, secondary- and tertiary stage. First the material immediately responds to the applied load by initiation of crack propagation, causing elastic strain (early primary stage) (Löw, 2013). As the rock “adjusts” to the stress, the crack propagation slows down, and the strain rate decelerates. Entering the secondary stage, the crack propagation reaches a stable almost constant rate during which the material slowly continues deforming. Tertiary stage initiates when the strain rate starts accelerating, and uncontrolled crack propagation continues until failure. Tertiary stage may be avoided with adequate support.

How long the creep process will last depends on the level of initial stress relative to the peak load of the rock mass. This can be described by the stress-strain curve, as shown in Fig.3.6. If the initial stress is close to the peak load, creep will terminate when accumulated stress is such as to intersect the falling part of the stress-strain curve (Goodman, 1989).

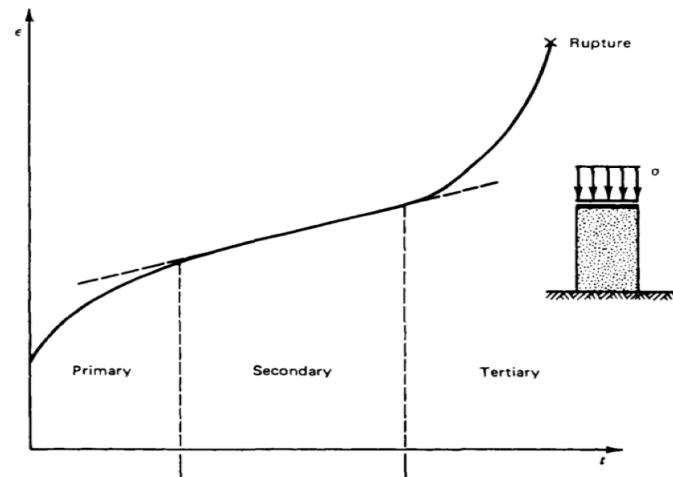


Figure 3.5.: Strain-time curve for creep, with the three characteristic stages (Goodman, 1989)

The G-U line marks the critical stress level. Above point G, crack propagation will accelerate into tertiary stage and terminate in rupture. This means that creep initiated at point A in Fig. 3.6 will terminate in failure at point B after a relatively short time. Creep starting in point C (initial stress further from peak load), will terminate in D after a much longer time than for A-B (Goodman, 1989). Creep initiated at point E below the critical stress level will approach point F, and stop at a finite strain level without rupture after a long time (Goodman, 1989). Point T marks the “creep threshold”, below which no creep will occur. The line T-U is the terminal locus for long-term creep tests (Shrestha, 2006). This illustrates how materials may creep to failure, even if it has not failed immediately after excavation.

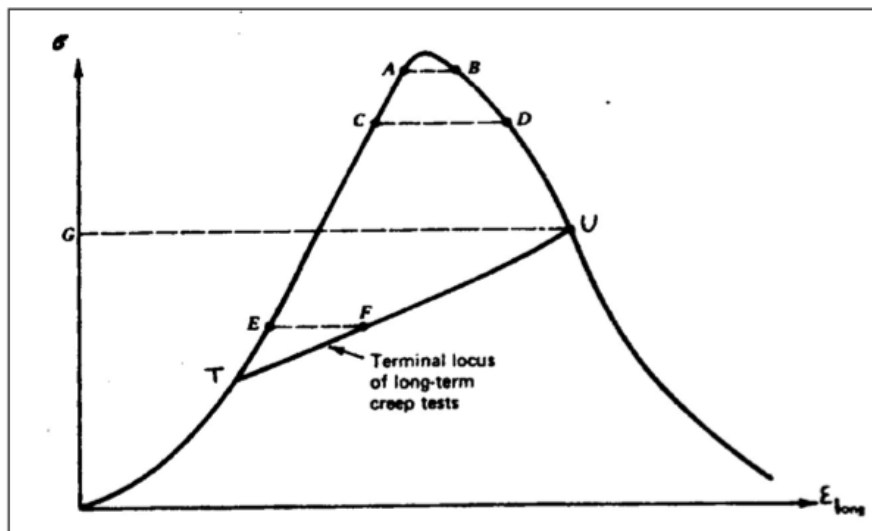


Figure 3.6.: Creep in relation to the complete stress-strain curve (Goodman, 1989)

3.3.3. Factors influencing squeezing

Squeezing ground conditions are influenced by several factors to different degrees. Many authors have analyzed case studies to identify the influencing factors, and have each presented their results differently (Steiner (2000, 1996); Panthi (2006); Shrestha and Panthi (2013); Kovári and Staus (1996); Aydan et al. (1996, 1993)). Shrestha (2006) gave the following summary of the factors influencing the occurrence and degree of squeezing:

- Stress conditions
- Strength and deformability of the rock mass
- Rock type
- Orientation of the geological structures
- Water pressure and porosity of the rock mass
- Construction procedures and support systems

The occurrence and degree of squeezing highly depend on the ratio between rock mass strength and in-situ stress. This means that for weak or strongly foliated (crushed) rocks, squeezing may occur even at low overburdens (low in-situ stress). At which ratio squeezing will occur is not defined, but a study on squeezing in tunnels in Japan showed that a ratio less than 2 resulted in squeezing (Aydan et al., 1996). According to Chapman, D., Metje, N. and Stärk, A. (2010) severe squeezing may occur when the uniaxial compressive strength (intact rock strength) of the rock is less than 30% of the in-situ stress.

The degree of squeezing depends on the rocks ability to deform; high deformability causes large deformation. Large long-term deformations or large long-term rock pressures is only possible in weak and deformable rocks (Shrestha, 2006).

Squeezing is typically seen in weak rocks like phyllite, shale, schist, claystone, mudstone, serpentine, flysh and weathered clayey and micaceous metamorphic rocks (Shrestha, 2006; Kovári and Staus, 1996). The presence and quality of minerals such as micas, chlorite, serpentine and clay is therefore particularly decisive (Kovári and Staus, 1996). According to Panthi (2013c) the high degree of schistosity (extent of thin foliation) in a rock is the dominating characteristic that leads to the formation of the visco-plastic zone around the opening. Accordingly, highly sheared material and fault gouge is especially prone to squeezing. Highly tectonized rocks lack sufficient bonding or confinement which results in a considerably reduced self-supporting capacity (Panthi, 2006).

Squeezing rock will also depend on the environmental conditions (alteration effects), rock durability (for example slaking of mudstone) and type of joint filling and gouge material (Shrestha, 2006).

The orientation of the rock foliation relative to the structure is critical for the degree of squeezing. As for all instability issues in tunneling, rock structures (e.g. foliation, fracture sets, fault zone) parallel to the tunnel alignment is the least preferable. According to Steiner (2000) substantially higher convergences, up to one order of magnitude greater, is observed where the foliation strikes parallel rather than perpendicular to the tunnel. For parallel structures also the dip relative to the opening is important. Overbreak due to buckling of schistose layers mainly occurs where the schistosity is parallel to the tunnel

perimeter (Shrestha, 2006). The different mechanical properties of joint structures and foliation may cause anisotropic closure of the excavation (Vu et al., 2013; Wang and Huang, 2014).

Porosity and ground water conditions may have a large influence on the degree of squeezing. High water pressures can cause significant reduction of the rock strength. For highly fractured rock, the water will reduce the rocks inner friction, and hence the shear strength of the rock (Nilsen and Broch, 2011). The water pressure may increase if there are confining materials (e.g. clay) in discontinuities in the vicinity of the tunnel (Shrestha, 2006). For porous rocks, high pore water pressure will reduce the strength of the rock. Draining the pores to reduce pore pressures may decrease squeezing over time. However, this will increase the empty pore volume of the rock, and high porosity rocks usually have low mechanical strength (Löw, 2013). Water present in faults and clay rich material may cause especially large convergences, and in extreme cases result in “flowing ground” (Shrestha and Panthi, 2013).

Finally, the choice of construction procedure and support measures may help reduce the extent of the deformation. Sequential excavation for large openings, or in extreme squeezing ground, is therefore often necessary. Methods may include heading and benching (Shrestha, 2006). Even if support is installed immediately after opening of the face, deformations behind the face may still continue (Shrestha and Panthi, 2013). Yielding support installed at the right time is therefore recommended to avoid destruction of the support. For extreme squeezing, it might be necessary to excavate a larger cross-sectional area, and let the rock deform for some time before the support is installed (Löw, S., 2013). If the installed support is able to provide sufficient loads, the inward displacement of the walls will decrease with time and approach an asymptote (not reach tertiary stage) (Goodman, 1989).

3.3.4. Time-dependency and the face-effect

In an advancing tunnel, the distance from the face will influence the behavior of the rock mass. According to Hoek (2007e) the radial displacement starts at about one half a tunnel diameter ahead of the advancing face (Fig. 3.7). The deformation reaches its final value about 1-1.5 tunnel diameters behind the face (according to Panthi (2006) maximum displacement occurs at approximately 2 diameters behind the face). This is because a part of the load that is redistributed around the opening is carried by the face itself (Carranza-Torres and Fairhurst, 2000). This phenomenon is referred to as the “face-effect”.

In a cavern with limited length, the face-effect will influence the deformation in the end-walls. The distribution of deformation is expected to have the same displacement profile as indicated in Fig. 3.7, with the least deformation close to the end-walls, and increasingly larger to finally reach maximum in the middle of the cavern.

This effect is important for understanding the principle behind the interaction between the installed support and the rock mass. If support is installed immediately behind the face, the support will not carry the full design load as some of the load is carried by the face itself. The effect of excavation progress and installation of support is further discussed in Sec. 5.3.1.

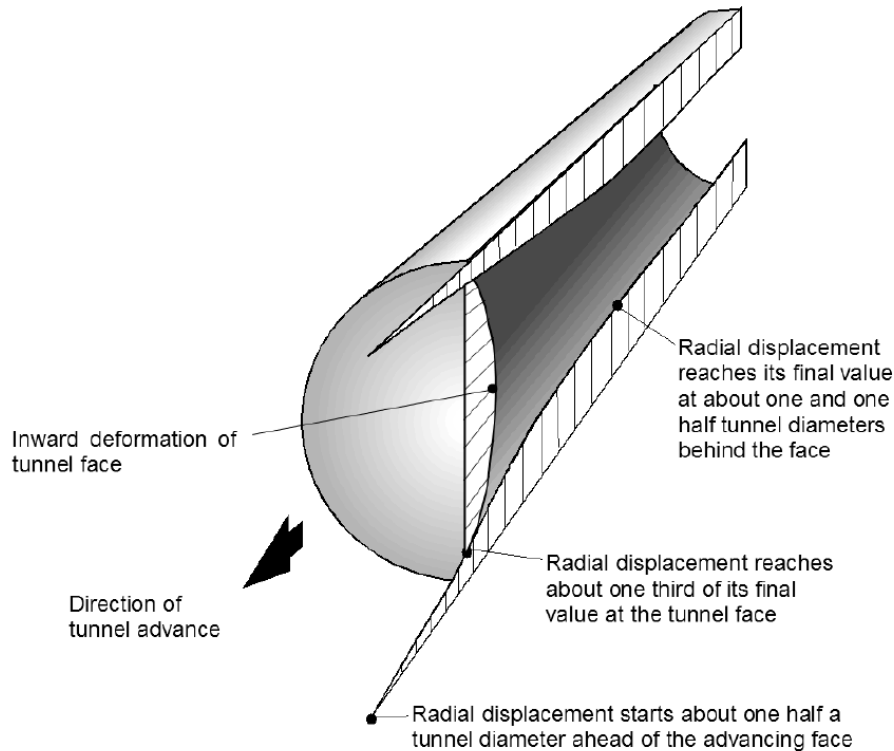


Figure 3.7.: Pattern of deformation in the rock mass surrounding an advancing tunnel (Hoek, 2007e)

3.4. CONSIDERATIONS FOR LARGE SCALE CAVERNS

Underground power stations require large openings, often with a span in order of 25 m. Both the geometry and the size of an excavation will highly influence its stability. In general, the deformations of an opening will increase with increasing width or radius of the opening (Palmström and Stille, 2010). Larger excavations will decrease the *in-situ* strength of the rock mass, since larger tunnels offer less confinement to the surrounding material (Goel et al., 1995; Palmström and Stille, 2010). This is why special considerations have to be made for the planning and design of large scale caverns. Based on the layout requirements, the orientation, size, and especially the shape, of the excavation have to be adjusted to fit the actual stability issues (Palmström and Stille, 2010).

For the design of an underground cavern, the general principle is a shape so that the compressive stresses are evenly distributed along the periphery of the opening (Nilsen and Broch, 2011). The underlying goal is to make sure there is enough confinement for the roof to be self-bearing; and in the same time not to cause high stress concentrations along points in the periphery which cause failure. This is best achieved by an arched roof, and by avoiding intruding corners and edges. If the distance between smooth bedding planes is less than 0.5 m, the roof should have a high arch (Nilsen and Thiedemann, 1993). Under high stresses, or highly anisotropic conditions, straight high walls should be avoided.

Hoek (2007a) performed numerical analysis to investigate the effect of three different

cavern shapes. The study was done for the design of the powerhouse cavern in the Mingtan project in Taiwan. The vertical stress in the cross-sectional plane of the cavern was 5 MPa, with a vertical to horizontal stress ratio $k=0.9$. Hoek (2007a) performed *Phase²* numerical analysis for three cavern shapes; (a) Mushroom shaped with a concrete arch, (b) conventional horseshoe, and (c) elliptical cavern designed for optimal stress distribution. The mushroom shaped cavern resulted in failure of the concrete arch, and the design was found not acceptable. The unsupported horseshoe shaped cavern, and the unsupported elliptical cavern, both resulted in failure in the roof and walls so that extensive support would be required. The elliptical shape would require less support than the horseshoe shaped, however not significantly different. The conventional horseshoe shape was chosen as the most appropriate cavern shape. This was believed to give the simplest construction procedure and the overall underground complex would be cheaper than involving an elliptical cavern (Hoek, 2007a).

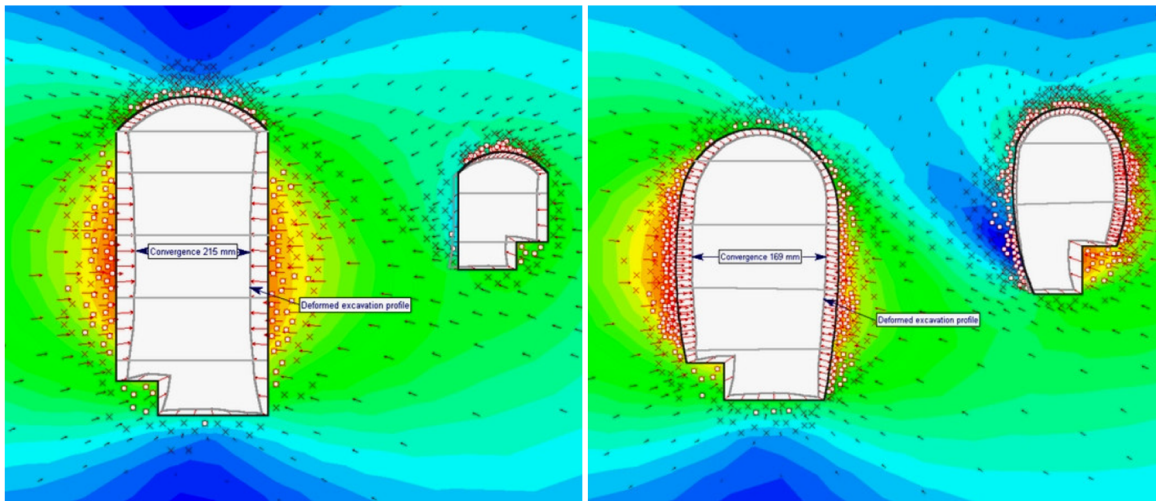


Figure 3.8.: Numerical stability analysis of horseshoe shaped cavern (left), and elliptically shaped caverns (right). (Hoek, 2007a)

For underground hydropower stations, an additional challenge will be adjacent openings mutually influencing each other. For larger projects the transformers are typically placed in a smaller cavern parallel to the power house, to reduce the size of the main cavern. The engineers have to weigh the cost between having a longer distance between the two caverns for better stability, versus a shorter distance to reduce the length and cost of the busbars (Hoek, 2000). In general there should be enough rock mass between the openings for the stresses to normalize. For squeezing ground it will be especially important that the plastic zones do not overlap, which in worst case may cause complete failure of the pillar. According to Hoek (2007a), a study was carried out to find the optimum pillar width between the transformer gallery and the machine hall. The results showed that the optimum pillar width is obtained when the distance between the two openings is approximately equal to the height of the larger of the two caverns. In very poor quality rock with larger overstressed zones, it may be advisable to increase the pillar width to 1.5 times the height of the larger cavern (Hoek, 2000). According to Hoek (2007b) this rule of thumb is generally applicable for all cavern designs in weak rock masses.

3.5. MEASURING AND MONITORING DEFORMATIONS

Besides visual inspection, deformation measurements are the most frequently used monitoring method. The deformation measurements can be carried out in different ways, and usually depend on the type of instability problems that should be monitored. The most common measuring variables include movements, rock stress/strain, and pressure/load or strain measurements (Panthi, 2013a). In principle, deformations can be measured at the excavation surface or inside the rock mass.

3.5.1. Convergence measurements

Convergence measurements are used for monitoring the deformations inside the opening. The measurements can give useful information about the loads transferred to the support, and in general indicate the behavior and stability of the rock mass. For best representation of the total deformation profile, it is important to have a sufficient number of installations placed so as to cover the roof and other critical parts of the cross-section (Fig. 3.9).

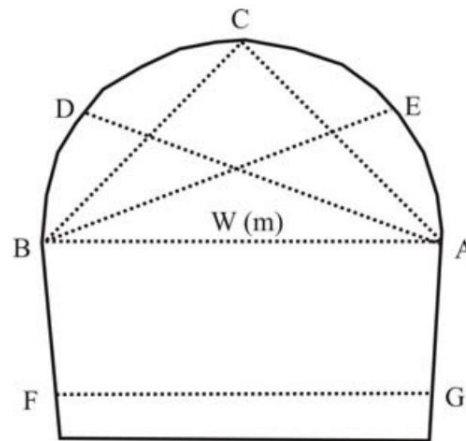


Figure 3.9.: Typical convergence monitoring program (Panthi, 2013a)

The simplest and least costly method for measuring convergence is the use of measuring tape, which measure the relative displacement between two points. However, this method will block the opening during the excavation. The results are only relative, and give no information about total deformation. This method is therefore not preferable for long term monitoring of instabilities. The use of theodolite is another fast and accurate method, which can have an accuracy of 1 mm per measurement. The system is computerized, and the absolute deformation may be established in relation to some fixed points. Normally, the same equipment used for setting the excavation alignment, and the boreholes for the blasting can be used (Palmström and Stille, 2010).

3.5.2. Extensometer measurements

Extensometers can be installed to measure the deformation inside the rock mass. In principal, an extensometer measures the distance from one or more installed anchors to a fixed head installed at the outer end of a borehole at the excavation surface. The measurement can be done mechanically with the aid of a dial gauge, or electronically using inductive transmitters, i.e swinging cord (linear variable differential transformer, LVDT)

(Palmström and Stille, 2010). The accuracy is $\pm 1-2$ mm for mechanical extensometers, and up to $\pm 0.1-0.5$ mm for electronic extensometers (Myrvang, 2001). The extensometer should be so long as to allow the inner anchor to be placed in rock that is not influenced by the excavation. This means that for plastic deformation the inner anchor should be placed outside the expected plastic radius.

3.5.3. Load cell and pressure cell measurements

Load cell and pressure cell measurements are installed on the support, and measure the load or pressure imposed on the support. Hydraulic load cells are typically used for monitoring of tiebacks, rock bolts and cables. They are basically a fluid-filled deformable chamber connected to a pressure gauge or electronic pressure transducer. By recording the change in pressure of the fluid in the pressure pad, the load can be determined (Nagaraj, 1993). Hydraulic load cells instruments typically consist of two ring-shaped stainless steel plates welded together around their circumference. The annular space between the plates is filled under vacuum with deaired oil (Sisgeo, 2014). Four or more strain gauge rosettes are bonded to the spool, and the pressure can be measure directly by a manometer connected to the cell body (DGSI, 2014; Sisgeo, 2014).

Radial total pressure cells (TPC) can be used for monitoring the pressure of the rock acting on the lining (between the rock and support interface). Radial TPCs are installed with its sensitive side to the rock, and are not completely embedded in the shotcrete. Tangential total pressure cells are installed with the sensitive side perpendicular to the rock surface, and measure the pressure within the tunnel lining. It is therefore completely embedded to the shotcrete. The device typically consists of two rounded steel plates with unequal thickness; the thicker side is for stabilization and the thinner side to minimize stiffness for the sensitive measuring side. The oil-filled space between the plates is connected via a pressure tube to a vibrating wire pressure sensor (DGSI, 2000).

3.5.4. Concluding remarks on deformation measurements

How the measured data is interpreted and applied depends on the type of instability one wish to monitor. In any case, it is very important to evaluate the data with respect to other factors. Most importantly the data should be matched to the excavation progress and other disturbances. For surface and close to surface excavations the data should be matched to weather data, especially large temperature changes and rainfall.

The advantage of extensometers compared to convergence measurements is that the approximate location of highest movement in the rock mass can be detected. This is especially useful for detecting shear movements along joints or faults inside the rock mass. This has proved especially useful for stability monitoring of deep seated rock instabilities, slope stability in natural slopes and quarry stability.

The installation for convergence measurements can only take place after the excavation. Depending on the time of installation and rate of deformation, an unknown amount of deformation will already have occurred in the rock mass and will be omitted from the measurements. The same applies to extensometers drilled in the cavern rock. The deformation before excavation can be monitored by installing extensometers from an outside surface, with the inner anchor as close to the actual work face as possible without being destroyed by the immediate blasting (Palmström and Stille, 2010).

4. THE CASE: NEELUM JHELUM HPP, PAKISTAN

The selected case study for the thesis is the Neelum Jhelum Hydropower Project, located in northern Pakistan. The project was selected in cooperation with Multiconsult AS (Norplan AS). Challenges due to squeezing deformation were experienced while excavating the powerhouse cavern and busbar tunnels. The deformations were monitored with convergence meters and multipoint extensometers, 31 measuring stations in total for the powerhouse cavern. Geologic data and deformation measurements were made available for the study, and form the basis for the analysis.

4.1. PROJECT DESCRIPTION

4.1.1. General

Neelum Jhelum Hydropower Project (NJHPP) is a massive run-of-the-river project located in the northern part of Pakistan. The scheme is designed to divert water from the dam site by the Neelum River, to the underground power station by the Jhelum River. Installed capacity will be 969MW, with an annual production of 5.15 billion units of electricity (WAPDA, 2013).

The project is owned and constructed under the supervision of the Pakistani Water and Power Development Authority (WAPDA). The project was initially approved in 1989 with intended construction start in 2002. During the early 1990s the project was reevaluated for major capacity improvements, and the construction start had to be postponed. In 2005 a devastating earthquake occurred near Muzzafarabad, which caused further delays for the construction works (WAPDA, 2013).

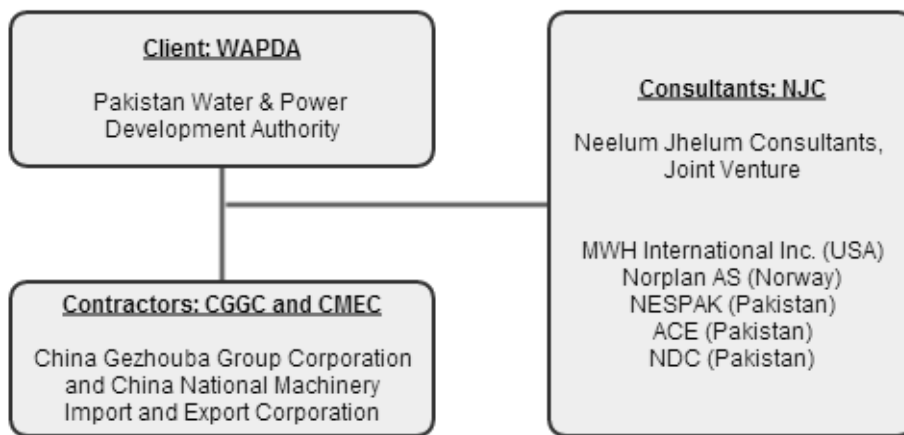


Figure 4.1.: Neelum Jhelum HPP organization

In 2008 WAPDA appointed Neelum Jhelum Consultants (NJC) to perform design review and the engineering supervision of the construction works. NJC is a joint venture between 5 companies; MWH International Inc. (USA), Norplan A.S. (Norway), National Engineering Services Pakistan Pvt. Limited (NESPAC), Associated Consulting Engineers Pvt. Limited (ACE, Pakistan) and National Development Consultants of Pakistan (NDC). The construction work is carried out by two Chinese construction companies, CGGC and

CMEC. Constructions finally began in January 2008 and are expected to be finalized during November 2016.

Information about the project was supplied by Norplan AS. The following documents were made available:

- “NJHPP: Rock Parameters NJHPP Final Draft”, NJC (2011)
- “Memo: Simulation of the crane level displacement during the excavation”, Norplan A/S (2013)
- Geologic plan and section from surface mapping, NJC (2012)
- Geologic long wall mapping of the powerhouse, NJC (2011)
- Convergence and extensometer measurements from the powerhouse cavern and busbar tunnels, NJC (2013)
- Technical drawings of the powerhouse complex, NJC (2009-2011)

Information was additionally received through conversations and e-mails with employees at Norplan A/S.

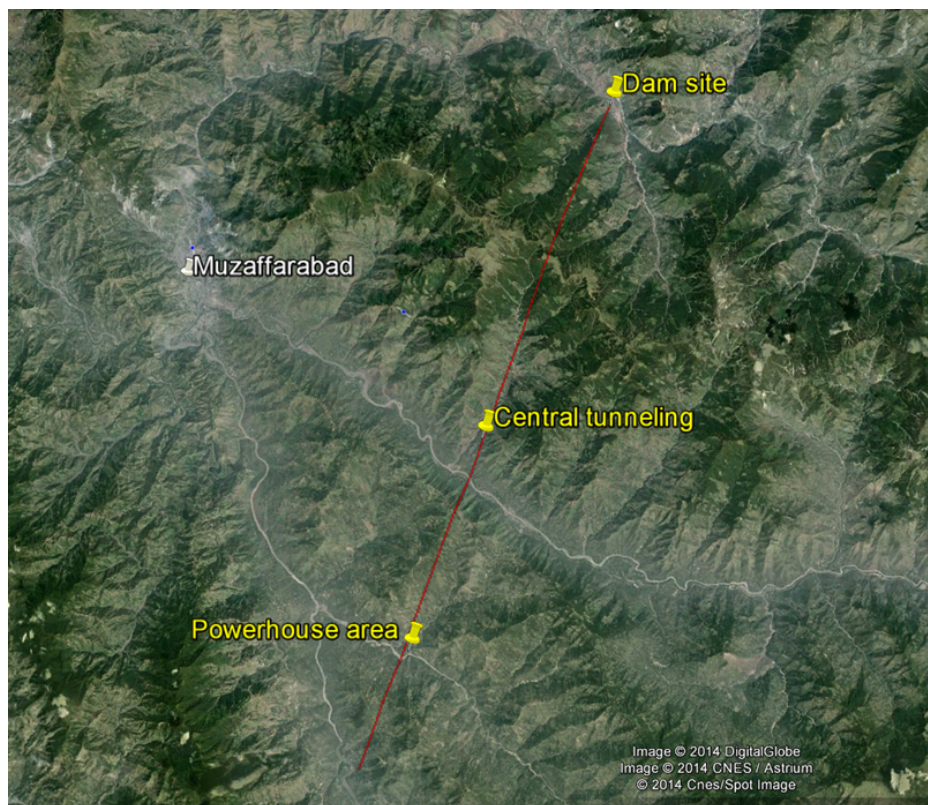


Figure 4.2.: Google earth image of project area

4.1.2. Project location

NJHPP lies by the town of Muzaffarabad, within the Kashmir region in the northern part of Pakistan (Fig.4.3). The area extends from the dam site located by Nauseri on the Neelum River (41 km east of Muzaffarabad), to the powerhouse in Azad Kashmir 22 km

4.1 PROJECT DESCRIPTION

south of Muzaffarabad. From the powerhouse the water will be discharged through the tailrace tunnel into the Jhelum River, about 4 km south of Chatter Kalas.

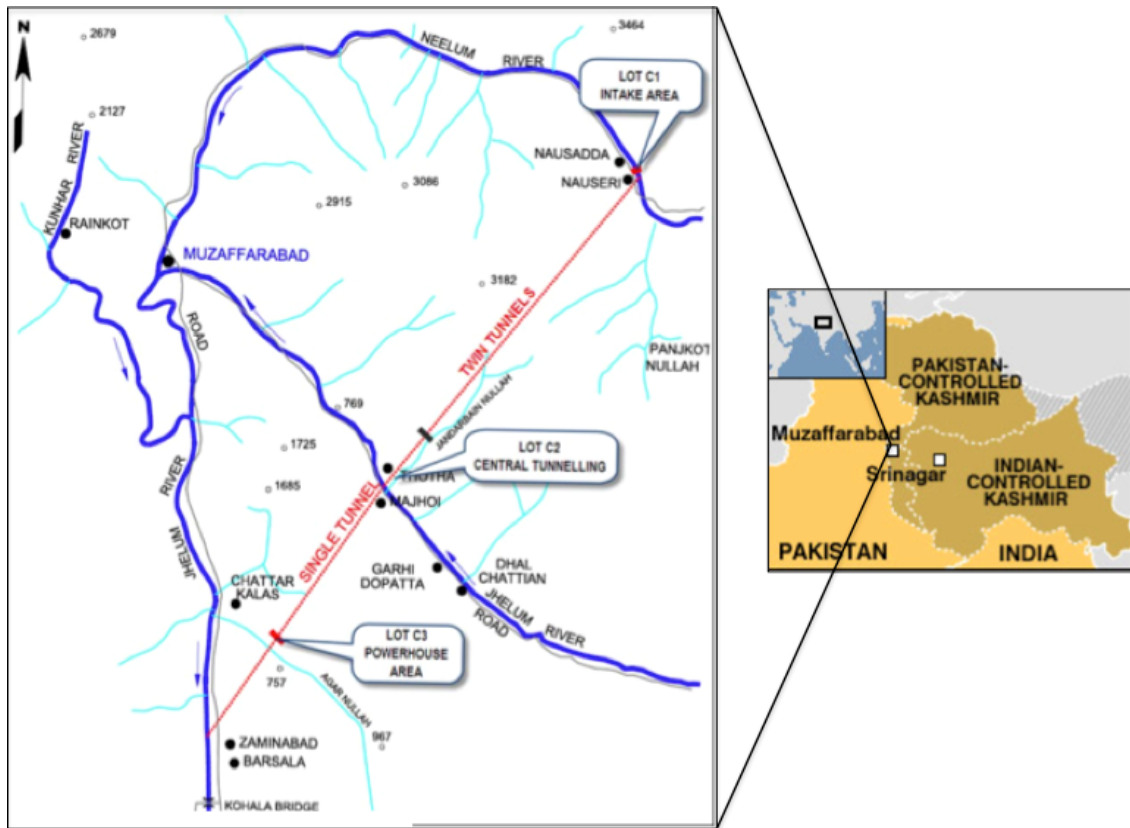


Figure 4.3.: Project location

4.1.3. Project layout features

The project area is divided into three main project sites: *Nauseri area (C1)*, *Majhoi/Thota area (C2)* and *Chatter Kalas area (C3)* (Fig.4.4). In total the project includes about 67.7 km of tunneling, where 46.1 km are excavated per December 2013, equal to 67.8% (WAPDA, 2013).

Nauseri area - Lot C1 - Intake area

The intake area is located at the Neelum river, close to the town of Nauseri. The Neelum-Jhelum dam is a 160 m long and 60 m high composite gravity dam. The gate diversion dam has 3 No. Radial gates and 2 No. Flap gates, designed to pass floods of a 1000 year recurrence period. The dam will create a head pond of 10 million cubic meters which allows for a peak reservoir volume of 3.8 million cubic meters. The area includes a six gate tunnel intake structure of 280 cumecs (m^3/s) capacity, which is connected to three conventional flushing surface basins. C1 also include the first 7.4 km of the single headrace tunnel, excavated with drill and blast. (WAPDA, 2013).

Majhoi/Thota area - Lot C2 - Central tunneling

The C2 area include most of the ~48 km long headrace tunnel, assemble- and disassemble chamber for TBM and 8 construction adit tunnels. A 19.54 km stretch of the tunnel from

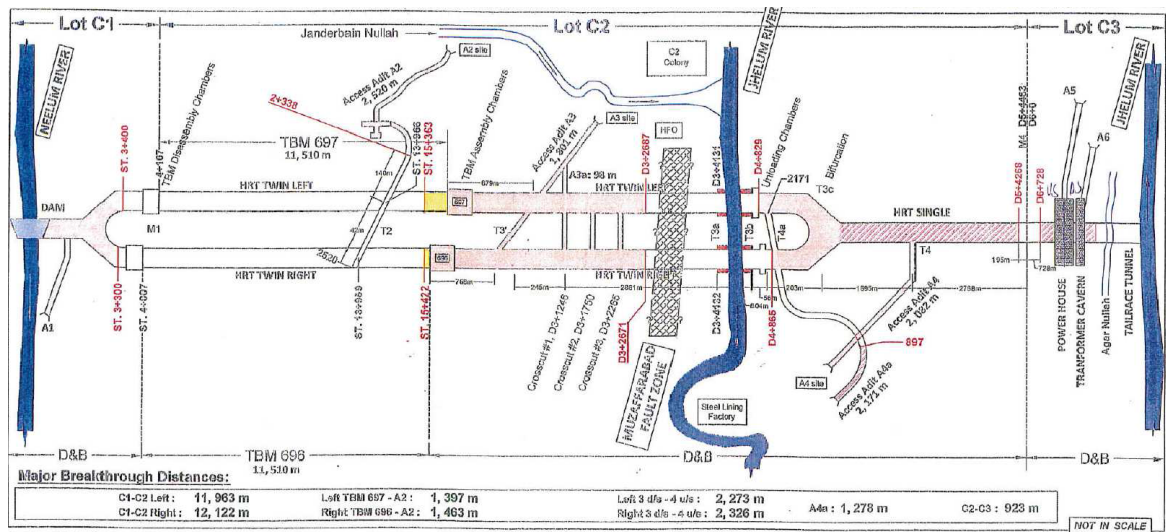


Figure 4.4.: Project layout features (not in scale) (Norplan A/S, 2013a)

the Nauseri site is constructed as a twin tunnel system. Due to high overburdens and weak rocks, two tunnels with smaller cross-sectional area (52-58 m²) were believed to create better stability (Norplan A/S, 2013b). The remaining headrace tunnel down to the surge chamber is a single tunnel with approximately 100 m² cross-sectional area. 11.5 km long sections of the twin tunnels are excavated with TBM, and are shotcrete lined with a concrete invert. The sections excavated by drill and blast are full face concrete lined. The headrace tunnel crosses under the Jhelum river at el. 602 m asl, approximately 180 m below the riverbed. The tunnel section below the Jhelum river, as well as the section crossing the Muzzafarabad fault, will be steel lined. (Norplan A/S, 2013b).

Chatter Kalas area - Lot C3 - Powerhouse area

Powerhouse area, including transformer hall, surge shaft, penstock/draft tube/busbar tunnels (4 of each), tailrace tunnel, access tunnels and other housing facilities for operation and maintenance. The headrace tunnel will feed four vertical shaft Francis turbines, with an installed capacity of 969 MW. The water will be discharged into the Neelum river, near Zamainabad through a 3.54 km long tailrace tunnel. (WAPDA, 2013).

4.1.4. Powerhouse complex design

The general layout of the powerhouse area is displayed in Fig. 4.5. It's a complex network of tunnels and larger caverns being excavated, with a mean overburden of about 530 m above the powerhouse complex. The approximate dimensions of the powerhouse cavern and transformer hall is shown in Fig. 4.6. The length of the powerhouse cavern is about 137 m.

4 bonneted gate niches are constructed in the downstream wall of the powerhouse cavern, with connection to the draft tube tunnels and busbar tunnels. The top level of the niche is at el. 601.95 m, bench level at el. 592.6 m and the bottom level is at el. 569.98 m. The design of the niches was changed from the original design. The lower halves of the niches were rotated 30 degrees, and buttresses were included for better stability (Norplan A/S, 2013b).

size and correct time progress of the excavation is not known for this study. However, it is known that the excavation had a temporary hold up from summer 2012 until early winter 2013, when the excavation was at el. 593 m. The excavation was stopped due to the bonneted gate niches (Norplan A/S, 2013a). The excavation of the main cavern was completed with the final blast in the floor on the 11th of November 2013. The 5-10 bottom meters of the two middle niches were still not excavated per December 2013.

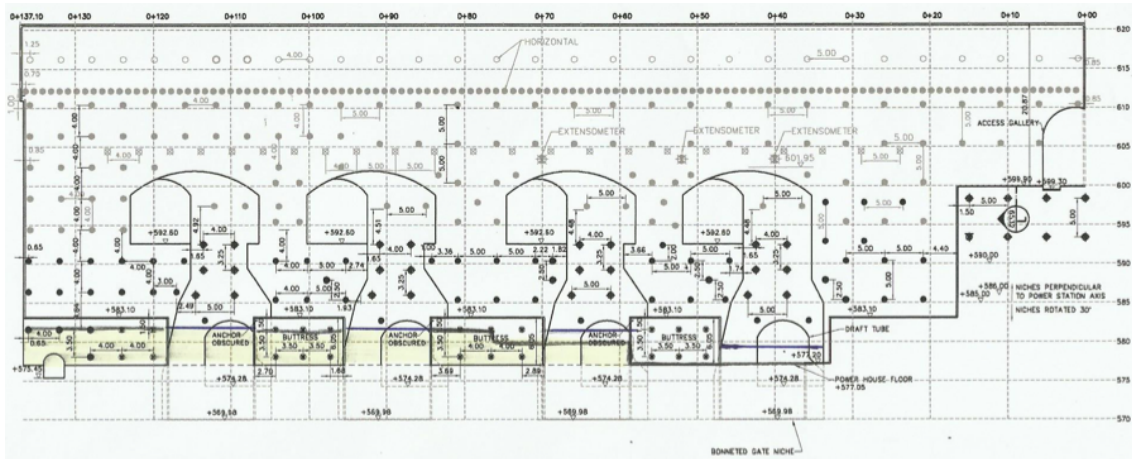


Figure 4.7.: Downstream wall of powerhouse cavern (NJC, 2013b)

4.2. GEOLOGICAL AND ENGINEERING GEOLOGICAL CONDITIONS

4.2.1. Regional geology

Northern Pakistan lies within the western region of the Himalaya mountain range. O'Brian (2001) made an important effort in summarizing the sequence of the Himalayan formation (Panthi, 2006). According to O'Brian (2001), the Himalayas are a result of the collision between the major lithospheric plates (Indian plate and the Asian plate) as well as the intervening microplates and arch units from the late Mesozoic time until today (about 50 Ma). O'Brian (2001) further explained how the northern boundary of the Himalaya is comprised of a series of continental blocks that accreted to the Asian margin during Paleozoic and Mesozoic time, each showing ophiolitic sutures along its boundaries. The most important with respect to the Himalaya evolution is the Lhasa block. During Jurassic time it collided with the northern Qiangtang block along the Bangong structure. At the end of Cretaceous, the oceanic island arc Kohistan-Ladakh collided with the Asia plate, and is now found in the northwest Himalaya (Fig.4.8). (O'Brian, 2001).

According to Panthi (2006), the continental collision has caused crustal imbrications, staking and under-thrusting of the Indian plate beneath the southern Asian margin. The collision also caused strike-slip movements along faults well away from the collision zone in northern Tibet and Southeast Asia. As a result of the compressional and extensional faulting, the Himalayas are comprised of several litho-tectonic units with a general northwest-southeast trend. As shown in Fig.4.9, from south to north, the Himalayas can be subdivided into five major tectonic subdivisions; the Gangetic plate (Terai), the Siwaliks zone, the lesser Himalayan zone, the higher Himalayan zone and the Tibetan-Tethys

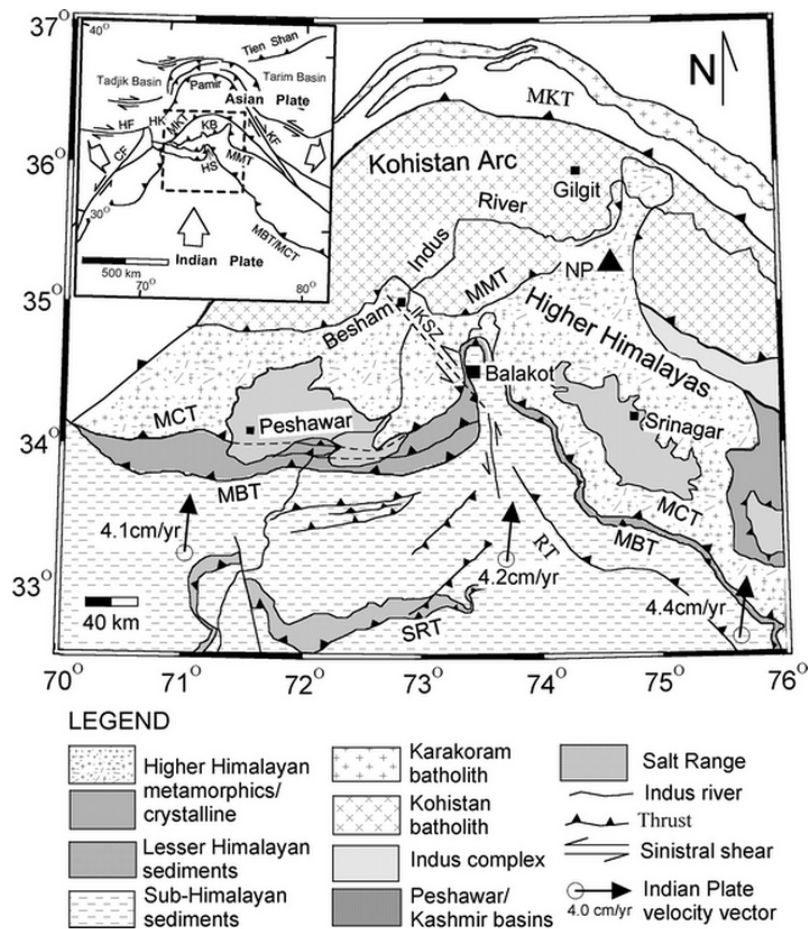


Figure 4.8.: Regional tectonic map of North Pakistan and adjoining areas. NJHPP lies right south of Balakot (Khan et al., 2010)

zone. These tectonic zones are characterized by special lithology, tectonics, geological structures and geologic history. The major geologic units in each tectonic subdivision is summarized in Tab.4.1.

4.2.2. Geologic and tectonic conditions in the project area

The Neelum Jhelum project is located in the western lower part of the Himalayas (Sub Himalayan), mainly in the Siwalik and lower part of the lesser Himalayan zone. The geologic units found in the project area are mainly molassic sedimentary rocks of the Murree formation, of Paleocene to Mid-Eocene age (NJC, 2011a).

The project area extends through the Hazara Kashmir Syntaxis, an area defined within an almost 180 degree Northwest trending bend of the Main Boundary Thrust (MBT), as shown in Fig.4.10 (the Murree fault is the MBT). The MBT is one of the major thrust zones of the Himalayas, separating the older formations of the Lesser Himalayan zone from the younger Siwalik and Terai formations. The Panjal thrust running almost parallel to the MBT is considered to be the basal sliding plane of a larger Kashmir nappe (Calkins et al., 1975). Stratigraphically, the syntaxis contains the youngest rocks of the Murree formation in its core (axial core), and successively older rocks wrap around the periphery.

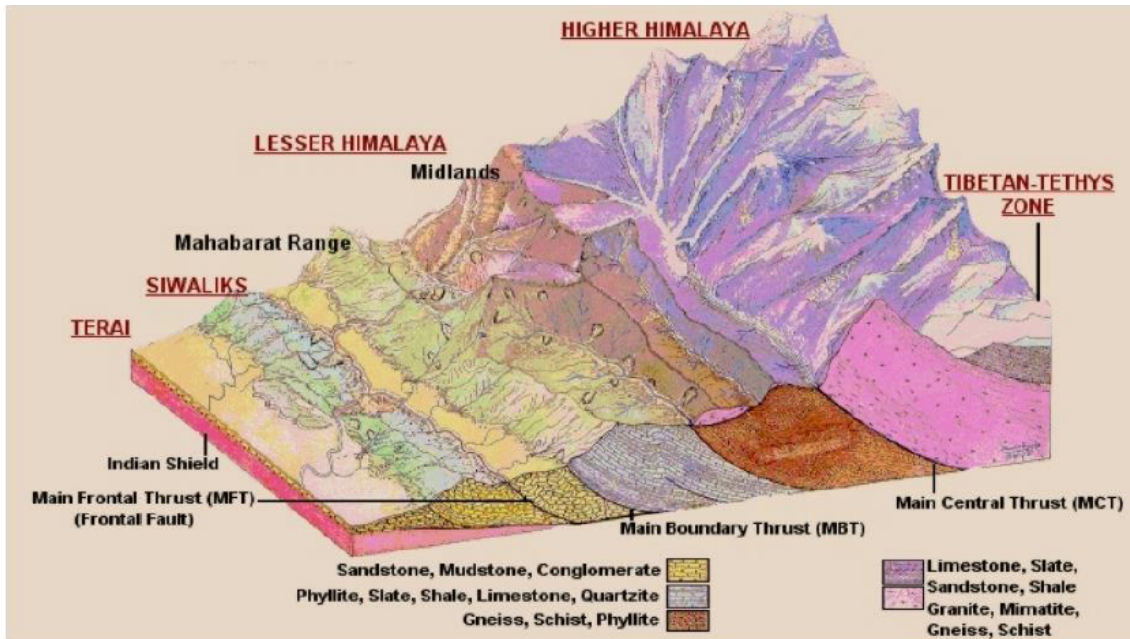


Figure 4.9.: Block diagram of the Himalaya giving different litho-tectonic units (De-oja et al., 1991)

Table 4.1.: Type of Himalayan rocks and their geomorphic units (Panthi, 2006)

Geomorphic Units	Width (km)	Altitude (m)	Main Rock Types	Age
Gangetic plane and inner Terai valleys	20-50	100-200	Alluvial deposits, coarse gravel at the foot of the Siwaliks mountain.	Recent
Siwaliks zone	15-30	200-1,000	Sandstone, mudstone, siltstone, shale, conglomerates etc.	Mid-Miocene to Pleistocene
Lesser Himalayan zone	70-165	200*-5,000	Shale, slate, phyllite, limestone, dolomite, marble, schist, quartzite, gneiss and granite.	Precambrian to Mesozoic
Higher Himalayan zone	10-60	>5,000	Gneiss, schist, marble, granite, quartzite, amphibole etc.	Precambrian
Tibetan-Tethys zone	-----	>2,500	Gneissic schist, marble, shale, slate, limestone, sandstone etc.	Late Proterozoic to early Cambrian

* In the lesser Himalayan valleys the elevation ranges from 200 to 2000 meters.

The Neelum Jhelum dam is located on the MBT itself, with the left embankment in the Murree formation and the right in the igneometamorphic Panjal formation. From there the headrace tunnel follows a Southeast direction through the Murree formation, crossing the active Muzaffarabad Fault (MF). Continuing to the powerhouse cavern, the MBT is

4.2 GEOLOGICAL AND ENGINEERING GEOLOGICAL CONDITIONS

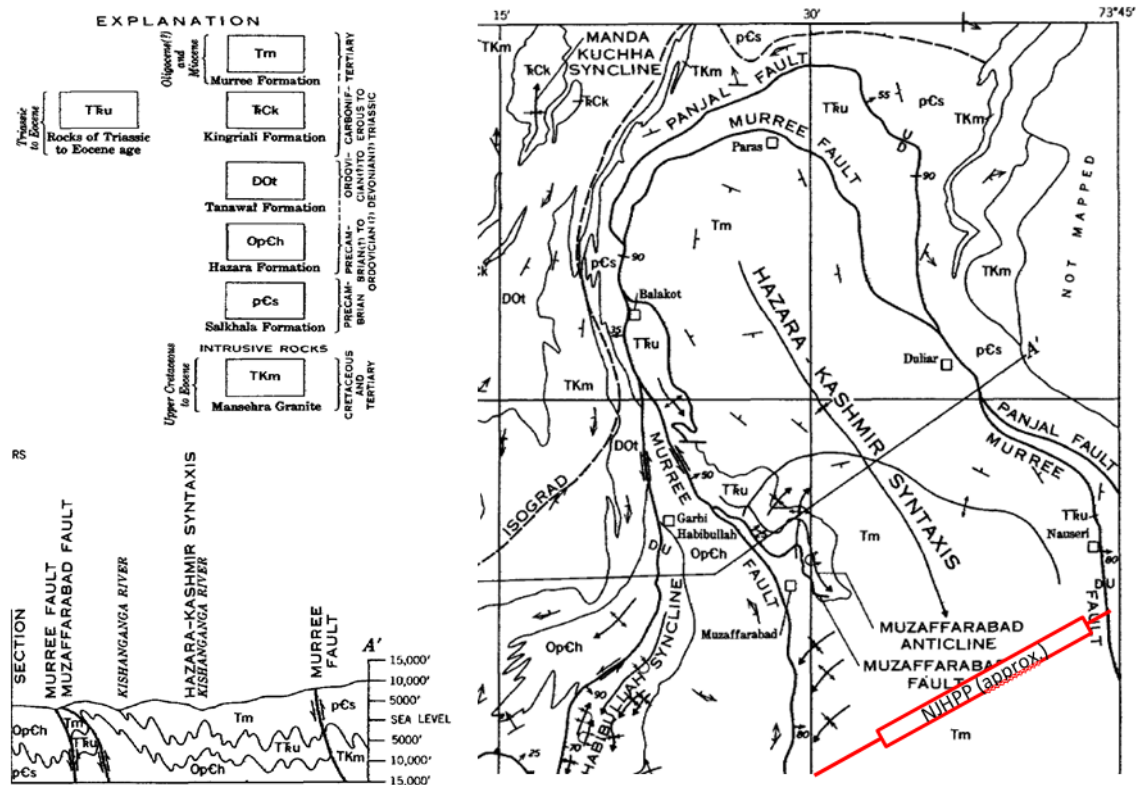


Figure 4.10.: The Hazara-Kashmir syntaxis. The Murre fault is also known as the Main Boundary Thrust. Modified from Calkins et al. (1975)

encountered once more close to the Jhelum river, on the opposite margin of the Hazara Kashmir Syntaxis (NJC, 2011a). In October 2005, there was a 7.5 magnitude earthquake, accompanied by rupture along the NW-SE trending Muzaffarabad fault. The surface average displacement was at 4 m, and caused the lives of 87,000 people and millions became homeless (Khan et al., 2010).

The Murree formation is comprised of strong grayish sandstone with layers of reddish brown sandstone, siltstone, mudstone and shale (NJC, 2011a). The formation shows a high degree of compression in the form of tight folding with repeated faulting and fractures. Open folds have been weathered into steep ridges and valleys.

4.2.3. Geological investigations

Norplan AS, the source to information about NJHPP, entered the project in the late stages. Therefore little information about the preliminary and first design phase investigations was made available for this study. NJC have produced one report with the combined results of 3 testing programs; the first conducted at the feasibility/detailed design stage (1997), the second after construction commenced (2009-2010) and the third which was being completed when the report was written in 2011. The third program was initiated to investigate siltstones and mudstones, which had been under-represented in previous investigations. The third testing program consisted of samples from short dedicated boreholes in C3 tunnels (cable tunnel, manifold tunnel, drainage gallery, probe tunnel and access tunnel) and C2 tunnels (Adit 2, 3 and 4). (NJC, 2011a).

The majority of the tests were performed by WAPDA's Central Materials Testing Laboratory, with very limited supervision from NJC staff. According to NJC (2011a) some unexpected results were obtained. The details for these are unknown. The report made by NJC form the basis for the geological and engineering geological conditions presented in this study, along with geological profiles of the project area and geological long wall mapping of the powerhouse cavern.

4.2.4. Rock units classified in the project area

During preface and detail design stage it was assumed monotonous series of alternating beds of shales and sandstones. After construction commenced it was observed that interbedded siltstones and mudstones appear far more frequently than shale at all three construction sites (C1, C2 and C3)(NJC, 2011a). The later revision therefore classified the appearing rocks into 5 units as given in Tab.4.2. All units seem to have a calcareous content, with calcite occurring both in matrix and as grains (NJC, 2011a).

Table 4.2.: Rock units classified in the project area. Summarized from NJC (2011a)

Rock Unit	Descriptive comment
Sandstone (SS-1)	(Very) strong, gray color, sharp non-gradational bedding contact to other units.
Sandstone (SS-2)	Reddish brown, strong-medium strong. SS-2 Sandstone-siltstone-mudstone occur in a continuous downward-fining sequence. Sand and silt size material frequently varying, making distinction between silty sandstone and sandy siltstone difficult.
Siltstone	Reddish brown. Strong-medium strong. Occurring as described above.
Mudstone	Reddish brown. Strong-medium strong. Occurring as described above.
Shale	Rare, found interlayered with SS-2 mostly and occasionally SS-1. Weak-medium strong.

4.2.5. Geology along the headrace tunnel

The topography and geology vary greatly along the headrace tunnel. Of the about 20 km stretch from the intake site to the Jhelum River crossing, about 80% of the tunnel is located below 500 m overburden. About 40% have more than 1000 m overburden and about 15% more than 1500 m overburden (Fig.4.11). For the 10 km between Jhelum River and the powerhouse, about 80% have an overburden more than 500 m.

The geology along the headrace tunnel is dominated by SS-1 and SS-2 sandstone, with varying thickness of intersecting layers of shale, siltstone and some mudstone (Norplan A/S, 2014). Based on surface mapping, the last 7-8 km down to the Jhelum River crossing are assumed to be highly tectonized and sheared. According to the excavation progress

4.2 GEOLOGICAL AND ENGINEERING GEOLOGICAL CONDITIONS

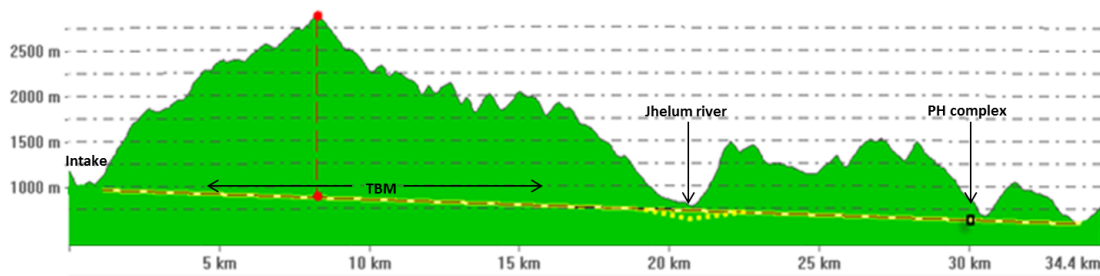


Figure 4.11.: Profile along headrace tunnel

updated 21.04.14, few of the surface mapped shear zones reached down to the tunnel alignment, as shown in Fig.4.12 (Norplan A/S, 2013b).

The three major concerns for the headrace tunnel are:

- High overburden combined with sectionally highly jointed and sheared rock, with special reference to sections excavated by TBM.
- Crossing of the Muzaffarabad fault zone. Estimated thickness of the weakness zone is 1 km.
- Crossing with the headrace tunnel under the Jhelum river with a water pressure of 410 m, about 180 m below the riverbed.

Unfortunately no more details about the geologic conditions for the headrace tunnel were made available for the study.

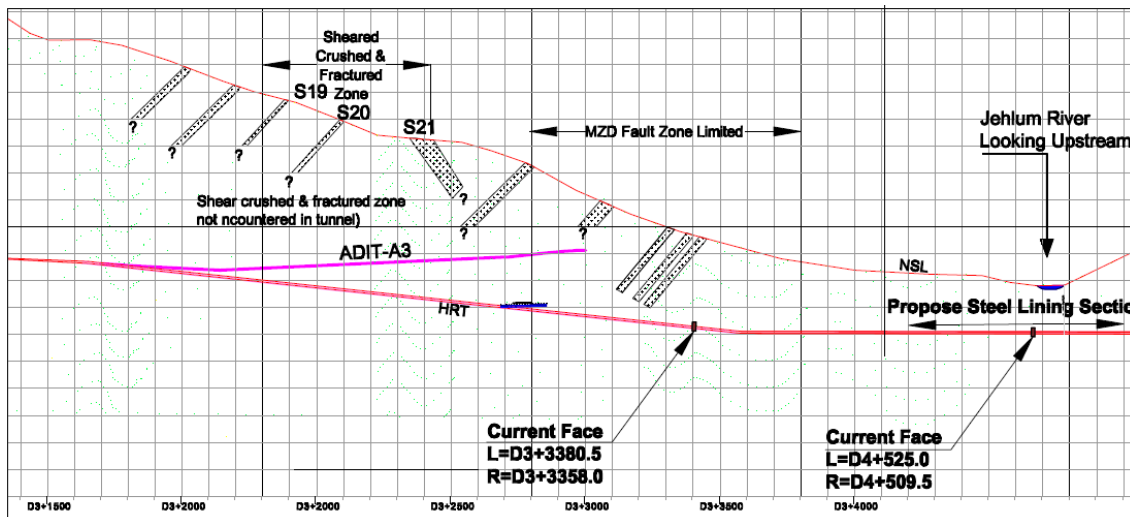


Figure 4.12.: Face location at Muzaffarabad fault and Jhelum crossing

4.2.6. Geology of the powerhouse complex

Layered SS-1 sandstone, siltstone and mudstone have been encountered in the powerhouse cavern. Some SS-2 sandstone was encountered in the access tunnels above the

powerhouse. Fig.4.13 shows the occurrence of the geologic units in the powerhouse cavern. The west-end of the cavern is mostly excavated in fractured sandstone, with increasing occurrence of siltstone and mudstone towards the east-end of the cavern. Geologists investigating the cavern during constructions described the mudstone as distinctly different from siltstone in the appearance of color and degree of shearing (Norplan A/S, 2013b). The blue lines in Fig.4.13 mark the crane beam level of the cavern. The dip direction/dip angle of the bedding is around 050-065/45-60. The possible shear zone in the middle west-end has a dip direction/dip angle of about 040-050/45-60 (Norplan A/S, 2013b).

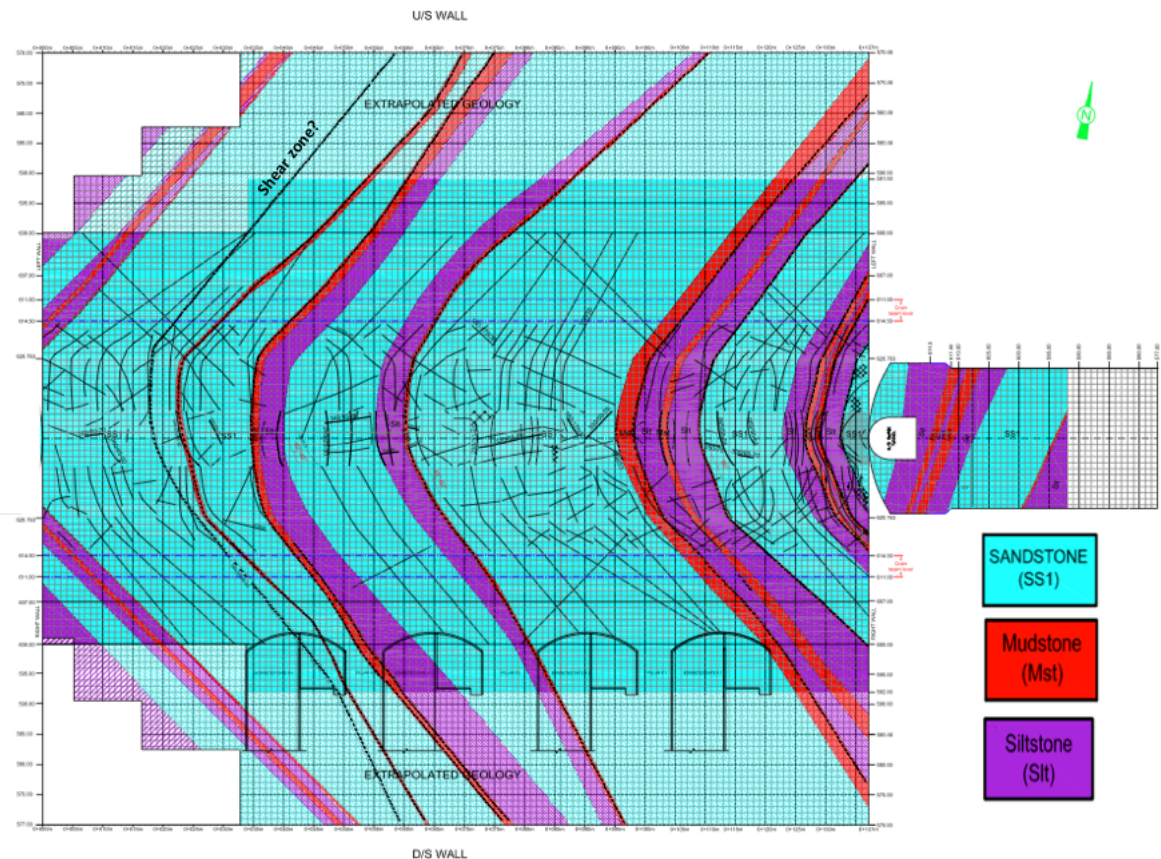


Figure 4.13.: Geological long wall mapping of the powerhouse cavern (NJC, 2011b)

4.3. ROCK MASS CONDITIONS OF THE POWERHOUSE COMPLEX

4.3.1. Intact rock properties

Based on the report by NJC (2011a) a summary of the intact rock properties are given in Tab.4.3. The SS-1 sandstone can be described as a high strength rock, and as average strong sandstone (SINTEF, 2013; Nilsen and Palmström, 2000). The elastic modulus and modulus ratio are in the typical interval for sandstone (Nilsen and Palmström, 2000).

The results for sandstone and mudstone show to be less consistent compared to reported values in literature (BGS, 2002; Nilsen and Palmström, 2000; Dwivedi et al., 2006). The strength values for siltstone are somewhat lower than what is typical for siltstone. For

4.3 ROCK MASS CONDITIONS OF THE POWERHOUSE COMPLEX

mudstone the strength is found to be much higher than what is referenced in the literature. The laboratory report comments that the results for mudstone are highly uncertain, and more tests are to be carried out. Additionally, the mudstone is highly sheared so finding good samples representing intact rock was challenging (NJC, 2011a). Given that the siltstone and mudstone may appear as a downward fining sequence, the distinction between each unit may be difficult.

Table 4.3.: Summary of intact rock properties from laboratory testing

Intact Rock Parameter		Rock Unit		
		SS-1	Siltstone	Mudstone
Specific gravity (Gs)	Average	2.73	2.8	2.703
UCS (MPa)	Average	86	66	42
	St.dev	36.14	24.62	22.67
	95% C.I	75.55 - 97.16	55.41 - 76.99	34.66 - 49.53
Tensile Strength (MPa)	Average	7.72	6.93	5.24
	Range	2.7-8.95	4.68-6.8	5.27 - 8.22
Elastic Modulus (GPa)	Average	58.1	40.6	27.4
	St.dev	21.17	13.0	14.54
	95% C.I	33.52 - 62.32	22.87 - 45.43	17.34 - 37.49
Poisson's ratio	Mean	0.27	-	0.21
Cohesion (MPa)	Average	6.02	8.91	5.87
	St.dev	1,68	9,23	-
	95% C.I	4.76 - 7.02	0.10 - 16.29	-
Friction angle (deg)	Mean	45.98	54.31	33.33
	St.dev	3.56	14.49	-
	95% C.I.	41 - 50	41.60 - 67.01	-

Slake durability test for siltstone and mudstone have been performed. In general, both rocks showed high percentage of durability against slaking. The single lowest value appeared for sheared mudstone (37.7%). Mudstone samples with the same petrographic composition showed inconsistent results, which indicate that the shearing of the mudstone is the main feature contributing to its behavior. During construction of the adit tunnels, slaking of sheared mudstone have been observed where it was encountered with water, and showed maximum convergence in comparison to other rock types. (NJC, 2011a).

4.3.2. Discontinuities

The majority of observed joints follow the direction of the bedding (black lines in Fig.4.13). Additionally there looks to be 2 more fracture sets, in an oblique angle to each other and the bedding. From the 4 cores taken in the powerhouse surface area the joints have been described as mostly planar, rough and weathered (NJC, 2011a). A thin possible shear

zone is observed in the west-end of the cavern. Observation of cross-going cracks in the shotcrete indicate that there are some shear movement along this zone. Dripping water around this zone has also been observed, indicating an open, connected water bearing fracture (Norplan A/S, 2013b).

4.3.3. Rock mass properties

NJC (2001) performed rock mass analysis using Roc-Lab, based on the latest borehole cores (from C3 and C2). Their recommended rock mass parameters are shown in Tab.4.4.

Table 4.4.: Estimation of rock properties with Roc-Lab

Parameter	Rock type		
	Sandstone SS-1	Siltstone	Mudstone
GSI	65	50	50
m_i	17	7	9

The material constant m_i were quoted form the Roc-Lab database (see App. A.1)(NJC, 2011a). GSI values were calculated using Q-values evaluated during face mapping. The following relationship between GSI and Q was used for the conversion:

$$GSI = 9 \ln Q + 44 \quad (4.1)$$

4.3.4. Rock mass classification

The rock mass have been classified according to the Q-system, both from rock cores and during construction (NJC, 2011a). The RQD distribution from core drilling are shown in App. E.1, where core nr. 9-12 are from the powerhouse area.

Estimated Q-values have been recorded by site personnel, but are only available as intervals for the sections where the deformations are recorded (Tab.4.5). Using the given GSI values, and calculating back with Eq. 4.1 gave a Q-value of 10.3 for sandstone, and 1.95 for siltstone and sandstone.

Table 4.5.: Rock mass classification per chainage (NJC, 2011a)

Chainage	Rock mass classification	Q-value interval	Class
0+015	Q2/Q3	4 – 40	Fair - Good
0+031	Q2/Q3	4 – 40	Fair - Good
0+050	Q2/Q3	4 – 40	Fair - Good
0+065	Q3/Q4	0.1 – 10	Very poor - Fair
0+078	Q3	4 – 10	Fair
0+085	Q3/Q4	0.1 – 10	Very poor - Fair
0+096.8	Q3	4 – 10	Fair
0+103	Q3/Q4	0.1 – 10	Very poor - Fair
0+110.5	Q3	4 – 10	Fair
0+127.8	Q3	4 – 10	Fair

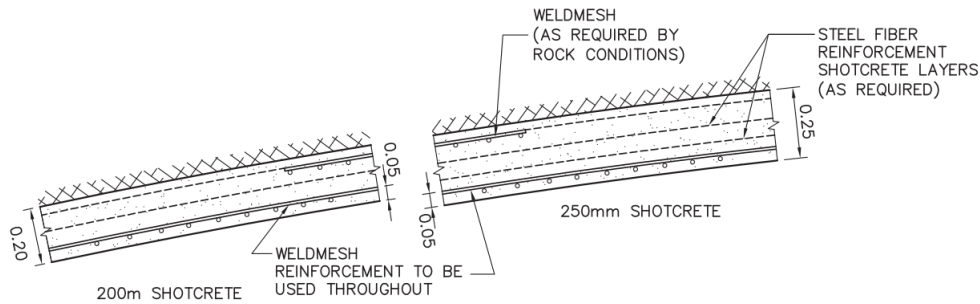


Figure 4.15.: Shotcrete support. From NJC (2011b)

angle from horizontal. The installation angle was decided based on numerical simulations showing this gave better stability with regard to the given bedding (Norplan A/S, 2013b). In the downstream wall (right side in Fig.4.14) the anchors were installed horizontally above the gate niches and busbar tunnel, and staggered 2 m with respect to the above installed 15 m anchors to avoid conflict (NJC, 2011b). Installed support is summarized in Tab.4.6, with notation as in Fig.4.14.

Table 4.6.: Summary of installed support

Support type	Description
Strand anchors, L=15m	Crown: Spacing 4×4m. Zone A: 5×5m grid, initially pretensioned to 30t. Zone B: 4×4m grid, initially pretensioned to 10t
Strand anchors, L=10m	Crown: Spacing 4×4m. Zone A: 5m×5m grid, initially pretensioned to 15t. Zone B: 4m×4m grid, initially pretensioned to 5t
Rock bolts, L=7m	Fully grouted. Ø25mm Crown: 1×1m staggered grid. Walls: spacing 1.3×1.3m staggered grid.
Rock bolts, L=5m	Fully grouted. Ø25mm, spacing 1.3×1.3m staggered grid.
Anchor bar #11	Fully grouted embedment length in rock 7m (5°upwards) in upstream wall, and 5 m in downstream wall
Strand anchor #8	L=15 m. Strand post-tensioned anchor, capacity 1325 kN
Shotcrete	200mm or 250mm thick. Mostly sprayed in three layers with total thickness 250mm including two layers of mesh 10cm*10cm and 5mm thickness (Norplan A/S, 2013b).

Initially all wall strand anchors were pre-tensioned at levels 30t and 10t for 15 m anchors, and 15t and 5t for 10 m anchors, for zone A and B respectively. They were tied at low stress to allow the walls to deform. According to Norplan A/S (2013b) the site engineers

4.5 DEFORMATION IN THE POWERHOUSE CAVERN

later recommended higher pre-tension stress levels, so anchors installed below el. 593 were tied up to higher stress levels. The anchors installed in the pillars are tied up to 80 tons. (Norplan A/S, 2013b).

The whole cavern is sprayed with weld mesh layered shotcrete. The shotcrete arrangement can be seen in Fig.4.15. The thickness varies between 200-250 mm, with one or two layers of weld mesh depending on the rock conditions (NJC, 2011b).



Figure 4.16.: (a) Squeezing in pillar wall. (b) Concrete jacket installed for niche pillar. Photos byNorplan A/S (2013b).

Special support measures had to be made for the pillars between the niches. The pillars showed pervasive cracking, resulting in severe squeezing (Fig.4.16a). A “concrete jacket” was installed, with 1000 mm thick reinforced concrete with 25 mm diameter and 300 mm steel reinforcement (compressive strength for concrete is 35 MPa) (Fig.4.16b). In addition, post-tension anchors with 2 m spacing were installed at surfaces in three directions (Norplan A/S, 2013b).

4.5. DEFORMATION IN THE POWERHOUSE CAVERN

4.5.1. Overview of available deformation data

The deformations in the powerhouse cavern have been continuously monitored since constructions commenced 2011. Both electronic extensometers and convergence stations have been installed. The recordings up until December 2013 were made available for the study. Deformations in the bonneted gate niches and busbar tunnels have also been monitored; however these were installed as late as in June 2013. The measuring plan for the cavern is shown in Fig.4.17, and the cross-sectional locations of the measuring points are illustrated in Fig.4.18a. The installed extensometers are of the type multipoint borehole extensometers, and are illustrated in Fig.4.18b; the inner anchor is 25 m, middle anchor 15 m and the closest anchor is 5 m from the reference point at the cavern wall.

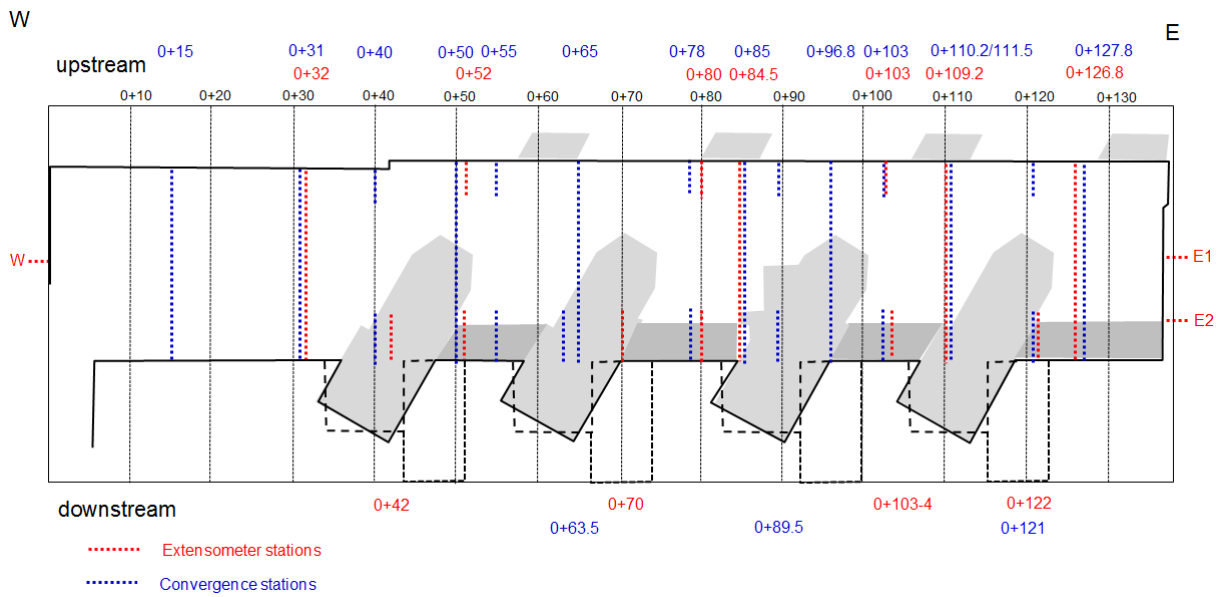


Figure 4.17.: Overview of measuring stations in the powerhouse cavern (NJC, 2013a)

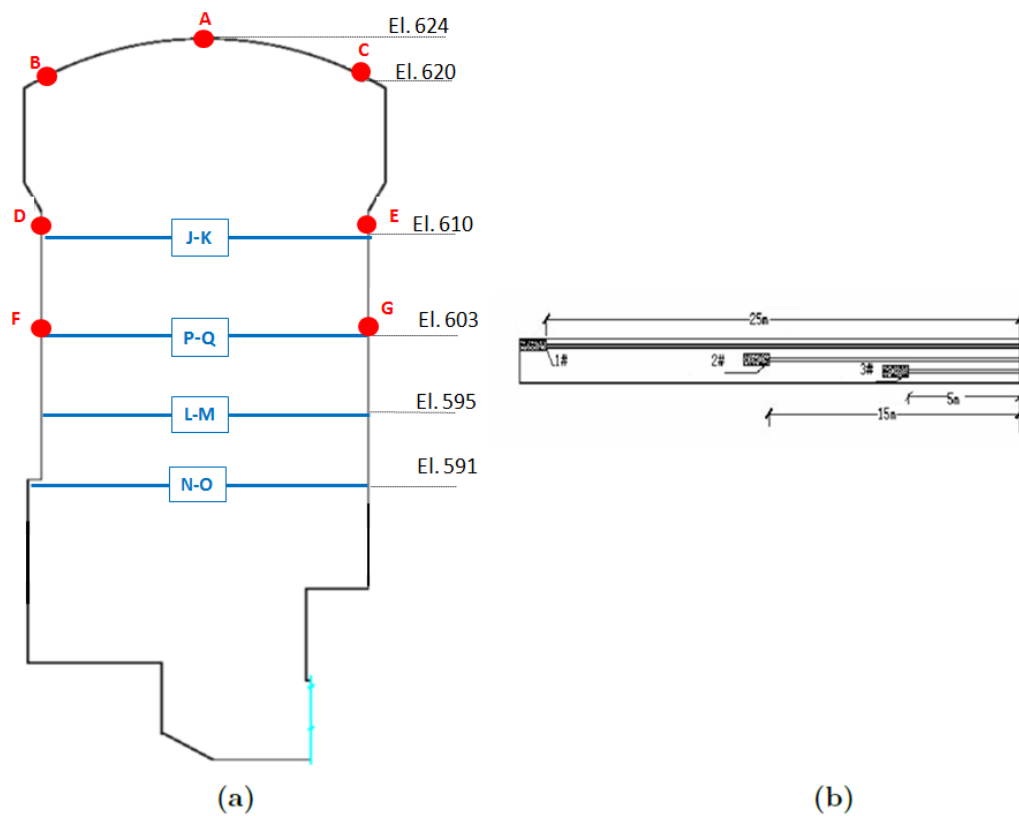


Figure 4.18.: a) Cross-sectional view of the measuring points. Blue lines represent convergence measurements, red dots are the extensometer points. b) Illustration of installed extensometers

4.5 DEFORMATION IN THE POWERHOUSE CAVERN

4.5.2. Analysis of measured deformation in the cavern

The deformation data have been assessed in detail, and compared to the location in the cavern, type of rock conditions, excavation progress and cavern layout. Fig.4.19 show a plot of all deformation data, based on the latest reading 08.12.13. The bars marked with a star were destroyed during construction. The data from the extensometers are plotted as the sum of total measured displacement in the two points at the same height as the convergence measurement (only relevant for extensometers D+E and F+G).

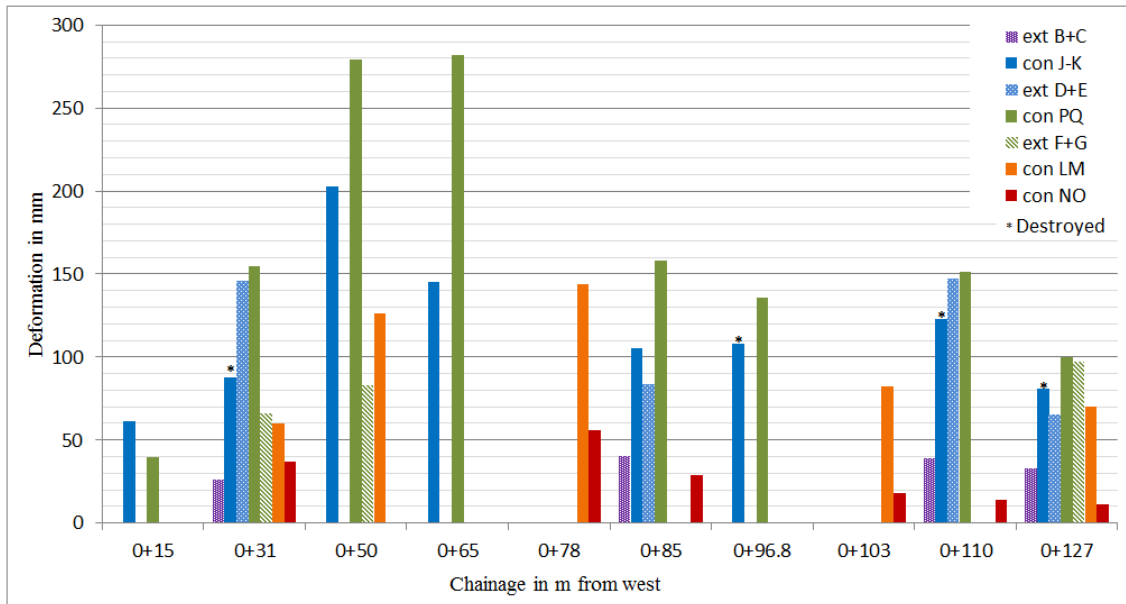


Figure 4.19.: Summary of all measured deformation along the cavern

The deformation is lowest in the west-end of the cavern (40-60 mm), where the cross-sectional area is smaller than for the rest of the cavern. The convergence of the walls increases towards the middle of the cavern. This is in accordance with theory about decreasing support from the end-walls. The data also indicate that the greatest deformation occurs in the upper middle part of the cavern walls, as the greatest deformation is measured at convergence line P-Q. This is right above the top level of the niches, and it is reasonable to assume this is the main cause for the high deformation. Given that it occur more siltstone and mudstone in the east-end of the cavern, it was expected to be higher deformation towards the east. Whether this is the case is difficult to conclude since the surrounding conditions change from west to east; the cross-sectional area is different, more support is added, and the closest measuring points are located at different distances from the end-walls.

Chainage 0+050 and 0+065 show unexpectedly high deformations, up to 282 mm for chainage 0+065. Observations describe water dripping around this area, which is known to influence the degree of squeezing. According to NJC (2011a), slaking of mudstone have been observed where it was encountered with water in the adit tunnels, where it showed maximum convergence in comparison to other rock types. The intersecting shear zone may also indicate that the rock mass is in general more sheared and fractured at these

sections. No observations from site personnel can confirm any of these theories for why the deformation is higher at this location (Norplan A/S, 2013a).

The measured data was compared and plotted against anchoring in either sandstone or siltstone/mudstone (based on site descriptions of location of the anchors). The plots are shown in App. B.3. The data indicate a slight tendency for lower convergence in sandstone than for mudstone/siltstone. Based on the descriptions of the rock mass the difference is much smaller than expected. Considering the relatively high degree of fracturing in the sandstone, it would appear that the rocks deform as a single mass.

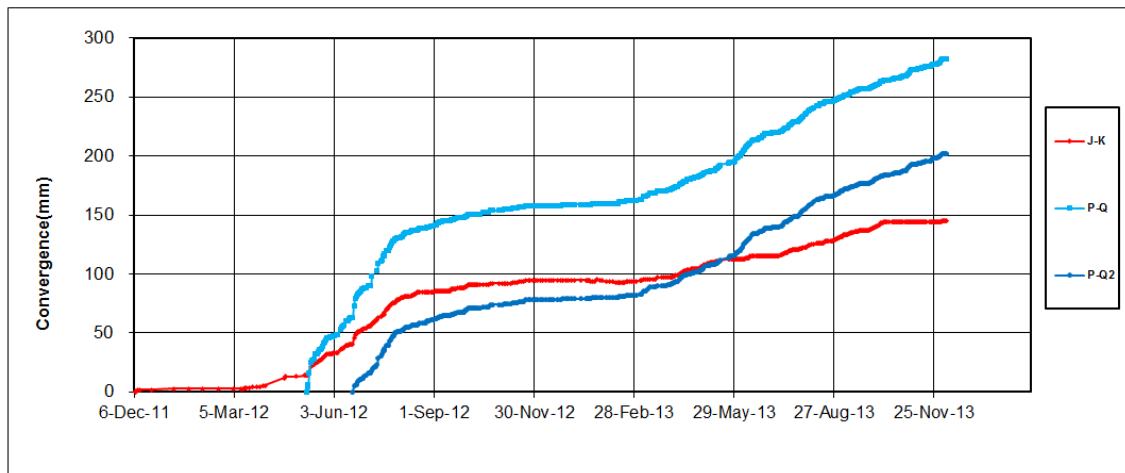


Figure 4.20.: Convergence over time for chainage 0+065

Correlating the development of deformation against the excavation progress revealed two significant events; the excavation of the bonneted gate niches, and excavation of the bottom floor level. All graphs show a rapid increase in deformation from about May 2012, before it starts decelerating around August-September 2012. This was the time when the bulleted gate niches were excavated. The second acceleration period was initiated around the beginning of the excavation of the bottom floor level. None of the graphs show a clear development towards an asymptote, which indicate that the deformation is ongoing and not yet reached its final value (per Dec. 2013).

4.5.3. Correlation between convergence and extensometer data

The correlation between the extensometer data and the convergence data is relatively good, for the few sections they are comparable. In Fig.4.19, the extensometers and convergence measurements for the green and blue bars are measured at approximately the same location. Most of the deviation can be explained by destruction of the convergence points or different time for installation.

The largest deviation is seen in the data for chainage 0+032 and 0+050. Analysis of the extensometer plots revealed some irregular behavior; the E extensometer at 0+032 shows the highest deformation between 5 and 15 m into the rock mass (Fig.4.21), while the F extensometer at chainage 0+052 decrease rapidly for the same distance (see App. B.2). The deformation behavior for extensometer E at chainage 0+032 would indicate failure of

4.5 DEFORMATION IN THE POWERHOUSE CAVERN

the rock mass inside the wall. No report from site personnel indicate failure of the cavern wall at this location, so measuring error is the more likely cause (NJC, 2013a).

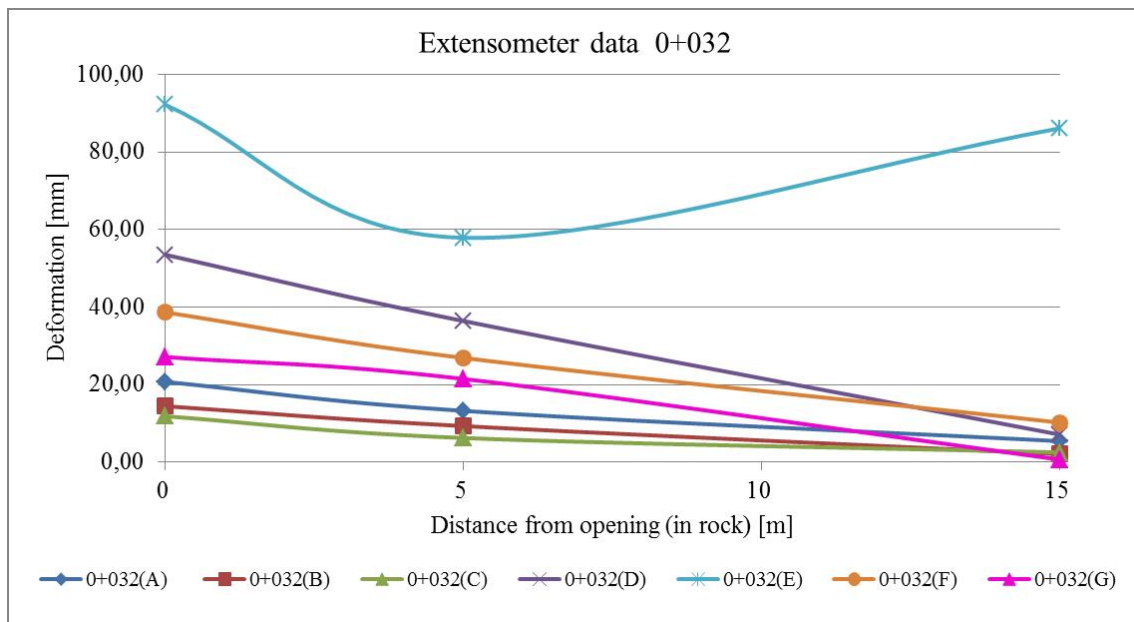


Figure 4.21.: Extensometer data for chainage 0+032

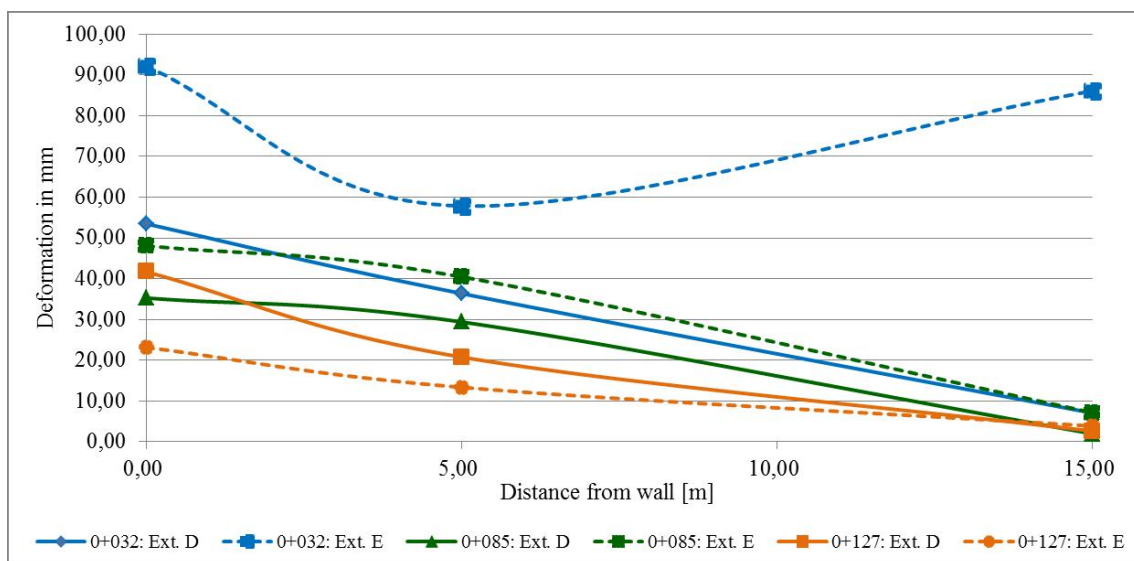


Figure 4.22.: Extensometers at el. 610, for section 0+032, 0+085 and 0+127

Fig.4.22 shows the extensometer data for three selected sections, at el. 610 right below the crane beam. For section 0+032 and 0+085, the extensometers indicate that the deformation is higher in the downstream wall (D extensometer in Fig.4.22). For section 0+127, the deformation is highest in the upstream wall. This may be related to the orientation of the bedding relative to the cavern alignment. More likely the higher deformation in the downstream wall is related to the niches. This may be why section 0+127 is different

than the two middle sections. Further the extensometers indicate that about 60-80% of the deformation occur in the first 5 meters of rock mass. The data indicate a radius of plastic zone of at least 10-15 meters around the cavern.

4.5.4. Concluding remarks

The extensive monitoring program gives important information about the deformation behavior of the cavern. Most importantly, the data reveal a complex set of influencing factors. The deformation is not significantly higher for the sections dominated by mudstone and siltstone, and the highest deformation cannot be fully explained by geological observations. The deformation behavior at the cavern follow the basic concepts of theory, like increasing deformation towards the middle of the cavern, highest deformation in the middle of the walls, and the highest deformation is potentially caused by influence of water and weaker rock mass. Construction of the niches and excavation of the bottom floor level have been identified as the two single most accelerating events. The highest deformation is measured at el. 603, in the wall right above the niches. The varying external factors pose a challenge for interpreting deformations in a powerhouse cavern versus a tunnel; multistage excavation progress, different geometry and intersecting niches and tunnels changing the distribution of stresses.

Additionally, the excavation progress naturally influence the time of measuring. The monitoring stations installed in the lower half of the cavern wall (L-M and N-O) have measured for a much shorter time interval. Significant deformation data is lost in the interpretation. At the time of installation, the rock mass has already deformed significantly; as the theory states that the deformation starts about 1-2 tunnel radii ahead of the face. The omitted deformation is difficult to estimate, as the cavern is excavated in non-systematic sequences due to the niches.

5. REVIEW ON SQUEEZING ANALYSIS

5.1. INTRODUCTION

The main cause for instability in the NJHPP cavern is squeezing deformation, and the convergence of the cavern roof and walls have been monitored during excavation. This makes for a potentially rare opportunity to evaluate the deformation characteristics of a powerhouse cavern, as well as to evaluate available methods for prediction and assessment of squeezing in large scale caverns. Many researchers have developed different methods to aid the engineer in the assessment of potential for tunnel squeezing and necessary support measures. However, there is a major limitation to the methods with regard to the analysis of non-circular excavations and anisotropic stress conditions.

The available methods for prediction of squeezing include empirical method such as Singh et al. (1992), Q-system (Grimstad and Barton, 1993), Goel et al. (1995), Palmström (1995); and the semi-analytical method proposed by Hoek and Marinos (2000). Analytical methods include more extensive analysis with estimation of necessary support pressure, like the Convergence-Confinement Method (CCM) by Carranza-Torres and Fairhurst (2000). Numerical modeling is recommended for substantial analysis, where the 2-dimensional elasto-plastic finite element program *Phase²* is commonly applied. This thesis will present, apply and evaluate the following methods in relation to the measured deformations at NJHPP: Goel et al. (1995), Q-system by Barton (2002), Hoek and Marinos (2000a), CCM and finally numerical modeling in *Phase²*.

5.2. EMPIRICAL AND SEMI-ANALYTICAL METHODS

Analysis of numerous case histories has lead authors to propose empirical relationships for the prediction of tunnel squeezing. Depending on the indicators used, Shrestha (2006) grouped the different methods into the following categories; (i) strength-stress ratio, (ii) strain estimation approach, and (iii) rock mass classification approach. The first two groups do not prescribe support requirements, and are therefore not considered to be complete methods (Shrestha, 2006). Rock mass classification approaches can be used for a wider range of underground constructions, and some assess the extent of support. For the analysis of NJHPP two empirical methods have been chosen: Goel's approach and the Q-method. Both are methods based on rock mass classification, and will be further explained in the following.

Among the known semi-analytical methods available for analysis of tunnel squeezing are Kovári, K. (1998), Aydan et al. (1993) and Hoek and Marinos (2000). In this study only the approach developed by Hoek and Marinos (2000) will be discussed further. The method can be viewed as a strain estimation method, and can include an internal pressure to simulate the effect of support.

5.2.1. Q-method

The Q-system for rock mass classification was first developed at the Norwegian Geotechnical Institute (NGI) by Barton et al. (1974), and later updated by Grimstad and Barton (1993). Based on numerical assessment of rock mass quality, the method is used for estimation of necessary tunnel support. The following six parameters are evaluated for the rock mass:

- Rock Quality Designation (RQD)
- Number of joint sets (J_n)
- Joint roughness (J_r , for the most unfavorable joint orientations)
- Degree of alteration or filling along the weakest joints (J_a)
- Water inflow (J_w)
- Stress reduction factor (SRF)

Based on the six parameters the overall rock mass quality (Q-value) is calculated as follows:

$$Q = \frac{RQD}{J_n} \times \frac{J_r}{J_a} \times \frac{J_w}{SRF} \quad (5.1)$$

Details for determination of Q-value parameters are shown in App.A.4. The last term in Eq. 5.1 can be named the “active stress” term, and evaluates the relative effect of water, faulting, strength/stress ratio, squeezing or swelling (Barton, 2002). This means squeezing is taken into account in the choice of value for SRF, which for squeezing conditions are defined according to the following criteria:

Table 5.1.: Squeezing condition according to Q-system (based on Barton, 2002)

Squeezing rock: plastic flow of incompetent rock under the influence of high rock pressure	$\sigma_{\theta max}/\sigma_{cm}$	SRF
Mild squeezing rock pressure	1 - 5	5 - 10
Heavy squeezing rock pressure	> 5	10 - 20

The Q-system rates squeezing as either “Mild” or “Heavy”, depending on the ratio between maximum tangential stress ($\sigma_{\theta max}$) and rock mass strength (σ_{cm}). Maximum tangential stress at the tunnel opening in plastic rock will for normal stress conditions be the overburden stress (σ_v).

According to NGI (2013) the “Determination of squeezing rock conditions must be made according to relevant literature (i.e. Singh et al., 1992 and Bhasin and Grimstad, 1996)”. Previous versions of the system only considered the determination by Singh et al. (1992) which states that squeezing rock occurs at a depth $H > 350Q^{1.5}$. Further the rock mass strength could be found by $\sigma_{cm}=0.7\gamma Q^{1/3}$ where γ is rock mass density in kN/m^3 (Shrestha, 2006). According to Shrestha (2006) this would lead to a loop of dependency; to determine σ_{cm} the Q-value has to be found, which again depend on SRF. To estimate SRF it should be know whether there is squeezing or not. To overcome this loop of dependency, other methods for determination of σ_{cm} will be used, as presented in Sec.2.3.3.

High stress conditions in weak rock will give a relatively high SRF, resulting in a lower value for rock mass quality (Q-value). The Q-system assign support classes based on Q-value, and the equivalent dimensions of the underground opening (D_e). D_e is a function of type and size of the excavation (D_t) and the excavation support ratio (ESR):

$$D_e = \frac{D_t}{ESR} \quad (5.2)$$

ESR depends on type and intended use of the underground excavation. Determination of ESR and classification chart for support according to the Q-system is given in App.A.5.

5.2.2. Goel (1994) approach

To overcome the problem with defining SRF, Goel developed an empirical method to predict squeezing based on rock mass number N. The rock mass number N is defined as Q-value with SRF=1.

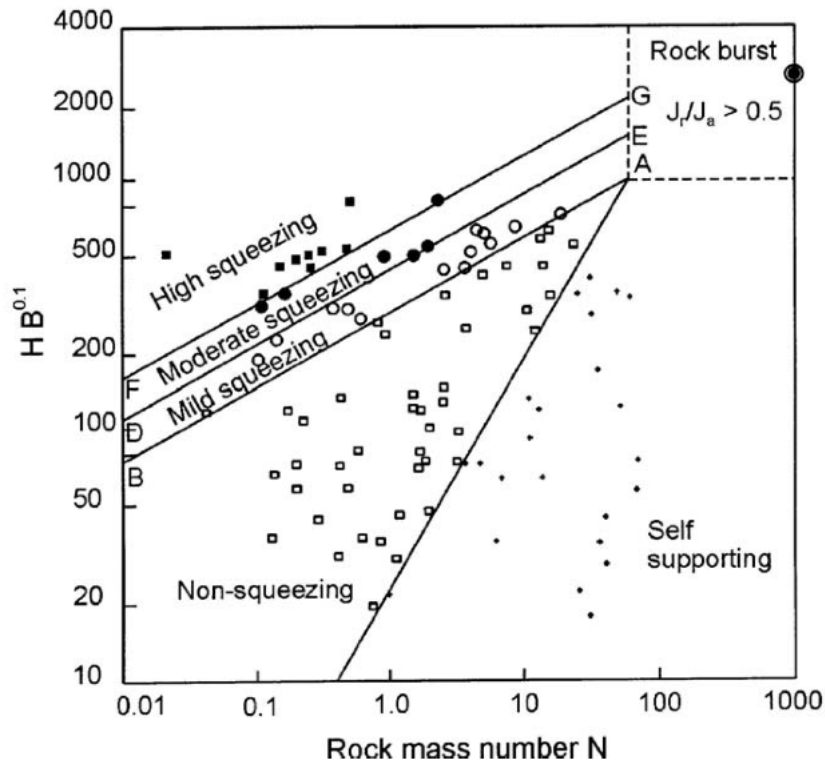


Figure 5.1.: Goel’s approach for predicting squeezing by rock mass number (N).

Goel studied 99 tunnel sections in the hopes of finding an empirical relationship between overburden depth (H), tunnel span/diameter (B) and rock mass number (N) (Shrestha, 2006). The study resulted in a log-log plot of $HB^{0.1}$ and N, as shown in Fig.5.1. Squeezing conditions are defined above the AB line, described by the following relationship:

$$H = (275N^{0.33}) B^{-0.1} \tag{5.3}$$

where H (overburden depth) is given in meters. In other words; the method can be used for prediction of maximum overburden depth for which squeezing will occur, for the given rock mass number. Or for which rock mass number, for the given tunnel diameter and overburden, squeezing will occur.

Goel also suggested formulas for determining support pressure and convergence deformation estimation. However, the deformation calculation depends upon the stiffness of support, which makes the calculation complicated (Shrestha, 2006).

5.2.3. Hoek and Marinos (2000) approach

Hoek and Marinos (2000) proposed that the ratio between the uniaxial compressive strength of the rock mass (σ_{cm}) and the in-situ stress (p_o) can be used to indicate the potential squeezing problems of a circular tunnel. According to the authors their methodology can give a “reliable first estimate” of the severity of squeezing, and indicate which type of support solutions could prevent the deformation.

The analysis by Hoek and Marinos (2000) followed an approach by Sakurai, S. (1983) to find the relationship between σ_{cm}/p_o and the percentage strain (ϵ) of the tunnel. Percentage strain is defined as ϵ (%) = $100 \times [\text{tunnel closure} / \text{tunnel diameter}]$. They used the results of a study on closed form analytical solutions for a circular tunnel in a hydrostatic stress field, published by Duncan Fama (1993) and Carranza-Torres and Fairhurst (1999). Performing Monte Carlo simulations for a wide range of tunnel conditions, they found a clearly defined pattern which could be predicted by the equation given in Fig.5.2.

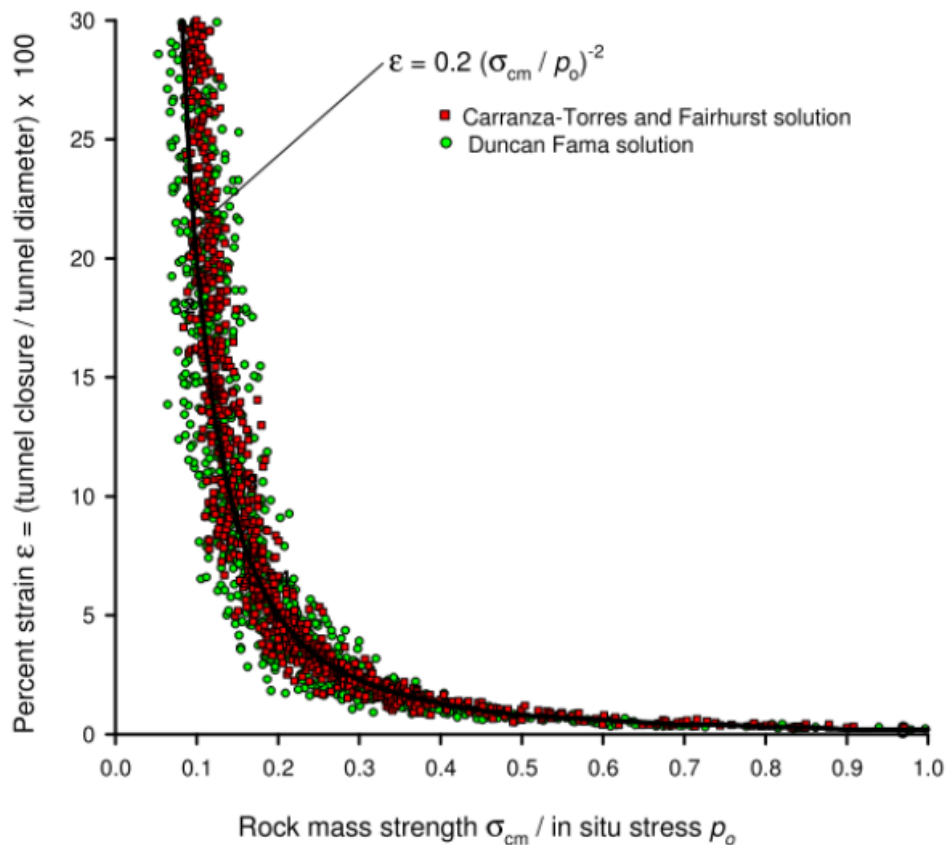


Figure 5.2.: Tunnel convergence against ratio of rock mass strength to in-situ stress, found by Hoek and Marinos (2000).

Hoek and Marinos (2000a) found that the size of the plastic zone surrounding the tunnel followed a very similar trend as that illustrated in Fig.5.2. Extending the analysis to include internal pressure to simulate the effect of support, they developed the following equations for determination of the size of the plastic zone (Eq. 5.4), and the deformation

5.2 EMPIRICAL AND SEMI-ANALYTICAL METHODS

of a tunnel in squeezing ground (Eq. 5.5):

$$\frac{d_p}{d_o} = \left(1.25 - 0.625 \frac{p_i}{p_o} \right) \frac{\sigma_{cm}}{p_o} \left(\frac{p_i}{p_o} - 0.57 \right) \quad (5.4)$$

$$\varepsilon = \frac{\delta_i}{d_o} = \left(0.002 - 0.0025 \frac{p_i}{p_o} \right) \frac{\sigma_{cm}}{p_o} \left(2.4 \frac{p_i}{p_o} - 2 \right) \quad (5.5)$$

Where,

d_p is the diameter of the plastic zone [m]

d_b is the original tunnel diameter [m]

δ_i is the tunnel sidewall deformation [m]

p_i is the internal support pressure [MPa]

p_o is the in-situ stress [MPa]

σ_{cm} is the rock mass strength [MPa]

Additionally, Hoek and Marinos (2000a) proposed a classification system for squeezing severity based on strain percentage, as presented in Fig.5.3. The five classes range from “Few support problems” (A) to “Extreme squeezing problems” (E), and are further described as in Tab.5.2.

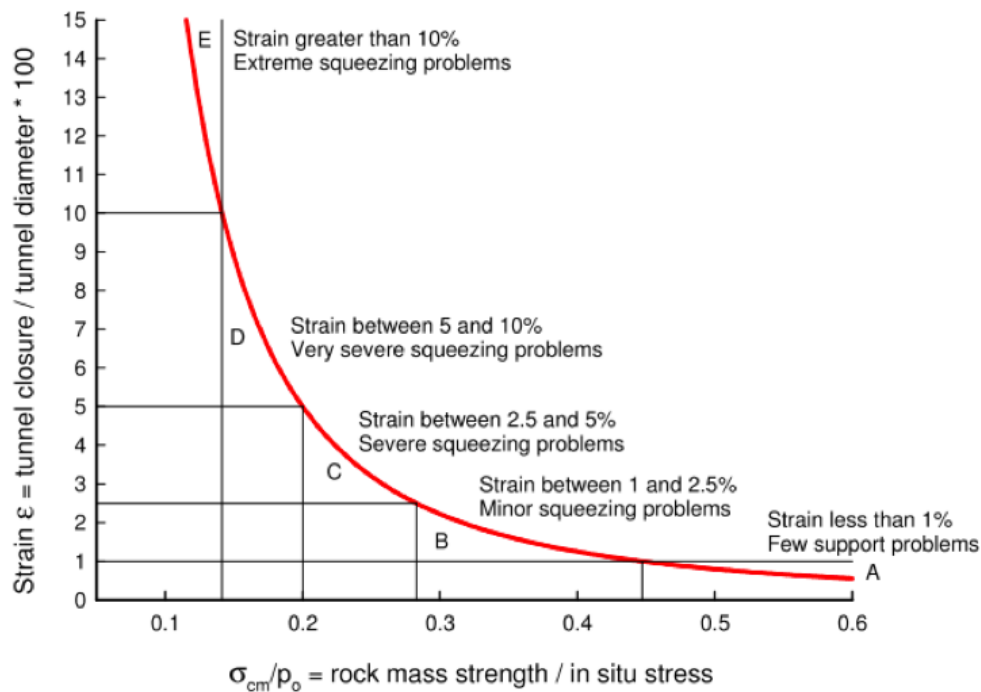


Figure 5.3.: Suggested classification of severity of squeezing, proposed by Hoek and Marinos (2000a).

Table 5.2.: Geotechnical issues and suggested support types for the 5 classes of squeezing severity Hoek and Marinos (2000a).

	Strain ϵ %	Geotechnical issues	Support types
A	Less than 1	Few stability problems and very simple tunnel support design methods can be used. Tunnel support recommendations based upon rock mass classifications provide an adequate basis for design.	Very simple tunnelling conditions, with rockbolts and shotcrete typically used for support.
B	1 to 2.5	Convergence confinement methods are used to predict the formation of a 'plastic' zone in the rock mass surrounding a tunnel and of the interaction between the progressive development of this zone and different types of support.	Minor squeezing problems which are generally dealt with by rockbolts and shotcrete; sometimes with light steel sets or lattice girders are added for additional security.
C	2.5 to 5	Two-dimensional finite element analysis, incorporating support elements and excavation sequence, are normally used for this type of problem. Face stability is generally not a major problem.	Severe squeezing problems requiring rapid installation of support and careful control of construction quality. Heavy steel sets embedded in shotcrete are generally required.
D	5 to 10	The design of the tunnel is dominated by face stability issues and, while two-dimensional finite analyses are generally carried out, some estimates of the effects of forepoling and face reinforcement are required.	Very severe squeezing and face stability problems. Forepoling and face reinforcement with steel sets embedded in shotcrete are usually necessary.
E	More than 10	Severe face instability as well as squeezing of the tunnel make this an extremely difficult three-dimensional problem for which no effective design methods are currently available. Most solutions are based on experience.	Extreme squeezing problems. Forepoling and face reinforcement are usually applied and yielding support may be required in extreme cases.

5.3. ANALYTICAL METHOD

Estimation of required support for a tunnel excavation can essentially be viewed as a four-dimensional problem. The three-dimensional redistribution of stresses around the excavation is mutually influenced by the time-dependent weakening of the rock mass, and the nature of the rock is unknown until exposed in the face. According to Carranza-Torres and Fairhurst (2000), Labasse described the dilemma as early as in 1949. Labasse first explained how the support should be standardized, to minimize the disruption of other underground operations. This standardization makes precise calculations for each cross-section useless. Labasse further explained how the need for immediate support behind the face does not allow for detailed calculations or for the fabrication of the support for each section. For a precise determination of the support, each cross-section had to be analyzed separately; including geological mapping, experiments and calculations. During this time, the excavation would be in danger of failing, and the support would be futile.

Considering these constraints, analytical methods have proved to be useful tools in the simplification of the interplay between the rock mass and installed support. The methods consider the effect of variation in assumed rock properties and on the support loads. Until now there are no available methods especially developed for squeezing deformation, but the general methods for tunnel stability are commonly used. The Convergence-Confinement Method (CCM) proposed by Carranza-Torres and Fairhurst (2000) has gained wide acceptance as one of the more competent analytical methods, and will be used in this study. Application of the method requires knowledge of the deformation characteristics of the rock mass and support. The Hoek-Brown criterion is widely used for the assessment

of the mechanical response of a jointed rock mass (see Sec.2.3.2). The following sections describe the practical implementation of CCM to rock-masses that can be described by the Hoek-Brown criterion.

5.3.1. Convergence-Confinement Method (CCM)

The term 'Convergence-Confinement' was developed in the 1960's and 70's, although the method itself has been known since at least 1938 (Carranza-Torres and Fairhurst, 2000). CCM allows for estimation of the load imposed on the support installed immediately behind the face. Support installed immediately behind the face of a tunnel will not carry the full load for which it is designed; a part of the load will be carried by the face itself. As the tunnel advances, this 'face-effect' will decrease, and the support progressively carries more load. When the face has moved sufficiently far from the installed support, the full design load of the support is reached.

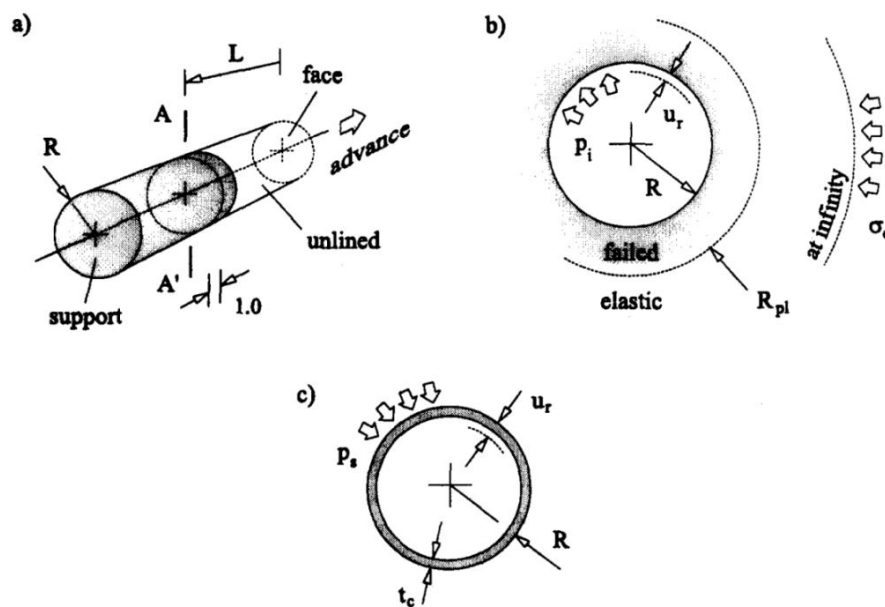


Figure 5.4.: a) A cylindrical tunnel of radius R driven in the rock mass. b) Cross-section of the rock mass at section $A-A'$. c) Cross-section of the circular support installed at section $A-A'$ (Carranza-Torres and Fairhurst, 2000).

Carranza-Torres and Fairhurst (2000) illustrated the problem as shown in Fig.5.4. Considering a tunnel with radius R driven in a rock mass subjected to a uniform far-field stress σ_0 . Support, with unit length in the direction of the tunnel, is installed at a distance L from the face. The objective of the CCM analysis is to determine the load that the rock mass will transmit to the installed support at section $A-A'$ from the time of installation until the time when the face has moved sufficiently far ahead. The variables involved in the analysis are shown in Fig.5.4b and c; R_{pl} is the radius of the plastic zone, u_r is the radial displacement of the wall, p_i is the internal pressure symbolizing the effect of the face moving away from the support, p_s is the pressure transmitted by the rock mass to the support. For simplicity, it is assumed that the deformation occur in a plane perpendicular

to the axis of the tunnel. For compatibility, the deformation of the rock support interface must equal the radial displacement of the wall.

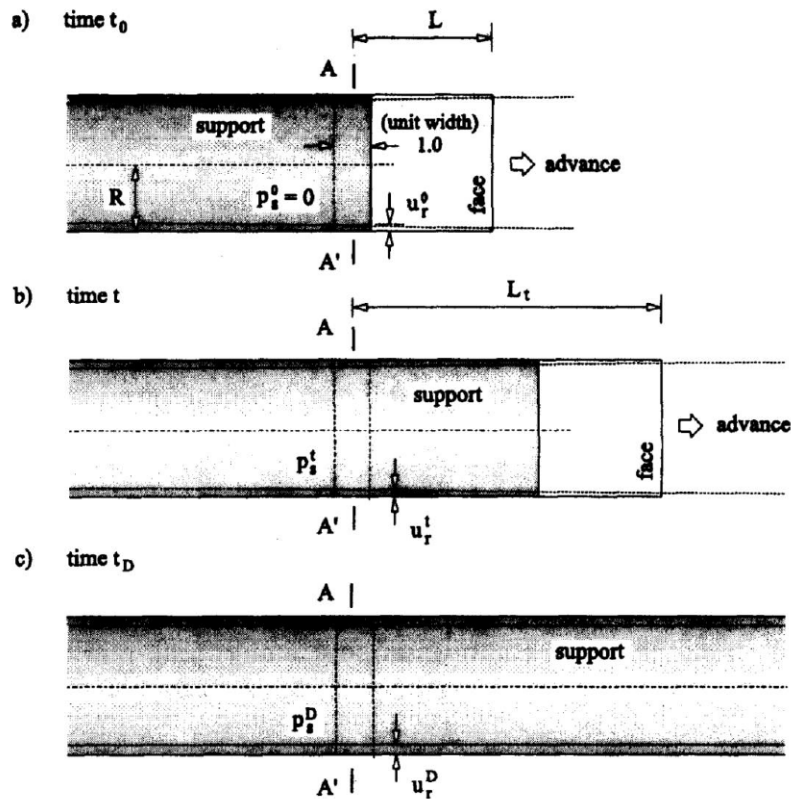


Figure 5.5.: Loading of the support at section A-A' due to progressive advance of the tunnel face (Carranza-Torres and Fairhurst, 2000)

The basis of the CCM is illustrated in a) through c) in Fig.5.5. At time t_0 support is installed at section A-A' at a distance L from the face, and the tunnel wall have then converged by the amount u_r^0 . Provided that the face does not advance, the support carries no load, so that $p_s = 0$ at this stage; i.e time-dependent weakening of the rock mass is not considered in CCM. As the tunnel advances, the rock mass and the support deform together; load is transmitted to the support (p_s increases) as the internal pressure decreases. At time t , at a distance L_t from the face, the ground will have converged by $u_r^t > u_r^0$ (Fig.5.5b). When the face has moved sufficiently far from the support, the ground support system at A-A' is in equilibrium and the support carries its full design load (p_s^D). At this time t_D , the effect of the face has disappeared ($p_i=0$) and the support and ground have converged together with the final amount u_r^D (Fig.5.5c).

To determine the load transferred to the support requires an analysis of the load-deformation characteristics of the elements comprising the system; (i) the progression of the tunnel (ii) the section of excavation perpendicular to the tunnel axis and (iii) the installed support at this section. Carranza-Torres and Fairhurst (2000) therefore defined CCM to include three main components; (i) the Longitudinal Deformation Profile (LDP), (ii) the Ground Reaction Curve (GRC) and (iii) the Support Characteristics Curve (SCC). The details of each component will be further discussed in the following.

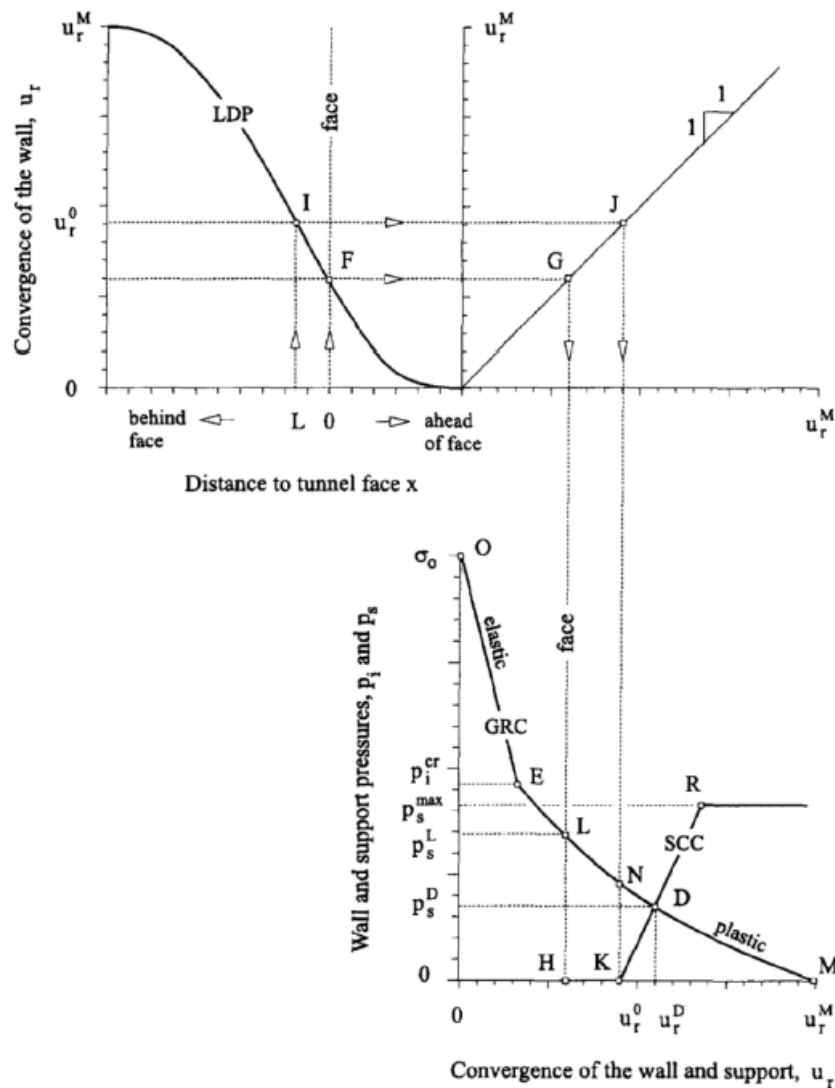


Figure 5.6.: Schematic representation of Longitudinal Deformation Profile (LDP), Ground Reaction Curve (GRC) and Support Characteristics Curve (SCC) (Carranza-Torres and Fairhurst, 2000)

The Ground Reaction Curve (GRC)

GRC describes the relationship between the decreasing internal pressure (p_i) and the increasing radial displacement of the wall (u_r) (OEM in Fig.5.6). The internal pressure is not a true representation of reality, but rather a surrogate for the effect of the gradual reduction of the radial resistance provided by the initially present tunnel core (Vlachopoulos and Diederichs, 2009). Initially (at point O, about one diameter ahead of the face), the internal pressure will equal the far-field stress (σ_0). As the tunnel advances, the support provided by the rock mass decreases, meaning the internal pressure p_i decreases. The rock mass will respond elastically until it reaches a critical internal pressure p_i^{cr} at point E, where plastic failure of the rock mass initiates. For $p_i < p_i^{cr}$ the rock mass deforms plastically, and a plastic region of radius R_{pl} is formed around the opening. Plastic de-

formation of the rock mass continuous until point M ($p_i = 0$), where the wall will have reached its final and maximum displacement (u_{max}).

Carranza-Torres and Fairhurst (2000) found that for a section of a circular tunnel with radius R , the uniform internal pressure p_i and far-field stress σ_0 can be 'scaled'. Assuming that the rock mass satisfies the Hoek-Brown criterion, the scaled internal pressure P_i and the scaled far field stress S_0 can be found by:

$$P_i = \frac{p_i}{m_b \sigma_{ci}} + \frac{s}{m_b^2} \quad (5.6)$$

$$S_0 = \frac{\sigma_0}{m_b \sigma_{ci}} + \frac{s}{m_b^2} \quad (5.7)$$

where m_b and s are rock mass parameters explained in Sec.2.3.2. σ_{ci} is the intact rock strength in MPa.

The critical point marking the transition from elastic to plastic behavior (point E in Fig.5.6) is found by first defining the scaled critical internal pressure P_i^{cr} (Eq.5.8). The actual critical internal pressure p_i^{cr} is further found by the inverse of Eq. 5.6, expressed by the scaled critical internal pressure (Eq. 5.9).

$$P_i^{cr} = \frac{1}{16} \left[1 - \sqrt{1 + 16S_0} \right]^2 \quad (5.8)$$

$$p_i^{cr} = \left[P_i^{cr} - \frac{s}{m_b^2} \right] m_b \sigma_{ci} \quad (5.9)$$

In the elastic region of the GRC ($p_i > p_i^{cr}$, OE in Fig.5.6), the radial displacement of the wall is defined by the following relationship:

$$u_r^{el} = \frac{\sigma_0 - p_i}{2G_{rm}} R \quad (5.10)$$

$$G_{rm} = \frac{E_{rm}}{2(1 + \nu)} \quad (5.11)$$

where R is the radius of the tunnel. G_{rm} is the shear modulus of the rock mass in GPa, defined as in Eq. 5.11, where E_{rm} is the elastic modulus of the rock mass in GPa and ν is the Poisson's ratio. E_{rm} is suggested to be found by the formula proposed by Hoek et al. (2002) in Tab.2.3, with $D=0$ (Carranza-Torres and Fairhurst, 2000).

Carranza-Torres and Fairhurst (2000) found that the plastic region of the GRC (EM in Fig.5.6) needs to be derived by a flow rule for the material. The flow rule defines the relationship between the strains that produce distortion, and those that produce volumetric changes during plastic deformation (Carranza-Torres and Fairhurst, 2000). The suggested flow rule solution is characterized by the dilation coefficient K_ψ , which depends on the dilation angle ψ (Eq.5.12). For $\psi = 0^\circ$ the material will have no volumetric change, while a volume increase in the material will occur for $\psi > 0^\circ$.

$$K_\psi = \frac{1 + \sin \psi}{1 - \sin \psi} \quad (5.12)$$

With the flow rule defined by the dilation coefficient K_ψ , the radial displacement of the plastic region, u_r^{pl} , is given by the following:

$$\frac{u_r^{pl}}{R} \frac{2G_{rm}}{\sigma_0 - p_i^{cr}} = \frac{K_\psi - 1}{K_\psi + 1} + \frac{2}{K_\psi + 1} \left(\frac{R_{pl}}{R} \right)^{K_\psi + 1} + \frac{1 - 2\nu}{4(S_0 - P_i^{cr})} \left[\ln \left(\frac{R_{pl}}{R} \right) \right]^2 - \left[\frac{1 - 2\nu}{K_\psi + 1} \frac{\sqrt{P_i^{cr}}}{S_0 - P_i^{cr}} + \frac{1 - \nu}{2} \frac{K_\psi - 1}{(K_\psi + 1)^2} \frac{1}{S_0 - P_i^{cr}} \right] \times \left[(K_\psi + 1) \ln \left(\frac{R_{pl}}{R} \right) - \left(\frac{R_{pl}}{R} \right)^{K_\psi + 1} + 1 \right] \quad (5.13)$$

where R_{pl} is the radius of the plastic region in meters:

$$R_{pl} = R \exp \left[2 \left(\sqrt{P_i^{cr}} - \sqrt{P_i} \right) \right] \quad (5.14)$$

The Longitudinal Deformation Profile (LDP)

The LDP is a graphical representation of the radial displacement occurring along the axis of an unsupported cylindrical excavation, for sections ahead and behind the face (Carranza-Torres and Fairhurst, 2000). The upper diagram in Fig.5.6 illustrates a typical LDP. The profile indicates that at some distance behind the tunnel face, the supporting effect from the face is negligibly small. Beyond this distance the unlined tunnel has converged by the final amount u_{max} . Similarly, at some distance ahead of face the advancing tunnel has no effect on the rock-mass, and the radial displacement is zero (Carranza-Torres and Fairhurst, 2000). As one of the three components in CCM, the LDP provides the important insight into how quickly the support begins to interact with the rock mass behind the face of the tunnel (defines point K in Fig.5.6). The LDP can therefore prove useful for the determination of the appropriate timing for the installation of stiff support, or for optimization of the installed support with specific displacement capacities (Vlachopoulos and Diederichs, 2009).

Consider a uniform far-field stress acting on a circular tunnel with radius R , with a final displacement u_{max} at a distance x behind the face. According to Carranza-Torres and Fairhurst (2000), Panet (1995) suggested the following relationship between radial displacement and distance behind the face:

$$\frac{u_r}{u_{max}} = 0.25 + 0.75 \left[1 - \left(\frac{0.75}{0.75 + x/R} \right)^2 \right] \quad (5.15)$$

Chern et al. (1999) presented measured data for convergence in the vicinity of the face in a tunnel in the Mingtam Power Cavern project (Carranza-Torres and Fairhurst, 2000). Compared with the measured values, the relation by Panet was found to overestimate the radial displacement. Based on the same empirical data, Hoek (1999) suggested a best-fit relationship between radial displacement and distance to the face:

$$\frac{u_r}{u_{max}} = 1 + \exp \left(\frac{-x/R}{1.10} \right)^{-1.7} \quad (5.16)$$

Vlachopoulos and Diederichs (2009) later found that the available formulas for LDP would only be reasonable if the radius of plastic zone does not exceed 2 tunnel radii, and provided that the yielding zone in the tunnel face does not interact with the developing yield zone around the tunnel walls. They explained how a larger yield zone takes a relatively longer normalized distance to develop. They saw the need for a more robust formulation, since the failure to use the appropriate LDP for support estimation could result in significant errors of appropriate installation distance (from the face).

To account for the influence of the increased overall yielding on the shape of the LDP, Vlachopoulos and Diederichs (2009) introduced the term normalized plastic zone radius, $R^* = R_{pl}/R$, where R_{pl} is the radius of the plastic zone and R is the radius of the tunnel. Based on *Phase²* analysis for plain strain cross-sections and axisymmetric models, they developed a new set of best-fit relationships for the construction of LDP as a function of R^* . The normalized closure, u_0^* is related to normalized plastic radius as follows:

$$u_0^* = \frac{u_0}{u_{max}} = \frac{1}{3}e^{-0.15R^*} \quad (5.17)$$

The deformation in the rock mass ahead of face ($X^* \leq 0$, where $X^* = X/R$) is:

$$u^* = \frac{u}{u_{max}} = u_0^*e^{X^*} \quad (5.18)$$

And the deformation in the tunnel (behind the face $X^* \geq 0$):

$$u^* = 1 - (1 - u_0^*)e^{-\frac{3X^*}{2R^*}} \quad (5.19)$$

u_{max} and R_{pl} is found when constructing the GRC. Eq. 5.17 to Eq. 5.19 can be used to construct the LDP for a circular tunnel in a uniform stress field, regardless of the radius of the plastic zone.

The Support Characteristics Curve (SCC)

SCC is defined as the relationship between the increasing internal pressure on the support (p_s), and the increasing radial displacement of the support (u_r). KR in Fig.5.6 show a typical SCC, where point K corresponds to a support pressure equal to zero (at time of installation). Point R corresponds to the maximum pressure the support can accept before collapsing, p_s^{max} . The SCC can be constructed from the elastic relationship between the applied stress p_s , and the resulting closure u_r for a section of the support of unit length in the direction of the tunnel (Carranza-Torres and Fairhurst, 2000):

$$p_s = K_s u_r \quad (5.20)$$

where K_s [MPa/m] is the elastic stiffness of the support.

The plastic part of the SCC, i.e the horizontal segment starting in point R, is defined by the maximum pressure p_s^{max} . This pressure depends on type of support and its stiffness. Carranza-Torres and Fairhurst (2000) have adapted equations from Hoek and Brown (1980) and Brady and Brown (1985) for three different support systems; *i*) concrete or shotcrete linings, *ii*) ungrouted bolts and cables and *iii*) blocked steel sets. As shotcrete and bolts are the only support relevant for this project, only these will be presented below. The reader is referenced to the original sources for further details.

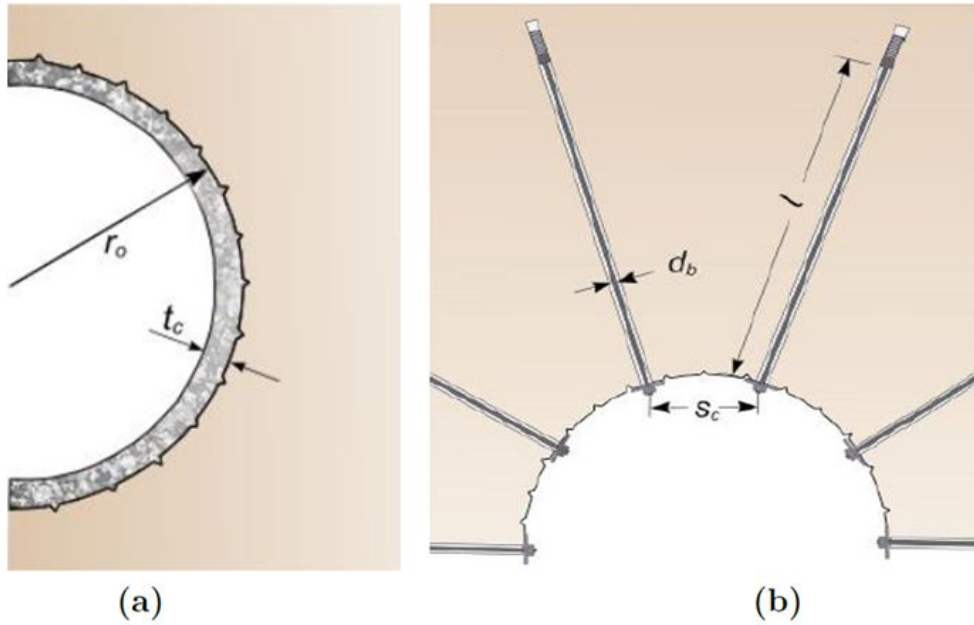


Figure 5.7.: Representation of sections of a) concrete/shotcrete rings and b) ungrouted mechanical-anchored bolts (Hoek, 2007e)

i) Concrete or shotcrete linings

For a closed ring of shotcrete or concrete, the maximum pressure provided by the support is given by:

$$p_s^{max} = \frac{\sigma_{cc}}{2} \left[1 - \frac{(R - t_c)^2}{R^2} \right] \quad (5.21)$$

The elastic stiffness is defined as:

$$K_s = \frac{E_c}{(1 - \nu_c)R} \frac{R^2 - (R - t_c)^2}{(1 - 2\nu_c)R^2 + (R - t_c)^2} \quad (5.22)$$

Where,

σ_{cc} is the unconfined compressive strength of the concrete/shotcrete [MPa]

E_c is the Young's modulus for concrete/shotcrete [MPa]

ν_c is Poisson's ratio for concrete/shotcrete [-]

t_c is the thickness of the ring [m]

R is the external radius of the support [m] (same as radius of the tunnel)

ii) UngROUTED bolts and cables

With the assumption of equally spaced bolts in the circumferential direction, the maximum pressure provided by the bolt system is:

$$p_s^{max} = \frac{T_{bf}}{s_c s_l} \quad (5.23)$$

The stiffness is:

$$\frac{1}{K_s} = s_c s_l \left[-\frac{4l}{\pi d_b^2 E_s} + Q \right] \quad (5.24)$$

Where,

T_{bf} is the ultimate load obtained in a pull-out test [MN]

s_c and s_l are the circumferential and longitudinal bolt spacing, respectively [m]

l is the free length of the bolt or cable [m]

d_b is the bolt/cable diameter [m]

E_s is the Young's modulus of the bolt or cable [MPa]

Q is the deformation-load constant for the anchor and head [m/MN]

Eq. 5.24 assumes that the reaction forces developed by the bolt are concentrated at the ends of the bar, and should for this reason not be applied to grouted bolts where the load is distributed throughout the length of the bolt (Carranza-Torres and Fairhurst, 2000).

Combined effect of support systems

If one or more support systems have been applied, their combined effects can be determined by adding the stiffnesses for each of the individual supports (Carranza-Torres and Fairhurst, 2000). This will increase the slope of the elastic part of the curve, as seen from Eq. 5.20. The combined stiffness of all installed support is assumed to be valid until one of the individual supports achieves its maximum possible elastic deformation. At this value of u_r^{max} the combined support is assumed to fail. Hence, the lowest value of u_r^{max} determines the maximum support pressure available for the individual supports acting together.

5.3.2. Limitations of CCM

The CCM is built on two major assumptions; i) uniform or hydrostatic stress conditions with constant magnitude, and ii) a circular tunnel cross-section (Carranza-Torres and Fairhurst, 2000). However, the reality is seldom as simple. For traditional tunnel excavations the cross-section are typically non-circular depending on the purpose of the tunnel, and the far-field stresses are generally unequal. For such conditions the loads will not be uniform, and bending moments will be induced in the support. Under such circumstances, the validity of the CCM should be assessed considering additional assumptions.

The in-situ stresses at a site depend on the geological history of the ground. As discussed in Sec. 3.1, world stress measurements indicate that the principal stresses are often unequal (see Fig. 3.1). Vertical stress measurements from regions around the world has given a best fit relation between vertical stress and depth:

$$\sigma_z = 0.027z \quad (5.25)$$

where σ_z is in MPa and z is the depth in meters. 0.027 correspond to the mean unit weight for silicates (in MN/m^3), a major component of many rocks (Carranza-Torres and

5.3 ANALYTICAL METHOD

Fairhurst, 2000). The horizontal component of the in-situ stress (σ_x) can be expressed as a function of the mean vertical stress:

$$k = \frac{\sigma_x}{\sigma_z} \quad (5.26)$$

As indicated in Fig.3.1, the magnitude of the horizontal stress vary between 0.5 and 3.5 of the mean vertical stress, although higher values have been observed (Carranza-Torres and Fairhurst, 2000). These data suggest that the in-situ stresses are often unequal, and that the vertical stress vary with the lithostatic gradient. The CCM can account for unequal stress conditions, if the uniform far-field stress input is taken as the average of the two stresses;

$$\sigma_0 = \frac{\sigma_z + \sigma_x}{2} \quad (5.27)$$

The validity of the CCM analysis for non-uniform stress conditions can be verified by checking the limiting stress ratio, k_{lim} . If the normal stress ratio is less than the limiting stress ratio ($k < k_{lim}$), it is shown that the mean radius of the plastic region around the opening and the mean convergence in the crown and sidewalls are comparable to that obtained by uniform CCM analysis (Fig.5.8a) left). However, for $k > k_{lim}$ the failure zone forms a 'butterfly' shape, and has no apparent relationship to the uniform loading analysis (Fig.5.8a) right). For $k > k_{lim}$ the conditions will be to variable to apply the CCM method (Carranza-Torres and Fairhurst, 2000).

The lower diagram in Fig.5.8 can be used for the verification of the level of k. This diagram applies to Mohr-Coulomb materials characterized by a friction angle ϕ and unconfined compressive strength σ_{ci} (linear failure envelope). For Hoek-Brown materials, an equivalent diagram can be constructed.

According to Carranza-Torres and Fairhurst (2000), the CCM can be used to provide a first estimate for the yield zone and convergence of the walls in non-circular tunnels. Within certain limits, an equivalent radius of the cross-section can be used:

$$R_{eq} = \sqrt{\frac{A_{cs}}{\pi}} \quad (5.28)$$

where A_{cs} is the area of the cross-section in m^2 . However, the authors do not propose an interval for the limit for which an equivalent radius would be valid. Given that the assumption for the CCM is a circular tunnel, it would be reasonable that the height to width ratio is close to one.

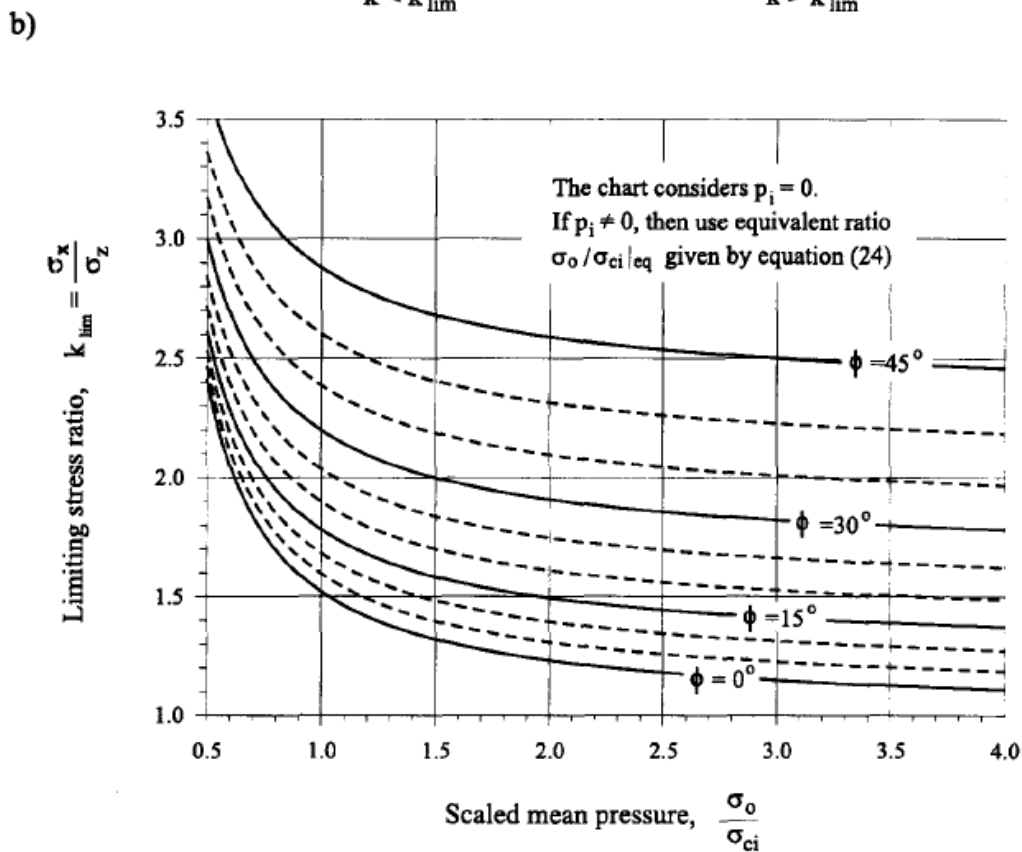
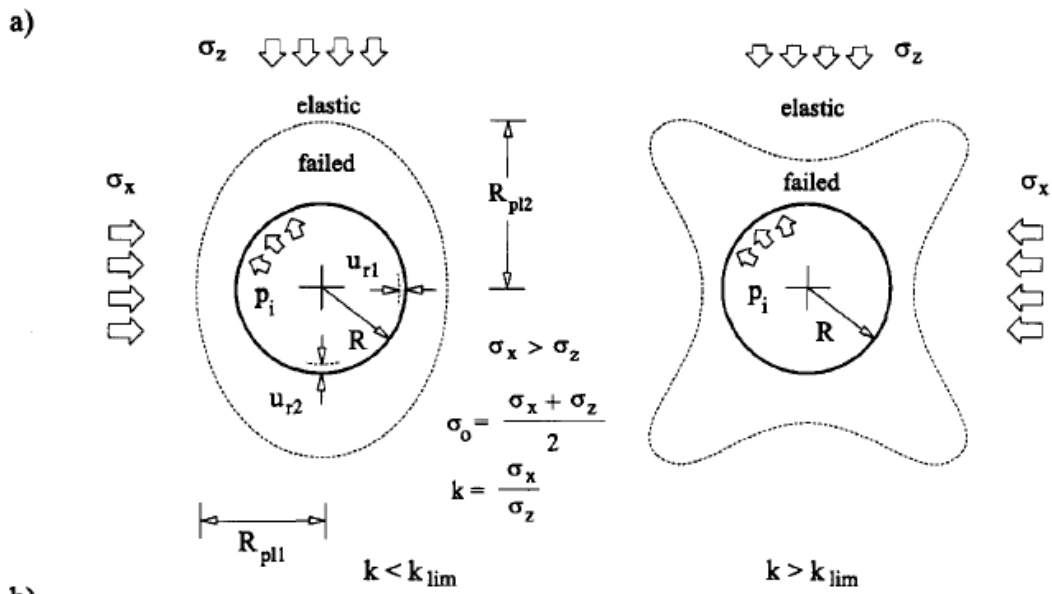


Figure 5.8.: a) A circular cavity in a Mohr-Coulomb material subjected to a uniform internal pressure and unequal far-field stresses. b) Limiting values of stress ratio k_{lim} as a function of scaled mean stress σ_o/σ_{ci} and friction angle ϕ (Carranza-Torres and Fairhurst, 2000)

5.4. NUMERICAL ANALYSIS

5.4.1. General

In rock engineering numerical modeling is mainly used for analyzing rock stresses and deformations. There is still no specialized program for analysis of the squeezing phenomenon, but there are programs which may be used for identifying and assessing the deformations around an excavation. The models may be used for comparison with results from empirical and analytical methods. The models may provide an even broader understanding and assistance for design purposes. In reality every ground condition is unique, and the complex interplays of the rock mass, support, layout and time cannot be fully reflected by models. However, numerical analysis has proven to be a helpful tool in the attempt to simulate reality. Since all analytical and empirical methods assume homogeneous material and simple geometry (circular), the numerical models have the clear advantage in allowing complex geology and specified layouts.

Numerical modeling often has the disadvantage of being time consuming, and will for a reliable analysis depend on numerous parameters. The advantages compared to other methods are still many and significant, including:

- allows complex geometry (i.e in-homogeneity, isotropy, groundwater, topography etc.)
- allows for inclusion of measurement and laboratory data
- quantitative analysis for rock mass, deformation, support etc.
- provides better understanding of mechanisms, both through quantitative values and qualitatively by visual effects/interpretations
- can be used to verify other simplified methods

The term “numerical modeling” means “discretization” of the rock mass into a large number of individual elements (Nilsen and Palmström, 2000). The way this is done, how the elements are treated in the calculation, are divided into two main categories:

Continuous models

Continuous model means that the rock mass is modeled as a continuous mass, and only a limited number of discontinuities may be included here (Nilsen and Palmström, 2000). This is the most commonly used category, and include 3 important methods: Finite Element Method (FEM), Boundary Element method (BEM) and Finite Difference Method (FDM). The most common programs include ABAQUS, ANSYS, PHASE2, PLAXIS2D/3D, FLAC3D etc.

Discontinuous models

Discontinuous models treat the rock mass as a system of individual blocks interacting along their boundaries, and therefore better represent the true nature of the rock (Nilsen and Palmström, 2000). The Distinct Element Method (DEM) is the most known method of this category, and is the basis for the program UDEC.

The world of numerical modeling offer many options for rock engineering, and the program should be chosen based on knowledge and purpose of the analysis. Often the analysis has the character of parameter study more than exact calculation with definite answers

(Nilsen and Palmström, 2000). For this reason it is recommended that the evaluation by an experienced engineering geologist is included in the interpretation. And equally important, that the user is aware and known to the limitations and assumptions behind the model.

The main objective for the numerical analysis in this study is to verify, assess and analyze the rock mass parameters, stresses and resulting deformations around the powerhouse cavern. This would be done by comparison to existing measured deformation in the cavern. Another element would be to verify the validity of the empirical and analytical methods, as well as the numerical model itself. For the analysis, the 2D finite element program *Phase²* by Rocscience was selected.

5.4.2. The *Phase²* program

Phase² is a 2-dimensional elasto-plastic finite element program for calculating stresses and displacements around underground openings (Rocscience, 2013). The program can be used to solve a wide range of mining, geotechnical and civil engineering problems, and is one of the most commonly used programs in rock engineering. The program is user friendly and easy to learn, operate and interpret. Some of the basic features offered in *Phase²* include (Rocscience, 2013):

- Elastic and plastic analysis
- Plain strain or axisymmetric analysis
- Constant or gravitational loading conditions, with load splitting
- Multistage excavations
- Multiple materials
- Jointed rock/construction joints
- Support analysis (bolts, concrete or shotcrete liners, reinforced liners etc.)
- Slope stability analysis

Phase² consists of three basic program modules; model, compute and interpret. The model is the pre-processing module used for entering and editing model boundaries, material properties, in-situ stresses, support etc. The model can be computed on a file, and then the interpretation can be initiated. Input parameters for the model, as well as possibilities for interpretation will be discussed below. For details about finite element computations and theory the reader is referred to the program documentation (Rocscience, 2013).

5.4.3. Input parameters for the model in *Phase²*

Input parameters for rock deformation analysis in *Phase²* include (1) loading conditions, (2) material properties, (3) support properties and (4) joint properties. The most important input features for loading conditions, materials and support are further explained below. Input options for joint properties, groundwater etc. can be found in the user manual for the *Phase²* software.

(1) Loading conditions

The loading conditions can be defined as constant field stress (3 components in MPa, and optional angle), or gravitational field stress. The option of gravity field stress defines a state of stress which varies with depth from a user-specified ground surface level. Gravity field stress is typically used for surface or near surface models at shallow depth, and where the effect of topography and/or tectonics influence the magnitude and direction of the stress. The stress ratio between vertical and horizontal stress is calculated by the Poisson's ratio. 'Locked in' stress can be included, and is estimated from the tectonic stress with two 'in plane' and 'out of plane' components.

(2) Material properties

Unit weight, initial element loading, strength properties (failure criterion), and elastic properties are the most important variable material input parameters for rock deformation analysis.

Initial element loading

The initial element loading can be defined as; 'none', 'body force', 'field stress' or 'field stress and body force'. For a constant field stress, the default is 'field stress', and will be equal to the defined constant stress. For gravity field stress, the default will be 'field stress and body force'. The body force represents the self-weight of the elements, and is derived from the unit weight of the material.

Strength properties

The strength properties allows for defining (i) the material type (elastic or plastic), and (ii) the failure criterion for a material.

(i) Material type

For the material type 'Elastic', the entered failure criterion parameters will be used for calculating and plotting of strength within the material (Rocscience, 2013). The failure envelope allows a degree of overstress to be calculated, although the material cannot 'fail'. The strength properties do not affect the analysis (i.e stresses and displacements are not affected).

For material type 'Plastic', the entered material parameters will be used in the analysis if yielding occurs. Depending on the failure criterion, residual properties and dilation factor for the material are defined. An 'ideally' elastic-plastic material is defined if residual strength parameters are equal to the peak parameters. (Rocscience, 2013).

(ii) Failure criterion

Seven different failure criteria is included in the software. Amongst the most commonly used criteria for rocks are Mohr-Coulomb, Hoek-Brown and Generalized Hoek-Brown. Input parameters for Mohr-Coulomb are cohesion, friction angle and tensile strength. The generalized Hoek-Brown criterion needs the intact rock strength (UCS) and the parameters m_b , s and a (see Sec.2.3.2 for details). The non-generalized Hoek-Brown assumes $a=0.5$. All plastic analysis require residual parameter values and dilation angle.

Elastic properties

The following elastic models can be defined; Isotropic, Transversely Isotropic, Orthotropic and Duncan-Chang Hyperbolic. Isotropic behavior is assumed for plastic analysis in *Phase²*. The elastic properties of an isotropic material is only defined by a single value of Young's modulus (E) and a single value of Poisson's ratio (ν). *Phase²* does not consider strain softening, but assumes an abrupt drop from peak to residual strength after failure (Fig. 5.9). A residual value of Young's modulus can be defined, and will be used in the analysis under the following conditions:

- Material yielding has occurred (peak strength envelope exceeded)
- After yielding, the material is subjected to a change in load state (i.e. unloading / reloading)

In effect; if the material yields but the load state is constant, the residual modulus will not be applied.

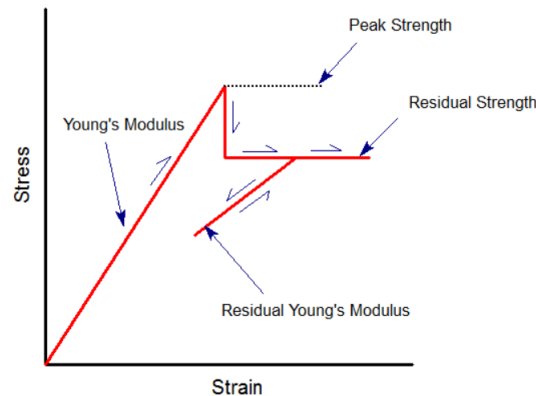


Figure 5.9.: Illustration of residual Young's modulus

(3) Support properties

Phase² has an inbuilt database for support modeling options for geotechnical and mining application. The support is grouped into two main categories; i) Bolts and ii) Liners, where the liner category can be used for many different types of support systems. The two categories are briefly presented here, and further discussed for the relevant analysis is Ch. 6.

i) Bolts

The following 5 bolt types can be modeled: End Anchored, Fully Bonded, Plain Strand Cable, Swellex / Split Set and Tiebacks. Depending on bolt type, different properties can be entered: bolt and borehole diameter, Young's modulus of the bolt steel, peak and residual tensile capacity, bolt pattern (staggered grid not possible), pre-tensioning force, shear properties etc. For further description see the *Phase²* documentation. It is important to notice that the different bolt types have different failure mechanisms.

5.5 CONCLUDING REMARKS ON SQUEEZING ANALYSIS

ii) Liners

Liner support can now be used to model simple liners (e.g. a single layer of shotcrete), reinforced concrete, composite liners (e.g. liners consisting of multiple layers of material), pile walls (e.g. a structural beam element with a joint on both sides) etc. For the more traditional excavations in rock, simple liners, reinforced concrete and composite liners are most relevant. For reinforced concrete, the properties can be defined to respond to flexural, axial and shear loads. The properties of the reinforcement and concrete are defined separately. Composite liners are defined as layers with the properties of each liner layer (up to 4 layers).

5.4.4. Interpretation of results

The interpretation of data will depend on the intended use of the analysis. For elastic analysis, it is possible to display the strength factor of the rock mass with contours. If the strength factor is greater than 1 everywhere around the tunnel, the results will be the same for plastic analysis. If the strength factor is less than one (elastic failure), plastic analysis should be performed. For plastic analysis it is possible to visualize and display stress trajectories, yield in rock mass and support, support capacity of reinforced concrete, location and progress of vertical, horizontal and total displacements etc. Displacement profiles along the excavation boundary can be used to compare the model results to measured cavern deformation, both from extensometer points and convergence. Sensitivity analysis and calibration of the model to estimate stress conditions and rock mass properties are possible when the deformation is known.

5.5. CONCLUDING REMARKS ON SQUEEZING ANALYSIS

Empirical and semi-analytical methods can primarily be used to find the the extent of squeezing. Empirical methods are based on experiences from numerous underground projects. The geometrical features of discontinuities and other parameters of the rock mass cannot be represented in the support charts (Shrestha, 2006). A good understanding of the geological conditions of the rock mass is a prerequisite of using the empirical methods.

The method by Hoek and Marinos (2000a) includes support pressure, but as emphasized out by the authors themselves; their methodology does not provide a final design for the tunnel excavation sequence and support system. The CCM is the only method, besides numerical modeling, that consider the interaction between rock mass deformation and installed support. However, the methods is constraint by many non-realistic assumptions, making the method limited for design purposes.

The empirical and analytical methods are developed for circular tunnels. The Q-method does not directly depend upon the dimension of the opening, and makes it applicable to all underground structures. However, the degree of squeezing depends upon the size and shape of the excavation. This non-dependency is therefore an advantage as well as a limitation of the Q-system. In this regard, numerical modeling show as the the most applicable option for analysis of large scale caverns, as few limitations are set for the geometry of the excavation.

6. SQUEEZING ANALYSIS

6.1. GENERAL

As presented in the previous chapters, the main challenge for the NJHPP cavern is squeezing deformation. The methods reviewed in Ch. 5 will be applied for 5 selected cavern sections, and compared to the measured deformations presented in Ch.4. The rock mass parameters provided by NJC (2011a) summarized in Ch.4 were used for the assessment of rock mass quality and strength. Rock mass parameters were estimated according to the theory presented in Ch.2, and evaluated in comparison to previous project work (Vestad, 2013).

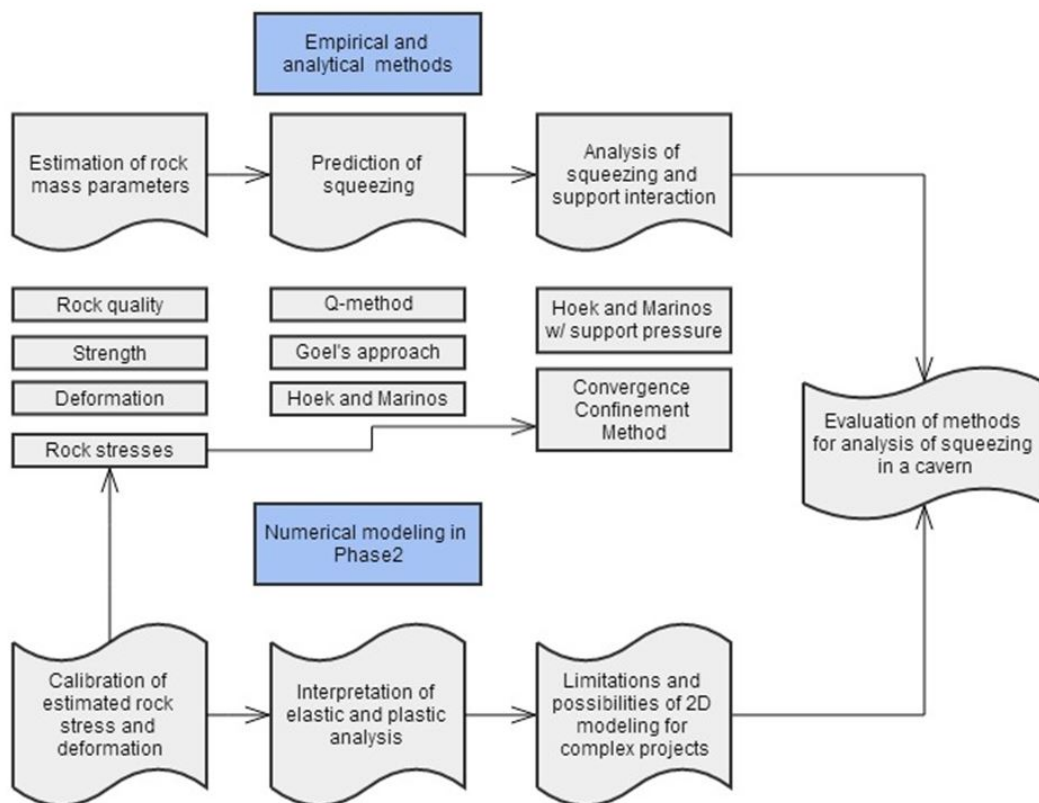


Figure 6.1.: Overview of performed analysis

Mudstone and siltstone was treated as one unit for all analysis. The rock mass properties were estimated as the mean of the two units. The two geologic layers are difficult to distinguish in reality, and the site descriptions imply that they behave relatively similar. As the jointing of the rock mass is more determining for its behavior than the intact rock strength or grain size, this simplification was regarded as valid for the complete analysis.

The empirical methods were applied using the estimated rock mass parameters, and the results compared to the measured deformations. Based on the comparison, the applicability and sensitivity of the methods with regard to analysis of deformations in large scale caverns could be assessed.

The CCM was applied using the same rock mass parameter inputs as for the empirical methods. The applied stress was selected after *Phase*² calibration to find the best fitted

horizontal stress conditions. Extensive analysis using CCM was done to properly evaluate the sensitivity of the method. The support pressure estimated by CCM was used for analysis with the semi-analytical method by Hoek and Marinos (2000).

Numerical modeling in *Phase²* was performed using the same rock mass parameters as for empirical and analytical methods. Plastic analysis with support was used to evaluate the rock mass deformability and stress conditions to find the best representation of the actual deformations. Unsupported elastic analysis and plastic analysis for unsupported ground was assessed. The overall correlation to measured deformations for all sections was evaluated, and the yield of support assessed.

Adjusting the rock mass strength parameters in *Phase²* to find the best correlation to the measured deformations was not done for two reasons. Firstly, this was regarded as too extensive for thesis work. Secondly, the objective of the study was selected so as to best evaluate the applicability of the methods with regard to the “known” parameters. When designing a cavern, a set of rock mass parameters will be available from laboratory and field work. The analysis of deformations will be performed before the excavation has commenced, so that the proper support can be designed. It was therefore regarded as most appropriate to apply the rock mass parameters available to the engineers before excavation of the cavern. Only a few adjustments were done, discussed in the next section.

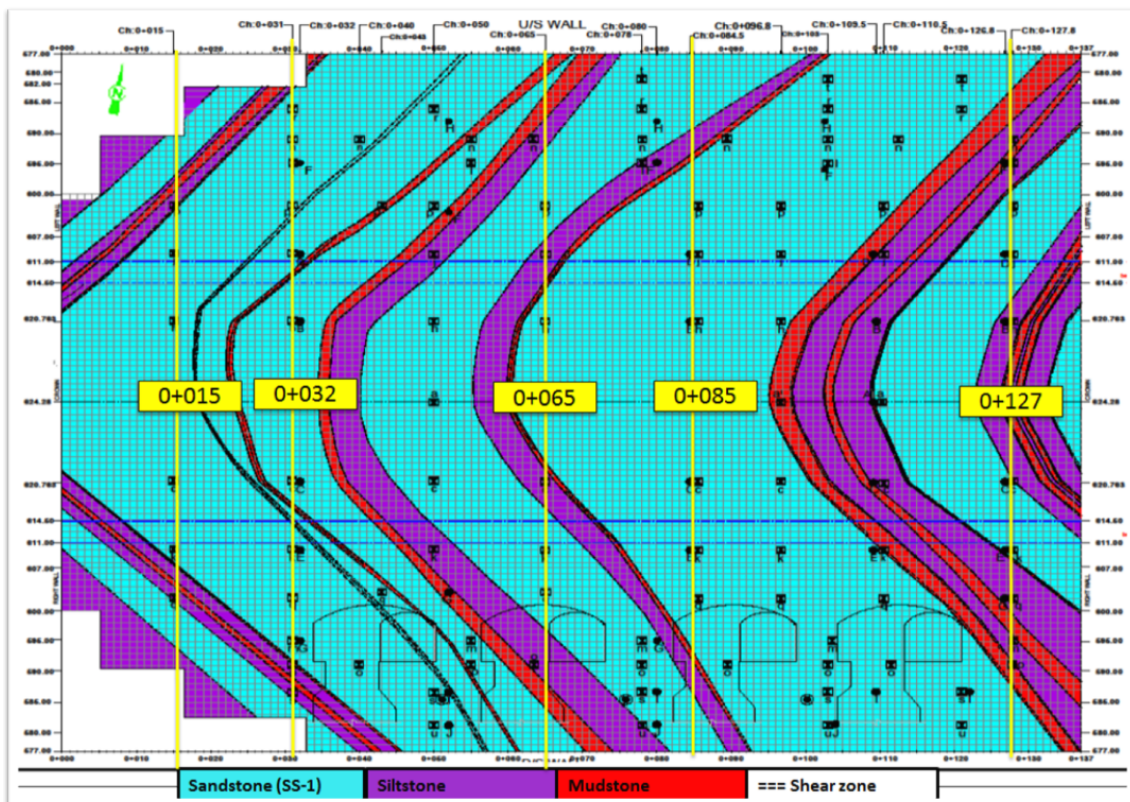


Figure 6.2.: Selected sections for the analysis

6.2. INPUT DATA

6.2.1. Selected sections for the analysis

Since the overburden and geologic conditions are relatively consistent in the cavern, the sections were mainly selected based on the quality and amount of available deformation data. A representative selection based on location in the cavern was also emphasized.

The 5 selected sections are shown in Fig.6.2. Section 0+065 was included for the reason of having the highest deformation. Some notable differences between the selected sections include:

- All sections have different cross-sectional area. The bottom floor elevation is higher for ch. 0+015 and 0+032 than for the other sections. Ch. 0+065 and 0+085 both intersect the bonneted gate niches on the downstream wall.
- Considerably more mudstone and siltstone is observed for section 0+127
- The reported shear zone intersect section 0+032 and 0+065. At section 0+065, the shear zone intersect in the top/middle cavern wall.
- Different distance from the end-walls. Ch. 0+127 is 10 m from the east end-wall.

6.2.2. Estimation of rock mass quality

Considering the significantly high measured deformations, the rock mass quality rated by the NJC (2011a) was regarded as too high (see Sec.4.3.3). New GSI, Q- and N-values were therefore estimated in discussion with supervisor (Panthi, 2014a). Determination of the parameters for the Q-system is given in App.A.4.

According to Norplan A/S (2013b), J_w and SRF are both 1 for the powerhouse cavern, so the rock mass rating N and Q-value will be equal. $J_w=1$ corresponds to minor or no inflow, meaning the water inflow for the sections with observed dripping is less than 5 l/min locally. RQD was estimated based on the 4 available cores in the area (borehole core 9-12 in App.E.1). RQD for sandstone was set to be 50-60, while for the sections including mudstone RQD=30-40 was assumed. Based on Fig.4.13 it was concluded with $J_n=9$ (3 fracture sets). According to NJC (2011a), the joints in sandstone appear rough and planar, corresponding to $J_r=1.5$. The joints in mudstone are assumed smooth and undulating, with $J_r=1$. The final parameter, joint alteration coefficient J_a , was assumed to vary based on appearance of mudstone in the sections. For sections in only sandstone the value is believed to be around 2-3, corresponding to slightly altered joints with little to no non-softening infill. For sections with intersecting mudstone layers, the value was set higher, believably around 5-6 (Panthi, 2013b).

Minimum and maximum Q- and N-value was estimated based on the assumptions above, as given in Tab.6.1. The GSI was estimated using the formulas by Barton (2002) (Eq. 2.8 and Eq. 2.9) using the estimated Q-values, and further discussed together with supervisor (Panthi, 2014a).

Table 6.1.: Estimation for rock mass quality ratings

Rock type	Q- and N- value			GSI		
	Min	Max	Mean	Min	Max	Mean
Sandstone SS-1	2.7	5	3.9	51	55	54
Mudstone/siltstone	0.6	0.9	0.75	41	44	43

6.2.3. Estimation of rock mass parameters

Rock mass strength and rock mass deformability was estimated based on empirical formulas presented in Ch.2.

Rock mass strength

The rock mass strength was estimated using the relationships by Hoek et al. (2002) and Panthi (2006), as given in Tab.2.2. For the estimation by Hoek et al. (2002) the GSI values from Tab.6.1 were used, and the parameter m_i was quoted from the standard chart in App.A.1. According to results during project work, the relation by Panthi (2006) was found to show the highest correlation with the actual deformations, when applied to the empirical and semi-analytical methods (Vestad, 2013). Back calculation from the measured deformations using Hoek and Marinos (2000) with support pressure indicate that the rock mass strength estimated by the relation by Panthi (2006) vary in the same interval (Vestad, 2013). The estimated rock mass strengths are given in Tab.6.2.

Rock mass deformability

The rock mass deformability is needed for the numerical analysis in *Phase*². The rock mass deformability was estimated using two of the relations presented in Tab.2.3; Hoek et al. (2002) and Panthi (2006).

Table 6.2.: Estimated rock mass strength and deformability

Relationship by	Rock mass strength, σ_{cm} [MPa]		Rock mass deformability, E_{rm} [GPa]	
	Hoek et al. (2002)	Panthi (2006)	Hoek et al. (2002)	Panthi (2006)
Sandstone SS-1	2.57 ± 0.32	13.39 ± 2.51	7.02 ± 0.44	8.98 ± 0.56
Mudstone/Siltstone	0.67 ± 0.11	6.67 ± 1.70	2.93 ± 0.25	4.17 ± 0.35

6.2.4. Estimation of support

The support pressure for the installed support had to be estimated for the analysis with Hoek and Marinos (2000a) and for the CCM. The CCM defines the support pressure in the construction of the SCC. The relations presented in Sec.5.3.1 were used for estimation of the combined support pressure. The theory presented by Carranza-Torres and Fairhurst (2000) is the same as recommended for estimation of support pressure for support in weak rocks by Hoek (2007d). The combined support pressure from plain strand cables, rock bolts and shotcrete was estimated.

The available method only provides relations for estimation for plain shotcrete and ungrouted bolts, limiting the representation of the actual installed support. The formulation

6.2 INPUT DATA

for shotcrete assumes a closed ring lining with no reinforcement, which is not the case for the installed shotcrete at NJHPP. The relation for mechanically anchored bolts assumes that the reaction forces developed by the bolt are concentrated at the ends of the bolt. According to Carranza-Torres and Fairhurst (2000), this formulation for rock bolts should not be used for grouted bolts where the load is distributed through the length of the bolt. According to Lie (2011), results of pull-out tests by Stillborg (1994) indicate that grouted bolts might decouple from the grout in a limited length close to the loading point. The stiffness of grouted bolts is associated to the length of the decoupled section rather than the whole length of the bolt.

Lie (2011) presents a formulation for the estimation of the stiffness of grouted bolts. This requires the input of the length of the decoupled bolt section. Since this was not known, using this formulation was regarded as just as uncertain as the standard relation for mechanically anchored bolts. The standard relations presented by Carranza-Torres and Fairhurst (2000) were therefore applied. The assumed support properties were decided in conversations with Norplan A/S (2013b), and are summarized in Tab.6.3.

Table 6.3.: Support properties

End anchored bolts		Plain Cables		Plain Shotcrete	
Bolt length, l	7 m	Cable Length, l	15 m	Thickness, t_c	250 mm
Bolt Diameter, d_b	25 mm	Cable Diameter, d_b	60.9 mm	Young's Modulus, E_c	20 GPa
Bolt Modulus, E_s	205 GPa	Cable Modulus, E_s	205 GPa	Poisson's ratio, ν	0.25
Tensile Capacity, T_{bf}	0.25 MN	Tensile Capacity, T_b	1.325 MN	Compressive strength, σ_{cc}	20 MPa
Bolt spacing	1.2m \times 1.2m	Cable Spacing	A: 5m \times 5m B: 4m \times 4m		

The combined support pressure was found by the added stiffness of the 3 support types, and limited by the maximum allowable displacement of the shotcrete (lowest allowable displacement). The details of the calculation is given in App.C.4, and will be further discussed in Sec.6.4.4. The estimated combined support pressure for each section is given in Tab.6.4.

6.2.5. Summary of input parameters for selected section

For section 0+127 mudstone is the predominant rock type, so mudstone/siltstone properties were used for this section. For section 0+065 the mean of the two was used. For the other sections, sandstone properties were assumed.

Table 6.4.: Summary of input parameters for each section

Section	Overburden [m]	Dominant rock type	Max. Measured Def. [mm]	Eq. tunnel radius R_{eq} [m]	Rock mass strength σ_{cm} [MPa]	Support pressure p_s [MPa]
0+015	420	SS-1	61	14.7	13.4 \pm 2.5	0.38
0+032	420	SS-1	155	18.2	13.4 \pm 2.5	0.33
0+065	420	SS-1/Mud/Silt	282	21.6	10.1 \pm 2.1	0.30
0+085	420	SS-1	158	21.5	13.4 \pm 2.5	0.30
0+127	450	Mud/Silt	100	18.7	6.8 \pm 1.7	0.33

6.3. PREDICTION OF SQUEEZING

6.3.1. Prediction of squeezing using empirical methods

The empirical methods were used to assess the potential for prediction of squeezing in the cavern. The semi-analytical method by Hoek and Marinos (2000) without support pressure was also included in this part of the analysis. Only the results using the rock mass strength estimated with the relation by Panthi (2006) will be discussed. This is justified on the basis of previous analysis using σ_{cm} estimated by Hoek et al. (2002), which showed to greatly underestimate the strength of the rock mass (Vestad, 2013). The prediction of squeezing for the 5 sections are summarized in Tab.6.5. Detailed calculations are presented in App.C.1.

Table 6.5.: Squeezing prediction according to Geol (1994), Q-method and Hoek and Marinos (2000a)

Section	In-situ stress [MPa]	N and Q	Goel (1994)		Q-method		Hoek and Marinos (2000)	
			HB ^{0.1}	Prediction	P ₀ /σ _{cm}	Prediction	Strain (%) without support	Prediction
0+015	11.25	2.7 – 5	589	Moderate	0.84 ±0.16	No (Mild)	0.14±0.06	Few stability problems
0+032	11.25	2.7 – 5	602	Moderate/High	0.84 ±0.16	No (Mild)	0.14±0.06	
0+065	11.25	0.75 – 3.9	612	High/Moderate	1.12 ±0.24	Mild	0.25±0.11	
0+085	11.25	2.7 – 5	612	Moderate/High	0.84 ±0.16	No (Mild)	0.14±0.06	
0+127	12.10	0.6 – 0.9	646	High	1.79 ±0.47	Mild	0.64±0.35	

The approach by Goel is the most conservative, and predict moderate to high squeezing for the whole cavern. Sections dominated by sandstone is predicted to have moderate squeezing, while the east-end dominated by mudstone and siltstone was predicted to experience high squeezing. The Q-method and Hoek and Marinos (2000) predict that the cavern should experience no to mild degree of squeezing, with few stability problems.

In reality there have been experienced problems while constructing the cavern and the design had to be reviewed several times. The pre-tensioning of the support was changed during construction, and heavier support was added for the mudstone/siltstone dominated sections. This considered, the prediction by Goel (1994) can be said to be best fitted to predict the actual conditions.

6.3.2. Discussion of applicability of the empirical methods

Prediction by the Q-method and Hoek and Marinos (2000) are both highly dependent on the quality of the estimated rock mass strength. The methods are only as precise as the estimated rock mass strength, making the rock mass strength estimation the most critical element of the prediction.

Theoretically the method by Goel (1994) depends on 7 parameters; the 5 included in the evaluation of rock mass number N, overburden and tunnel diameter. However, for projects with considerable overburden, the method will almost regardless of rock quality result in squeezing. This major sensitivity to rock cover limits the value of the method, as the

6.4 ANALYSIS OF SQUEEZING

prediction basically can be done by just looking at overburden depth. For an experienced geologist, knowing the overburden and occurrence of weak rock will in either case be argument enough for conducting more extensive analysis.

For prediction of squeezing in a cavern, the Q-method has the advantage of being independent on excavation geometry. However, the degree of squeezing is influenced by the size of the excavation. This non-dependency is therefore an advantage, as well as a limitation. Both the method by Goel, and Hoek and Marinos, depend on the tunnel dimensions, such that for a cavern an equivalent tunnel radius has to be assumed. This is not realistic, as the shape of the plastic zone as well as the degree of squeezing will be different for a cavern with height/width ratio different from 1.

Comparing the results from Hoek and Marinos (2000) is difficult, as the method evaluates squeezing based on strain. Estimated percentage strain depends on the tunnel diameter. For a large scale cavern, the evaluation of deformation is misguided when discussing strain. For large dimensions the weak rock will fail much before the calculated strain will reach alarming values. For the NJHPP cavern, the deformations transformed to strain all lie below 1 %, which in the definition by Hoek and Marinos (2000) is characterized as non-squeezing conditions. The deformations relative to the equivalent diameter of the cavern are too low, and the deformations in the walls should in reality be related to the width of the cavern. In either case, the dimensions in a cavern are so large that the rock would completely fail before the calculated strain would become as high as to predict stability issues.

6.4. ANALYSIS OF SQUEEZING

The analysis of squeezing was performed using Hoek and Marinos (2000) with support pressure, and with the CCM suggested by Carranza-Torres and Fairhurst (2000). The results from Hoek and Marinos (2000) will be presented and discussed in the first section. The CCM analysis will be presented in sections depending on the part of analysis, and an overall discussion of applicability will be presented in Sec.6.4.5.

6.4.1. Hoek and Marinos (2000) with support pressure

The results of the analysis using Hoek and Marinos (2000a) with support pressure changed the percentage strain for section 0+127; from 0.64% without support to 0.60% with support pressure. The strain for section 0+065 was reduced by 0.01% with support. For the other three sections, the results were unchanged (see Tab.6.5). The details for the calculation are given in App.C.2.

For comparison to the measured deformations, the radial wall deformation was calculated using the equivalent tunnel diameter (Fig.6.3). For all sections excluding 0+127, the method underestimates the deformation. The maximum calculated deformation for section 0+015 is the only result close to the measured deformation. The largest deviation is found for chainage 0+127, the only section where mudstone/siltstone was assumed. In general the method could not reflect the deformation characteristics of the cavern.

Radius of the plastic zone was calculated using Eq.5.4. The size of the plastic zone was smallest for section 0+015, with a diameter of 33 m. The largest diameter of 63 meters

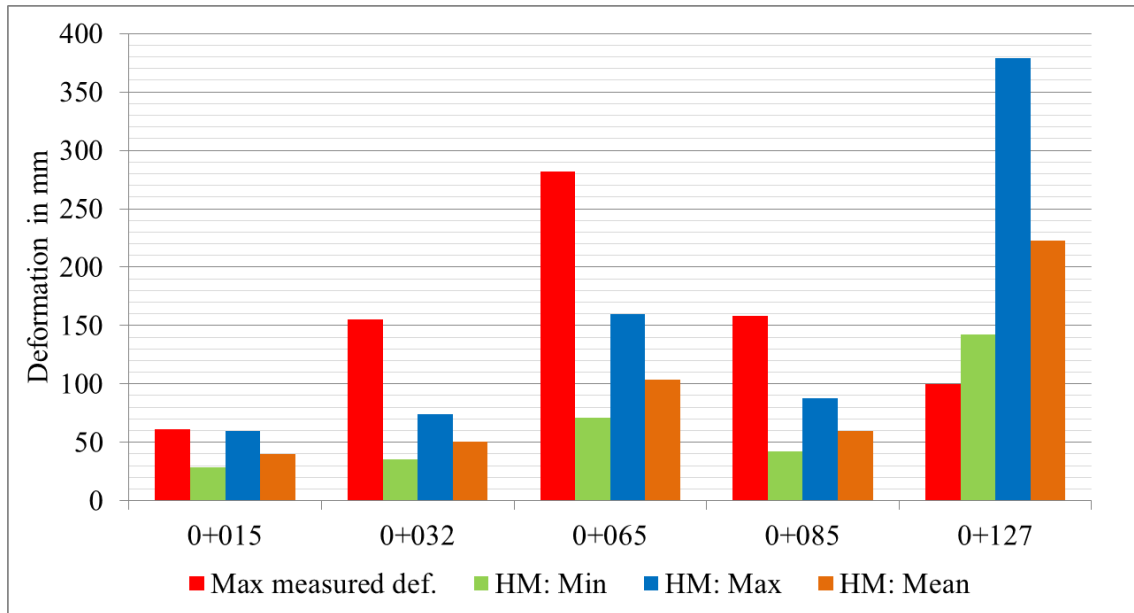


Figure 6.3.: Deformation by Hoek and Marinos compared to measured deformation

was found for section 0+127. The extensometer data indicate a plastic zone less than 25 meters. The results for section 0+015 is therefore in the correct range, while as for the other sections the radius is slightly overestimated.

Arguments for the applicability of the method are much the same as for the method applied without support. The dependency to quality of the rock mass estimation is the most critical part of the analysis, as well as the estimation of support pressure. On the other hand, the quality of the estimated rock mass strength is an uncertainty in basically all rock mechanical analysis. Still, this sensitivity is emphasized in Hoek and Marinos (2000) as rock mass strength is one of the two key input parameters.

For prediction of squeezing in a cavern where support is not yet designed, the method could potentially be used for evaluation of the necessary precautions (see Sec.5.2.3). A limited strain can be decided, and necessary support pressure can be estimated. However, as discussed in the previous section, the rock mass in a large scale caverns would fail much before the calculated strain predict failure. The method is designed for circular tunnels with limited cross-section, and defined based on strains experienced in smaller tunnels. This makes the suggested classification by Fig.5.3 and Tab.5.2 futile.

Based on the analysis presented here, the method by Hoek and Marinos (2000) is concluded to be little applicable for analysis of large scale caverns. The potential and degree of squeezing would due to the large dimensions not be represented by the classification suggested in the method.

6.4.2. CCM: Longitudinal displacement profiles

The Longitudinal Displacement Profile (LDP) determines the ground behavior as a function of distance to the advancing face. The LDPs were constructed using the method proposed by Carranza-Torres and Fairhurst (2000), and the updated version by Vlachopoulos and Diederichs (2009) (see Sec.5.3.1). Additionally, the method was applied considering

6.4 ANALYSIS OF SQUEEZING

both vertical stress and mean stress. To account for the excavation progress, analysis of deformation for the top two benches (above the bulleted gate niches) was performed. In total, the method was applied so as to evaluate the variation with stress condition, rock mass conditions and excavation progress (smaller cross section). The assumed input parameters for the analysis are shown for the detailed calculations in App.C.3.

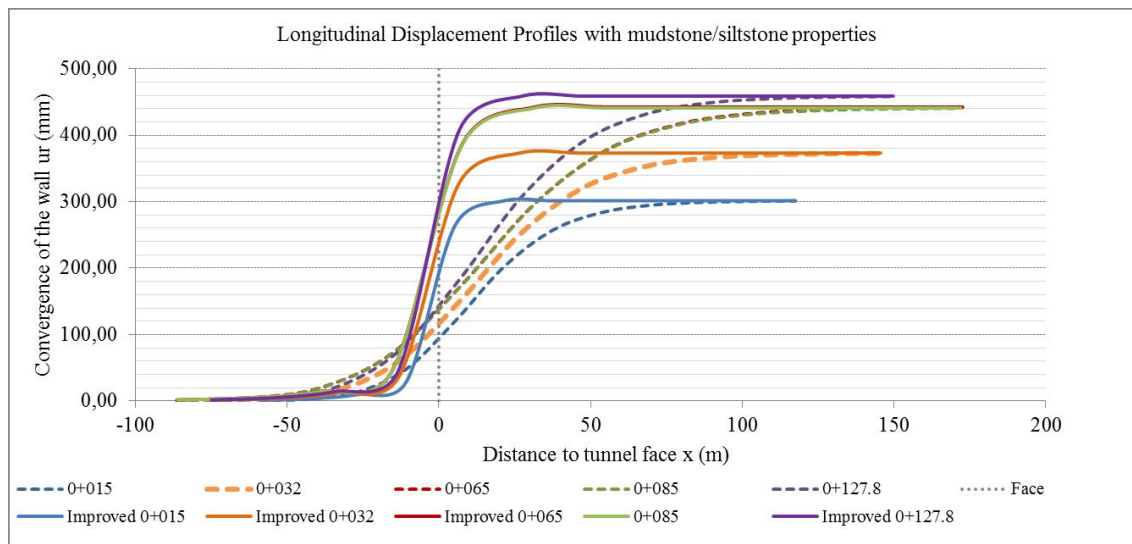


Figure 6.4.: Original LDP and improved LDP for the 5 sections

Fig.6.4 shows the LDPs for the 5 sections, constructed with the initial LDP relationship by Carranza-Torres and Fairhurst (2000) and the improved LDP by Vlachopoulos and Diederichs (2009). The vertical stress was used for the field stress. The motivation for the improved LDP is that a larger cross-section will influence the size of the plastic zone, hence influence the progress of deformation in the rock mass. This effect is clearly reflected in Fig.6.4; the improved LDPs are much steeper than the originals. A larger portion of the deformation will occur ahead of the face, as the large cross-section will produce a much larger radius of the plastic zone. About half of the total deformation will occur ahead of the face. Given the large cross-sectional area for the cavern, only the improved LDP will be discussed further.

The CCM can in practice only consider one type of rock condition per section. For this reason, construction of the longitudinal displacement profiles was done for both sandstone and mudstone/siltstone properties to show the potential variation for the sections. Another possibility would be to estimate mean rock parameters for each section. However, it was decided that the uncertainty in the analysis was better displayed by constructing LDPs for mudstone/siltstone and sandstone separately.

Fig.6.5 shows the improved LDPs for all sections, with either mudstone/siltstone or sandstone properties. The resulted deformation is highly dependent on rock type; for sandstone the deformation is maximum 40 mm for sections 0+065, 0+085 and 0+127; while the same sections will have almost 460 mm convergence if only mudstone/siltstone properties were used. The highest deformation will occur at section 0+127, which are caused by the slightly higher overburden (higher vertical stress). It can also be seen that the

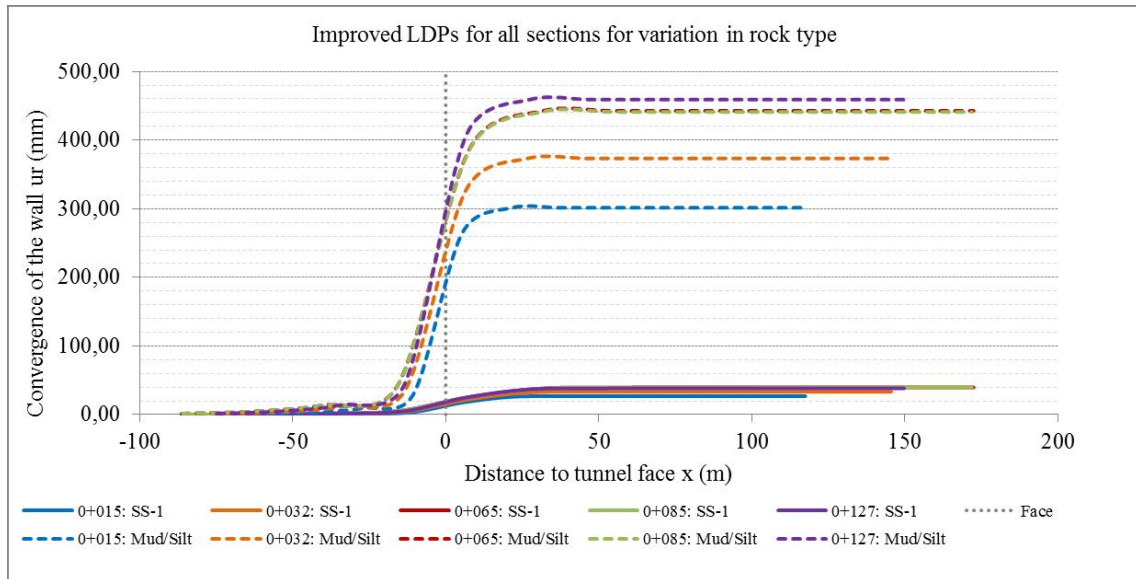


Figure 6.5.: Improved LDPs for variation in rock type

deformation for section 0+065 and 0+085 is almost equal, due to approximately same equivalent tunnel radius. For all sections, the measured deformations are between what is predicted by the CCM for sandstone and mudstone/siltstone. This is reasonable given that both rock types occur in all sections. It is clear that only assuming sandstone highly underestimates the deformation, while only considering mudstone/siltstone highly overestimate the convergence for all sections.

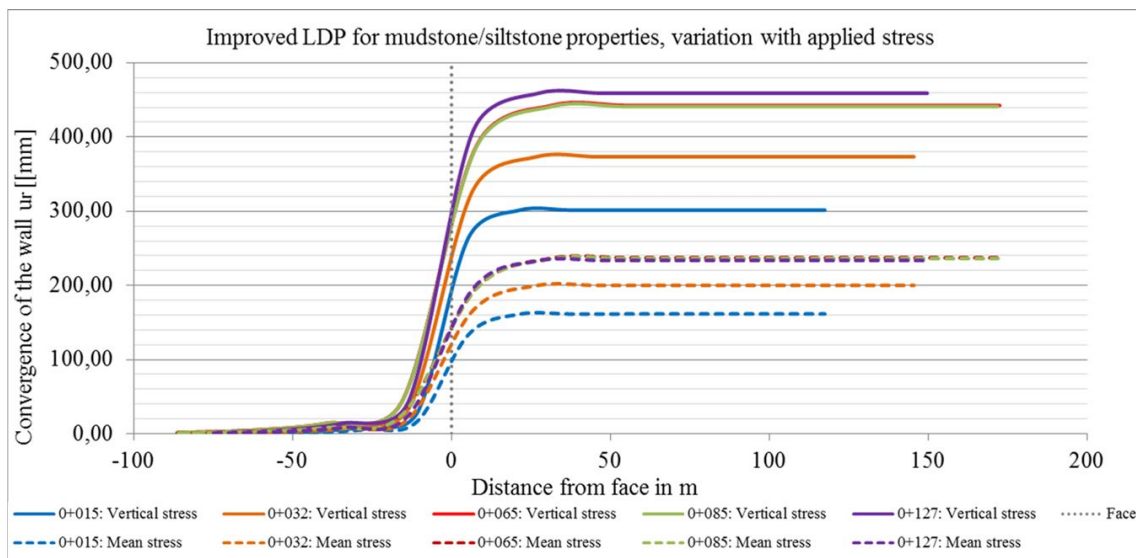


Figure 6.6.: Improved LDPs with variation to applied stress

The LDPs were constructed for two types of field stress; vertical stress or mean stress. The mean stress was calculated by Eq. 5.27, using the calibrated horizontal stress from numerical analysis (see Sec. 6.5.3). The stress ratio k was found less than the limiting

6.4 ANALYSIS OF SQUEEZING

stress ratio k_{lim} for all sections, so applying mean stress is valid for the complete analysis. Fig.6.6 show the results for mudstone/siltstone properties, with variation to applied stress. Using the mean stress greatly reduce the total resulting deformation, as well as reducing the slope of the profile. The deformations when using mean stress is closer to the actual measured deformations for all sections, if assuming mudstone/siltstone properties.

The LDP for the top two benches will be the same for all sections, as the shape of the cavern is the same above the elevation of the niches. Slightly higher deformation is found for section 0+127, caused by the somewhat increased overburden. As for the other LDPs, about half of the total deformation will have occurred ahead of the face. The total deformation for the top two benches can be seen in Fig.6.7.

6.4.3. CCM: Comparison to measured deformation

The total deformation from the CCM analysis compared to the measured deformations are shown in Fig.6.7. The CCM results presented here are for unsupported ground, while the measured deformations are recorded after installation of the support. Therefore the deformation by CCM should be expected to be higher than the measured.

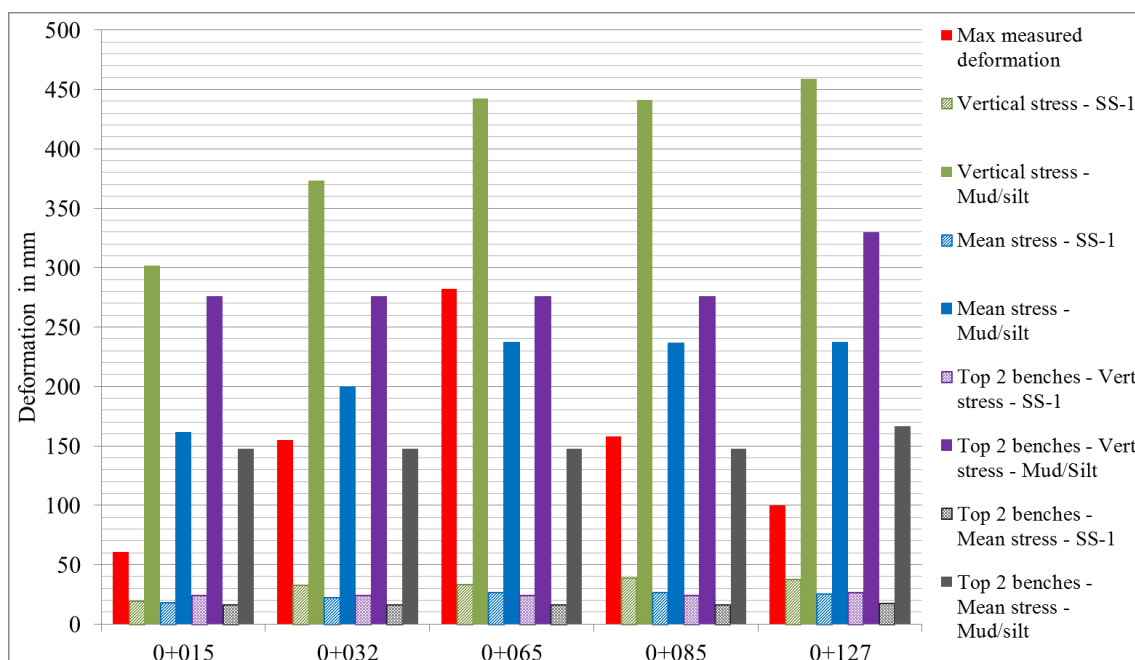


Figure 6.7.: Total deformation from CCM compared to measured deformation

What becomes evident is that assuming only sandstone would lead to a gross underestimation of the deformation for all sections. Considering the stress conditions, it is clear that applying only vertical stress leads to a major overestimation of the deformation, when assuming only mudstone/siltstone. Applying mean stress conditions for mudstone/siltstone properties seem the best fit for all sections, excluding 0+065 (underestimated by about 50 mm). The largest deviation is seen for the end-sections 0+015 and 0+127, which are influenced by the face-effect. For sections 0+015 and 0+127, the CCM resulted in higher deformation than measured also for the top two benches with mudstone/siltstone proper-

ties. In general, about 2/3 of the deformation will already have occurred for the top two benches, compared to the full profile CCM analysis.

For evaluation of the face-effect, the deformation at the actual distance from the end-walls was plotted for each section with mean stress and mudstone/siltstone properties (Fig. 6.8). Considering the LDP at 10 m behind the face, section 0+127 would have deformed about 105 mm (close to the maximum measured). For section 0+015, the CCM predicts 30 mm more than measured deformation. For section 0+032 and 0+065 the convergences were underestimates by 10 mm and 70 mm respectively. According to the analysis, excavating the top two benches would result in more than 3/4 of the total deformation for all sections. At this stage during excavation the measured deformations were considerably less.

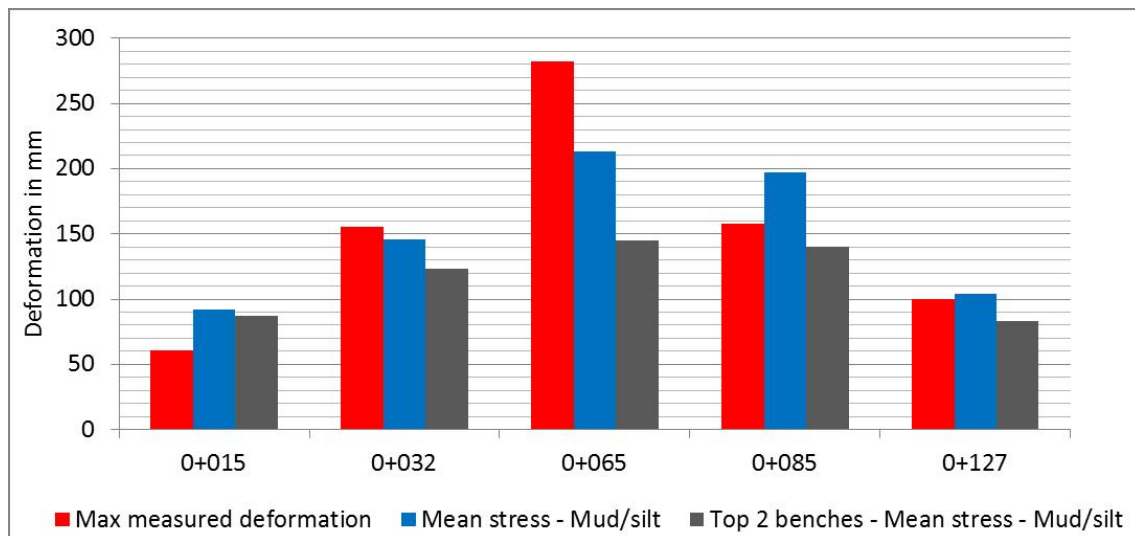


Figure 6.8.: Deformation at correct distance from the end-walls

In general, analyzing the LDPs at the actual distance from the face gave an overall better representation of the true deformation pattern. However, the magnitude of the deformations is less than the actual deformation for the middle sections of the cavern. On the other hand, the deformations at 0+032 and 0+065 are unexpectedly high, and as explained the rock mass may here be more fractured and influenced by water. These factors were not considered in the CCM analysis.

The CCM predicts the radius of the plastic zone to be between 40-60 m, depending on the equivalent radius of the section. This is unreasonably high compared to the extensometers, which indicate a plastic region less than 25m.

6.4.4. CCM: Ground and support interaction

As explained in Sec.5.3.1, the CCM can be used to analyze the interaction between rock and support, by constructing the GRC and the SCC. The full profile GRCs for all sections with assumed mean stress is shown in Fig.6.9. It can be seen that for sandstone properties, the rock will deform elastically for almost the entire deformation profile. For the mudstone/siltstone profiles, the ground will deform elastically until about 25 mm deformation is reached. At the face, the CCM predicts that about 70 mm deformation has already occurred.

6.4 ANALYSIS OF SQUEEZING

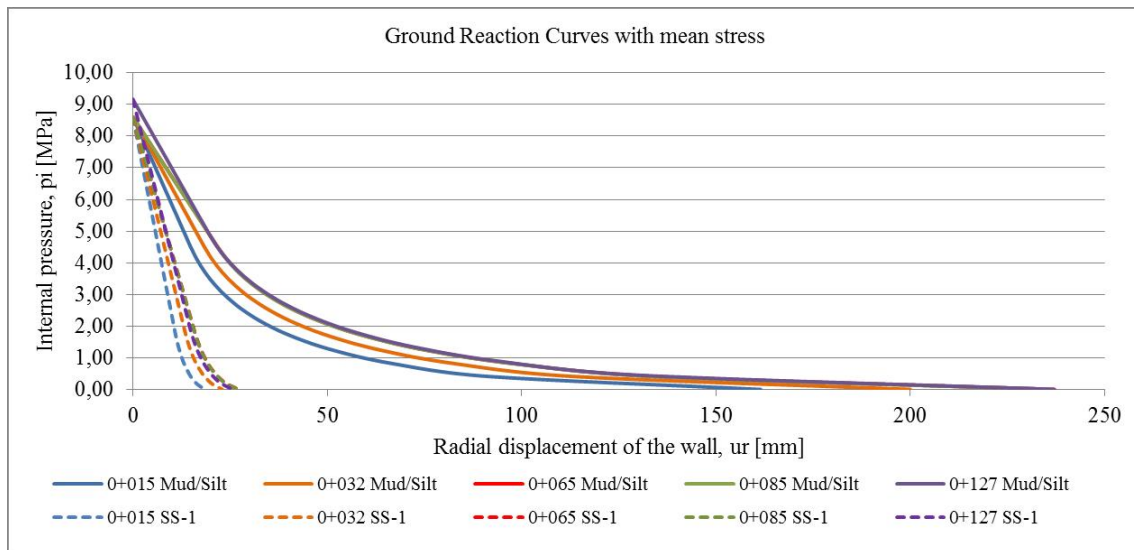


Figure 6.9.: GRC for all sections with applied mean stress

SCC was constructed for all sections, but will be discussed based on the results for section 0+085. Chainage 0+032 and 0+085 seem to be the sections best represented by applying mean stress for assumed mudstone/siltstone properties. The CCM predicts about 50 mm more deformation than measured, which in theory would be reasonable for unsupported ground. Section 0+085 is also sufficiently far from the end-walls, and is believed to be little influenced by the face-effect (2 cavern heights from the end-wall). However, it should be noted the 0+085 profile includes part of a bulletted gate niche.

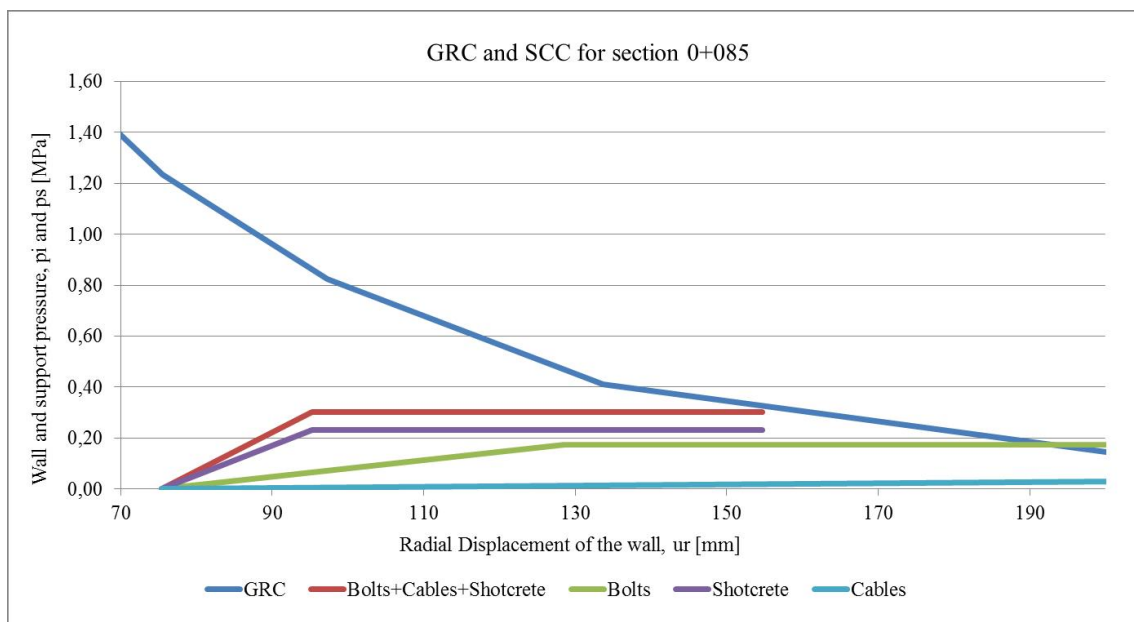


Figure 6.10.: GRC and SCC for section 0+085, for support installed 5m behind face

Fig.6.10 show the SCC for all three support types and the combined support, installed 2 m behind the face (the GRC starts at face). As the maximum support pressure estimated

by the SCC was 0.30 MPa, the CCM predicts failure of the support unless it is installed over 25 m behind the face. Here the ground would already have deformed by over 140 mm. The measured convergence for section 0+085 is at maximum 158 mm. Compared to this, the SCC and GRC do fit quite well considering.

Regardless, the assumption behind this result do not fit the reality: the actual support was installed immediately after opening of the face. In reality the support and rock have deformed together from time of installation, and only some downfall of shotcrete has been observed in the cavern. Considering the practical installation of the support, the CCM would predict failure. For the given GRC, installation of support 1-2 m behind the face (immediate support) would require a support pressure of over 1 MPa to prevent the support from failing.

6.4.5. Discussion of the applicability of the CCM to cavern analysis

A major discrepancy of the analysis can be related to the non-circular cross-section of the cavern. The height to width ratio of the cavern is almost 2, resulting in an equivalent tunnel diameter almost twice the width of the cavern. Just analyzing the top two benches gave much higher convergence than was measured at this excavation step. When the overburden and rock type is assumed relatively consistent throughout the cavern, the method only responds to changes in equivalent radius. The different results in the analysis were basically only influenced by the different dimensions of the cross-sections. Although this is considered an important effect, it is not the only contributing factor to the large spread in the deformation data. When interpreting the results of the CCM it is therefore critical to know which parameters change for each section, so the 'influencing factors' can be considered.

The convergence calculated by the method was compared to the maximum measured convergence, which for all sections are measured at el. 603 (in the wall right above the niche). Although the results are relatively promising when looking at the actual distance from the end-walls, it must be known when interpreting the results that the deformation predicted by CCM will not be valid for the whole height of the wall. It seems that that the CCM best predict for the interval of highest deformation, which is also most critical to determine.

Based on the analysis, the SCC is regarded the least applicable component of the CCM. In general, the few choices for the applied support limit the representation of reality. Support for large scale caverns usually include a complex scheme of bolts, long cables, arches and reinforced shotcrete. Additionally, there are two major concerns for the calculation of the combined support for SCC: the maximum pressure depends on the added stiffness, and the allowable deformation is limited by the smallest allowable deformation of the components. As seen in Fig. 6.11, the shotcrete is very stiff, and allow for very little deformation (steep curve). The cables however allow much deformation over its total length, and its stiffness becomes very low. In effect the combined support pressure becomes unreasonably low; low stiffness of cables combined with the small allowable deformation of the shotcrete.

The SCC does not consider the difference in installation time for the individual supports. In reality, the bolts and cables would be installed before the shotcrete is sprayed. The

6.4 ANALYSIS OF SQUEEZING

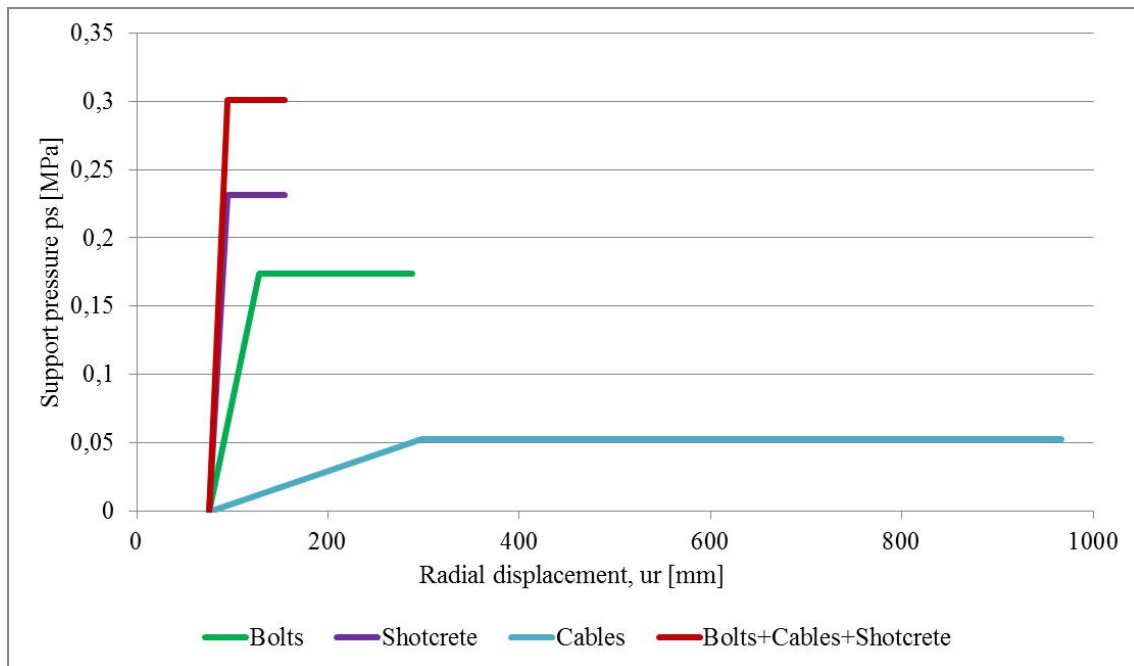


Figure 6.11.: Support characteristics curves for all installed support types

support characteristics curve would not be a straight line; it would be divided in segments depending on the installed support (Fig. 6.12). Assuming bolts are installed first, they will have time to act before the shotcrete is sprayed and dried (first segment). The shotcrete will make the support stiffer, but within the time the shotcrete takes into effect the wall and bolts will already have deformed a certain amount. The actual pressure exerted on the shotcrete, will be less than the combined SCC predicts.

An evaluation of the method should be done from a design perspective. Considering that the cavern is constructed in mostly jointed sandstone, with some mudstone and siltstone, would have lead to major underestimation of the deformations regardless of the other conditions. The assumption of worst case, only weak rock mass like mudstone/siltstone, give relatively good prediction if the mean stress is applied and the face-effect is considered (correct reading of the LDP). That the overall result is better for applied mean stress is reasonable, considering that the cavern is under anisotropic stress conditions. The method in general proves sensitive to the quality of the estimated rock mass strength, as for all the previously applied methods. The CCM applied in this study uses the Hoek-Brown criterion for determination of the rock mass strength. This criterion applied in previous analyses has shown to result in too high deformations, while the CCM seems less conservative in this regard.

Given that the analysis of a cavern in general fulfill few of the assumptions behind the method, the results have shown better than expected. However, the variety of the results depending on input parameters and interpretation highlight the many uncertainties of the method. Only knowing what to look for lead the method to give relatively representing results. Based on the analysis performed, it seems that mean stress (anisotropic stress conditions), worst assumed rock conditions and consideration for face-effect would give

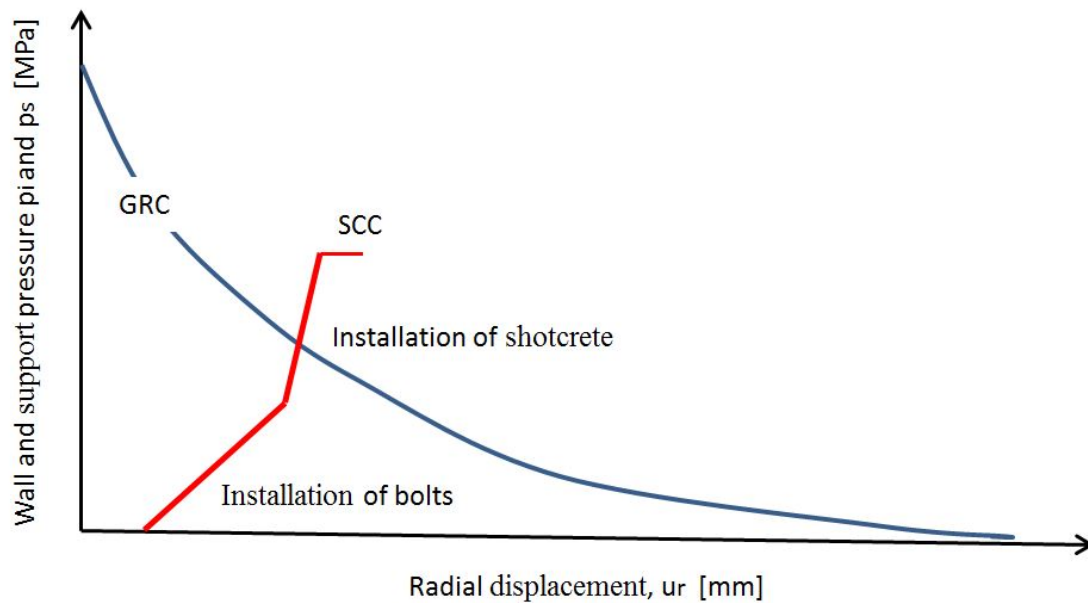


Figure 6.12.: Realistic shape of SCC

the best results. In general it should be said that for analysis of deformations in a cavern the CCM can be used for prediction of squeezing, however not for support interaction analysis. The effect of the large cross-section on the deformation and visualization of the deformation profile can prove quite useful. Compared to analysis of a tunnel, knowing how to interpret the results becomes a more critical process in cavern analysis. One must at all times be aware of which assumptions are violated, and which factors are changing. But as argued by Carranza-Torres and Fairhurst (2000); even if the assumptions are violated the method can still be useful in the early stages of the design.

6.5. NUMERICAL MODELING

6.5.1. Construction of the models in Phase²

The excavation boundaries for each section were found from project drawings of the cavern received from NJC (2011b) (App.E.3). The external boundary was set as a box with expansion factor 3, sufficient for the rock mass to normalize towards the boundary. The right and left boundary were restraint in the x-direction, and the upper and lower boundary restraint in the y-direction. The 4 corners were restraint in both x- and y-direction.

The geological conditions were set based on the long wall cavern surface mapping, according to Fig.4.13. Some simplifications had to be made: mudstone and siltstone were treated as one material, with a constant dip angle. The pattern interpreted from Fig.4.13 was interpolated to the remaining rock mass. After discussion with supervisor it was concluded that joints should not be added for any of the models (Panthi, 2014b). Groundwater conditions was not considered, since little to information about hydrogeologic conditions was available and its a deep excavation.

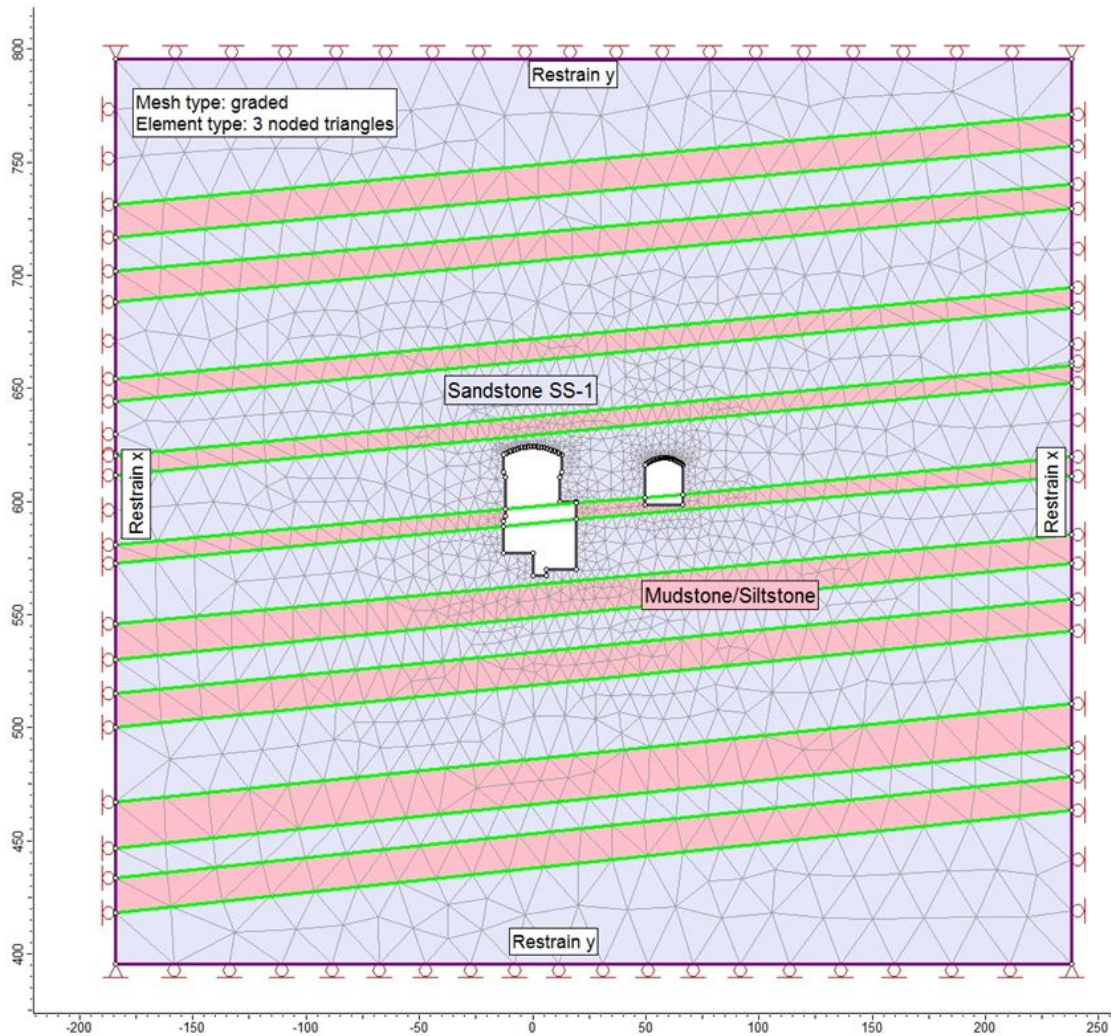


Figure 6.13.: Example model 0+085

6.5.2. Model input

The material properties were defined by the generalized Hoek and Brown criterion, as this is the most appropriate option for a heavily jointed rock mass. The mean intact rock strength and Poisson's ratio given by NJC (2011a) were used in the analysis. The Hoek Brown parameters were calculated based on the estimated GSI (Tab.6.1), and the m_i was quoted from the standard chart in App.A.1. After discussion with supervisor, the residual properties for plastic analysis were assumed 1/4 of the peak value, and the dilation angle assumed to be zero (Panthi, 2014b). The rock mass parameters are summarized in Tab.6.6.

The support properties were discussed and decided in cooperation with Norplan A/S (2014). The installed cables were decided best represented as "Plain Strand Cable", and the rock bolts as "Fully Bonded". The bolt properties were defined as for the CCM (Tab.6.3), but with a different bolt pattern for walls and crown. The bolts and cables in the cavern are installed in a staggered grid. *Phase²* cannot comprehend a staggered grid, so a simplification to quadratic grid had to be made. The residual tensile capacity of the bolts was set as 10% of the peak tensile capacity (Norplan A/S, 2014).

Table 6.6.: Model input for *Phase²* analysis

Material	Intact strength [MPa]	m_b (peak)	m_b (residual)	s (peak)	s (residual)	a (peak)	a (residual)
SS-1	86	1.1	0.275	0.001	0.00023	0.5	0.125
Mud/Silt	54.1	0.27	0.0675	0.0002	4.4e-005	0.51	0.1275

The installed shotcrete at NJHPP is reinforced with 2 layers of mesh with $10\text{cm} \times 10\text{cm}$ grid and 5 mm thickness. The *Phase²* database only includes 4 mm and 6 mm thick weld mesh, so a composite liner with two layers with 4 mm thickness mesh was applied. Except for reinforcement spacing, the default weld mesh properties were assumed. Otherwise the properties for shotcrete were assumed the same as for the CCM analysis.

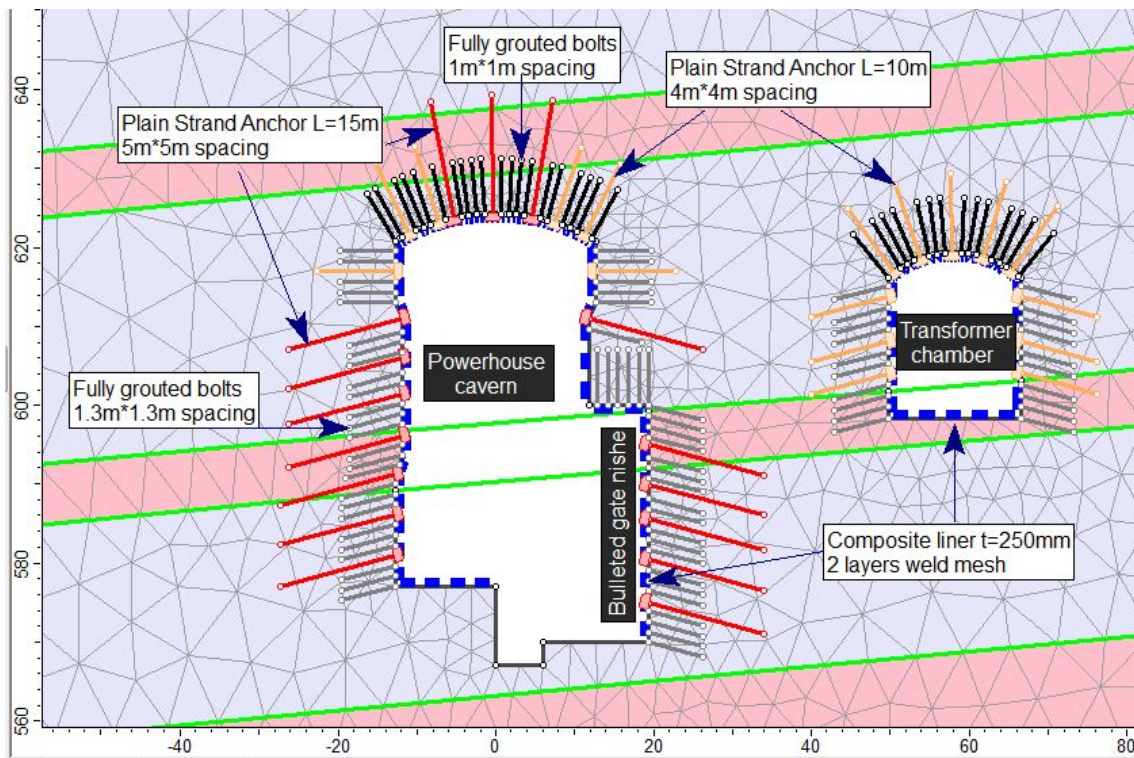


Figure 6.14.: Example of the model for section 0+085 with installed support

The support was installed in the cavern according to the project drawings for zone A and B, given in App.E.3. Chainage 0+127 is the only section in zone B. A few simplifications had to be made, especially above the niches in model 0+085 and 0+065 where the staggered grids are complicated. As the deformations in the cavern are measured before support of the bottom floor level, shotcrete was not added to the floor level of the cavern. The shotcrete was treated as plastic material in the analysis. The option for plastic shotcrete is justified as long as the liner is intended to yield. Plastic properties however prevent analysis of the support capacity of the shotcrete, and should therefore not be used for design purposes.

6.5.3. Calibration of models

The initial intent for the calibration was to find the appropriate level for the horizontal stresses and the rock mass deformability based on one model, and apply the best values for the other 4 sections. However, finding the appropriate model to represent the cavern was difficult due to the changing external factors. Section 0+127 has the most extensive deformation data from both convergence measurements and extensometers. This section is influenced by the east end-wall, which cannot be simulated with *Phase*². Section 0+032 may be sufficiently far from the end-walls, but some errors are seen in the deformation data. Section 0+085 has data from both extensometers and convergence installations, but there are some discrepancies between the data for the same measuring location, and the section is intersecting a niche. Finally, it was decided to perform numerous repetitions of the analysis for section 0+085, 0+127 and 0+032, as all three of these have considerably more deformation data than 0+065 and 0+015.

The procedure was to evaluate the change in total deformation for different levels of horizontal stress and rock mass deformability, for plastic analysis with support. The vertical stress was estimated using Eq. 3.1, and the horizontal stress by Eq. 3.2. The mean Poisson's ratio (0.24) was used for the estimation. The tectonic component was varied between 3.5 and 4 MPa magnitude, with direction N41°E. The cavern is oriented N78°E, so the angle between the cavern and the horizontal stress is 37°. The horizontal in-plane and out-of-plane components were calculated using basic geometry (see App.C.5). The modulus of deformation was varied in an interval around the estimated values seen in Tab.6.2.

The total deformation for the excavation boundary was evaluated using the “query boundary” and plot option. The total deformation was compared to the extensometer and convergence data at the correct location. It was decided that results within 25% of the actual deformation would be satisfying (Panthi, 2014a).

Calibration for section 0+085

For section 0+085, the D-E extensometers are installed about a month later than the convergence line, and show about 20 mm less deformation. For this reason, the maximum convergence for J-K was used for the comparison. Convergence location N-O (el. 596, middle of the wall) could not be used due to the short measuring interval. The layout for model 0+085 can be seen in Fig.6.14.

About 30 models were run with different combinations of stress and modulus of deformation in different combinations. Fig.6.15 illustrate the results for 10 of the most representative results for section 0+085. The details for the 10 runs are shown in Tab.6.7. The table shows the percentage deviation in total deformation for the models compared to the measured deformation for convergence J-K, P-Q and crown extensometers A, B and C. Positive values are percent higher deformation in the model compared to the measured.

In Fig.6.15 the points represent the deformation at the extensometer locations A, B, C, D and E (Fig.4.18). The deformation for point D and E was assumed to be 10-20 mm higher, based on the convergence measurements. In general, the modeled results for the downstream side of the crown do not correspond well with the measured deformations (A in the middle of the crown, C is the downstream corner).

Compared to the measured convergence, the best results were obtained for model 10, with a magnitude of 4 MPa for the tectonic stress and deformation modulus 7.05 GPa and 2.4 GPa for sandstone and mudstone/siltstone respectively. The deformation in the crown for this model was however way higher than what has been measured. As shown in Fig.6.15, the model could not recreate the deformation pattern in the crown.

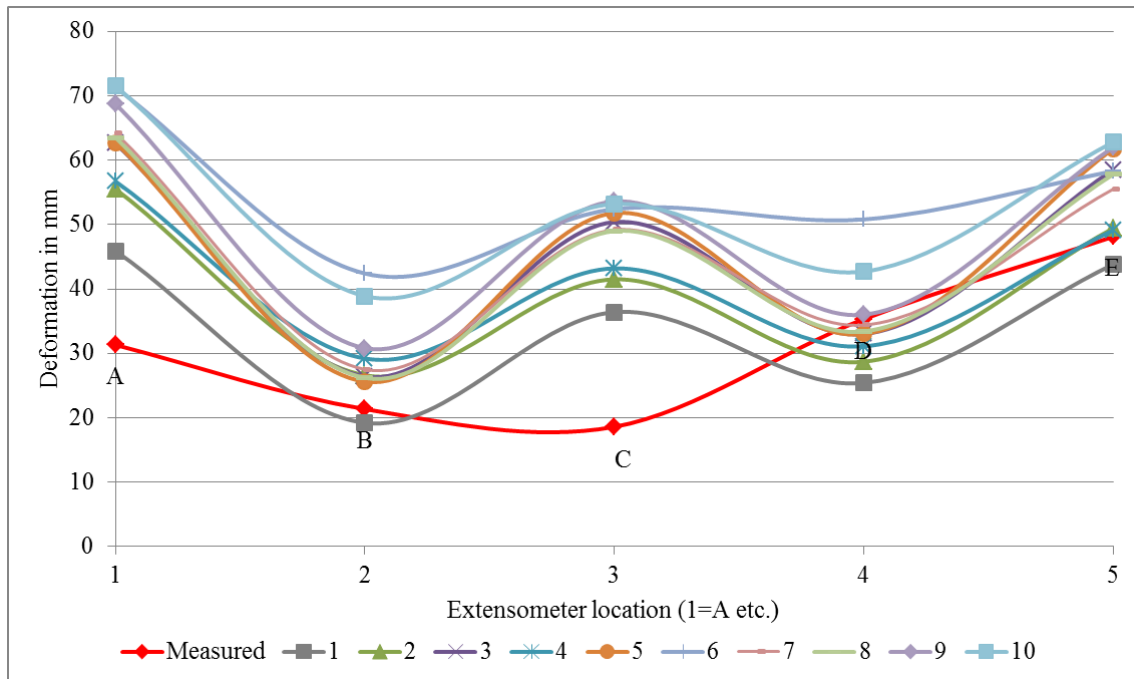


Figure 6.15.: Graph for calibration results of model 0+085

Table 6.7.: Model results for 0+085 compared to measured deformations

Model run	Magnitude tectonic stress [MPa]	Deformation modulus [MPa]		Percent deviance between model and measured deformation (%)				
		SS-1	Mud/Silt	Conv. J-K	Conv. P-Q	Ext. A	Ext. B	Ext. C
1	3.8	8980	4170	-49	-75	32	-11	49
2	3.8	8980	2930	-31	-47	44	20	55
3	3.8	7020	2930	-11	-32	50	19	63
4	4	8980	2930	-34	-58	45	27	57
5	4	7020	2930	-15	-34	50	17	64
6	4	7000	2500	4	-27	56	50	65
7	4	7500	2500	-17	-38	51	22	62
8	4	7200	2600	-15	-39	51	19	62
9	4	7050	2450	-7	-19	54	31	65
10	4	7050	2400	0	-17	57	47	66

6.5 NUMERICAL MODELING

Control analysis for section 0+127 and 0+032

The same procedure was performed for sections 0+127 and 0+032 as for section 0+085, except only for the 10 variations presented above. As can be seen from Tab.6.8, the results for section 0+127 show much less correspondence to the measured deformations for this section. The values best corresponding to model 0+127 are the values resulting in the least favorable results for model 0+085 (model run 1 and 2), and vice versa. Section 0+127 needs more optimistic rock and stress input to simulate better conditions, since the supporting effect of the end-wall cannot be considered in the model.

Table 6.8.: Model results for 0+127 compared to measured deformations

Model run	Magnitude tectonic stress [MPa]	Deformation modulus [MPa]		Percent deviance between model and measured deformation (%)				
		SS-1	Mud/Silt	Conv. J-K	Conv. P-Q	Ext. A	Ext. B	Ext. C
1	3.8	8980	4170	-9	-10	4	29	53
2	3.8	8980	2930	7	12	24	41	62
3	3.8	7020	2930	26	27	34	57	71
4	4	8980	2930	14	19	25	47	62
5	4	7020	2930	16	22	30	44	67
6	4	7000	2500	34	30	40	61	74
7	4	7500	2500	27	30	38	57	73
8	4	7200	2600	21	28	35	49	71
9	4	7050	2450	29	26	41	55	74
10	4	7050	2400	32	29	41	58	78

Table 6.9.: Model results for 0+032 compared to measured deformations

Model run	Magnitude tectonic stress [MPa]	Deformation modulus [MPa]		Percent deviance between model and measured deformation (%)				
		SS-1	Mud/Silt	Conv. J-K	Conv. P-Q	Ext. A	Ext. B	Ext. C
1	3.8	8980	4170	-53	-155	45	42	41
2	3.8	8980	2930	-35	-124	52	50	52
3	3.8	7020	2930	8	-72	61	58	64
4	4	8980	2930	-8	-114	51	39	58
5	4	7020	2930	-1	-99	57	48	59
6	4	7000	2500	4	-90	61	55	63
7	4	7500	2500	3	-103	58	50	61
8	4	7200	2600	0	-98	59	52	60
9	4	7050	2450	11	-87	61	56	62
10	4	7050	2400	6	-90	58	51	63

Section 0+032 showed better correspondence to both the measured values and the results gained for section 0+085. Convergence line P-Q showed most difficult to model. The deformations in the crown were as for model 0+085 overestimated with about 50%. The calibration graphs for sections 0+127 and 0+032 are given in App.D.1.

Conclusions for the calibrated values

The results for all three models vary both compared to the measured deformations and compared to each other. Deviant results were expected considering the different conditions for each section. The results for model 0+085 may suggest unreasonably low modulus of deformation and higher stress magnitude. This is because the section intersects the niche, which as discussed has shown to influence the deformation. Section 0+127 will predict too good conditions to simulate the effect of the non-represented face-effect. The results for section 0+032 are highly uncertain, as the deformation data for this section are inconsistent and may include several errors.

The results for section 0+032 and 0+085 seem to indicate that the most appropriate magnitude of the horizontal stress is 4 MPa. The deformation modulus for the rock mass is the most uncertain input for the analysis. Best case, it can be interpreted to lie within an interval of 7.05-7.2 GPa for SS-1 sandstone, and 2.4-2.6 GPa for mudstone/siltstone. To reduce the amount of presented data, the remaining analysis to be presented will be done for models with the input from model run nr. 10 for section 0+085, as this was regarded as the overall best result.

6.5.4. Elastic analysis

Elastic analysis to evaluate the strength factor and total elastic deformation was carried out for all sections. The strength factor is the most interesting result for elastic analysis; a strength factor less than one means the material will fail, and plastic analysis is necessary. The results for the elastic analysis for all sections are given in App.D.2.

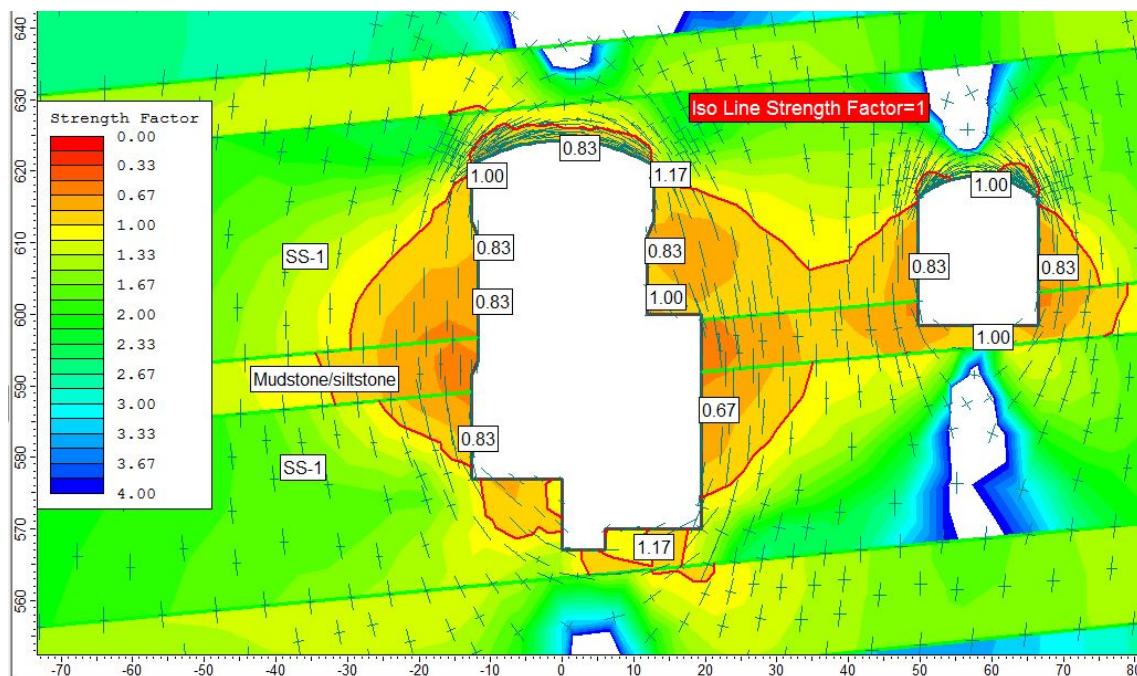


Figure 6.16.: Strength factor for model 0+085

For all sections the strength factor was found to be less than one around the whole contour of the powerhouse cavern and transformer chamber. More importantly, the strength factor

6.5 NUMERICAL MODELING

was less than one for the rock mass between the two openings, predicting failure in the pillar. The pillar will not reach complete failure in section 0+015 and 0+032, and the sandstone in the pillars have a strength factor above one (App.D.2). Fig.6.16 displays the strength factor for section 0+085, and it is seen how most of the pillar between the two chambers will fail. The model also shows how the strength factor depends on rock material; the critical line extends when crossing into the mudstone/siltstone layer. In section 0+032 there is no mudstone/siltstone layer intersecting the middle of the cavern, which is why the strength factor for the pillar is higher than for the other sections.

The stress trajectories are displayed in Fig. 6.16, and show that there is no confining stress along the walls of the cavern. This causes high concentration of compressive tangential stresses in the high walls. The total elastic deformation was briefly evaluated for all sections, and are shown in App.D.2. In general the deformations in the models are way less than measured for all sections, reinforcing the necessity of plastic analysis.

6.5.5. Plastic analysis

Plastic analysis with and without support was carried out for all five sections. The strength factor will for plastic analysis always be one or greater, and therefore provide little useful information. The strength factor will not be discussed further.

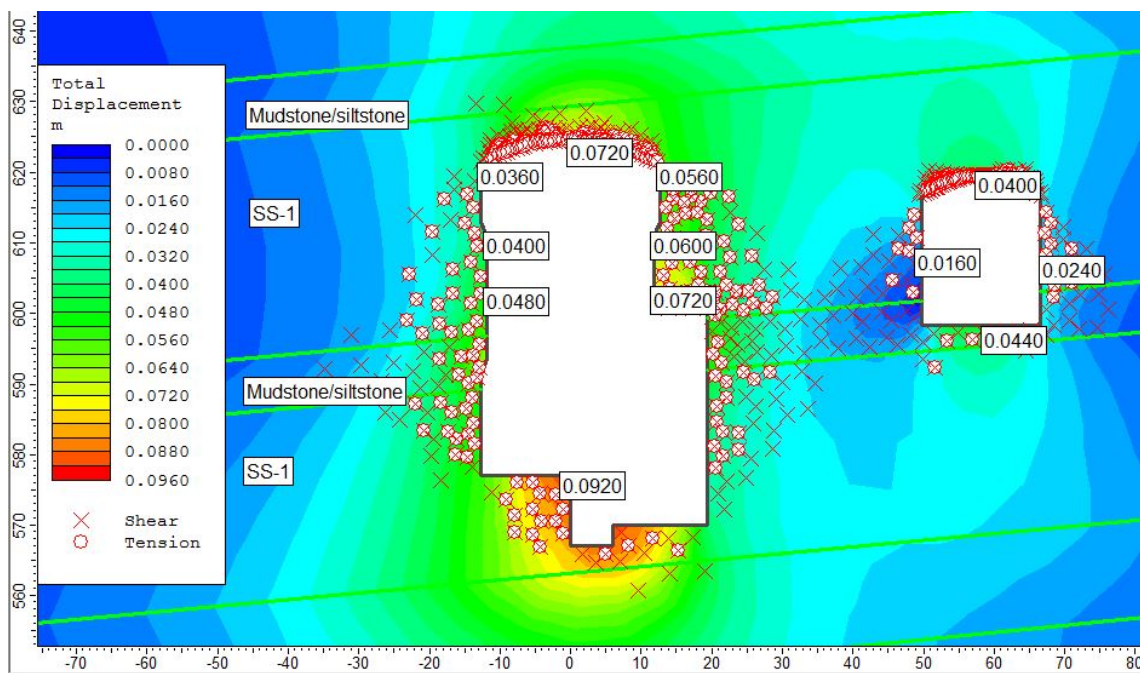


Figure 6.17.: Total deformation for unsupported plastic analysis for section 0+085

Fig.6.17 displays the total deformation and yielded elements for section 0+085 without support. The total deformation is slightly less than measured in the walls, and about twice the measured deformation is modeled in the crown. The yielded elements indicate that the pillar would suffer shear failure along the layer of mudstone/siltstone. Failure in both shear and tension is seen for the total length of the crown for both the powerhouse and the transformer hall, and in the rock mass in a radius of 5-15 meter around the powerhouse

cavern. The same extent of failure is seen for sections 0+065 and 0+127, whereas the pillar will not reach failure for sections 0+015 and 0+032 (see App.D.3).

Analysis for total plastic deformations with installed support was carried out for all sections (App.D.3). Fig.6.18 displays the total deformation and yield in rock mass and support at section 0+085. Number of yielded elements for the unsupported analysis is 565, while the support reduces the number of yielded elements to 528. However, the total deformation increases for all investigated points along the periphery of the cavern.

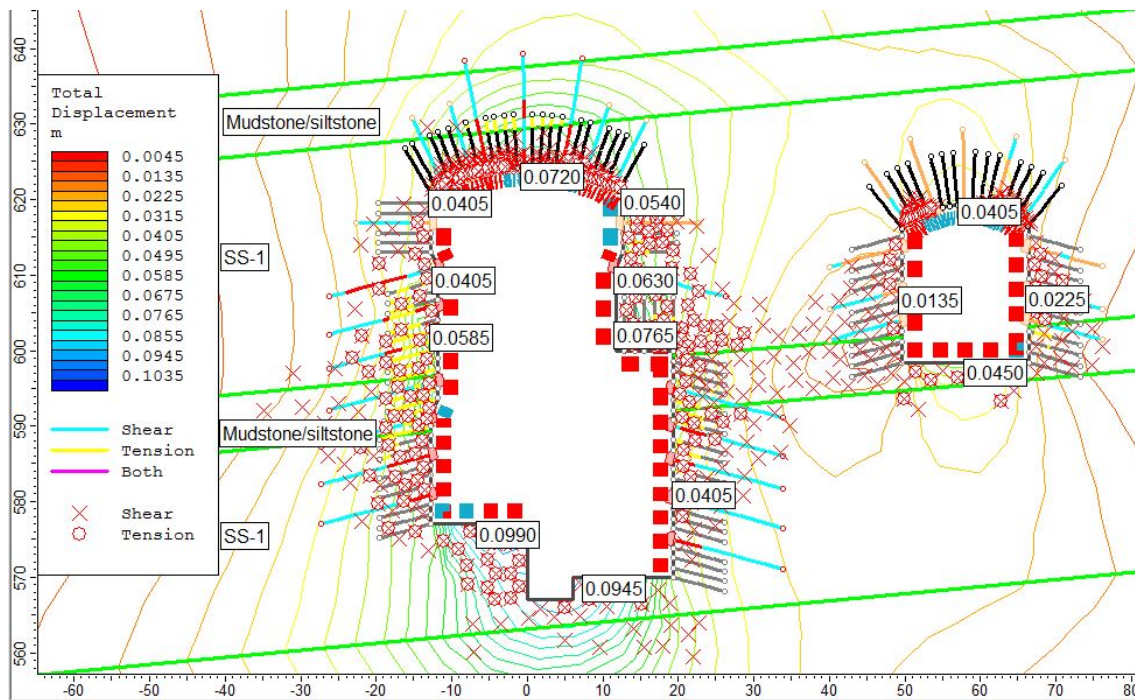


Figure 6.18.: Total deformation for plastic analysis with installed support for section 0+085

Yield of the support is seen as red for the shotcrete elements, and light blue for shear and yellow for tension in the bolts and cables. Many of the installed cables are fully sheared (light blue for the full length), but will not have failed as shear failure is not possible for plain strand cables in the program. Fully bonded bolts and plain strand cables can only fail in tension. The failure in the bolts and cables are defined in segments, determined by the intersection of each bolt with the solid elements of the mesh. As can be seen for the fully bonded bolts in the upstream wall and crown; the bolts will fail in tension close to the wall. In the crown they will fail for the segments installed in mudstone/siltstone. In the upstream wall, all bolts installed in the middle of the wall and in mudstone/siltstone will reach full tensile failure. For the failed bolts the peak tensile capacity is exceeded for all segments, and the load capacity of the bolts are reduced to equal or less than the defined residual capacity (0.025 MN). A few of the cables in the upstream wall also display tensile failure in selected segments.

The total deformation for all sections was compared to the measured deformations and the results from unsupported analysis, shown in Fig.6.19. Interestingly, the total deformation

6.5 NUMERICAL MODELING

in the wall increase for most sections when installing support. Section 0+127 is the only model having decreased deformation with installed support. Compared to the measured deformations, the models correspond best for convergence line J-K, installed right below the crane beam at el. 610. The P-Q convergence at el. 603 right above the crown of the niche, which measure the highest deformation for all sections, can not be modeled correctly for any of the sections. Hence, the models could not recreate the correct distribution of deformations around the contour. As for the results for the other methods, the highest deviance is seen for section 0+065.

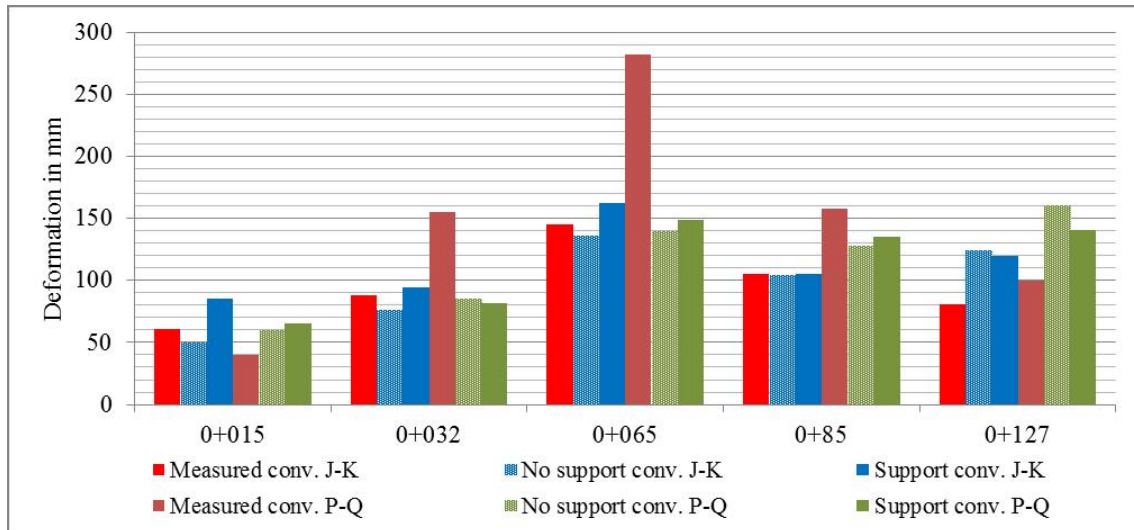


Figure 6.19.: Wall convergence for plastic analysis with and without support compared to measured deformations

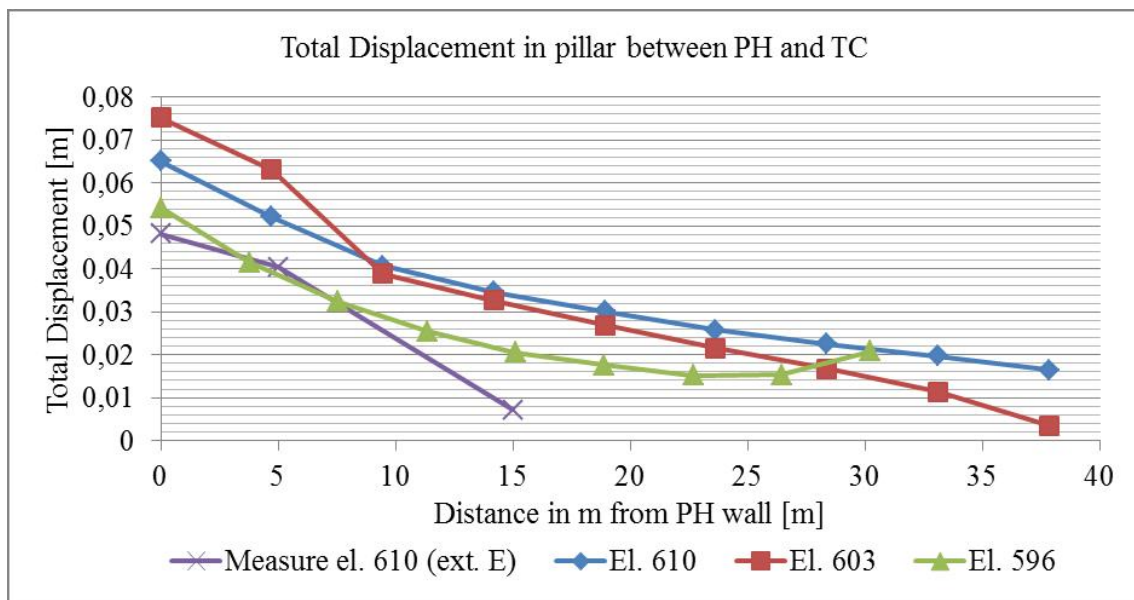


Figure 6.20.: Deformation in pillar between powerhouse and transformer chamber for section 0+085

The total deformation in the pillar between the powerhouse cavern and the transformer chamber for section 0+085, at three different elevations in the wall, is displayed in Fig. 6.20. The deformation measured for extensometer E is plotted for comparison. The plot indicates that the model is relatively correct with regard to the size of the plastic zone and area of highest deformation. Plotting the modeled deformation against the measured extensometers shows that the modeled deformations follow much the same development, but the magnitude for the wall and rock mass deformation is higher.

Section 0+085 was investigated for the progression in deformation for each excavation step. The excavation was performed in 6 stages, slightly simplified compared to the actual excavation progress. The total deformation for each excavation step is displayed in Fig. 6.22. The 6 excavation stages and explanation for the x-axis in Fig. 6.22 is shown in Fig. 6.21; the distance along the contour in Fig. 6.22 starts in the upper left corner of the crown and continue down the upstream wall. The two accelerating events for the deformation was the excavation of the niche, and excavating down to the floor level. The model could predict an increase in the deformation for excavation of the niche level, seen as the jump between the green and purple line in Fig. 6.22. The increase in the deformation for excavation down to the bottom floor level is less steep, just as for the actual measured deformation. The convergence graphs for P-Q show an increase of about 60-80 mm during excavation of the niche, and about 50 mm during the excavation down to the bottom floor level. The model predicts an increase of about 60 mm for the excavation of the niche, and 30 mm down to the bottom floor level.

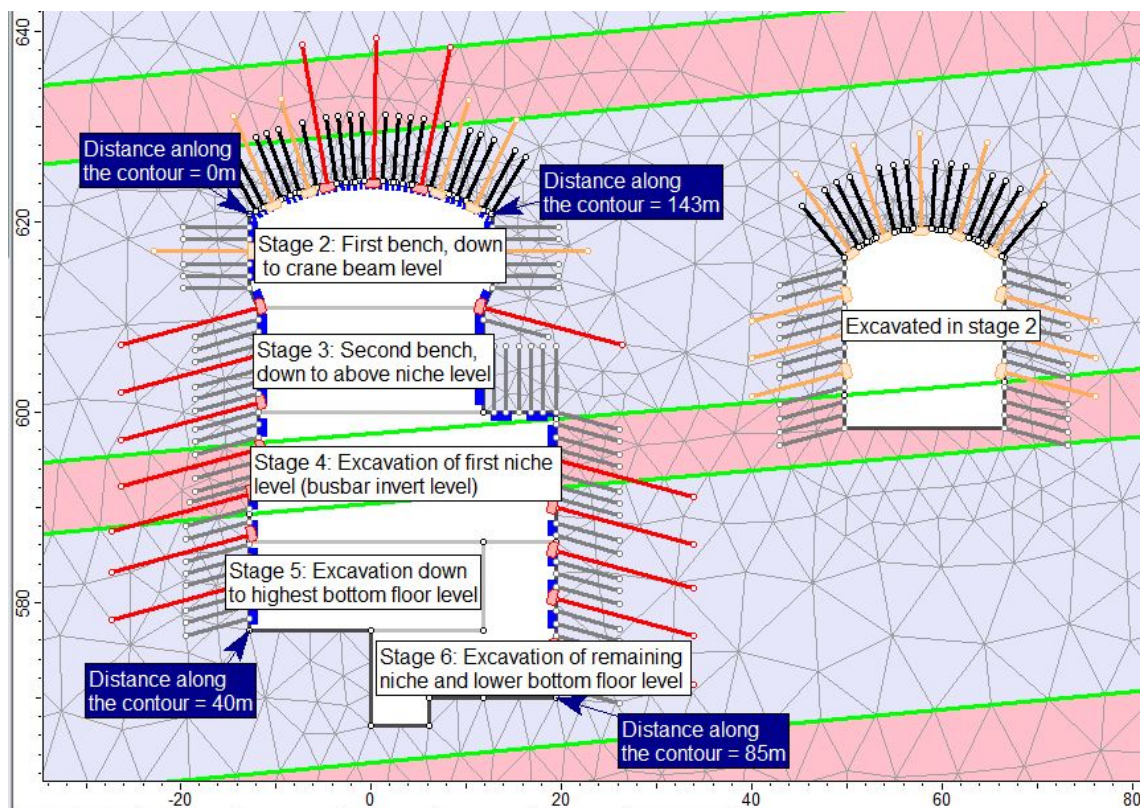


Figure 6.21.: Illustration of stages for section 0+085

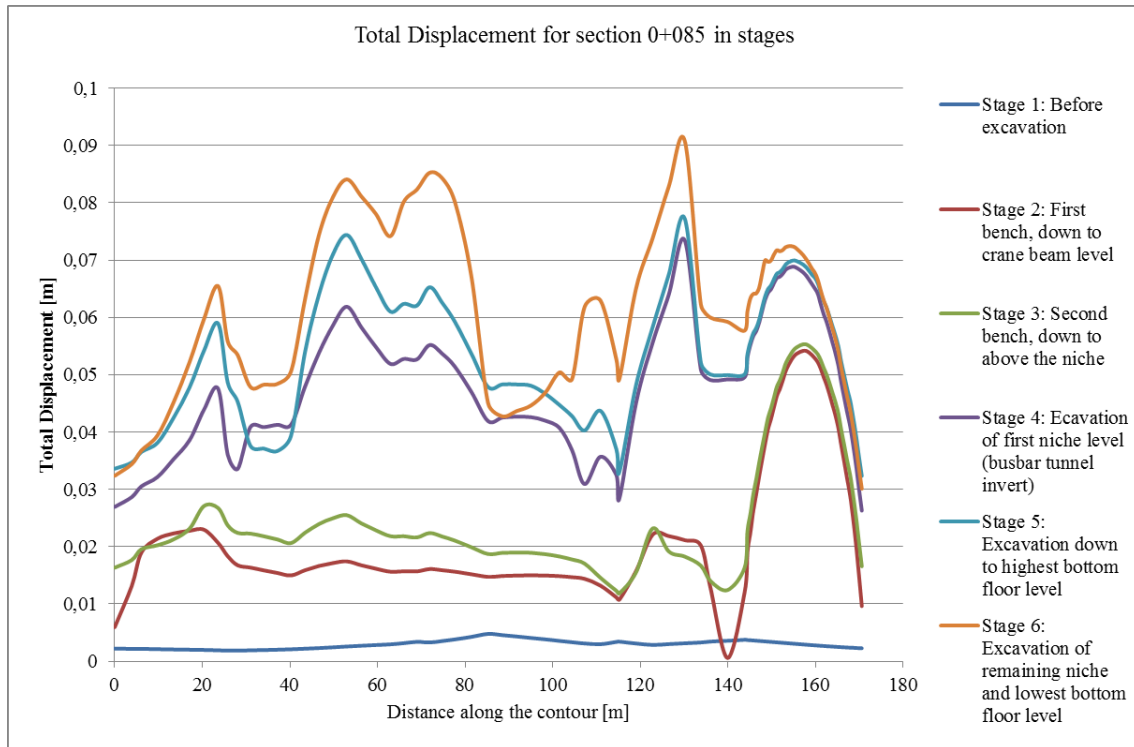


Figure 6.22.: Total displacement for excavation in stages for section 0+085

In summary, the model is almost able to predict the correct amount of increase in deformation when excavating the niche. The increase in deformation for excavation of the floor level is not interpreted correctly in the model. Still, considering the majorly simplifications in the model, it is difficult to conclude if the results are valid for the correct assumptions. In reality the excavation and installation of support of the niche was done over a long period of time, and additional support was added after severe yielding had occurred. Excavation and support of the niche is added 'simultaneously' per stage in the model. It is natural to assume that the effect in increased deformation in the model is just as much the result of excavating a wider cross-section and increasing the total excavated height.

6.5.6. Discussion of the applicability of 2D numerical modeling

Since the surrounding conditions for each section are different, the results for 2-dimensional analysis will not be able to reflect the true nature of the rock mass. Looking at the results compared to the extensometers for the sections where this is available, the highest discrepancy is seen for the downstream wall. The most obvious explanation would be that the niches influence more to the deformation at the downstream wall where they intersect. The modeled deformations were higher for the two models including a niche, so the effect of a larger cross-section was reflected. However, the magnitudes were highly underestimated. Additionally, the geologic layers are in reality not straight lines, which have been assumed in all models. This may have an influence onto why the model could not represent the distribution of deformation correctly along the crown and walls of the cavern.

The face-effect cannot be considered in 2-dimensional cross-sectional modeling using *Phase²*. The program considers the modeled cross-section to be infinite in the out-of-plane direction, hence neglecting the effect of the end-walls. This limits the potential for modeling of the deformation behavior of the whole cavern. The models will not be able to predict the difference in deformation relative to the location in the cavern. The analysis performed in this study especially highlights this effect, as the rock conditions are basically the same for the whole cavern. A potential solution could be to model the middle of the cavern for the worst assumed rock conditions and scale down the deformations intuitively for the remaining cavern.

In general the models predict a larger radius of the plastic zone than what has been experienced in the cavern. It might be that the rock anchors installed in the cavern affect the rock mass more than what is possible to model. The most peculiar result is how the deformation increase with support for the plastic analysis. A potential explanation might be that the installed support is too stiff, and not designed for plastic deformation. The shotcrete show yielding for almost all elements. If cracks in the shotcrete are included in the calculated total deformation, this may be why the program displays higher values for the models with support. Little information was found in the *Phase²* documentation to support this theory.

A clear advantage of 2-dimensional modeling is the visualization of the deformations, understanding the effect of geologic layers, and interaction between the adjacent openings. Numerical models are the only option for display of the changing deformation along the contour of the cavern. Even if the correct distribution in magnitude is not obtained, the model effectively highlights the consequence for high straight walls and the indent at the crane beam level.

The models displayed how the deformations increase in the mudstone/siltstone layers. Although the deformation do not indicate a clear difference in deformation depending on rock type, the potential danger in excavating in such bad rock conditions can be considered during design phase.

Evaluating *Phase²* with respect to being a design tool will provoke different conclusions. The program is relatively simple to use and interpret, and might be one of the better available methods for displaying potential deformations and stress conditions. However, the program exhibit significant limitations with regard to plastic analysis with support. It becomes clear that 3 dimensional modeling would be necessary for thorough analysis of the deformation behavior of a complex powerhouse cavern excavated in weak rocks.

6.6. DISCUSSION ON SQUEEZING ANALYSIS FOR A CAVERN

The empirical methods represent the simplest form of analysis. They exhibit the limited purpose of predicting occurrence of squeezing in a tunnel. The methods applied in the study consider the two factors regarded as most influential on the degree of squeezing; in-situ stress and rock mass strength or quality. The quality of the results are only as good as the estimated input, making the estimation of rock mass strength the most critical element in the analysis. Also the methods do not consider stress anisotropy.

The analysis of the deformations in the NJHPP cavern indicate that the non-ground related conditions contribute just as much to the deformation as the apparent rock mass conditions. The Q-method has the advantage of not being size or shape dependent. For prediction in a cavern, this can be considered both an advantage and a limitation as squeezing behavior is size and shape dependent. The method proposed by Goel considers the dimension of the excavation, a proven advantage compared to the Q-method. Still, the classification of squeezing proposed by Goel is based on empirical data for circular tunnels. The basic assumption for the method is therefore violated in the analysis of a cavern. The method by Goel was able to predict moderate to high squeezing in the cavern, while the Q-method and Hoek and Marinos without support pressure would predict no instabilities.

In theory the semi-analytical method by Hoek and Marinos (2000) can be used for a first hand estimate on the degree of squeezing and required support pressure. However, the assessment of squeezing as a function of strain is misguided in the analysis of a cavern. The rock mass will fail and cause instability in the cavern at much lower levels of strain than would be predicted in the method. Converting strain to deformation requires applying the equivalent radius, which for large a powerhouse can be twice the width of the cavern. Additionally, the support pressure applied in the analysis was estimated using the CCM. The combined support pressure for long cables and plain shotcrete becomes unrealistically low using the SCC. Even considering the low support pressure, the method by Hoek and Marinos underestimated the deformation for all sections excluding 0+127 where only mudstone/siltstone was assumed. In general the effect of the support pressure in the method was negligible; only 0.04% reduction of strain was seen for section 0+127.

The CCM is the only applied method that can consider the effect of the end-walls, giving the method an advantage for the analysis of caverns with a definite length. The LDP component of the CCM is the only method of the 5 applied, which could consider the effect of the end-walls. The CCM was therefore able to predict the pattern of deformation dependent on location in the cavern. In contrast, the numerical models proved to consider the effect of the adjacent openings, which may be an even more critical aspect during design phase. In addition the numerical models are able to analyze the difference in deformation along the contour of the cross-section, which is not possible for any of the other methods applied. Although the models presented could not recreate the actual deformation pattern, the effect of high straight walls and problems for the crown was reflected in the analysis.

In general it may seem that the most difficult part in the analysis is determination of adequate support. Only the CCM and numerical modeling can properly assess support, in estimation of support pressure and interaction with the rock mass. Regardless, none of the methods proved able to evaluate the effect of the installed support. The available types

of support in the CCM are limited, and the combined support pressure is not correctly assessed. *Phase²* is still not able to consider failure for both shear and tension for long cables, misinterpreting the effect of the support. A limitation for both seems to be the interaction between the installed supports, and between the support and the rock mass.

Determination of the size of the plastic zone is an important factor to consider for design of the required support. Long rock cables must be designed so as to be anchored in the competent rock outside the plastic zone. Although there are no definite data to confirm the size of the plastic zone around the NJHPP cavern, the extensometers indicate that the zone is less than 25 m and probably around 15 m. The estimate of radius of plastic zone was best represented in the numerical analysis, even if the models are too pessimistic for the pillars.

The apparent advantage of numerical methods is the possibility to model the true geometry of the cross-section. The method also considers more than one rock type. The other necessary assumptions for the rock mass is however still the same. The uncertainty of the estimated rock mass strength and deformability is just as relevant for numerical modeling.

For section 0+032 and 0+065, the effect of water bearing fractures or shear zone is a possible explanation to the unexpectedly high deformations. The effect of water is only considered in the empirical methods with the determination of the J_w parameter. The sensitivity of the methods to this parameter is however small compared to the theoretical effect in reality. Neither could the effect of one controlling discontinuity be investigated by the empirical or analytical methods. They all consider the rock mass in total; with definition of joint sets in the classification or with GSI for Hoek and Brown estimation. Local differences were not considered in this analysis, as they are difficult to predict until the face is exposed. The effect of joints and groundwater could be considered in *Phase²*, however the time available for the study did not allow for such investigations.

Analysis of deformations in large scale cavern has proven much more difficult than for a circular tunnel. In a tunnel, the deformations are less influenced by external factors. The methods typically only consider stress conditions and rock mass quality and strength. The analysis of the deformations in the NJHPP cavern indicate that for a powerhouse cavern the complex excavation layout, large dimensions and excavation progress are major influencing factors. The effects of these are not properly considered in any of the selected methods for the analysis. Even so, the limitations in the assumptions for ground behavior are a known paradox in all aspects of rock engineering.

7. CONCLUSIONS AND RECOMMENDATIONS

7.1. CONCLUSIONS

The major cause for instability in the Neelum Jhelum HPP cavern is squeezing deformation. The cavern is constructed in fractured sandstone with the intercalation of thin to thick layers of locally sheared siltstone and mudstone. Since constructions began in 2011, the deformations have been monitored progressively with convergence lines and extensometers. The highest deformation is seen for the middle sections, with up to 282 mm convergence of the walls. Analyses of the convergence data show that the two major influencing events accelerating the deformation were the excavation of the bulleted gate niches in the downstream wall (4 niches), and the excavation down to the bottom floor level. The data from extensometers indicate that the deformations are higher in the downstream wall for the middle sections of the cavern, probably due to the intersecting niches.

In this study, 5 methods for the analysis of squeezing deformation have been applied. This included two empirical methods, Geol (1994) and the Q-system, which both evaluate squeezing based on in-situ stress and rock mass classification or strength. The semi-analytical method by Hoek and Marinos (2000) can be used for prediction and analysis of tunnel strain in percent, based on the estimated rock mass strength and in-situ stress. The analytical Convergence-Confinement Method (CCM) proposed by Carranza-Torres and Fairhurst (2000) allow for more extensive analysis, considering the interaction of the rock mass with regard to excavation progress and support installation. Finally, numerical modeling using the 2-dimensional finite element program *Phase²* by Rocscience have been used for the analysis of plastic deformation, and determination of appropriate rock and stress parameters. All applied methods rely on the estimation of in-situ stresses and rock mass strength or quality, making the rock mass estimation and geological investigation the most critical part for all analysis.

The extensive deformation data for the NJHPP cavern have made it possible to perform an in depth evaluation of the applied methods with regard to deformation analysis of a large scale cavern. Following conclusions have been made:

- The most critical element in any analysis is the determination of appropriate rock mass parameters. All methods depend on rock mass strength or quality, and their results are only as good as the quality of the estimated input.
- The approach by Goel (1994) was the only empirical method able to predict squeezing in the cavern. The method considers the size of the excavation, which may be an important factor influencing the deformations. While this is true, the method by Goel is much more sensitive to the overburden depth and will almost regardless of quality predict squeezing for a considerable overburden. The prediction may therefore be less useful to an engineering geologist. Knowledge of the squeezing phenomenon will for considerable overburdens and occurrence of weak rocks in any case prompt the engineer to conduct more extensive analysis.
- The method by Hoek and Marinos (2000) has proven the least applicable to analysis of squeezing in a cavern. The classification and suggested support measures are evaluated with regard to percentage strain. Critical deformation and failure of the

rock mass will for large dimensions occur for much lower strains than would be predicted by the method. Further, the conversion from strain to deformation would require use of an equivalent tunnel diameter. For a cavern with height to width ratio around 2, the equivalent diameter becomes twice the width of the cavern. Even then the deformations estimated by Hoek and Marinos were grossly underestimated for the assumed rock conditions.

- The CCM is able to consider the supporting effect of the end-walls and anisotropic stress conditions. Still, reliable results were only obtained by assuming worst case rock conditions and mean stress (anisotropic rock conditions). The assumption of fractured sandstone results in a considerable underestimation of the deformation. The method showed highly variable results depending on input parameters and interpretation. The more extensive the analysis, the more critical the interpretation and geologic understanding becomes.
- The SCC has proven little applicable for support estimation. The SCC is restricted in the available choices for support types. Complex support measures are necessary for a large cavern, and cannot be considered in the SCC. The combined support pressure estimated is limited by the allowable displacement of shotcrete and the low stiffness of the long cables. In effect the estimated combined support pressure becomes unrealistically low. The large dimensions of a cavern will influence a larger plastic zone ahead of the face. About half the total deformation will already have occurred at face so that immediate installation will cause failure in the underestimated support.
- *Phase²* is considered a useful tool for the analysis of the deformation along the contour of the cavern. The effect of high straight walls and corners is seen in the model, although the correct magnitude of the deformation along the contour was not obtained. The model is able to predict the increase in deformation for excavation of the niche. However, the basis for the effect in the model may not be correct. The program can also be used for analysis of the effect of adjacent openings, which is a major aspect in design of a powerhouse complex. 2-dimensional modeling is however not an adequate method for design of support for complex installations.
- In sum, the CCM and numerical models give the best results for analysis of squeezing in a cavern. Still, the complexity involved for the deformation behavior in a cavern is not fully represented in any of the methods. The CCM is useful for the analysis of variation in deformation along the cavern length. Numerical modeling is the only option for analysis of variation in deformations in the cross-sectional plane, and for proper display of the effect of excavation steps. Understanding the effect of the complex cavern design has only proven possible in the numerical analysis. Numerical modeling is the method considering most of the factors involved in the behavior of the rock mass; geologic layers with different properties, orientation relative to the structure, anisotropic stress conditions, adjacent openings and cavern design.

7.2. RECOMMENDATIONS

The recommendations for the proper procedure for analysis of deformations in a cavern are affected by the limitations in this study. This study only considers the deformations measured in one cavern. To provide a definite strategy and recommendation for squeezing analysis in large cavern, the methods should be applied and compared to more than one case study. Regardless, the following recommendations can be said to apply to any analysis of deformations in large scale cavern:

- The most important factor for all analysis is proper input parameters. Field observations and laboratory tests are crucial for a soundly based estimation of rock mass properties. Stress measurements should be performed, as estimation of the horizontal stress is the most uncertain parameter experienced in this analysis.
- The CCM can be used for the analysis of potential levels of deformation relative to the location in the cavern. Worst assumed rock properties should be assessed, as the method is very sensitive to rock mass input.
- When severe squeezing is expected, deformation measurements in the adit tunnels should be performed before excavation of the cavern. The *Phase²* program can be used to correlate the deformations to rock mass parameters and stress conditions. Further an analysis of different cavern designs and potential support can be used to evaluate and compare options for the final design.
- For adequate estimation of the deformation for a complex cavern design, 3-dimensional numerical modeling will be necessary.
- The assumptions behind each method of analysis should be well known to the user. A proper interpretation can only be done while knowing the limitations of the method. One should always confirm the interpretations of the analysis with an experienced engineering geologist, and if possible compare to similar projects.

Bibliography

- Aydan, Ö., Akagi, T., Kawamoto, T., 1993. The Squeezing Potential of Rocks Around Tunnels ; Theory and Prediction. *Rock Mechanics and Rock Engineering* 26, 137–163.
- Aydan, Ö., Akagi, T., Kawamoto, T., 1996. The squeezing potential of rocks around tunnels ; theory and prediction with examples taken from Japan. *Rock Mechanics and Rock Engineering* 29 (3), 125–143.
- Barton, N., 2002. Some new Q-value correlations to assist in site characterisation and tunnel design. *International Journal of Rock Mechanics and Mining Sciences* 39, 185–216.
- Barton, N., Lien, R., Lunde, J., 1974. Engineering classification of rock masses for the design of rock support. *Rock Mechanics* 6, 189–236.
- BGS, 2002. Engineering geology of British rocks and soils: Mudstones of the Mercia Mudstone Group.
- Bieniawski, Z., 1989. *Engineering Rock Mass Classification*. New York: Wiley.
- Calkins, J. A., Offield, T. W., Abdullah, A. K. M., Tayyab Ali, S., 1975. Geology of the Southern Himalaya In Hazara, Pakistan, and Adjacent Areas. Geological Survey Professional Paper 716-C, United States Government Printing Office, Washington.
- Carranza-Torres, C., Fairhurst, C., Sep. 1999. The elasto-plastic response of underground excavations in rock masses that satisfy the Hoek–Brown failure criterion. *International Journal of Rock Mechanics and Mining Sciences* 36 (6), 777–809.
- Carranza-Torres, C., Fairhurst, C., 2000. Application of the Convergence-Confinement method of tunnel design to rock masses that satisfy the Hoek-Brown failure criterion. *Tunnelling and Underground Space Technology* 15 (2), 187–213.
- Chapman, D., Metje, N. and Stärk, A., 2010. *Introduction to Tunnel Construction*. Spon Press, New York.
- Deoja, B., Dhital, M., Wagner, A., 1991. Risk engineering in the Hindu Kush-Himalaya. International centre for intergrated mountain development (ICIMOD).
- DGSI, 2000. Radial and Tangential Total Pressure Cells. User’s Manual. Product information.
URL www.slopeindicator.com
- DGSI, 2014. Center-Hole Load Cell. Product information.
URL www.slopeindicator.com
- Dwivedi, S. K., Adhikary, P. C., Tamrakar, J. M., 2006. Engineering geological and geotechnical characteristics of the Kankai hydro-power tunnel in soft rock , Nepal Regional geology. *Bulletin of Engineering Geology and the Environment* (752), 1–11.
- Goel, R., Jethwa, J., Paithankar, A., 1995. Indian experiences with Q and RMR systems. *Tunnelling and Underground Space Technology* 10 (1), 97–109.
- Goodman, R. E., 1989. *Introduction to rock mechanics*. John Wiley and Sons.

- Hoek, E., 1990. Estimating Mohr-Coulomb Friction and Cohesion Values from the Hoek-Brown Failure Criterion. *Int. J. Rock Mech. Min. Sci & Geomech. Abstr.* 27, 227–229.
- Hoek, E., 2000. Large Powerhouse caverns in weak rock. In: *Rock Engineering*. Balkema Publishers, Ch. 13.
- Hoek, E., 2007a. Design of large underground caverns - a case history based on the Mingtan Pumped Storage Project in Taiwan. In: *Practical Rock Engineering*. Ch. 13.
- Hoek, E., 2007b. Design of underground caverns. In: *Practical Rock Engineering*. Rocscience, Ch. 13.
- Hoek, E., 2007c. Rock mass properties. In: *Practical rock engineering*. Rocscience, Ch. 11.
- Hoek, E., 2007d. Rock-Support Interaction analysis for tunnels in weak rock masses. In: *Practical rock engineering*, online PDF from previous edition. Ch. 12.
- Hoek, E., 2007e. Tunnels in weak rock. In: *Practical Rock Engineering*. Ch. 12.
- Hoek, E., Carranza-Torres, C., Corkum, B., 2002. Hoek-Brown failure criterion - 2002 edition. *Proc. NARMS-TAC Conference, Toronto (1)*, 267–273.
- Hoek, E., Diederichs, M., 2006. Empirical estimation of rock mass modulus. *International Journal of Rock Mechanics and Mining Sciences* 43, 203–215.
- Hoek, E., Marinos, P., Desember 2000a. Predicting Squeezing. *Tunnels and Tunneling International*, 33–36.
- Hoek, E., Marinos, P., 2000b. Predicting tunnel squeezing problems in weak heterogeneous rock masses. *Tunnels and Tunneling International* (November).
- Hudson, J. A., Harrison, J. P., 2000. *Engineering Rock Mechanics - An Introduction to the Principles*. Pergamon.
- Khan, P. K., Mohanty, S., Mohanty, M., 2010. Geodynamic Implications for the 8 October 2005 North Pakistan Earthquake. *Surveys in Geophysics* 31, 85–106.
- Kovári, K., Staus, J., 1996. Basic Considerations on Tunnelling in Squeezing Ground. *Rock Mechanics and Rock Engineering* 29 (4), 203–210.
- Kovári, K., 1998. Tunneling in squeezing rock. *Tunnel* 5, 12–31.
- Lie, C. C., 2011. *TGB4210 Rock and Soil Mechanics - supplements*. Tapir akademiske forlag.
- Löw, S., April 2013. Lecture notes for ETH Zürich course "Landslide analysis".
- Löw, S., 2013. Class notes for ETH Zürich course "Engineering geology of underground excavations".
- Myrvang, A., 2001. *Bergmekanikk*. Institutt for geologi of bergteknikk, NTNU.
- Nagaraj, T., 1993. *Principles of Testing SOils, Rocks and Concrete*. Elsevier.
- NGI, April 2013. Using the Q-system: Rock mass classification and support design. online pdf.

-
- Nilsen, B., Broch, E., 2011. *Ingeniørgeologi - Berg Grunnkurskompendium*. Institutt for geologi og bergteknikk, NTNU.
- Nilsen, B., Palmström, A., 2000. *Handbook nr.2: Engineering Geology and Rock Engineering*. Norwegian Group of Rock Mechanics.
- Nilsen, B., Thiedemann, A., 1993. *Rock Engineering*. Norwegian University of Technology, Division of Hydraulic Engineering.
- NJC, 2011a. NJHP: Rock Parameters NJHH Final Draft, project report.
- NJC, 2011b. Project drawings.
- NJC, 2013a. Convergence measurements, excel file. Updated 08.12.13.
- NJC, 2013b. Excavation progress, update from site personnel November 2013.
- Norplan A/S, 2013a. Internal project presentation, powerpoint presentation.
- Norplan A/S, 2013b. Personal correspondence during Project Work fall 2013.
- Norplan A/S, 2014. Personal correspondence during Master thesis work spring 2014.
- O'Brian, P. J., 2001. Subduction followed by collision: Alpine and Himalayan examples. *Physics of the Earth and Planetary Interiors* 127, 277–291.
- Palmström, A., Stille, H., 2010. *Rock Engineering*. Thomas Telford Limited, London.
- Panet, M., 1996. Two case histories of tunnels through squeezing rocks. *Rock Mechanics and Rock Engineering* 29 (3), 155–164.
- Panthi, K., 2014a. Discussion of estimation of rock mass quality, and limitations for the analysis. Date: 14.05.14.
- Panthi, K. K., 2006. Analysis of engineering geological uncertainties related to tunneling in Himalayan rock mass conditions. Ph.D. thesis, NTNU.
- Panthi, K. K., 2013a. Deformasjonsmålinger i tunneler langs svake og skifrige bergmasser. In: Conference contribution at Komplekse Undergrunnsanlegg - geometri og design. Hosted by NFF and Tekna.
- Panthi, K. K., Fall 2013b. Discussions with supervisor during Project Work.
- Panthi, K. K., 2013c. Predicting Tunnel Squeezing: A Discussion based on Two Tunnel Projects. *Hydro Nepal* (12), 20–25.
- Panthi, K. K., 2014b. Discussion of assumptions for numerical models. Date: 17.02.14.
- Rocscience, 2013. Phase2 Documentation.
- Sakurai, S., 1983. Displacement measurement associated with the design of underground openings. *Proc. Int. Symp. Field Measurements in Geomechanics*.
- Shrestha, G. L., 2006. Stress induced problems in Himalayan tunnels with special reference to squeezing. Ph.D. thesis, NTNU.
- Shrestha, P. K., Panthi, K. K., Aug. 2013. Groundwater Effect on Faulted Rock Mass: An Evaluation of Modi Khola Pressure Tunnel in the Nepal Himalaya. *Rock Mechanics and Rock Engineering* (123).

- Singh, B., Jethwa, J., Dube, A., Singh, B., 1992. Correlation between observed support pressure and rock mass quality. *Tunnelling and Underground Space Technology* 7 (1), 59–74.
- SINTEF, 2013. Materialdata for naturstein. Typiske verdier.
URL www.sintef.no
- Sisgeo, 2014. Hydraulic anchor load cells. Product information.
URL www.sisgeo.com
- Steiner, W., 1996. Tunnelling in Squeezing Rocks : Case Histories. *Rock Mechanics and Rock Engineering* 29, 211–246.
- Steiner, W., 2000. Squeezing rock in tunneling: identification and important factors. *Rivista Italiana di Geotecnica* (1).
- Vestad, M., 2013. Study on the Deformation Condition of Powerhouse Cavern of Neelum Jhelum HPP, Pakistan, TGB4500 Project work.
- Vlachopoulos, N., Diederichs, M. S., 2009. Improved longitudinal displacement profiles for convergence confinement analysis of deep tunnels. *Rock Mechanics and Rock Engineering* 42, 131–146.
- Vu, T. M., Sulem, J., Subrin, D., Monin, N., Lascols, J., 2013. Anisotropic Closure in Squeezing Rocks: The Example of Saint-Martin-la-Porte Access Gallery. *Rock Mech. Rock Eng.* 46, 231–246.
- Wang, T. T., Huang, T. H., 2014. Anisotropic Deformation of a Circular Tunnel Excavated in a Rock Mass Containing Sets of Ubiquitous Joints: Theory Analysis and Numerical Modeling. *Rock Mech. Rock Eng.* 47, 643–657.
- WAPDA, 2013. Neelum Jhelum Hydropower Project.
URL http://www.wapda.gov.pk/vision2025/htmls_vision2025/njhp.html
- World Stress Map, 2008.
URL www.world-stress-map.org







APPENDICES

A. STANDARD CHARTS AND FIGURES






A.1. Hoek and Brown constant m_i (Hoek and Marinos, 2000b)

Rock type	Class	Group	Texture			
			Coarse	Medium	Fine	Very fine
SEDIMENTARY	Clastic		Conglomerates (21 ± 3)	Sandstones 17 ± 4	Siltstones 7 ± 2	Claystones 4 ± 2
			Breccias (19 ± 5)		Greywackes (18 ± 3)	Shales (6 ± 2)
	Non-Clastic	Carbonates	Crystalline Limestone (12 ± 3)	Sparitic Limestones (10 ± 2)	Micritic Limestones (9 ± 2)	Dolomites (9 ± 3)
		Evaporites		Gypsum 8 ± 2	Anhydrite 12 ± 2	
Organic					Chalk 7 ± 2	
METAMORPHIC	Non Foliated		Marble 9 ± 3	Hornfels (19 ± 4)	Quartzites 20 ± 3	
				Metasandstone (19 ± 3)		
	Slightly foliated		Migmatite (29 ± 3)	Amphibolites 26 ± 6	Gneiss 28 ± 5	
	Foliated*		Schists 12 ± 3	Phyllites (7 ± 3)	Slates 7 ± 4	
IGNEOUS	Plutonic	Light	Granite 32 ± 3	Diorite 25 ± 5		
			Granodiorite (29 ± 3)			
	Dark	Gabbro 27 ± 3	Dolerite (16 ± 5)			
		Norite 20 ± 5				
	Hypabyssal		Porphyries (20 ± 5)		Diabase (15 ± 5)	Peridotite (25 ± 5)
Volcanic	Lava		Rhyolite (25 ± 5)	Dacite (25 ± 3)		
			Andesite 25 ± 5	Basalt (25 ± 5)		
	Pyroclastic	Agglomerate (19 ± 3)	Breccia (19 ± 5)	Tuff (13 ± 5)		

A.2. Determination of GSI (Hoek and Marinos, 2000b)

<p>GEOLOGICAL STRENGTH INDEX</p> <p>From the description of structure and surface conditions of the rock mass, pick an appropriate box in this chart. Estimate the average value of the Geological Strength Index (GSI) from the contours. Do not attempt to be too precise. Quoting a range of GSI from 36 to 42 is more realistic than stating that GSI = 38. It is also important to recognize that the Hoek-Brown criterion should only be applied to rock masses where the size of the individual blocks or pieces is small compared with the size of the excavation under consideration. When individual block sizes are more than approximately one quarter of the excavation dimension, failure will generally be structurally controlled and the Hoek-Brown criterion should not be used.</p>		<p>SURFACE CONDITIONS</p> <p>VERY GOOD Very rough, fresh unweathered surfaces</p> <p>GOOD Rough, slightly weathered, iron stained surfaces</p> <p>FAIR Smooth, moderately weathered and altered surfaces</p> <p>POOR Slackensided, highly weathered surfaces with coatings or fillings of angular fragments</p> <p>VERY POOR Slackensided, highly weathered surfaces with soft clay coatings or fillings</p> <p>DECREASING SURFACE QUALITY →</p>				
<p>STRUCTURE</p> <p> INTACT OR MASSIVE – intact rock specimens or massive in situ rock with very few widely spaced discontinuities</p> <p> BLOCKY - very well interlocked undisturbed rock mass consisting of cubical blocks formed by three orthogonal discontinuity sets</p> <p> VERY BLOCKY - interlocked, partially disturbed rock mass with multifaceted angular blocks formed by four or more discontinuity sets</p> <p> BLOCKY/DISTURBED - folded and/or faulted with angular blocks formed by many intersecting discontinuity sets</p> <p> DISINTEGRATED - poorly interlocked, heavily broken rock mass with a mixture of angular and rounded rock pieces</p> <p> FOLIATED/LAMINATED – Folded and tectonically sheared foliated rocks. Schistosity prevails over any other discontinuity set, resulting in complete lack of blockiness</p> <p>← DECREASING INTERLOCKING OF ROCK PIECES</p>		<p>90</p> <p>80</p> <p>70</p> <p>60</p> <p>50</p> <p>40</p> <p>30</p> <p>20</p> <p>10</p> <p>5</p> <p>N/A</p> <p>N/A</p> <p>N/A</p> <p>N/A</p> <p>N/A</p> <p>N/A</p> <p>N/A</p> <p>N/A</p>				
		<p>→</p>				

A.3. Disturbance factor D (Hoek et al., 2002)

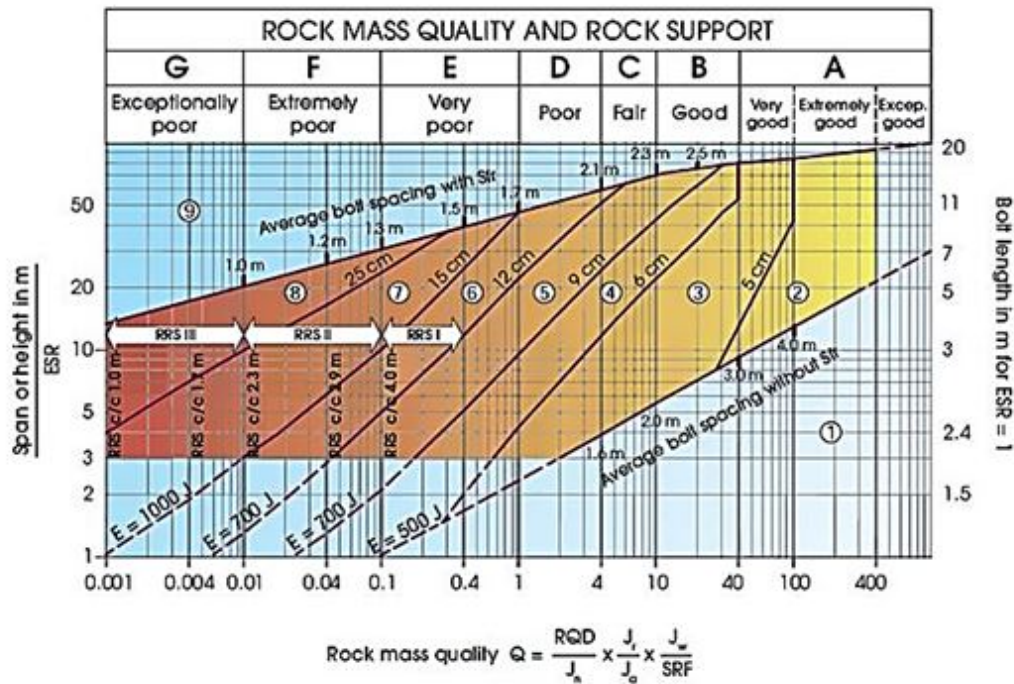
Appearance of rock mass	Description of rock mass	Suggested value of <i>D</i>
	Excellent quality controlled blasting or excavation by Tunnel Boring Machine results in minimal disturbance to the confined rock mass surrounding a tunnel.	<i>D</i> = 0
	Mechanical or hand excavation in poor quality rock masses (no blasting) results in minimal disturbance to the surrounding rock mass. Where squeezing problems result in significant floor heave, disturbance can be severe unless a temporary invert, as shown in the photograph, is placed.	<i>D</i> = 0 <i>D</i> = 0.5 No invert
	Very poor quality blasting in a hard rock tunnel results in severe local damage, extending 2 or 3 m, in the surrounding rock mass.	<i>D</i> = 0.8
	Small scale blasting in civil engineering slopes results in modest rock mass damage, particularly if controlled blasting is used as shown on the left hand side of the photograph. However, stress relief results in some disturbance.	<i>D</i> = 0.7 Good blasting <i>D</i> = 1.0 Poor blasting
	Very large open pit mine slopes suffer significant disturbance due to heavy production blasting and also due to stress relief from overburden removal. In some softer rocks excavation can be carried out by ripping and dozing and the degree of damage to the slopes is less.	<i>D</i> = 1.0 Production blasting <i>D</i> = 0.7 Mechanical excavation

A.4. Description of ratings for input parameters for Q-system (Barton, 2002)

RQD (Rock quality designation, %)		J_n (Joint set number)	
Very poor	0 - 25	Massive, no or few joints	0.5 - 1
Poor	25 - 50	One joint set	2
Fair	50 - 75	One joint set + random joints	3
Good	75 - 90	Two joint sets	4
Excellent	90 - 100	Two joint sets + random	6
<i>Notes:</i>		Three joint sets	9
(i) where RQD is reported or measured as ≤ 10 (including 0), a nominal value of 10 is used to evaluate Q.		Three joint sets + random	12
(ii) RQD intervals of 5 i.e. 100, 95, 90 etc., are successfully accurate.		Four or more joint sets, heavily jointed, sugar cube etc	15
		Crushed rock, earthlike	20
		<i>Note:</i> For tunnel intersections, use (3 x J _n) and for portals use (2 x J _n)	
J_r (Joint roughness number)			
<i>(a) Rock wall contact</i>		<i>(b) Rock wall contact before 10 cm shear</i>	
Discontinuous joints	4	Rough or irregular, undulating	1.5
Rough or irregular, undulating	3	Smooth, undulating	1
Smooth, undulating	2	Slickensided, undulating	0.5
Slickensided, undulating	1.5		
<i>© No rock wall contact when sheared</i>			
Zone containing clay minerals thick enough to prevent rock wall contact			1
Sandy, gravelly or crushed zone thick enough to prevent rock wall contact			1
<i>Notes:</i> (i) Description refers to small-scale features and intermediate scale features, in that order (ii) Add 1.0 if the mean spacing of the relevant joint set is greater than 3 m. (iii) J _r = 0.5 can be used for planar, slickenside joints having lineations, provided these are oriented for minimum strength. (iv) J _r and J _a classification is applied to the joint set that is least favorable for stability both from the point of view of orientation and shear resistance, $\tau \approx \sigma_n \cdot \tan^{-1} (J_r/J_a)$			
J_a (Joint alteration number)			
<i>(a) Rock wall contact (no mineral fillings, only coatings)</i>		<i>φ_r (appr.)</i>	J_a
Tightly healed, hard, non-softening, impermeable filling i.e., quartz/epidote		-	0.75
Unaltered joint walls, surface staining only		25 - 35	1
Slightly altered joint walls, non-softening mineral coatings, sandy particles, clay free disintegrated rock, etc.		25 - 30	2
Silty or sandy clay coatings, small clay fractions (non-softening)		20 - 25	3
Softening or low friction clay mineral coatings, i.e., kaolinite or mica. Also chlorite, talk, gypsum, graphite etc., and small quantities of swelling clay		8 - 16	4
<i>(b) Rock wall contact before 10 cm shear (thin mineral fillings)</i>			
Sandy particles, clay free disintegrated rock etc.		25 - 30	4
Strongly over-consolidated non-softening clay mineral fillings (continuous, but < 5mm thickness)		16 - 24	6

Medium or low over-consolidated non-softening clay mineral fillings (continuous, but < 5mm thickness)	12 - 16	8	
Swelling clay fillings, i.e., montmorillonite (continuous, but < 5mm thick)	6 - 12	8 - 12	
<i>(c) No rock wall contact when sheared (thick mineral fillings)</i>			
Zones or bands of disintegrated or crushed rock and clay	6 - 24	6, 8 - 12	
Zones or bands of silty or sandy clay, small clay fraction (non-softening)	-	5	
Thick, continuous zones or bands of clay	6 - 24	13 - 20	
<i>J_w (Joint water reduction factor)</i>	<i>Approx. P (bars)</i>	<i>J_w</i>	
Dry excavations or minor inflow, i.e., < 5 l/min locally	< 1	1	
Medium inflow or pressure, occasional outwash of joint fillings	1 - 2.5	0.66	
Large inflow or high pressure in competent rock with unfilled joints	2.5 - 10	0.5	
Large inflow or high pressure, considerable outwash of joint fillings	2.5 - 10	0.33	
Exceptionally high inflow or pressure at blasting, decaying with time	> 10	0.2 - 0.1	
Exceptionally high inflow or pressure continuing without noticeable decay with time	> 10	0.2 - 0.1	
<i>Notes: (i) The last four factors are crude estimates. Increase J_w if drainage measures are installed. (ii) Special problems caused by ice formation are not considered. (iii) For general characterization of rock masses distance from excavation influences. The use of J_w = 1, 0.66, 0.5, 0.33, etc. as depth increases from say 0-5, 5-25, 25-250 to >250m is recommended, assuming that RQD/J_n is low enough (0.5-25) for good hydraulic connectivity.</i>			
<i>SRF (Stress Reduction Factor)</i>			
<i>(a) Weakness zones intersecting excavation, which may cause loosening of rock mass</i>	<i>SRF</i>		
Multiple occurrence of weakness zones containing clay or chemically disintegrated rock, very loose surrounding rock at any depth	10		
Single weakness zone containing clay or chemically disintegrated rock (depth ≤ 50m)	5		
Single weakness zone containing clay or chemically disintegrated rock (depth > 50m)	2.5		
Multiple shear zones in competent rocks (clay free), loose surrounding rock at any depth	7.5		
Single shear zone in competent rocks (clay free), (depth of excavation ≤ 50m)	5		
Single shear zone in competent rocks (clay free), (depth of excavation > 50m)	2.5		
Loose, open joints, heavily jointed or sugar cube etc. at any depth	5		
<i>Note: Reduce these values of SRF by 25 - 50 % if the relevant shear zones only influence but do not intersect the excavation.</i>			
<i>(b) Competent rock, rock stress problems</i>	σ_c / σ_1	σ_t / σ_c	<i>SRF</i>
Low stress, near surface, open joints	> 200	< 0.01	2.5
Medium stress, favorable stress condition	200 - 10	0.01 - 0.3	1
High stress, very tight structures. Usually favorable to stability, may be unfavorable for wall stability	10 - 5	0.3 - 0.4	0.5 - 2
Moderate slabbing after > 1 hour in massive rock	5 - 3	0.5 - 0.65	5 - 50
Slabbing and rock burst after a few minutes of excavation	3 - 2	0.65 - 1	50 - 200
Heavy rock burst and immediate dynamic deformations	< 2	> 1	200 - 400
<i>Notes: (i) For strongly anisotropic virgin stress field (if measured): when $5 \leq \sigma_1 / \sigma_3 \leq 10$, reduce σ_c to $0.75 \sigma_c$ and when $\sigma_1 / \sigma_3 > 10$, reduce σ_c to $0.5 \sigma_c$. (ii) For general characterization of rock mass, overburden from excavation influences. The use of SRF 5, 2.5, 1 and 0.5 is recommended as depth increases from say 0-5, 5-25, 25-250 to > 250m respectively.</i>			
<i>© Squeezing rock: plastic flow of incompetent rock under the influence of high rock pressure</i>	σ_t / σ_c	<i>SRF</i>	
Mild squeezing rock pressure	1 - 5	5 - 10	
Heavy squeezing rock pressure	> 5	10 - 20	
<i>(d) Swelling rock: chemical swelling activity depending on pressure of water</i>	<i>SRF</i>		
Mild swelling rock pressure	5 - 10		
Heavy swelling rock pressure	10 - 15		

A.5. Q-system support charts (NGI, 2013)



Support categories

- ① Unsupported or spot bolting
- ② Spot bolting, SB
- ③ Systematic bolting, fibre reinforced sprayed concrete, 5-6 cm, B+Sfr
- ④ Fibre reinforced sprayed concrete and bolting, 6-9 cm, Sfr (E500)+B
- ⑤ Fibre reinforced sprayed concrete and bolting, 9-12 cm, Sfr (E700)+B
- ⑥ Fibre reinforced sprayed concrete and bolting, 12-15 cm + reinforced ribs of sprayed concrete and bolting, Sfr (E700)+RRS I+B
- ⑦ Fibre reinforced sprayed concrete >15 cm + reinforced ribs of sprayed concrete and bolting, Sfr (E1000)+RRS II+B
- ⑧ Cast concrete lining, CCA or Sfr (E1000)+RRS III+B
- ⑨ Special evaluation

Bolts spacing is mainly based on Ø20 mm

E = Energy absorption in fibre reinforced sprayed concrete

ESR = Excavation Support Ratio

Areas with dashed lines have no empirical data

RRS - spacing related to Q-value

Si30/6 Ø16 - Ø20 (span 10m)
D40/6+2 Ø16-20 (span 20m)

Si35/6 Ø16-20 (span 5m)
D45/6+2 Ø16-20 (span 10m)
D55/6+4 Ø20 (span 20m)

D40/6+4 Ø16-20 (span 5m)
D55/6+4 Ø20 (span 10m)
D70/6+6 Ø20 (span 20m)

Si30/6 = Single layer of 6 rebars,
30 cm thickness of sprayed concrete

D = Double layer of rebars

Ø16 = Rebar diameter is 16 mm

c/c = RSS spacing, centre - centre

A.6. Rock Mass Rating system (RMR) (Bieniawski, 1989)

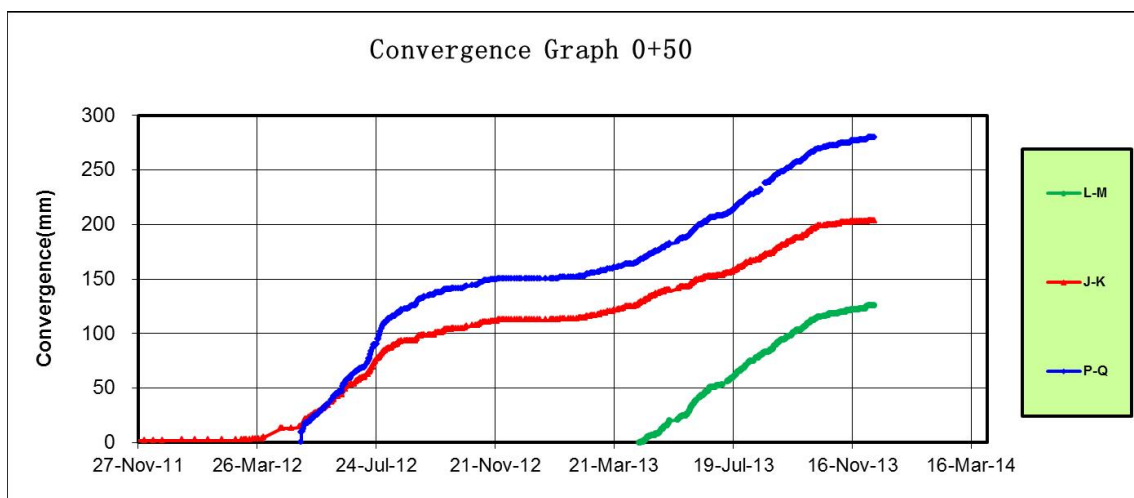
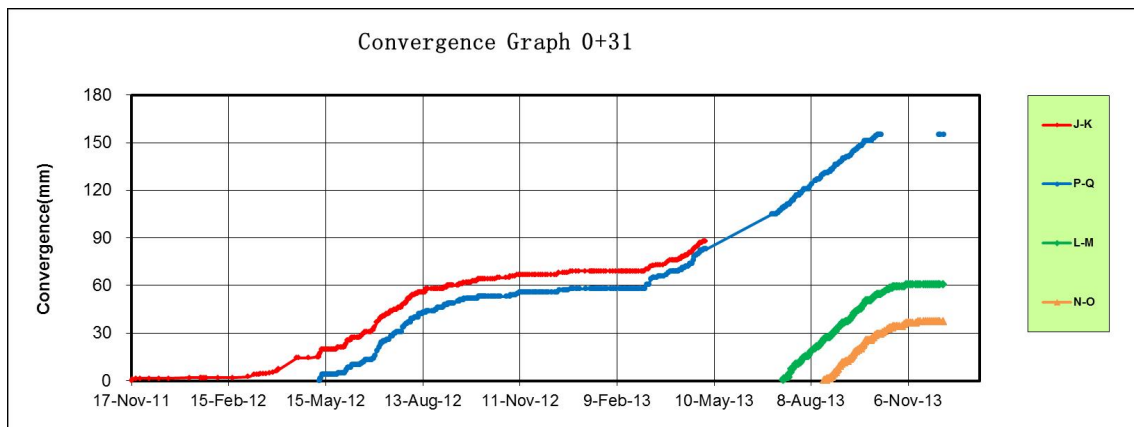
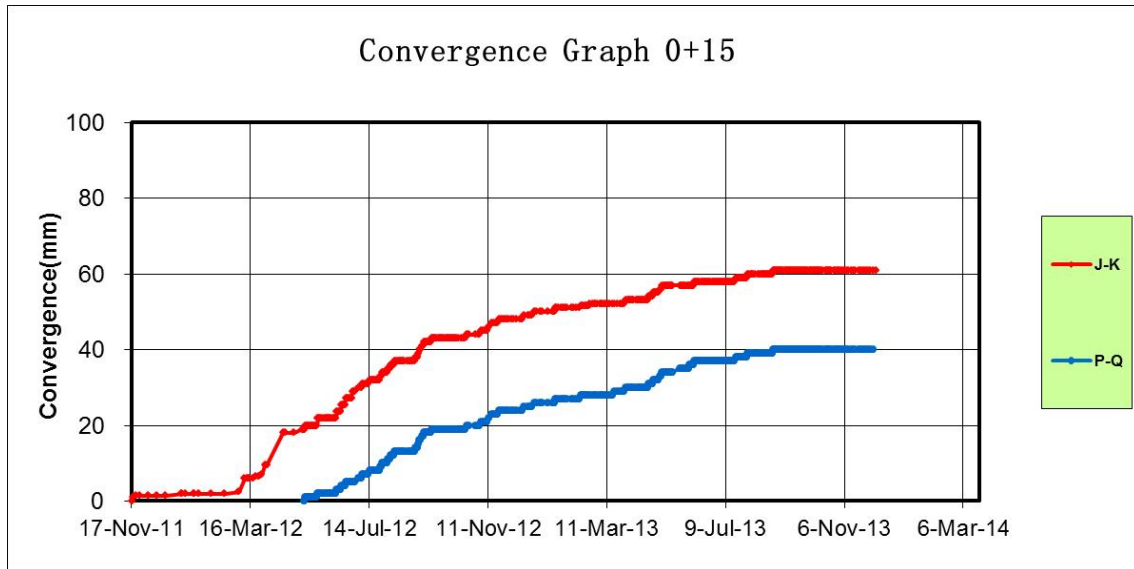
A. Classification parameters and their ratings									
Parameters			Range of values or ratings						
1	Strength of Intact Rock	Point load strength index (MPa)	> 10	4 - 10	2 - 4	1 - 2	Low range uniaxial strength is preferred		
		Uniaxial compressive strength (MPa)	> 250	100-250	50-100	25-50	5- 25	1 - 5	< 1
	Rating	15	12	7	4	2	1	0	
2	Drill core quality, RQD (%)		90-100	75-90	50-75	25-50	< 25		
	Rating		20	17	13	8	5		
3	Spacing of discontinuities (m)		> 2	0.6-2	0.2-0.6	0.06-0.2	< 0.06		
	Rating		20	15	10	8	5		
4	Condition of discontinuities	Length, persistence (m)	< 1	1-3	3-10	10-20	> 20		
		Rating	6	4	2	1	0		
		Separation (mm)	none	< 0.1	0.1-1	1-5	> 5		
		Rating	6	5	4	1	0		
		Roughness	very rough	rough	slightly rough	smooth	slickensided		
		Rating	6	5	3	1	0		
		Infilling (gouge) (mm)	none	hard filling		soft filling			
Rating	6	< 5	> 5	< 5	> 5	0			
4	Weathering	un-weathered	slightly weathered	moderately weathered	highly weathered	decomposed			
		Rating	6	5	3	1	0		
		here, ρ_w is joint water pressure and σ_1 is major principle stress							
5	Ground water	Inflow per 10 meter tunnel length (l/min)	none	< 10	10-25	25-125	> 125		
		ρ_w / σ_1	0	0.01	0.1-0.2	0.2-0.5	> 0.5		
		General conditions	dry	damp	wet	dripping	flowing		
		Rating	15	10	7	4	0		
B. Rating adjustment for discontinuity orientation									
Tunnel alignment		very favorable	favorable	fair	unfavorable	very unfavorable			
Rating adjustment		0	-2	-5	-10	-12			
C. Rock mass classes determined from total ratings									
Rating		100-80	80-61	60-41	40-21	< 20			
Class No.		I	II	III	IV	V			
Description		Very good	Good	Fair	Poor	Very poor			
D. Meaning or rock mass classes									
Class No.		I	II	III	IV	V			
Average stand-up time		Can be estimated from Figure 4-4							
Cohesion of the rock mass (kPa)		> 400	3-400	2-300	1-200	< 00			
Friction angle of the rock mass (degrees)		< 45	35-45	25-35	15-25	< 15			

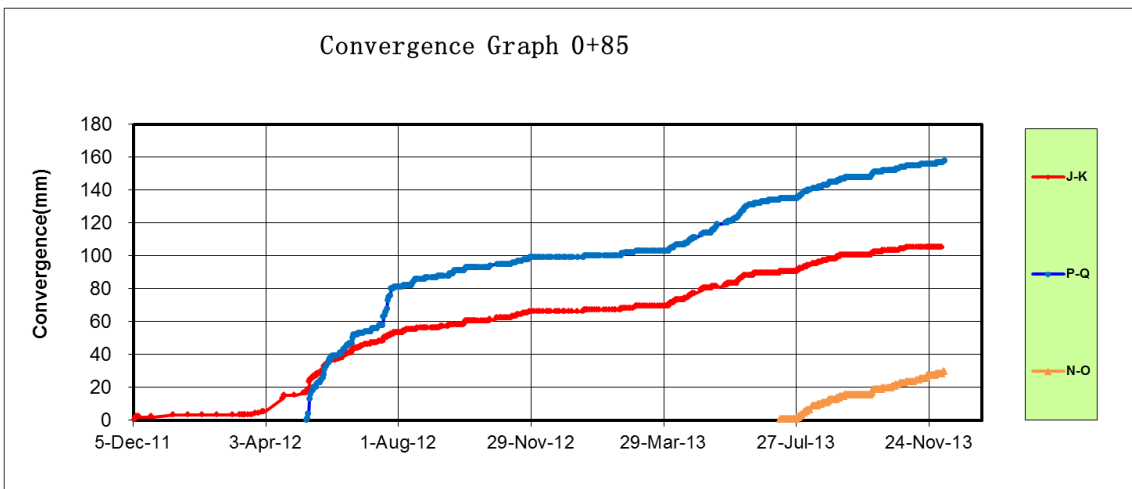
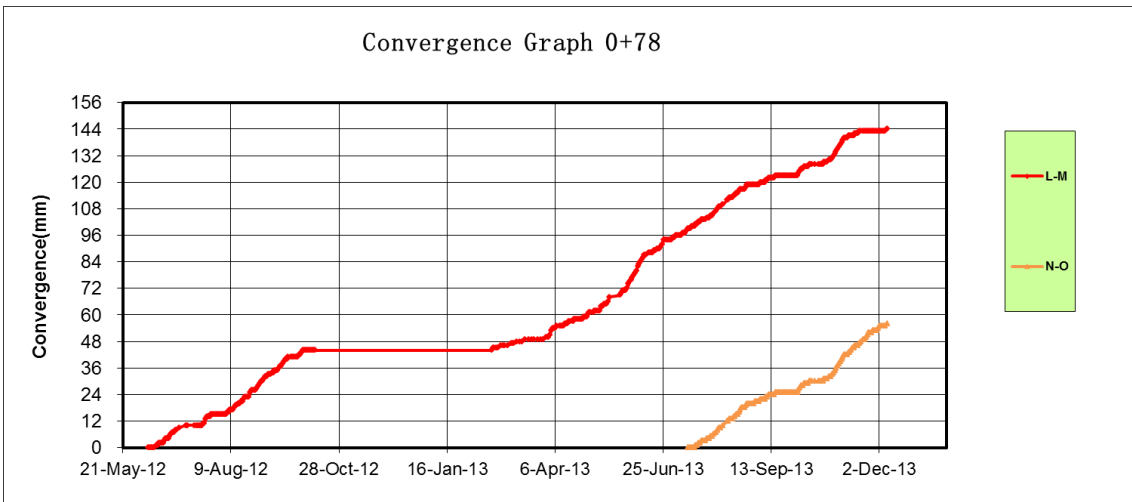
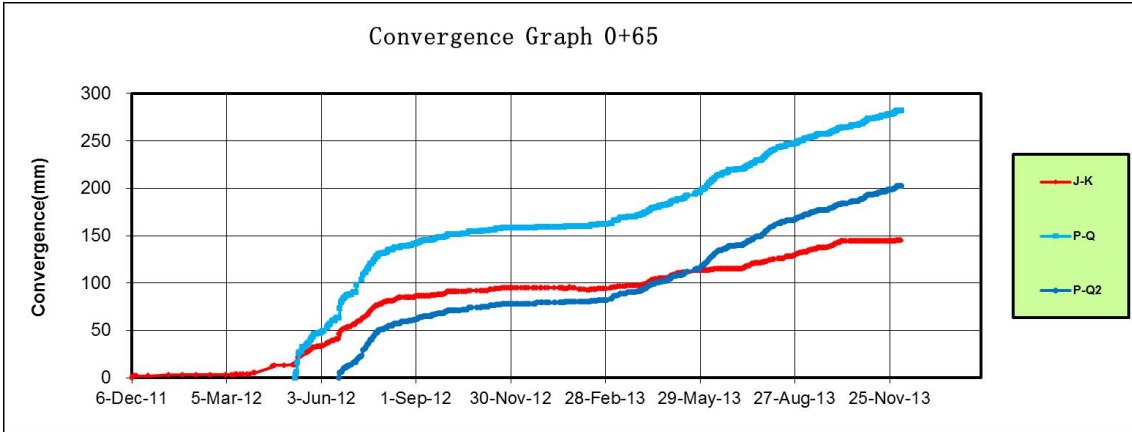
A.7. Relationship between Q-value and RMR (Panthi, 2006)

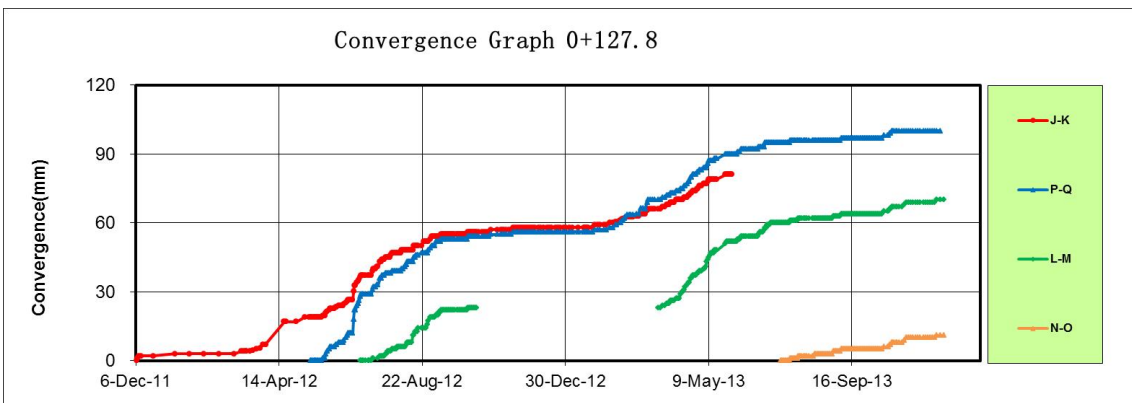
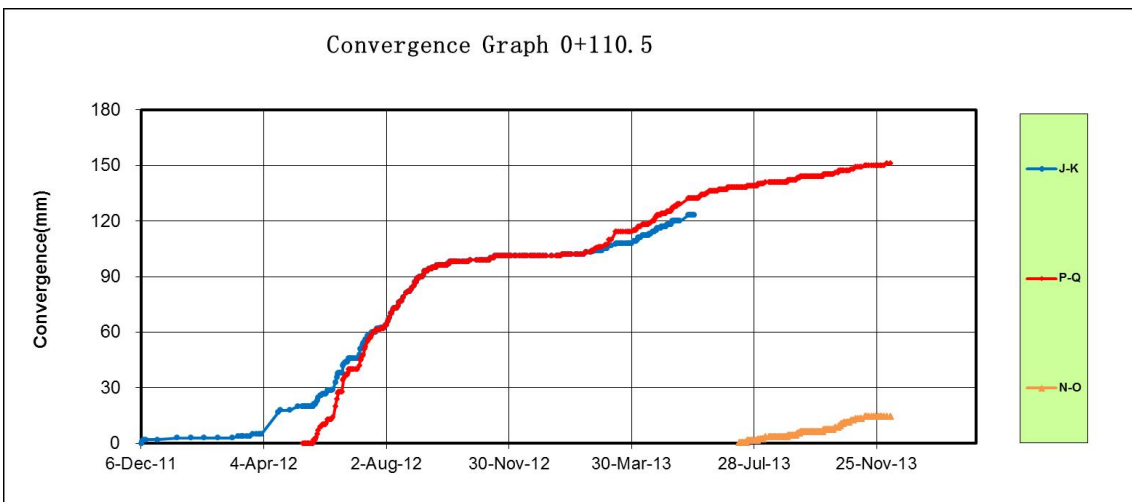
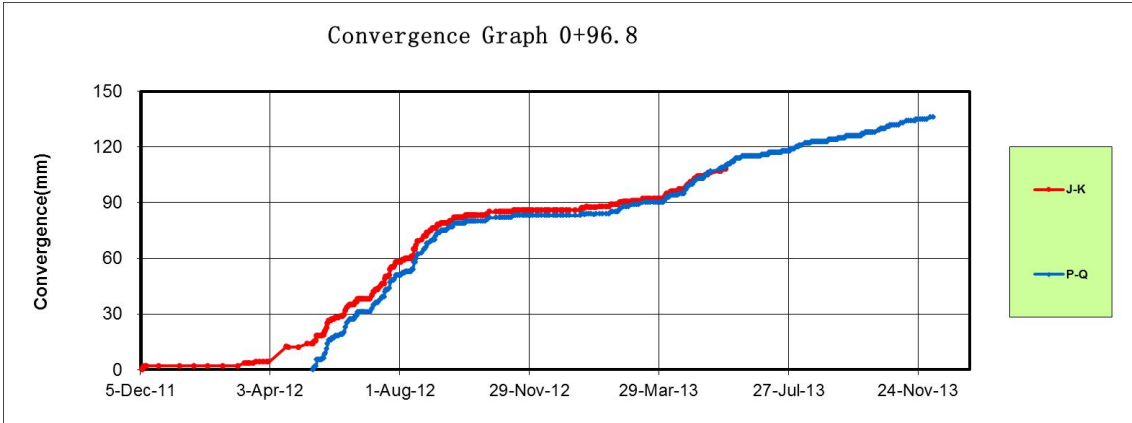
		$RMR \approx 9 \times \ln Q + 44$ (Bieniawski, 1989)		$RMR = 15 \times \log Q + 50$ (Barton, 1995)	
Descriptions		Range of Q-values		Range of RMR-values	
Rock Class	Quality descriptions	Minimum	Maximum	Minimum	Maximum
Class 1	Very good to excellent	100	1000	85	100
Class 2	Good	10	100	65	85
Class 3	Fair to good	4	10	56	65
Class 4	Poor	1	4	44	56
Class 5	Very poor	0.1	1	35	44
Class 6	Extremely poor	0.01	0.1	20	35
Class 7	Exceptionally poor	0.001	0.01	5	20

B. NJHPP DEFORMATION PLOTS

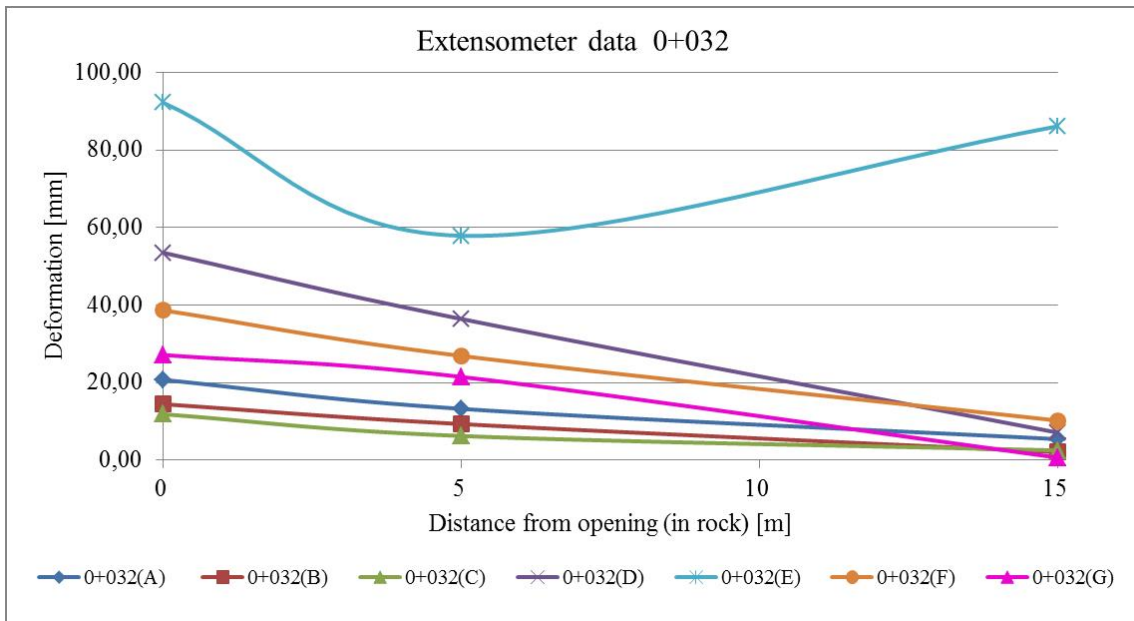
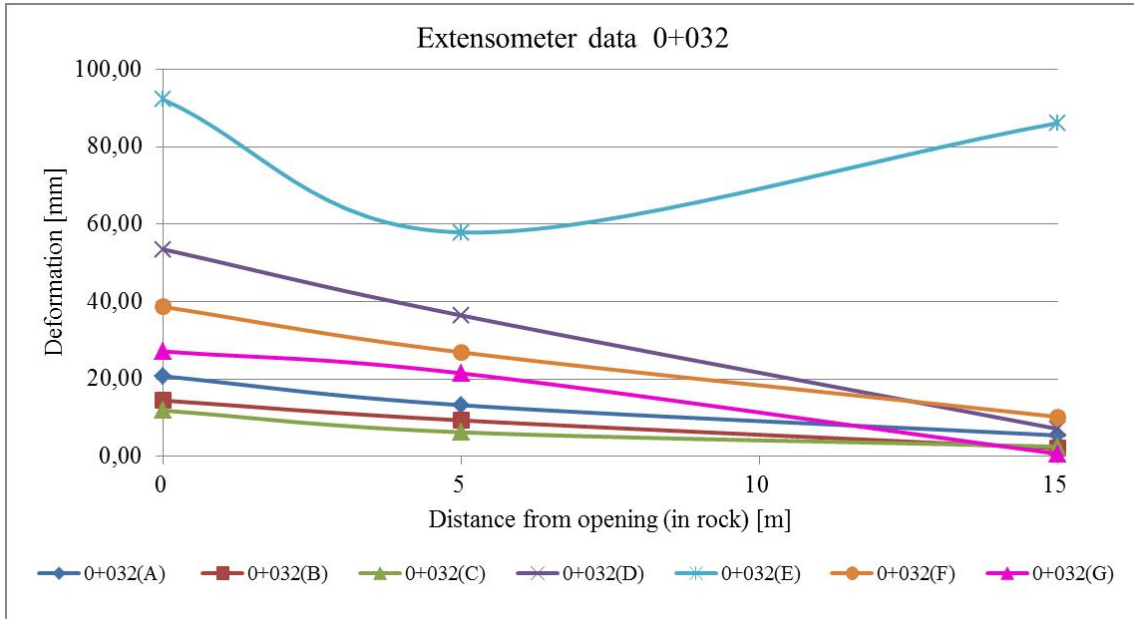
B.1. Convergence plots (NJC, 2013a)

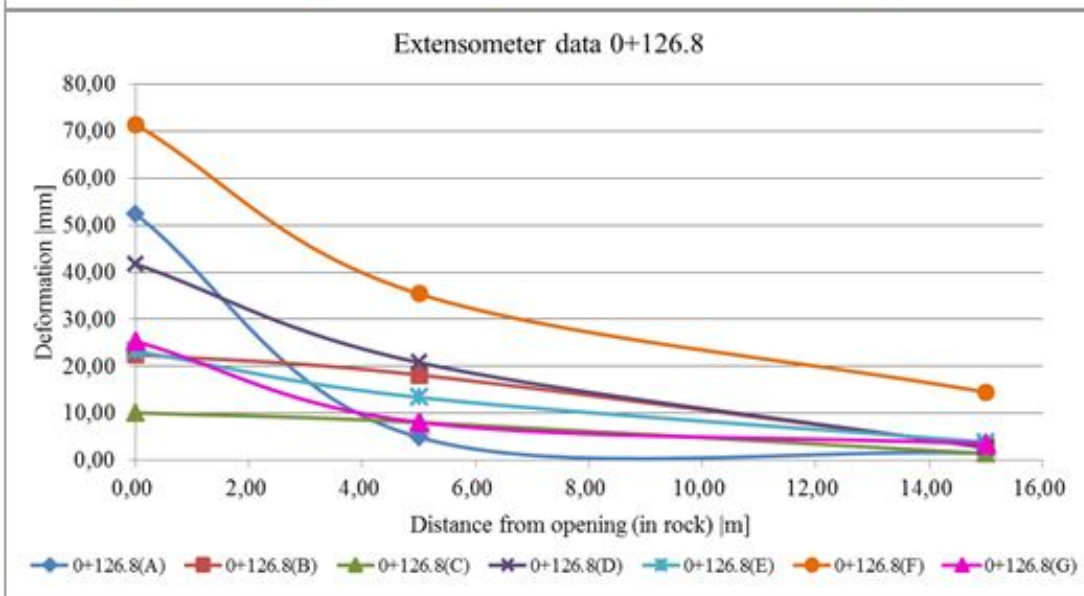
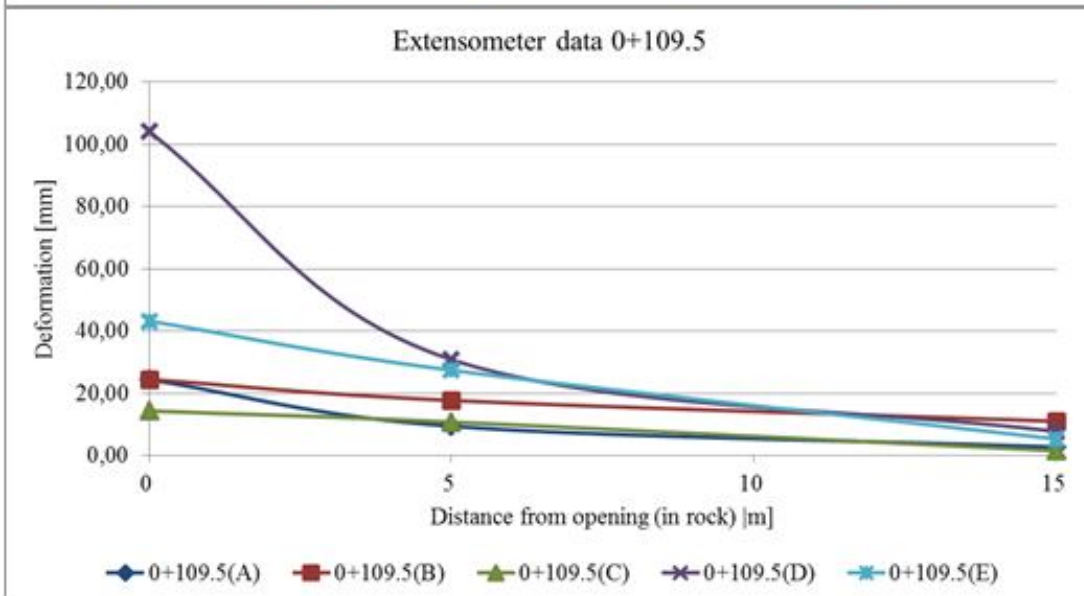
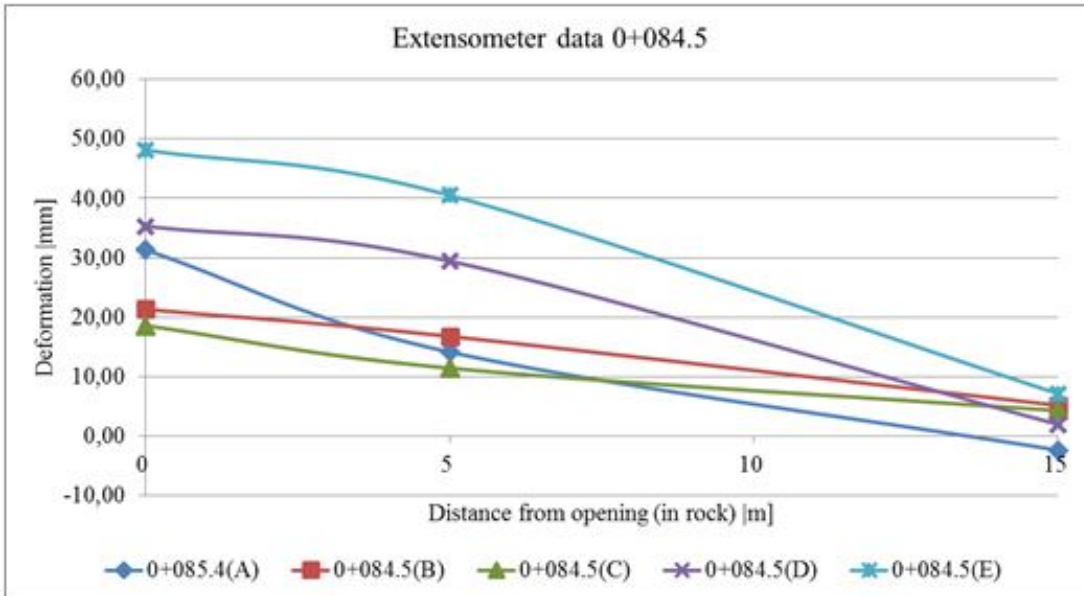




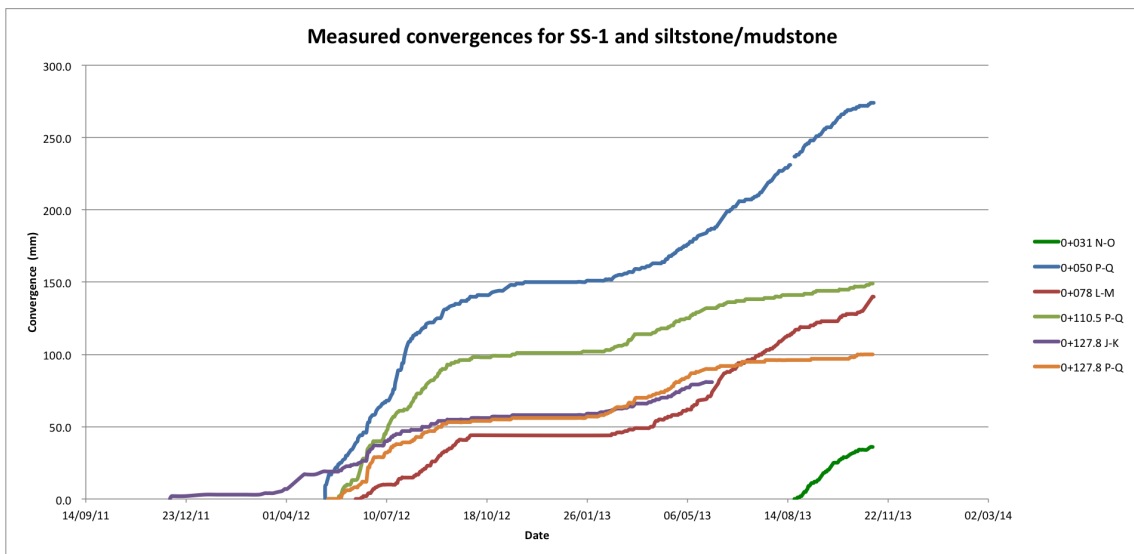
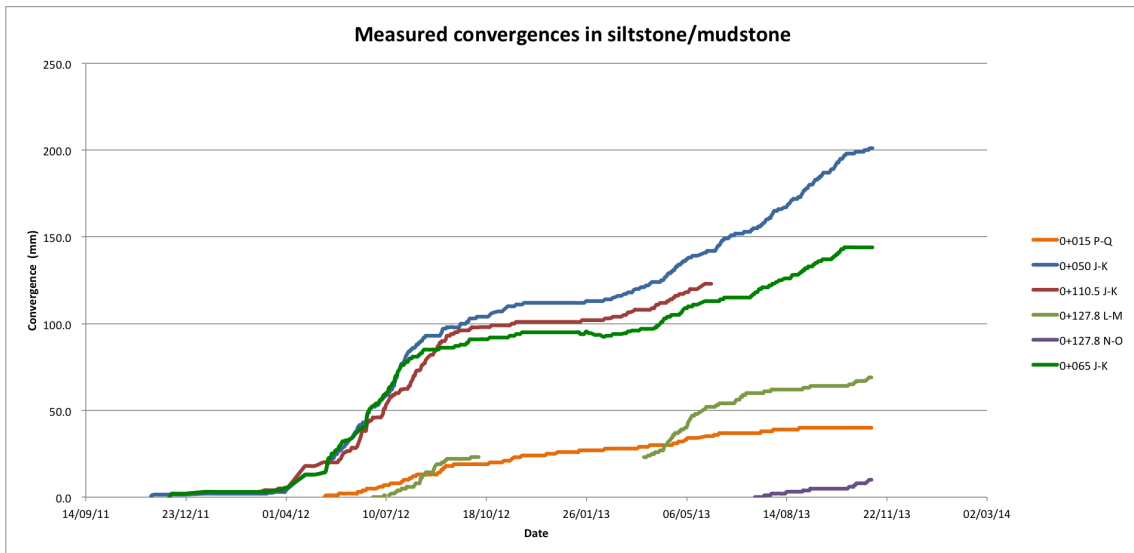
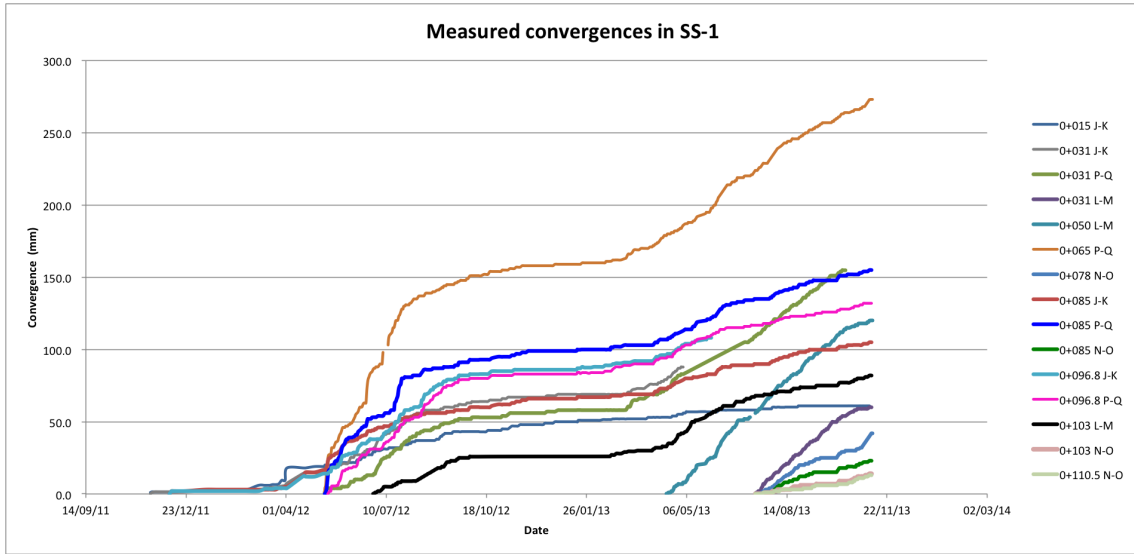


B.2. Extensometer plots





B.3. Convergence plotted based on rock type anchoring



C. DETAILED CALCULATIONS AND RESULT

C.1. Prediction by Goel (1994) and Q-method

1. Prediction by Geol (1994)

Prediction of squeezing using Goel (1994)					
Section	Overburden H [m]	Eq. Diameter [m]	HB ^{0.1}	Rock mass number	Prediction
0+015	420	29.3	589	2.7 - 5	Moderate
0+032	420	36.4	602	2.7 - 5	Moderate/ High
0+065	420	43.2	612	0.75 - 3.9	High/ Moderate
0+085	420	43.0	612	2.7 - 5	Moderate/ High
0+127	450	37.4	646	0.6 – 0.9	High

2. Prediction by Q-method

Section	Vertical stress p_0 [MPa]	Rock mass strength σ_{cm} [MPa] by Panthi (2006)			Prediction by Q-method			
		Min	Max	Mean	P_0/σ_{cm} Min	P_0/σ_{cm} Max	P_0/σ_{cm} Mean	Prediction
0+015	11.25	10.94	15.96	13.39	0.70	1.03	0.84	No (Mild)
0+032	11.25	10.94	15.96	13.39	0.70	1.03	0.84	No (Mild)
0+065	11.25	8.04	12.25	10.07	0.92	1.40	1.12	Mild
0+085	11.25	10.94	15.96	13.39	0.70	1.03	0.84	No (Mild)
0+127	12.10	5.14	8.53	6.76	1.42	2.36	1.79	Mild

C.2. Hoek and Marinos (2000) calculations

1. Prediction by Hoek and Marinos without support pressure

Section	Vertical stress p_0 [MPa]	Rock mass strength σ_{cm} [MPa] by Panthi (2006)			Prediction by Hoek and Marinos (2000) Strain (%) without support pressure			
		Min	Max	Mean	Min	Max	Mean	Prediction
0+015	11.25	10.94	15.96	13.39	0.10	0.21	0.14	Few stability problems
0+032	11.25	10.94	15.96	13.39	0.10	0.21	0.14	
0+065	11.25	8.04	12.25	10.07	0.17	0.39	0.25	
0+085	11.25	10.94	15.96	13.39	0.10	0.21	0.14	
0+127	12.10	5.14	8.53	6.76	0.40	1.11	0.64	

2. Prediction by Hoek and Marinos with support pressure. The combined support pressure was calculated by the CCM (SCC).

Section	Vertical stress p_0 [MPa]	Support pressure p_s [MPa]	Rock mass strength σ_{cm} [MPa] by Panthi (2006)			Prediction by Hoek and Marinos (2000) Strain (%) with support pressure			
			Min	Max	Mean	Min	Max	Mean	Prediction
0+015	11.25	0.38	10.94	15.96	13.39	0.10	0.20	0.14	Few stability problems
0+032	11.25	0.33	10.94	15.96	13.39	0.10	0.20	0.14	
0+065	11.25	0.30	8.04	12.25	10.07	0.16	0.37	0.24	
0+085	11.25	0.30	10.94	15.96	13.39	0.10	0.20	0.14	
0+127	12.10	0.30	5.14	8.53	6.76	0.38	1.01	0.60	

3. Size of the plastic zone, and strain (%) converted to deformation in mm

Section	Equivalent diameter [m]	Diameter plastic zone by Hoek and Marinos (2000) [m]			Deformation in mm based on strain (%) with support		
		Min	Max	Mean	Min	Max	Mean
0+015	29.3	29,9	36,6	32,8	28,72	59,25	40,27
0+032	36.4	37,1	45,5	40,8	35,71	73,96	50,15
0+065	43.2	50,9	63,9	56,6	70,85	160,00	103,41
0+085	43.0	43,9	53,8	48,3	42,23	87,68	59,38
0+127	37.4	55,7	73,4	63,2	141,95	378,91	222,54

C.3. CCM: GRC and LDP

The procedure and calculation are the same for all sections, just with different equivalent radius. Calculation for section 0+085 is shown below for two conditions; (1) sandstone properties with vertical stress as far-field stress and (2) mudstone/siltstone properties with mean stress as far-field stress.

1. Input and output for section 0+085 with sandstone properties and vertical stress

INPUT: Sandstone and vertical stress			
Geometry			
Cross sectional area cavern	A	1452	m ²
Equivalent tunnel radius	R _{eq}	21.5	m
Rock mass - SS-1			
Intact strength	σ_{ci}	86.4	MPa
Intact parameter	m_i	17	-
Poisson's ratio	ν	0,27	-
Dilation angle	ψ	0	deg
GSI	GSI	54	-
Unit weight	Υ	0.0273	MN/m ³
Elastic modulus	E_i	58.1	GPa
Basic friction angle	ϕ	32	deg
Loading			
Overburden	H	420	m
Vertical stress/Initial far field stress	σ_0	11.25	MPa
OUTPUT			
Rock Mass parameters SS-1	m_b	1.1	-
	s	0.001	-
	a	0.5	-
Rock mass modulus	E_{rm}	11.7	GPa
Rock mass shear modulus	G_{rm}	4.61	GPa
Dilation coefficient	K_v	1	-
Far field stress	S_0	0.12	MPa
Scaled critical internal pressure	P_{cr}	0.03	MPa
Actual critical internal pressure	p_{cr}	2.88	MPa

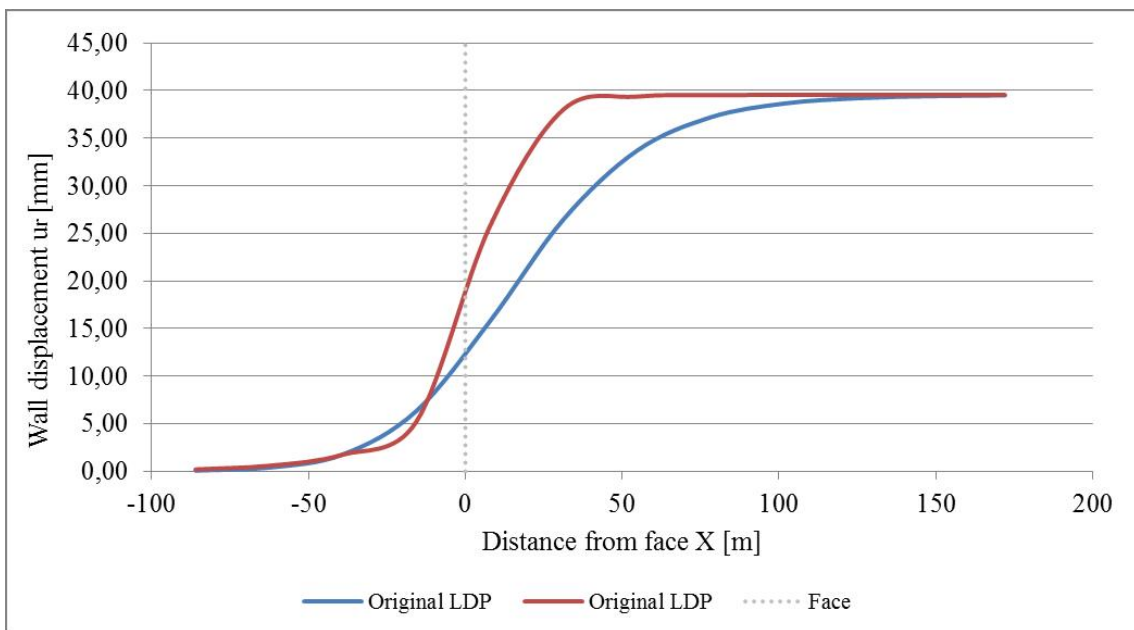
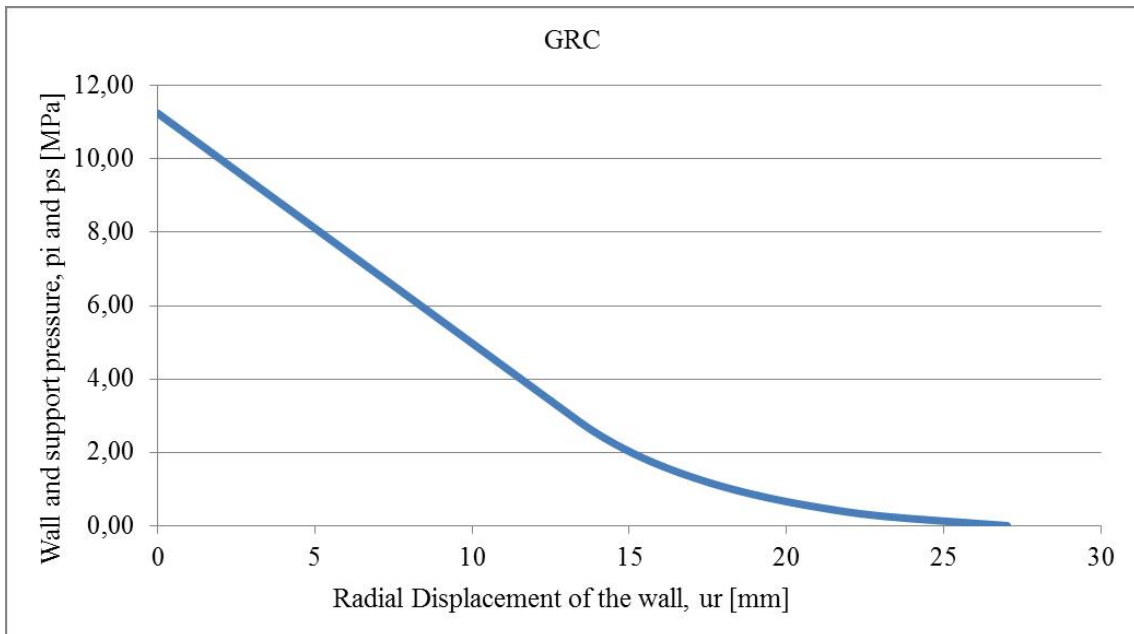
2. Calculation of GRC with sandstone properties with vertical stress as far-field stress

Ground Reaction Curve - GRC							
		Internal pressure	Int p_i crown	Int p_i floor		R_p/R	Radial disp., u_r
	Point	pip_grc [MPa]	pip_r_grc [MPa]	pip_f_grc [MPa]	pips_grc	xi_grc	ur_grc [mm]
Elastic	1	11,25	-	-	-	-	0
	2	2,88	-	-	-	-	19,53
Plastic region	1	2,88	2,88	2,88	0,03	1,00	19,53
	2	2,61	2,62	2,61	0,03	1,02	20,18
	3	2,35	2,37	2,33	0,03	1,03	20,90
	4	2,09	2,12	2,06	0,02	1,05	21,72
	5	1,83	1,87	1,79	0,02	1,07	22,65
	6	1,57	1,62	1,51	0,02	1,09	23,72
	7	1,31	1,38	1,24	0,01	1,12	24,96
	8	1,05	1,13	0,96	0,01	1,14	26,43
	9	0,78	0,89	0,68	0,01	1,18	28,23
	10	0,52	0,65	0,40	0,01	1,21	30,52
	11	0,26	0,42	0,11	0,00	1,26	33,71
	12	0,00	0,20	-0,20	0,00	1,35	39,55

3. Calculation of the original and improved LDP for sandstone properties with vertical stress as far-field stress

Equivalent tunnel radius	R_eq	21,5	m				
Max. Disp	u_max	39,5	mm				
Maximum normalized plastic zone radius	R*	1,3	-				
Normalized displacement at face	u_o*	0,3	-				
Original LDP				Improved LDP			
Point	lf_r	lf [m]	u_r [mm]	Point	X*=X/R	Dist to face X [m]	u_r [mm]
1	-4	-85,994	0,08	1	-4	-85,994	0,20
2	-2,909	-62,541	0,39	2	-2,909	-62,541	0,59
3	-1,818	-39,088	1,77	3	-1,818	-39,088	1,75
4	-0,727	-15,635	6,33	4	-0,727	-15,635	5,21
5	0,364	7,818	15,75	5	0,364	7,818	25,73
6	1,455	31,271	26,46	6	1,455	31,271	38,02
7	2,545	54,723	33,69	7	2,545	54,723	39,38
8	3,636	78,176	37,20	8	3,636	78,176	39,53
9	4,727	101,629	38,65	9	4,727	101,629	39,54
10	5,818	125,082	39,21	10	5,818	125,082	39,54
11	6,909	148,535	39,42	11	6,909	148,535	39,54
12	8	171,988	39,50	12	8	171,988	39,55

4. GRC and LDP for section 0+085



5. Input and output for section 0+085 with mudstone/siltstone properties and mean stress as far-field stress

INPUT: Mudstone/siltstone and mean stress			
Geometry			
Cross sectional area cavern	A	1452	m ²
Equivalent tunnel radius	R _{eq}	21.5	m
Rock mass			
Intact strength	σ_{ci}	54.1	MPa
Intact parameter	m _i	8	-
Poisson's ratio	ν	0.21	-
Dilation angle	ψ	0	deg
GSI	GSI	43	-
Unit weight	γ	0.027	MN/m ³
Elastic modulus	E _i	34	GPa
Basic friction angle	ϕ	30	deg
Loading			
Overburden	H	420	m
Vertical stress	σ_v	11.25	MPa
Horizontal in-plane stress	σ_h	5.96	MPa
Mean far-field stress	σ_0	8.61	MPa
OUTPUT			
Rock Mass parameters SS-1	m _b	0.27	-
	s	0.0002	-
	a	0.51	-
Rock mass modulus	E _{mm}	4.92	GPa
Rock mass shear modulus	G _{mm}	2.03	GPa
Dilation coefficient	K _{ψ}	1	-
Far field stress	S ₀	0.59	MPa
Scaled critical internal pressure	P _{cr}	0.31	MPa
Actual critical internal pressure	p _{cr}	4.53	MPa

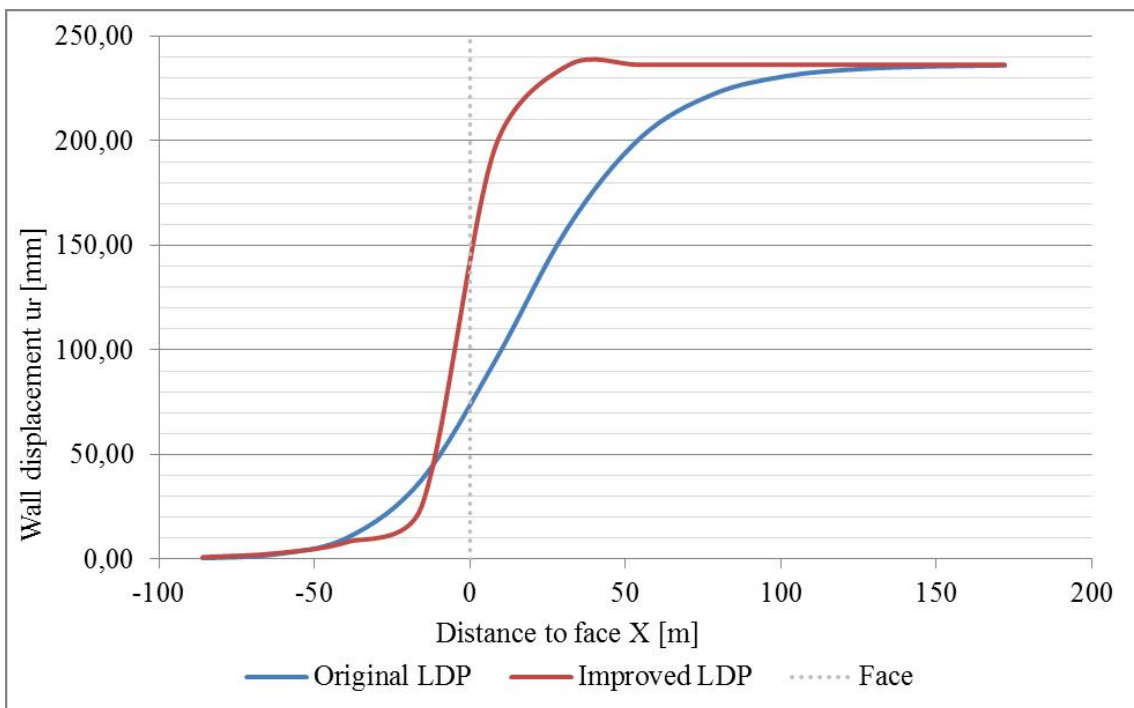
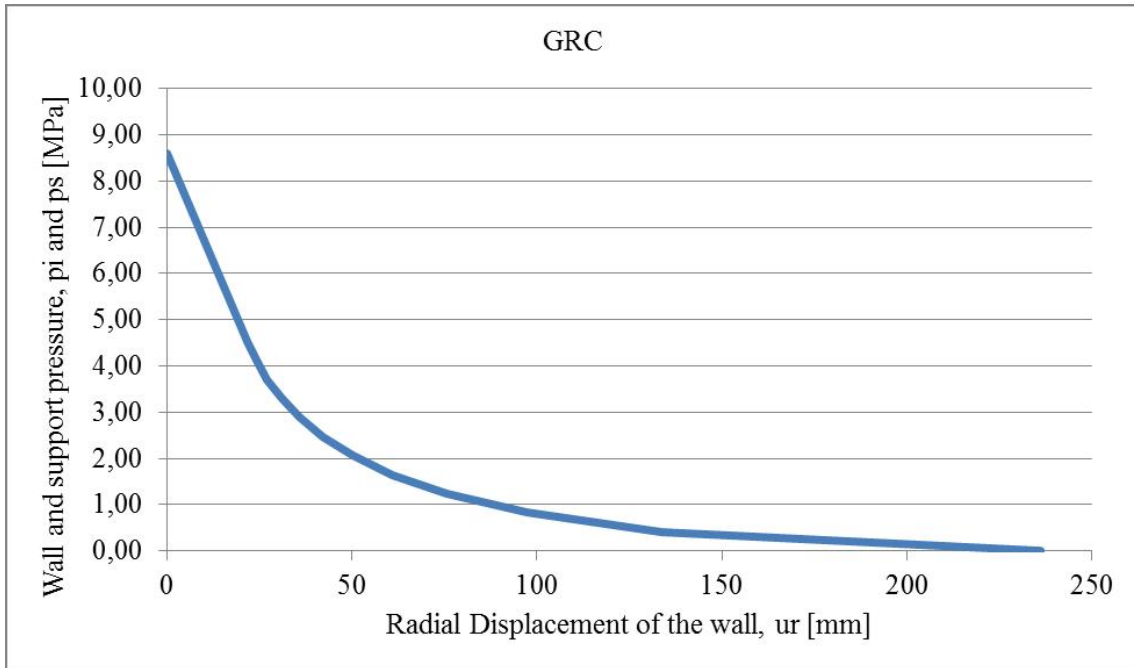
6. Calculation of GRC with mudstone/siltstone properties and mean stress as far-field stress

Ground Reaction Curve - GRC							
		Internal pressure	Int p_i crown	Int p_i floor		R _{pl} /R	Radial disp., u _r
	Point	pip_grc [MPa]	pip_r_grc [MPa]	pip_f_grc [MPa]	pips_grc	xi_grc	ur_grc [mm]
Elastic	1	8,61	-	-	-	-	0
	2	4,53	-	-	-	-	21,56
Plastic region	1	4,53	4,53	4,53	0,31	1,00	21,56
	2	4,12	4,15	4,09	0,29	1,05	24,01
	3	3,71	3,77	3,64	0,26	1,11	27,09
	4	3,29	3,40	3,19	0,23	1,18	30,95
	5	2,88	3,03	2,74	0,20	1,25	35,83
	6	2,47	2,67	2,28	0,17	1,34	42,05
	7	2,06	2,31	1,81	0,14	1,44	50,12
	8	1,65	1,97	1,33	0,12	1,55	60,82
	9	1,24	1,64	0,83	0,09	1,70	75,57
	10	0,82	1,34	0,31	0,06	1,89	97,28
	11	0,41	1,08	-0,26	0,03	2,16	133,67
	12	0,00	1,03	-1,03	0,00	2,78	236,32

7. Calculation of the original and improved LDP with mudstone/siltstone properties and mean stress as far-field stress

Equivalent tunnel radius	R _{eq}	21,50	m				
Max. Disp	u _{max}	236,32	mm				
Maximum normalized plastic zone radius	R*	2,78	-				
Normalized displacement at face	u _o *	0,22	-				
Original LDP				Improved LDP			
Point	lf _r	lf [m]	u _r [mm]	Point	X*=X/R	Dist to face X [m]	u _r [mm]
1	-4	-85,9940421	0,47	1	-4	-85,994	0,95
2	-2,909	-62,541	2,35	2	-2,909	-62,541	2,83
3	-1,818	-39,088	10,56	3	-1,818	-39,088	8,43
4	-0,727	-15,635	37,85	4	-0,727	-15,635	25,10
5	0,364	7,818	94,13	5	0,364	7,818	195,78
6	1,455	31,271	158,15	6	1,455	31,271	235,89
7	2,545	54,723	201,32	7	2,545	54,723	236,31
8	3,636	78,176	222,28	8	3,636	78,176	236,32
9	4,727	101,629	230,95	9	4,727	101,629	236,32
10	5,818	125,082	234,31	10	5,818	125,082	236,32
11	6,909	148,535	235,57	11	6,909	148,535	236,32
12	8	171,988	236,04	12	8	171,988	236,32

8. GRC and LDP for section 0+085



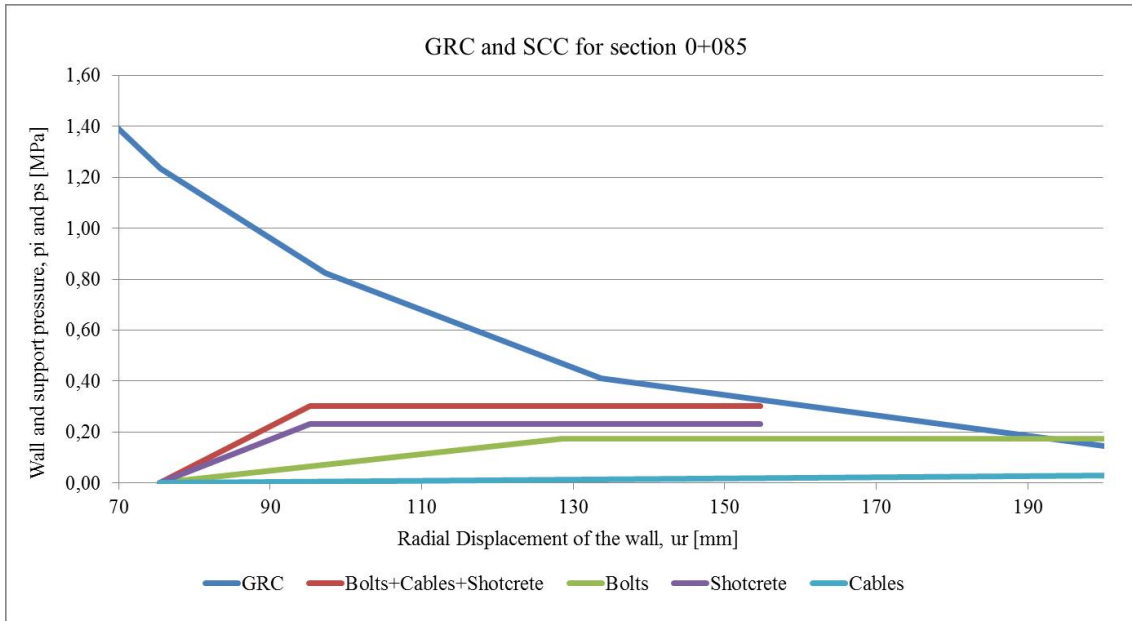
C.4. SCC calculations

Example of the SCC calculation for section 0+085 is given. The calculations are the same for all sections, only with different equivalent radius.

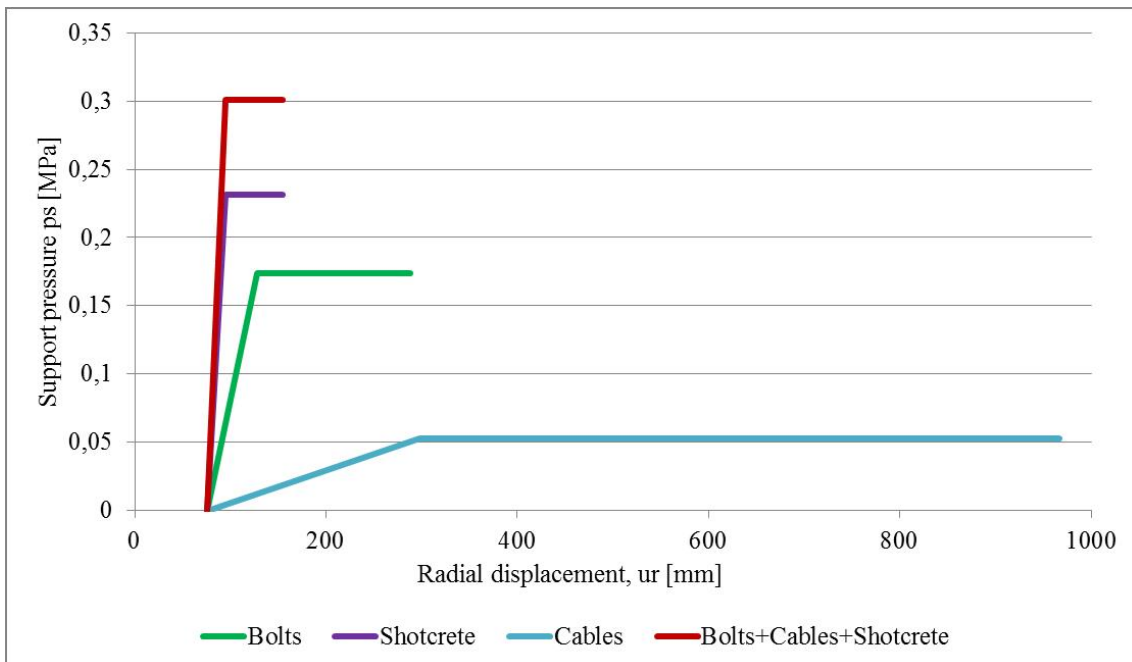
1. Input and output for the calculation for SCC for section 0+085, installed 5m behind face

Input Support Characteristics curve				Output	
A. Bolts				A. Bolts	
Bolt diameter	d_gb	25	mm	pi [MPa]	ur [mm]
Length	l_gb	7	m	0	86,23
Ultimate load	T-gbf	0,25	MN	0,17	139,37
Deformation load constant	Q_gb	0,143	m/MN	0,17	298,80
Youngs modulus bolt/steel	E_gb	205	GPa		
Number of bolts	n_gbolt				
Longitudinal bolt spacing	s_gb	1,2	m		
Circumferential spacing	sc_gb	1,2	m		
Maximum support pressure	Pmax_gb	0,17	MPa		
Elastic Stiffness	K_gb	3,27E+00	MPa/m		
Max displacement	umax_gb	53,14	mm		
B. Shotcrete				B. Shotcrete	
Unconfined Comp. Strength	sig_cc	20	MPa	pi [Mpa]	ur [mm]
Elastic modulus	E_c	20	GPa	0	86,23
Poisson's ratio	nu_c	0,25		0,23	106,61
Thickness of shotcrete	t_c	250	mm	0,23	165,61
Maximum support pressure	pmax_c	0,23	MPa		
Elastic stiffness	K_c	1,17E+01	MPa/m		
Max displacement	umax_c	19,84	mm		
C. Cables				C. Cables	
Bolt diameter	d_gb	60,91	mm	pi [MPa]	ur [mm]
Length	l_gb	15	m	0	86,23
Ultimate load	T-gbf	1,325	MN	0,05	308,98
Deformation load constant	Q_gb	0,143	m/MN	0,05	977,22
Youngs modulus bolt/steel	E_gb	205	GPa		
Number of bolts	n_gbolt				
Longitudinal bolt spacing	s_gb	5	m		
Circumferential spacing	sc_gb	5	m		
Maximum support pressure	Pmax_gb	0,05	MPa		
Elastic Stiffness	K_gb	2,38E-01	MPa/m		
Max displacement	umax_gb	222,75	mm		
Combined shotcrete+bolts+cables				Combined support	
Elastic stiffness	K_gb+c	1,52E+01	MPa/m	pi [Mpa]	ur [mm]
Max displacement	urmax_com	19,84	mm	0	86,23
Max support pressure	pmax_com	0,30	MPa	0,30	106,08
				0,30	165,61

2. SCC and GRC (displayed behind face) for section 0+085



3. Combined and individual support characteristics curves

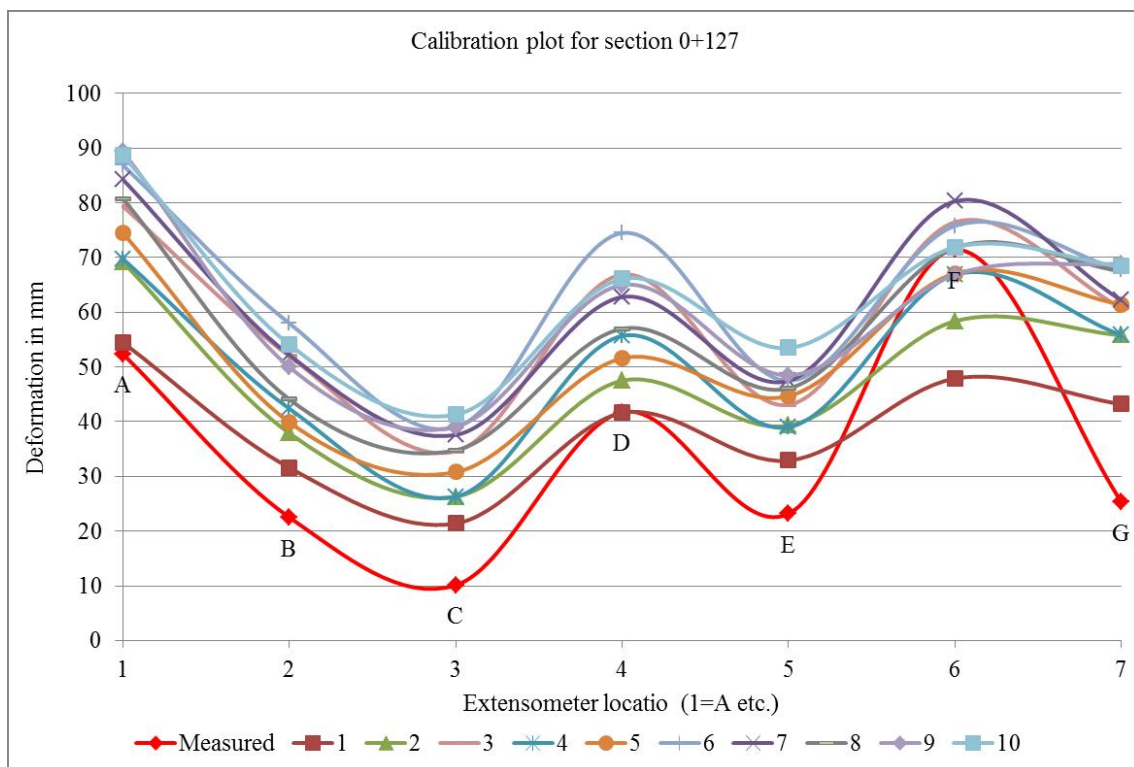
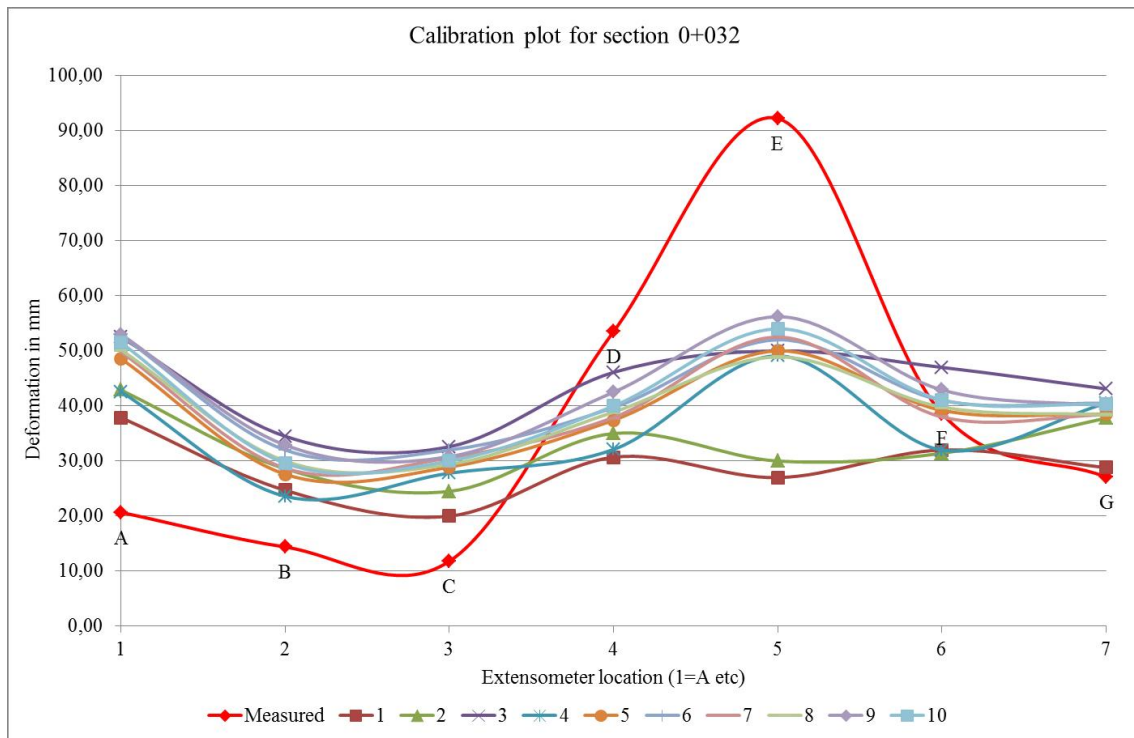


C.5. Estimation of stress

Overburden [m]	Poisson's ratio	Stress ratio k	Horizontal stress [MPa]	Vertical stress [MPa]	Tectonic out of plane [MPa]	Tectonic in-plane [MPa]	Horizontal stress out-of-plane [MPa]	Horizontal stress in-plane [MPa]
420	0.24	0.32	3.5	11.25	2.80	2.11	5.66	6.35
450	0.24	0.32	3.5	12.10	2.80	2.11	5.93	6.61
420	0.24	0.32	3.7	11.25	2.95	2.23	5.78	6.51
450	0.24	0.32	3.7	12.10	2.95	2.23	6.05	6.77
420	0.24	0.32	3.8	11.25	3.03	2.27	5.84	6.59
450	0.24	0.32	3.8	12.10	3.03	2.27	6.11	6.85
420	0.24	0.32	4	11.25	3.19	2.41	5.96	6.75
450	0.24	0.32	4	12.10	3.19	2.41	6.23	7.01

D. PHASE2 MODELING RESULTS

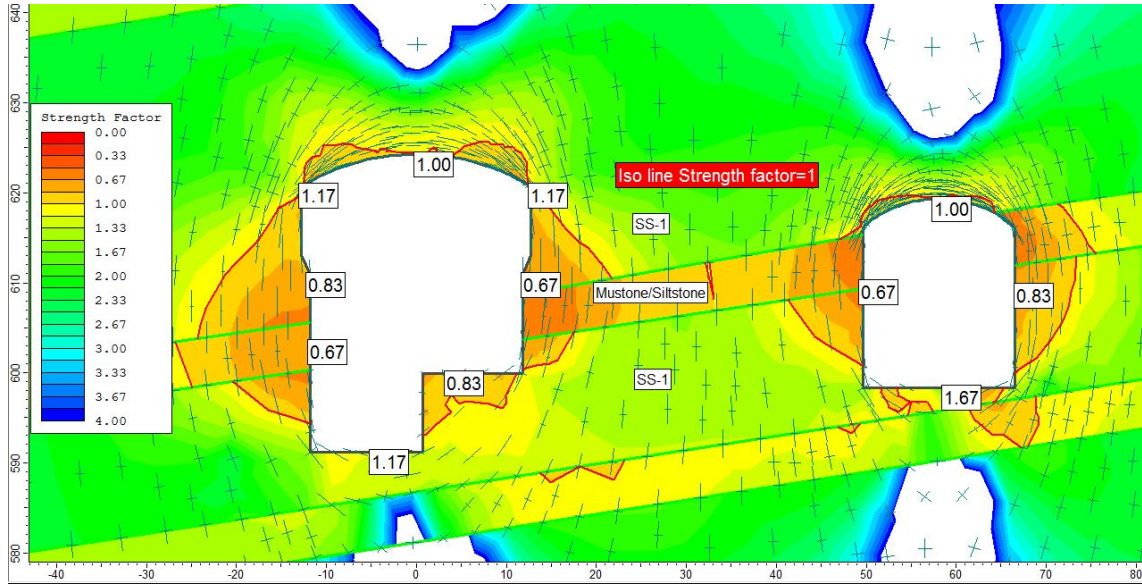
D.1. Calibration plots



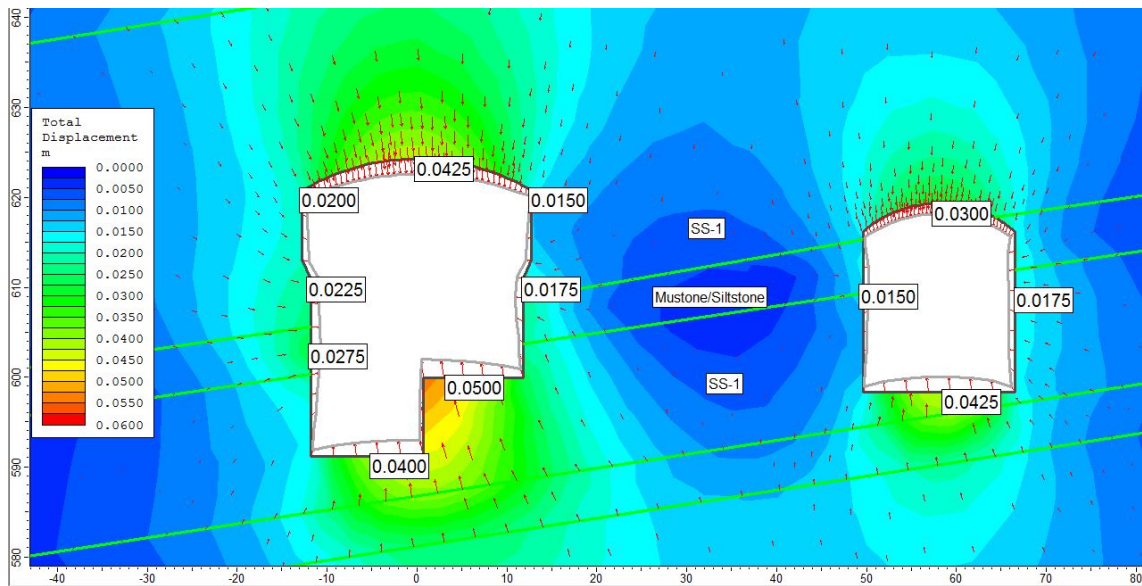
D.2. Elastic analysis

Section 0+015

1. Strength factor for section 0+015

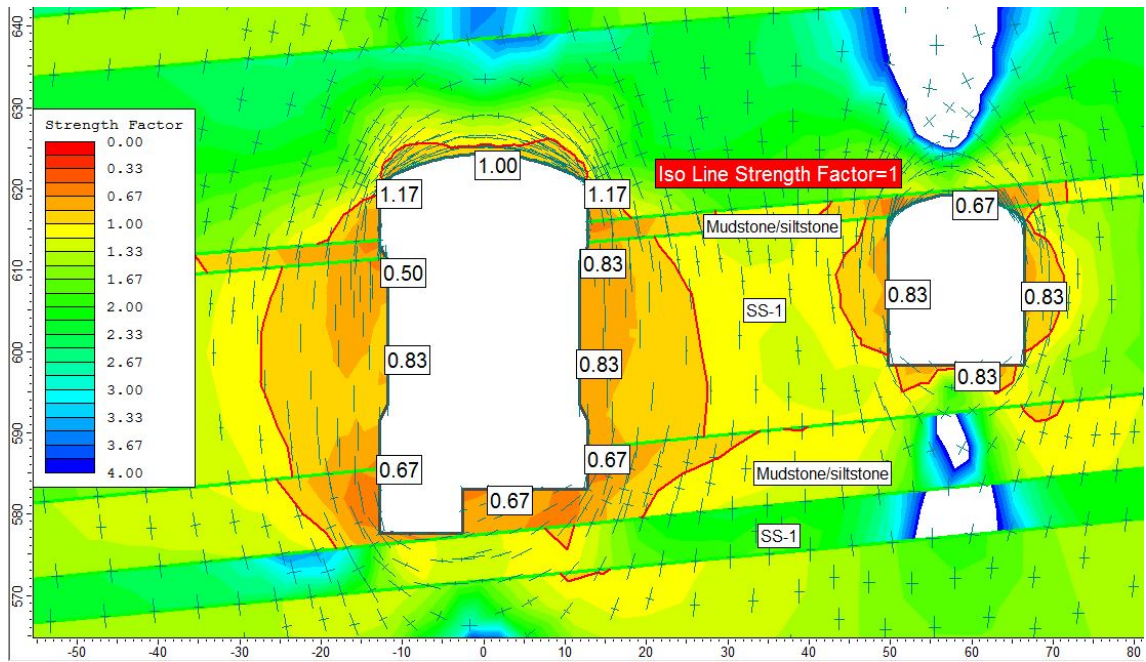


2. Total elastic deformation for section 0+015

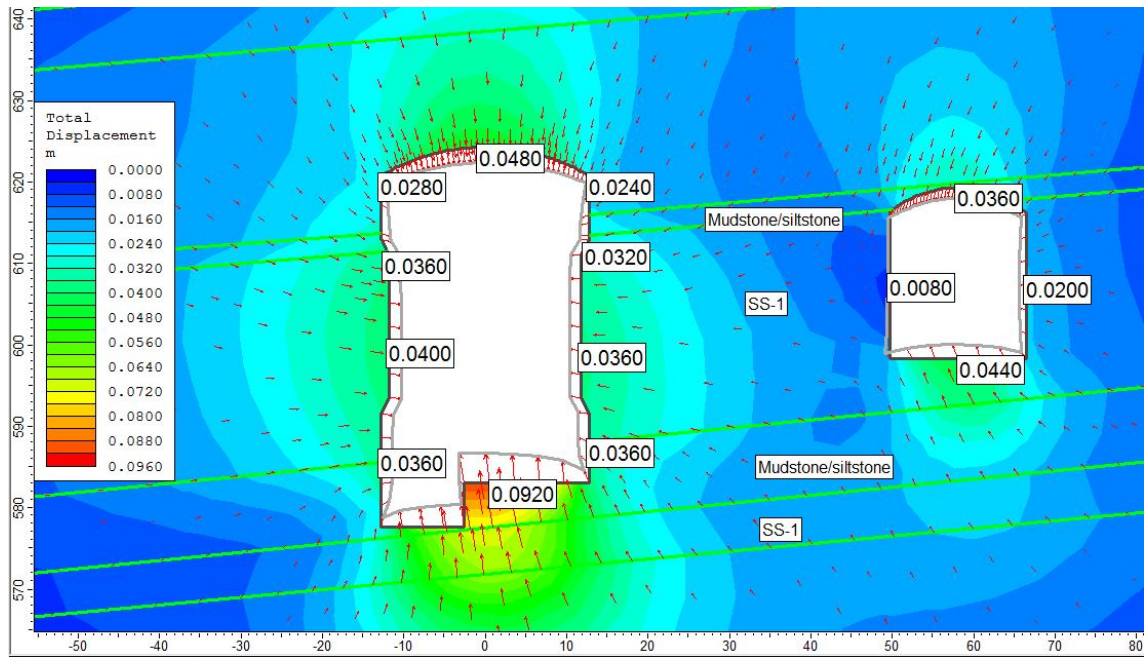


Section 0+032

1. Strength factor for section 0+032

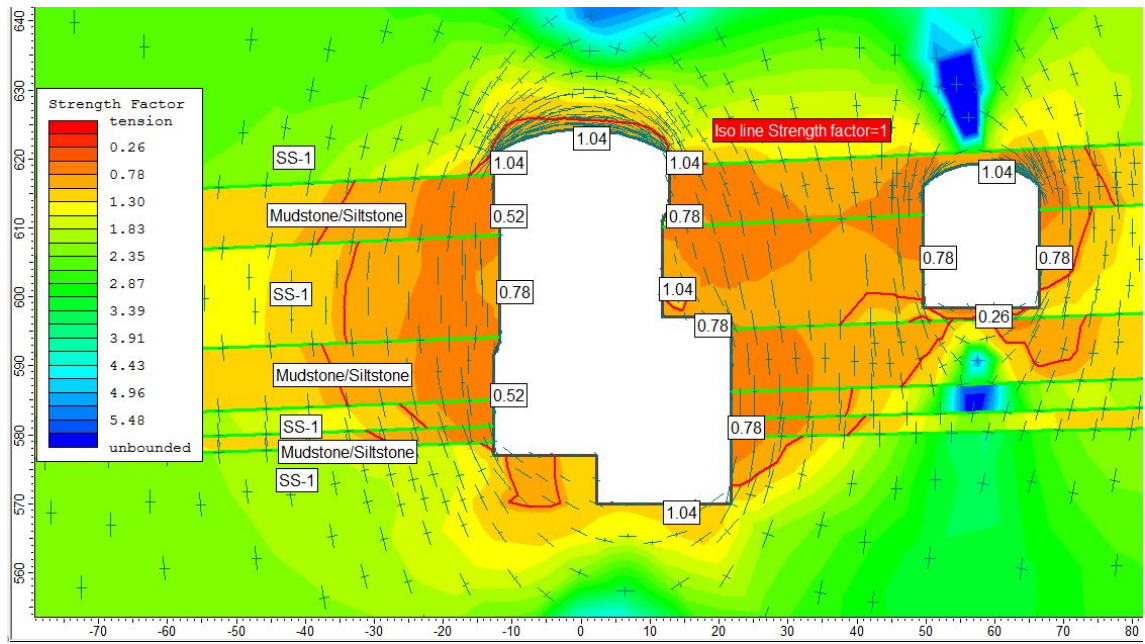


2. Total elastic deformation for section 0+032

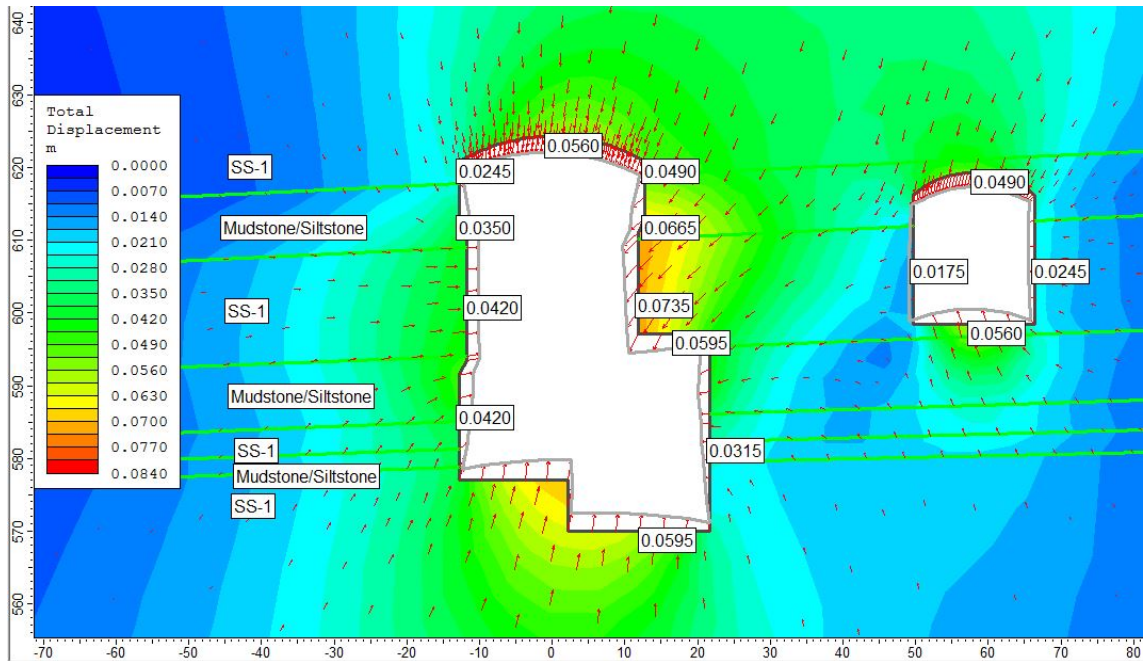


Section 0+065

1. Strength factor for section 0+065

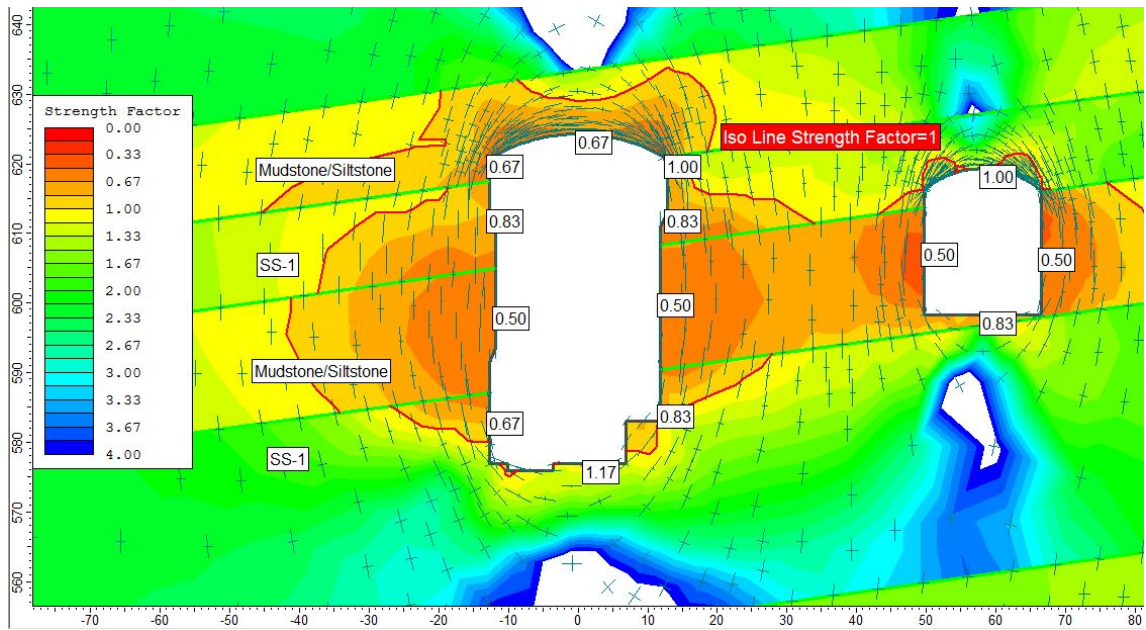


2. Total elastic deformation for section 0+065

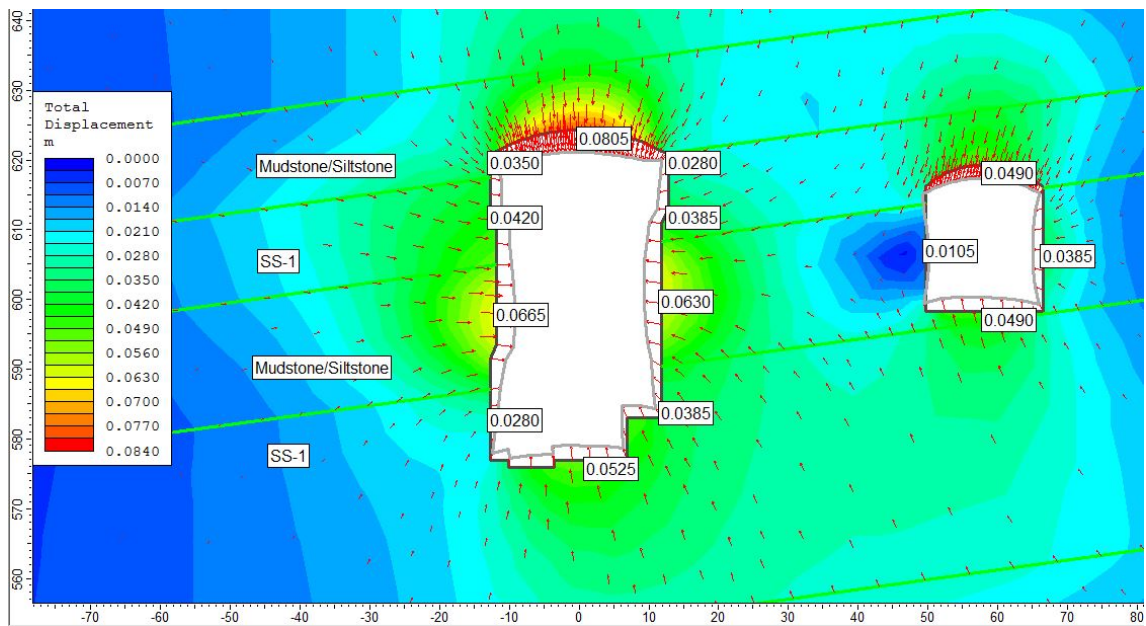


Section 0+127

1. Strength factor for section 0+127



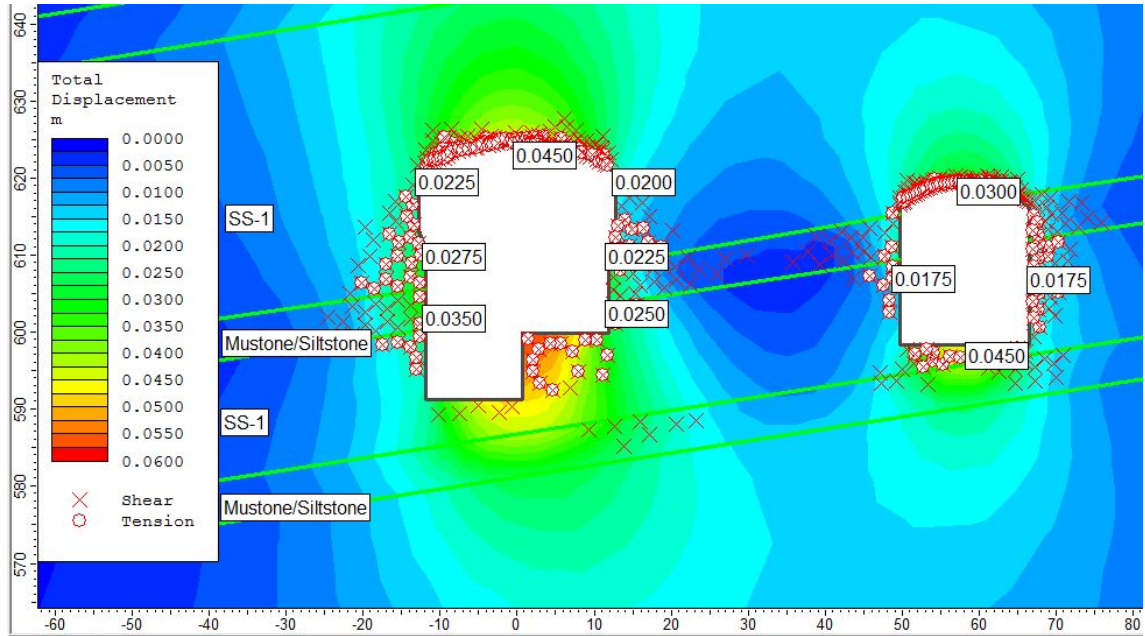
2. Total elastic deformation for section 0+127



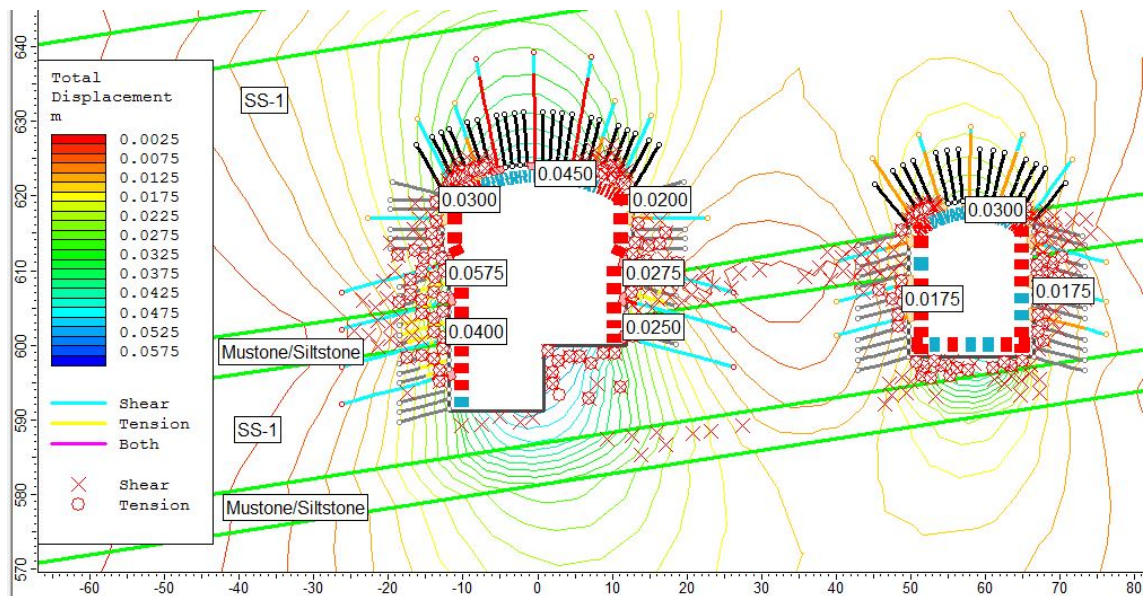
D.3. Plastic analysis

Section 0+015

1. Unsupported total plastic deformation for section 0+015

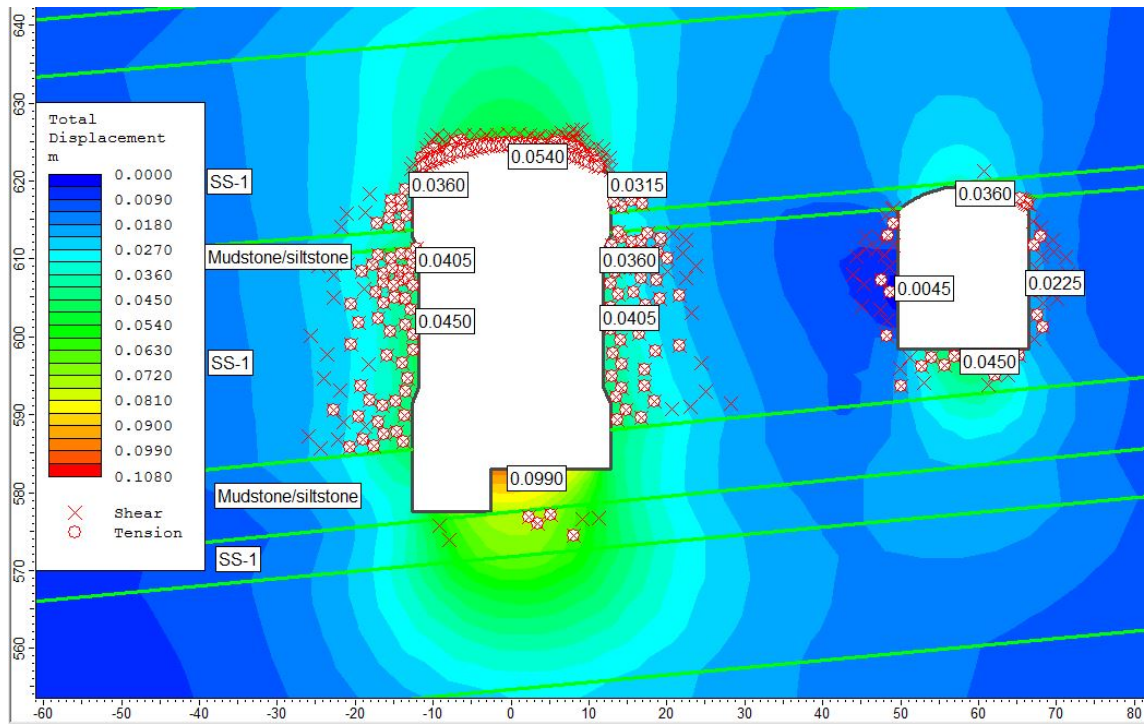


2. Total plastic deformation with applied support for section 0+015

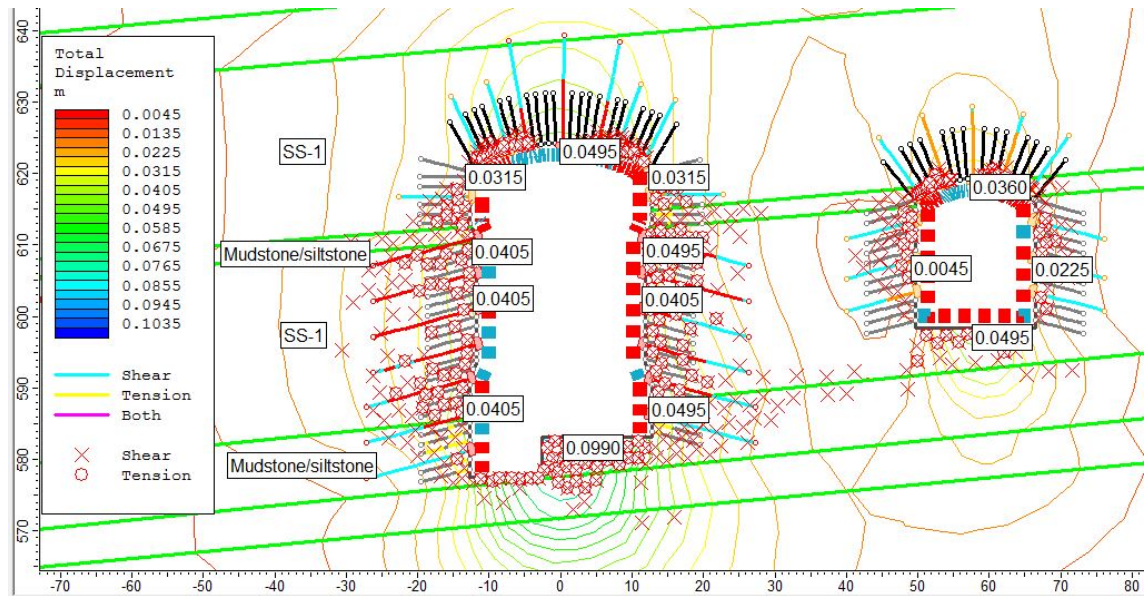


Section 0+032

1. Unsupported total plastic deformation for section 0+032

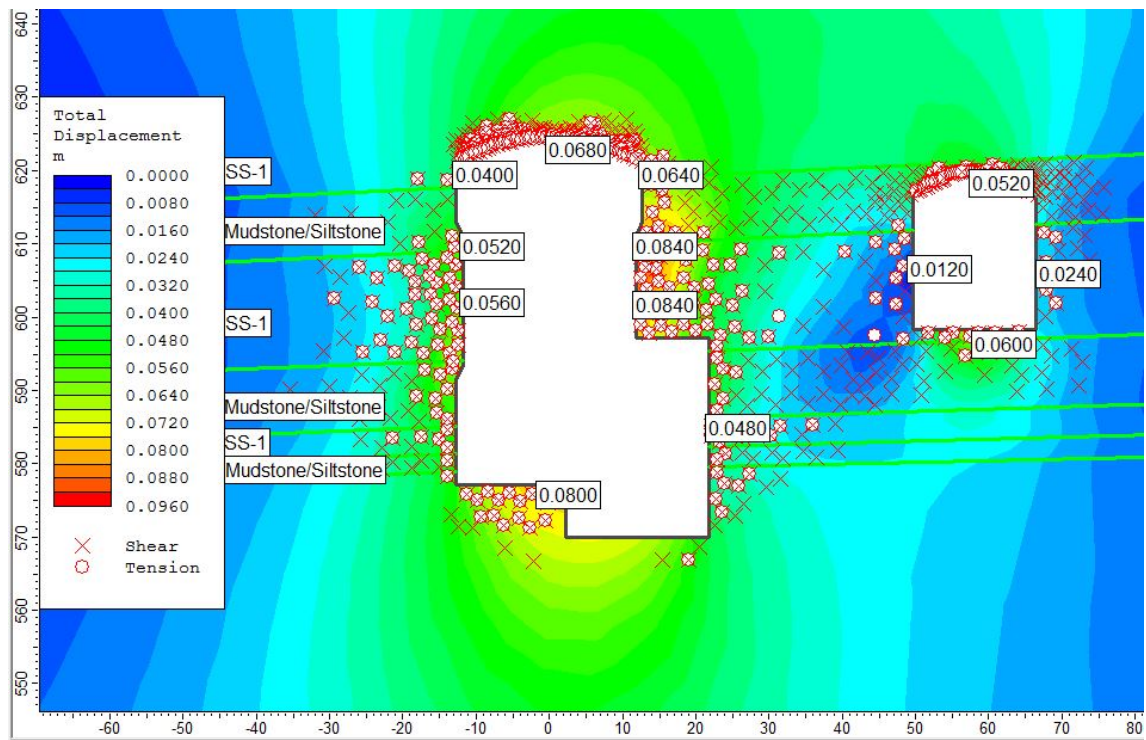


2. Total plastic deformation with applied support for section 0+032

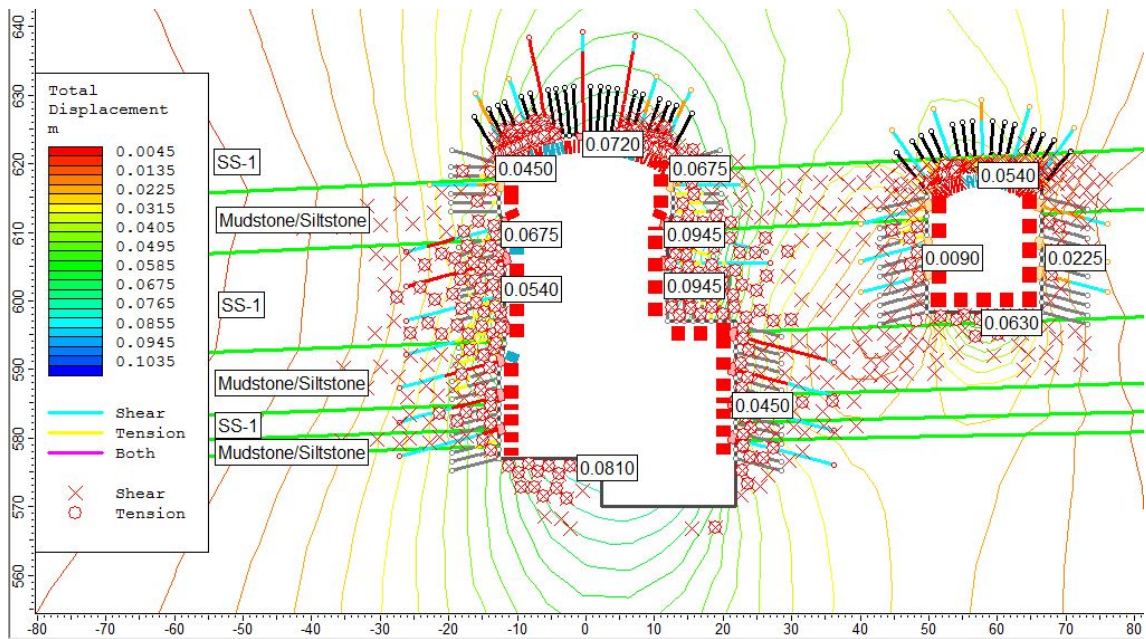


Section 0+065

1. Unsupported total plastic deformation for section 0+065

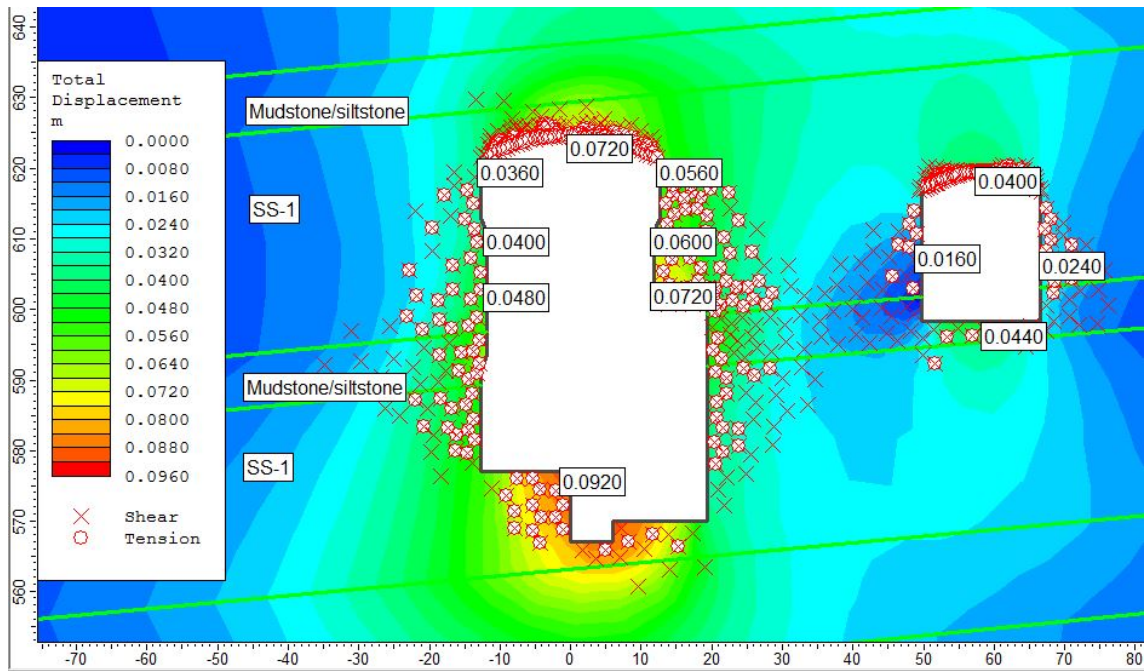


2. Total plastic deformation with applied support for section 0+065

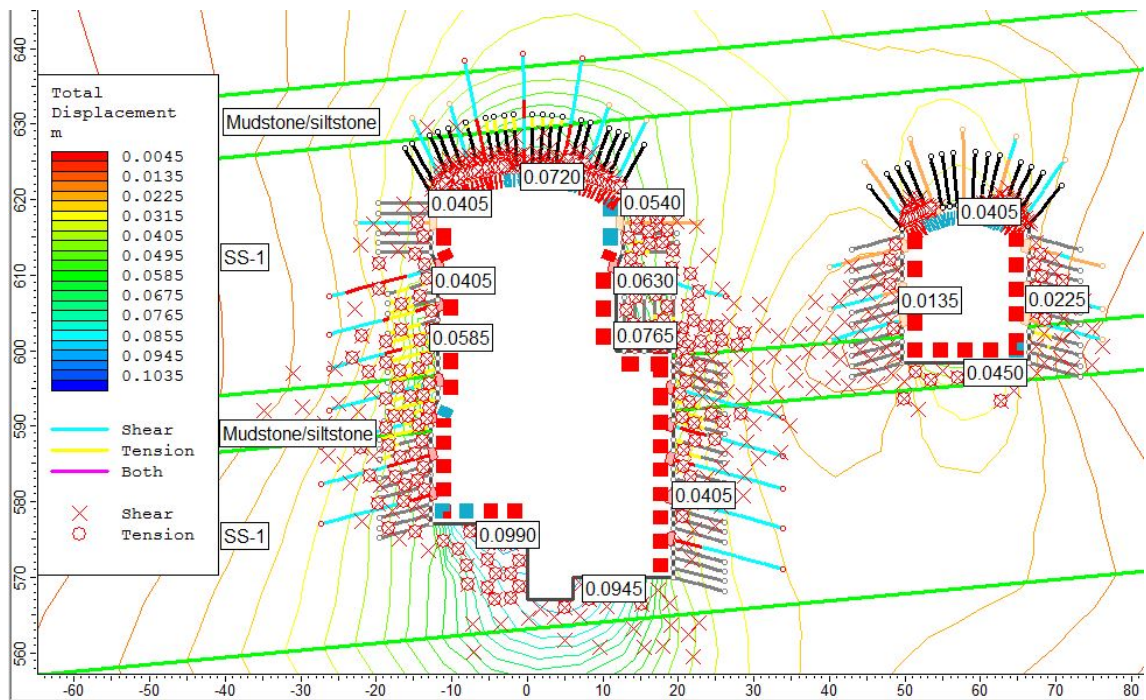


Section 0+085

1. Unsupported total plastic deformation for section 0+085

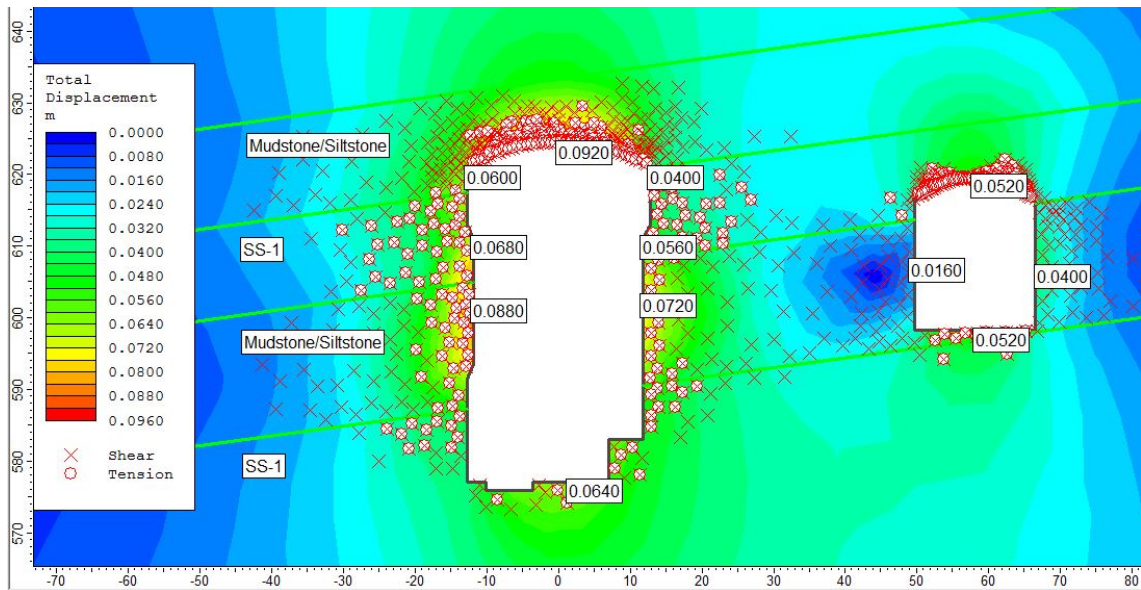


2. Total plastic deformation with applied support for section 0+085

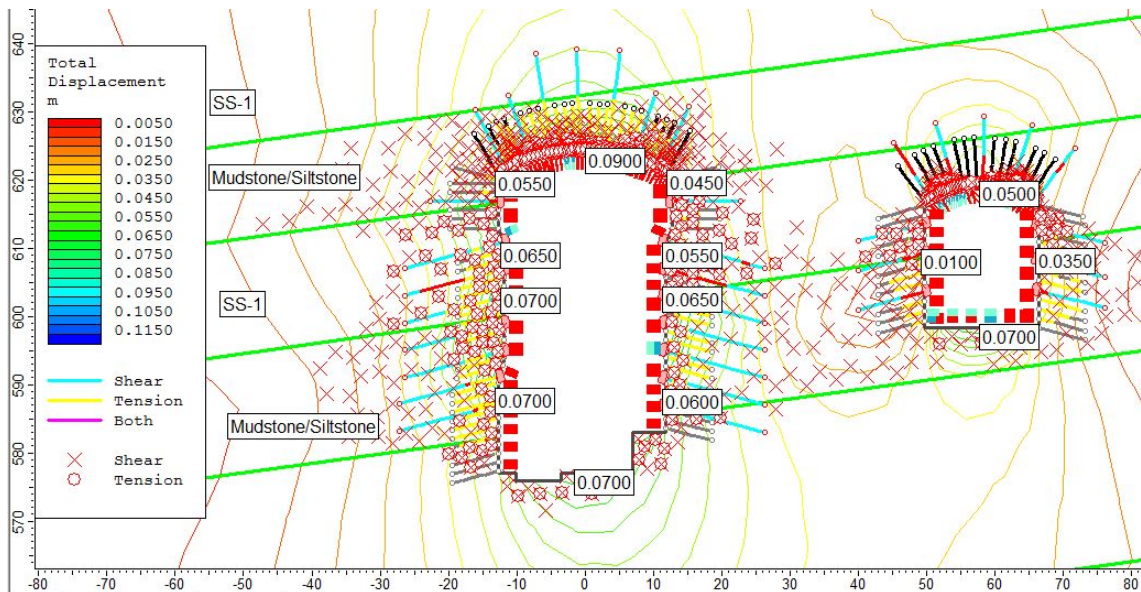


Section 0+127

1. Unsupported total plastic deformation for section 0+127

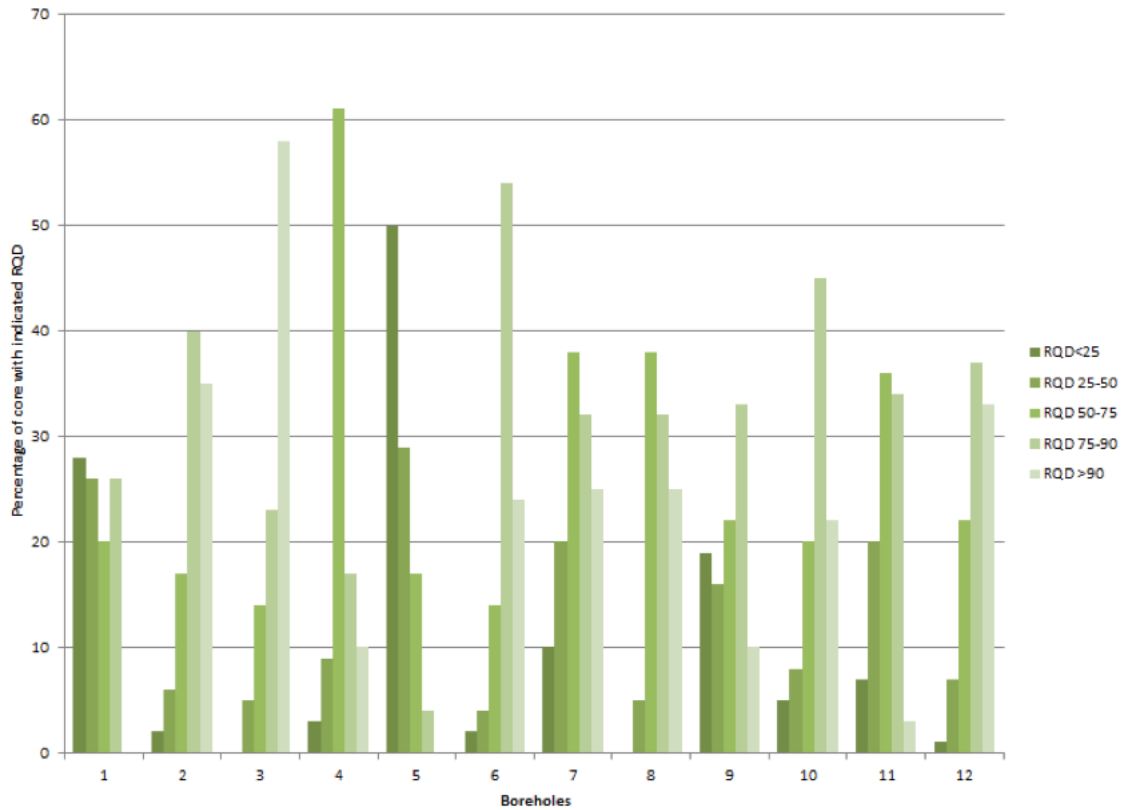


2. Total plastic deformation with applied support for section 0+127



E. PROJECT RELATED DOCUMENTS AND DRAWINGS

E.1. RQD frequency distribution in borehole cores below 60m (NJC, 2011a)



E.2. Geological surface maps and profiles

The geologic profiles are too large to include in the printed version. 4 profiles were added after printing, and made available to sensor.

E.3. Technical drawings

Drawing nr.	Description
C3 – C – 4490	Power station area: General layout
C3 – C – 4581	Power station area: Powerhouse base excavation, plan and section
C3 – C – 4582	Power station area: Powerhouse base excavation, sections
C3 – C – 4583	Power station area: Powerhouse base excavation, plan and section From chainage 0+00 to 0+41.85
C3 – C – 4584	Power station area: Powerhouse base excavation, plan and section From chainage 0+41.85 to 0+90.25
C3 – C – 4585	Power station area: Powerhouse base excavation, plan and section From chainage 0+90.25 to 0+137.10
C3 – C – 6531	Power station: Rock support sections, longitudinal section A
C3 – C – 6532	Power station: Rock support sections, cross-section L and M
C3 – C – 6533	Power station: Rock support sections, cross-section P and Q

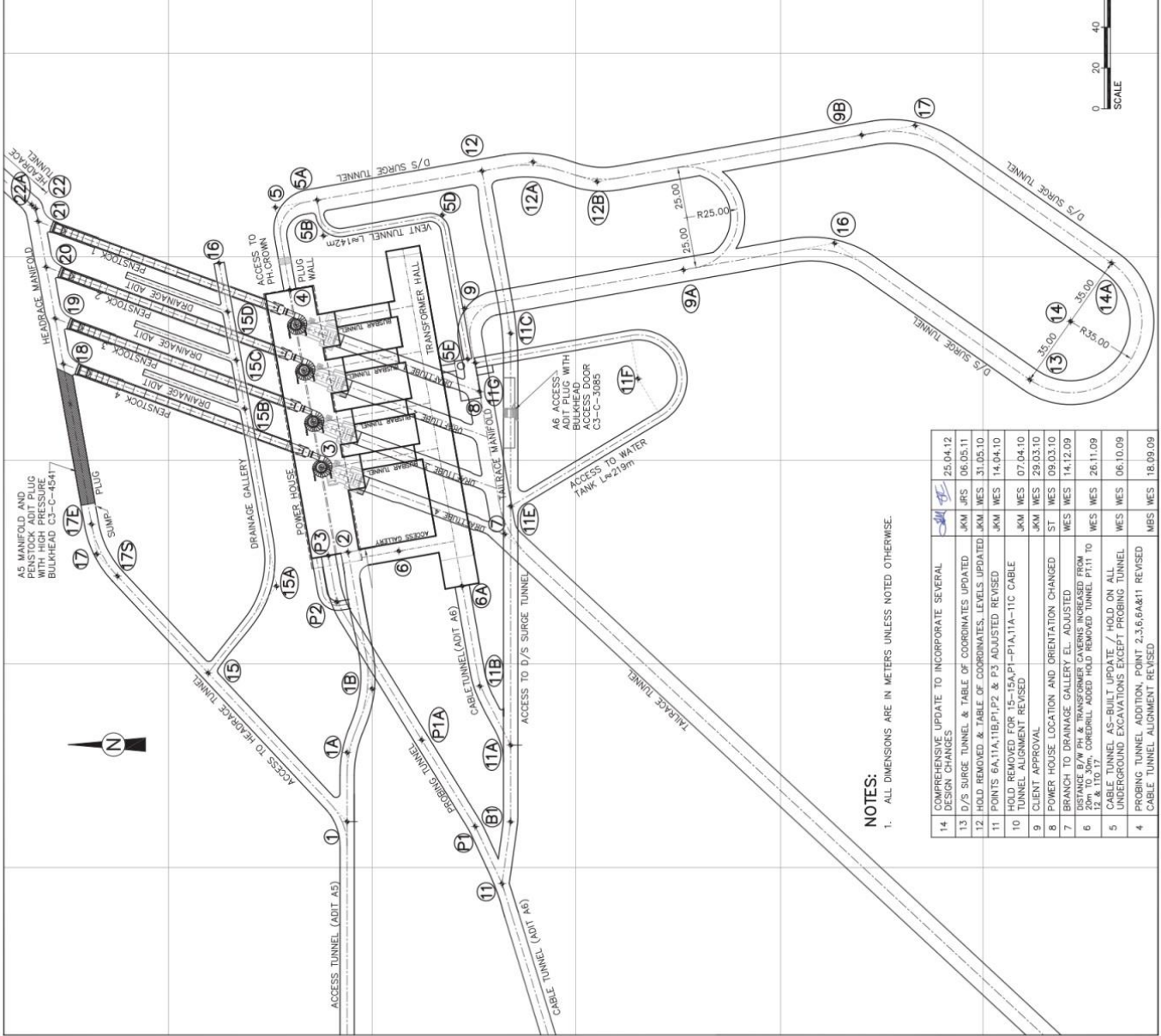
POINT	DESCRIPTION	EASTING	NORTHING	ELEVATION
1	Intersection Access tunnel (Adit A5) & Access to Headrace tunnel	363322.500	376512.000	598.50
1A	Access Tunnel (Adit A5) bend begin	363356.473	376512.300	599.41
1B	Access Tunnel (Adit A5) bend end	363387.771	3765300.026	600.30
2	Access Tunnel (Adit A5) Entrance to Power house	363454.926	3765311.867	600.50
3	C/L of Unit 4 Turbine	363496.580	3765325.000	-
4	Entrance to Power house Crown	363383.635	3765340.350	614.50
5	Intersection Point of 7th bend in D/S Surge Tunnel	363624.263	3765347.513	-
5A	Intersection: Access to Powerhouse Crown & Vent Tunnel	363627.879	3765326.995	609.68
5B	Intersection Point of 1st bend in Vent Tunnel	363610.295	3765333.895	-
5D	Intersection Point of 2nd bend in Vent Tunnel	363620.588	3765295.519	-
5E	End Point of Vent Tunnel	363549.780	3765253.034	625.00
6A	Access Gallery Power house to Transformer Hall	363455.470	3765286.902	600.50
6B	Cable Tunnel (Adit A6) Entrance to Transformer Hall	363438.287	3765255.803	611.30
7	17A: Intersection: Drift tube Unit 4 & Tailrace Mainfold	363463.795	3765234.928	573.70
8	Intersection: Drift tube Unit 1 & Tailrace Mainfold	363533.815	3765247.724	573.70
9	Intersection Point of 1st bend in D/S Surge Tunnel	363574.654	3765254.475	-
9A	Point of inflection, D/S Surge Tunnel (Change of Slope of Tunnel)	363593.591	3765147.134	585.00
9B	Point of inflection, D/S Surge Tunnel (Change of Slope of Tunnel)	363659.803	3765059.621	592.65
11	Intersection Cable Tunnel & Probing Tunnel	363392.070	3765236.221	610.22
81	Intersection Point of last bend in Cable Tunnel	363322.427	3765232.000	609.45
11A	Intersection: Cable Tunnel (Adit A6)/Access to D/S Surge Tunnel	363360.106	3765232.000	608.50
11B	Cable Tunnel (Adit A6) bend	363389.080	3765247.004	609.89
11C	Access to D/S Surge Tunnel bend	363562.368	3765232.000	604.30
11E	Intersection: Access to Water Tank Tunnel & Access to D/S Surge Tunnel	363477.346	3765232.000	609.91
11F	Intersection Point of 1st bend in Access to Water Tank Tunnel	363540.158	3765169.893	-
11G	End Point of Access to Water Tank Tunnel	363547.891	3765249.350	625.00
12	Intersection: Access to D/S Surge Tunnel / D/S Surge Tunnel	363442.143	3765246.666	604.30
12A	Intersection Point of 5th bend in D/S Surge Tunnel	363446.568	3765220.974	-
12B	Intersection Point of 6th bend in D/S Surge Tunnel	363436.873	3765189.991	-
13	Start of 3rd bend in D/S Surge Tunnel	363539.592	3764977.049	588.29
14	Center point of 3rd bend in D/S Surge Tunnel	363568.265	3764956.977	-
14A	End point of 3rd bend in D/S Surge Tunnel	363596.937	3764936.904	590.19
15	Intersection: Access to Headrace tunnel / Drainage Gallery	363395.499	3765346.881	-
15A	Intersection Point of 1st bend in Drainage Gallery	363438.193	3765346.881	591.75
15B	Start point of 1st Drainage Adt	363525.341	3765362.505	-
15C	Start point of 2nd Drainage Adt	363549.181	3765366.729	-
15D	Start point of 3rd Drainage Adt	363573.021	3765370.952	-
16	Drainage Gallery end	363596.917	3765375.186	596.00
17	Intersection Point of last bend in Access to Headrace tunnel	363453.993	3765435.239	585.00
18	Intersection: Access to Headrace tunnel & Headrace Mainfold & Penstock 4	363547.344	3765455.641	585.00
19	Intersection: Headrace Mainfold & Penstock 3	363569.699	3765455.641	585.00
20	Intersection: Headrace Mainfold & Penstock 2	363595.009	3765460.004	585.00
21	Intersection: Headrace Mainfold & Penstock 1	363617.364	3765464.046	585.00
22	Intersection Point of Bend at the end of Headrace mainfold	363623.769	3765465.179	585.00
22A	End of Headrace Tunnel	363625.517	3765467.133	585.00
P1	Intersection Point of 1st bend in Probing Tunnel	363362.640	3765275.639	-
P2	Intersection Point of 2nd bend in Probing Tunnel	363430.396	3765317.487	-
P3	Probing Tunnel Entrance to Power House Crown	363453.225	3765321.515	618.65

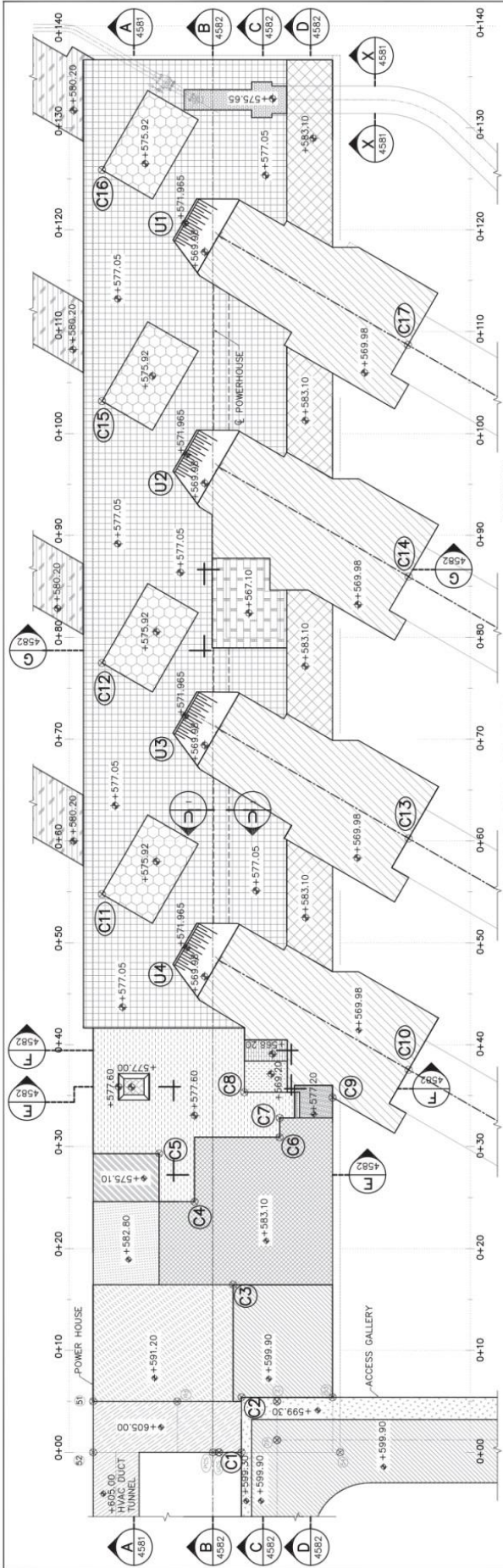
FOR CONSTRUCTION

3	PLUGS SHOWN	CB	CB	19.03.09
2	POINTS 18-21 ADJUSTED TO SUIT OMC	CB	CB	05.03.09
1	GENERAL MODIFICATION	CB	CB	25.02.09
Rev.	Description	Check	Appr.	Date

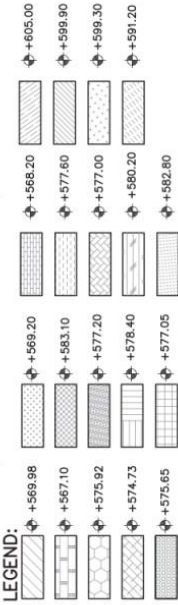
**NEELUM JHELUM HYDROELECTRIC PROJECT
POWER STATION AREA
GENERAL LAYOUT**

DRAWN	SHARIF/NAEED	CHECKED	CB/ST/AM	TENDER DWG. NO.
SUBMITTED	CB/ABS	APPROVED	CB/ABS	4001
DATE	26.11.09	PROJECT NO	1005800	
DWG. NO.	C3-C-4490	REV.	14	



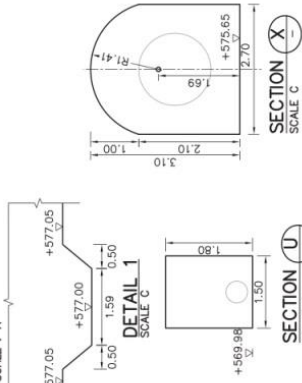


POWERHOUSE BASE PLAN
SCALE: A

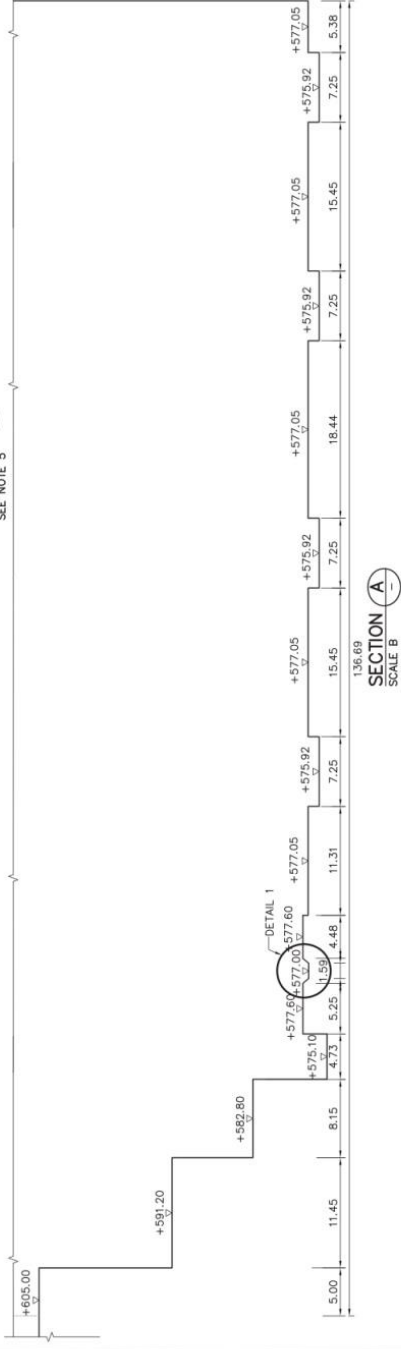


NOTES:

1. ALL DIMENSIONS AND ELEVATIONS ARE IN METERS UNLESS NOTED OTHERWISE.
2. ALL LEVELS SHOW TO ROCK/CAVATION LEVEL.
3. FOR COORDINATES OF CONTROL POINTS SEE DWG. C3-C-4490, C3-C-4491
4. FOR DIMENSIONS SEE DETAILED EXCAVATION PLANS AND SECTION DRAWINGS
5. GRADE - 450mm DIA. PIPE TUNNEL DIMENSIONS SHALL BE MINIMIZED AS MUCH AS POSSIBLE AND STILL ACCOMMODATE 450mm ϕ PIPE.



3D VIEW OF POWERHOUSE BASE



SECTION A
SCALE B

FOR CONSTRUCTION

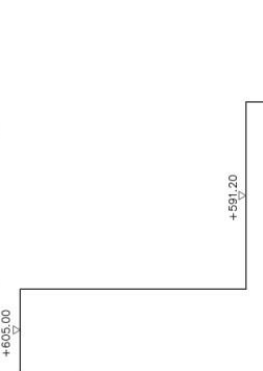
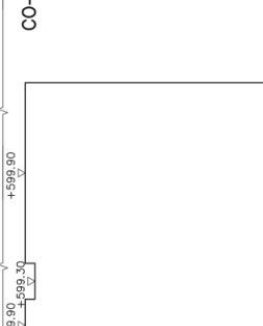
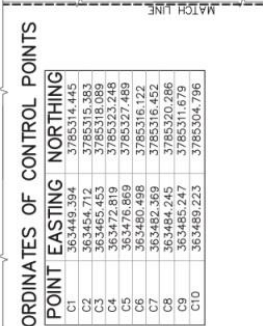
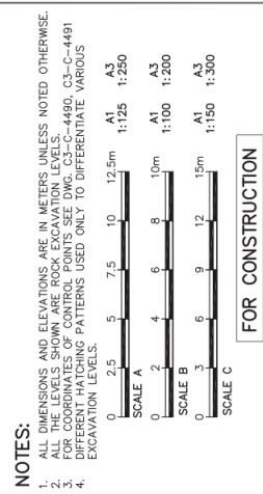
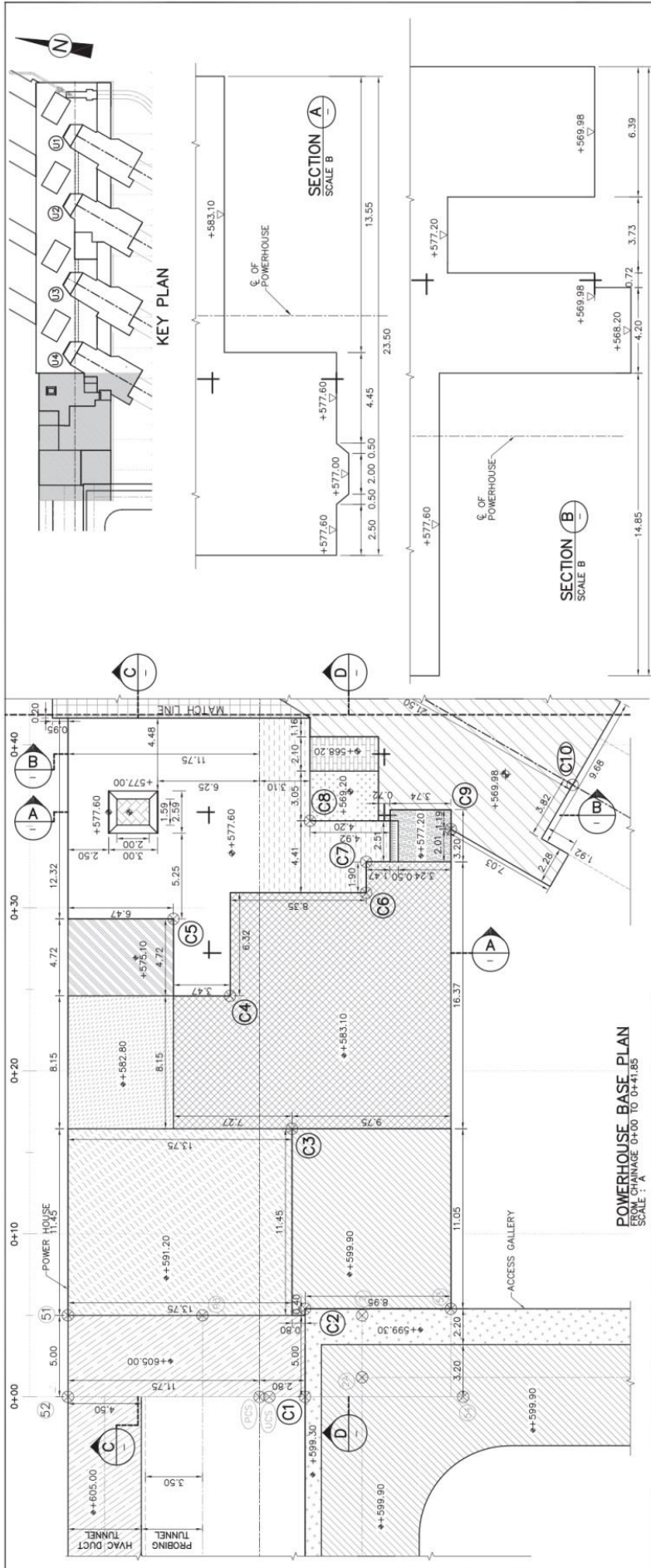
Rev.	Description	Check	Appr.	Date

PAKISTAN WATER & POWER DEVELOPMENT AUTHORITY
NEELUM JHELMUM HYDRO-POWER COMPANY

NEELUM JHELMUM HYDROELECTRIC PROJECT
POWER STATION AREA
POWERHOUSE BASE EXCAVATION
PLAN AND SECTIONS

DRAWN	SRM	CHECKED	JKM	TENDER DWG. NO.	4201-A
SUBMITTED	SRM	APPROVED	JRS	DATE	02.11.12
				PROJECT NO.	1005800
				DWG. NO.	C3-C-4581
				REV.	0

SHEET 1 OF 2



CO-ORDINATES OF CONTROL POINTS

POINT	EASTING	NORTHING
C1	363443.186	3785314.445
C2	363454.712	3785315.383
C3	363465.453	3785318.089
C4	363472.819	3785323.248
C5	363476.869	3785327.489
C6	363480.498	3785316.122
C7	363482.368	3785316.452
C8	363485.247	3785316.793
C9	363485.247	3785316.793
C10	363489.223	3785304.796

NOTES:
 1. DIMENSIONS AND ELEVATIONS ARE IN METERS UNLESS NOTED OTHERWISE.
 2. ALL THE LEVELS SHOWN ARE ROCK EXCAVATION LEVELS.
 3. FOR COORDINATES OF CONTROL POINTS SEE DWG. C3-C-4490, C3-C-4491
 4. DIFFERENT HATCHING PATTERNS USED ONLY TO DIFFERENTIATE VARIOUS EXCAVATION LEVELS.



Rev: _____ Description: _____ (Check) Appr: _____ Date: _____

PAKISTAN WATER & POWER DEVELOPMENT AUTHORITY
 NEELUM JHELUM HYDRO-POWER COMPANY

NEELUM JHELUM HYDROELECTRIC PROJECT
POWER STATION AREA
POWERHOUSE BASE EXCAVATION
PLAN AND SECTIONS

DRAWN: SRM CHECKED: JKM TENDER DWG. NO.: _____
 SUBMITTED: SRM APPROVED: JRS DATE: 02.11.12 PROJECT NO: 1005800
 SHEET 1 OF 3

NEELUM JHELUM CONSULTANTS
 DWG. NO. C3-C-4583 REV: 0

POWERHOUSE BASE PLAN
 SCALE 1:1
 SCALE CHANGE 0+00 TO 0+41.85

ACCESS GALLERY

POWERHOUSE

PROBING TUNNEL

HVAC DUCT

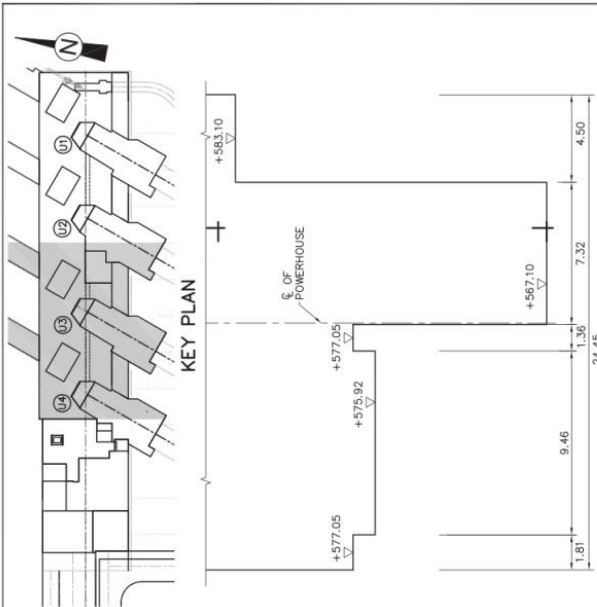
POWER HOUSE

SECTION A SCALE 1:250

SECTION B SCALE 1:250

SECTION C SCALE 1:250

SECTION D SCALE 1:250



SECTION A
SCALE A

CO-ORDINATES OF CONTROL POINTS

POINT	EASTING	NORTHING
U3	363518.834	3785326.941
U4	363496.579	3785324.999
C11	363500.959	3785337.438
C12	363523.317	3785341.381
C13	363511.578	3785306.737
C14	363536.887	3785313.199

NOTES:

1. DIMENSIONS AND ELEVATIONS ARE IN METERS UNLESS NOTED OTHERWISE.
2. ALL THE LEVELS SHOWN ARE ROCK EXCAVATION LEVELS.
3. FOR COORDINATES OF CONTROL POINTS SEE DWG. C3-C-4490, C3-C-4491
4. DIFFERENT HATCHING PATTERNS USED ONLY TO DIFFERENTIATE VARIOUS EXCAVATION LEVELS.



FOR CONSTRUCTION

Rev.	Description	Check	Appr.	Date

PAKISTAN WATER & POWER DEVELOPMENT AUTHORITY
NEELUM JHELUM HYDRO-POWER COMPANY

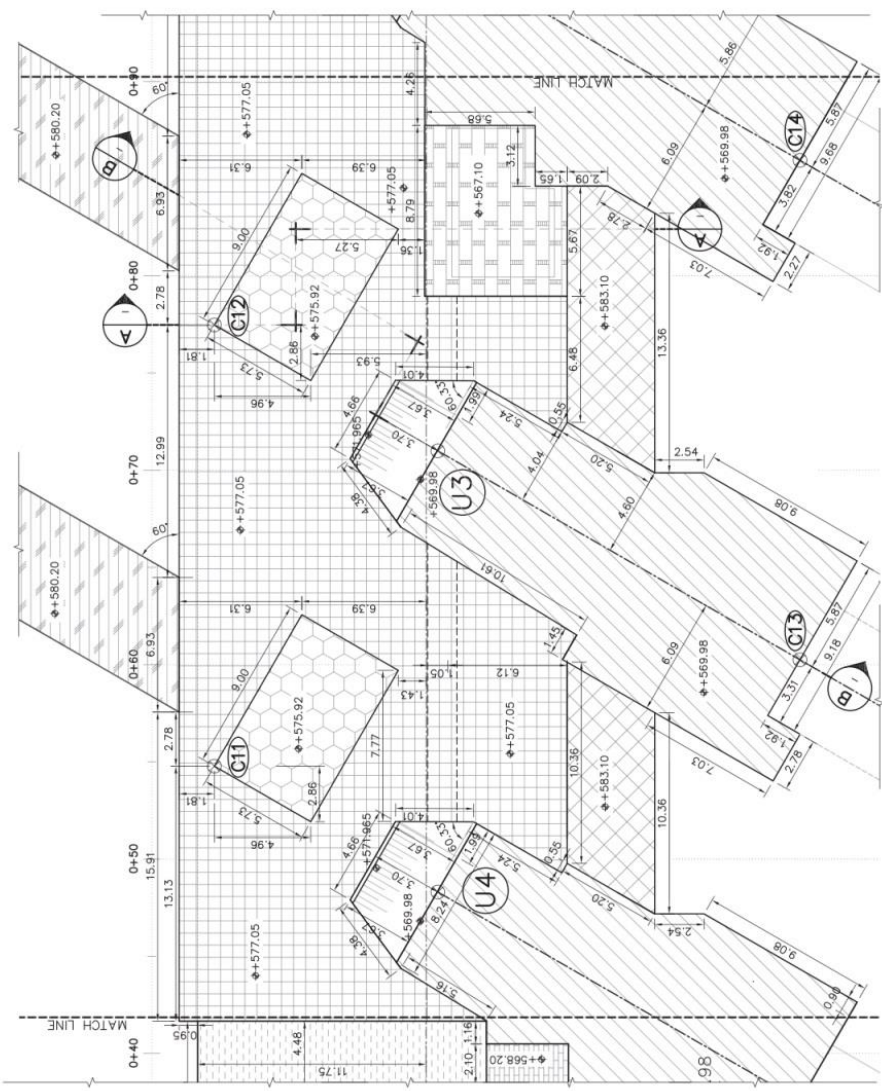
NEELUM JHELUM HYDROELECTRIC PROJECT
POWER STATION AREA
POWERHOUSE BASE
EXCAVATION PLAN AND SECTION

SHEET 2 OF 3

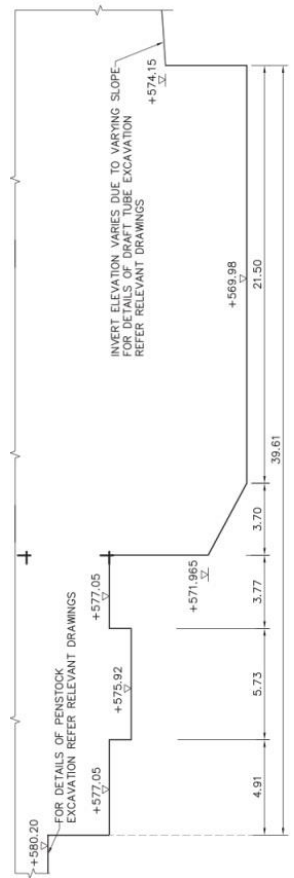
DRAWN	SRM	CHECKED	JKM	TENDER DWG. NO.

SUBMITTED	SRM	APPROVED	JRS	DATE	PROJECT NO.
				02.11.12	1005800

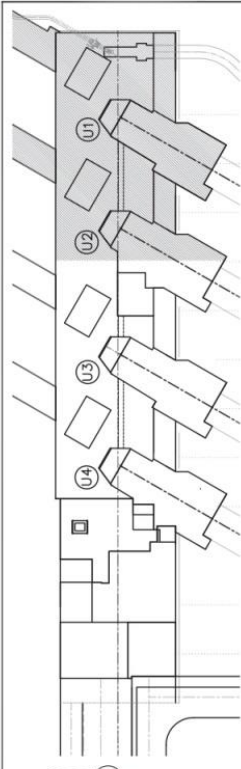
NEELUM JHELUM CONSULTANTS C3-C-4584 0



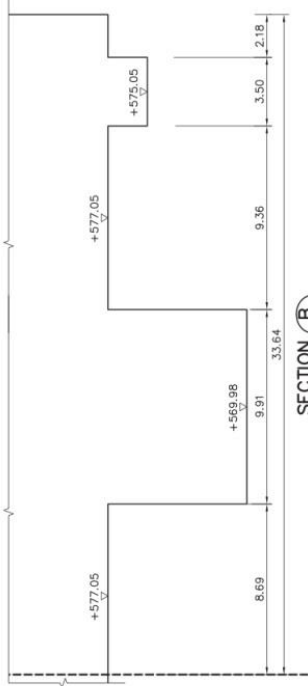
POWERHOUSE BASE PLAN
FROM CHAINAGE 0+41.85 TO 0+90.25
SCALE : A



SECTION B
SCALE A



KEY PLAN



SECTION B
SCALE A

CO-ORDINATES OF CONTROL POINTS

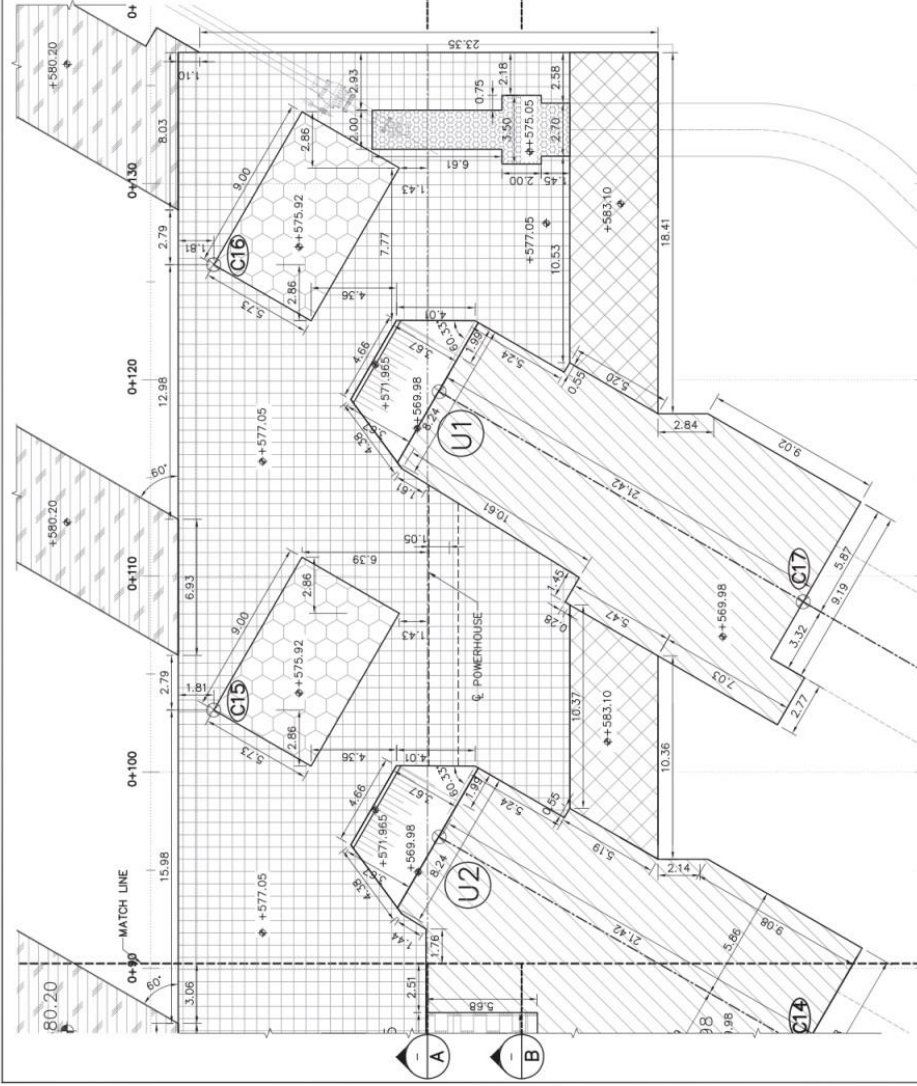
POINT	EASTING	NORTHING
U1	363596.599	3785337.346
U2	363544.243	3785333.404
C15	363548.619	3785345.842
C16	363570.974	3785349.784
C17	363559.270	3785317.217

NOTES:

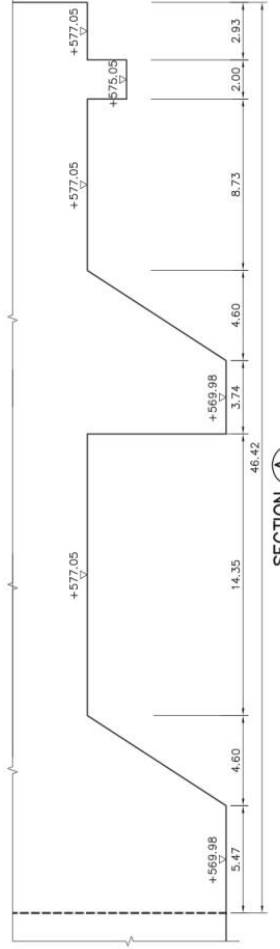
1. ALL DIMENSIONS AND ELEVATIONS ARE IN METERS UNLESS NOTED OTHERWISE.
2. ALL THE LEVELS SHOWN ARE ROCK EXCAVATION LEVELS.
3. FOR COORDINATES OF CONTROL POINTS SEE DWG. C3-C-4490, C3-C-4491.
4. EXCAVATION PATTERNS USED ONLY TO DIFFERENTIATE VARIOUS EXCAVATION LEVELS.



POWERHOUSE BASE PLAN
FROM CHAINAGE 0+80.25 TO 0+137.10
SCALE : A



SECTION A
SCALE A



FOR CONSTRUCTION

Rev	Description	Check	Appr.	Date

		PAKISTAN WATER & POWER DEVELOPMENT AUTHORITY NEELUM JHELUM HYDRO-POWER COMPANY		
NEELUM JHELUM HYDROELECTRIC PROJECT POWER STATION AREA POWERHOUSE BASE EXCAVATION PLAN AND SECTIONS				
DRAWN	SRM	CHECKED	JKM	TENDER DWG. NO.
SUBMITTED	SRM	APPROVED	JRS	DATE
SHEET 3 OF 3 PROJECT NO. 1005800 DWG. NO. C3-C-4585				REV
NEELUM JHELUM CONSULTANTS				0

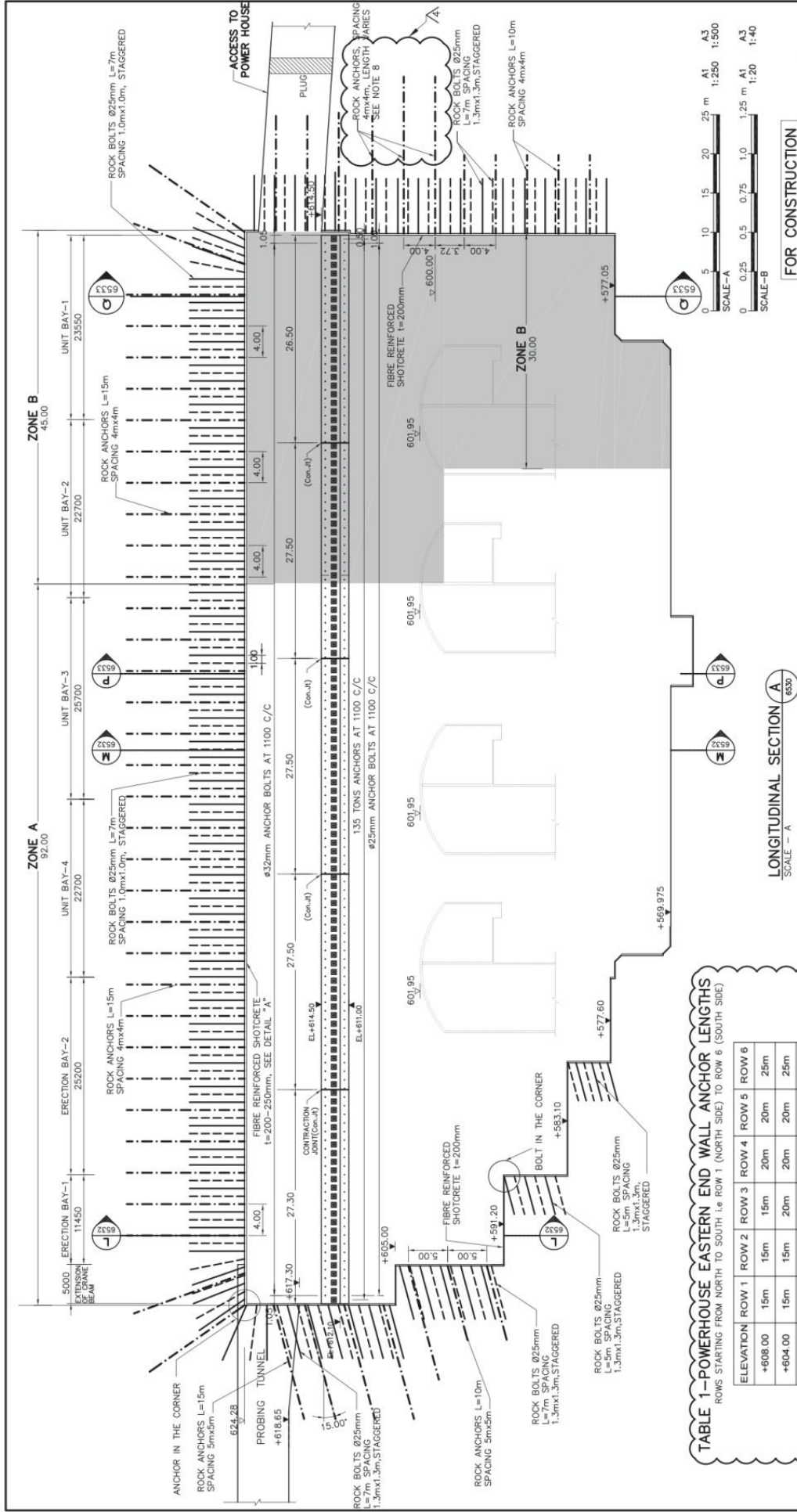
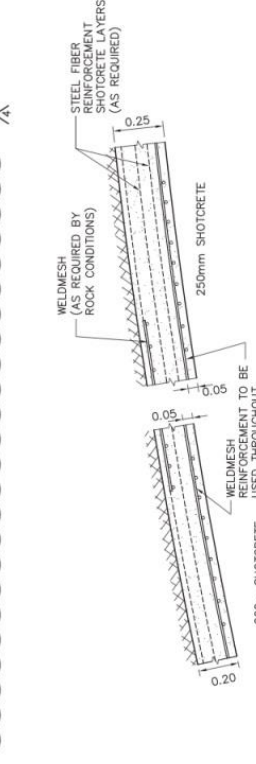


TABLE 1-POWERHOUSE EASTERN END WALL ANCHOR LENGTHS
ROWS STARTING FROM NORTH TO SOUTH (LE ROW 1 (NORTH SIDE) TO ROW 6 (SOUTH SIDE))

ELEVATION	ROW 1	ROW 2	ROW 3	ROW 4	ROW 5	ROW 6
+608.00	15m	15m	15m	20m	20m	25m
+604.00	15m	15m	15m	20m	20m	25m
+600.00	15m	15m	15m	20m	20m	25m



FOR CONSTRUCTION

4	ANCHOR LENGTH DETAILS FOR EASTERN END WALL INCORPORATED, NOTE 8 & TABLE 1 ADDED.	JKM/JRS	11.07.11
3	ROCK SUPPORT UPDATED, ZONES A&B REVISED	JKM/JRS	23.02.11
2	ROCK SUPPORT UPDATED, ZONES A&B INTRODUCED	JKM/JRS	08.09.10
1	ROCK SUPPORT REVISED FOR NEW SECTION	JKM/JRS	08.09.10

Check/Approve: _____ Date: _____

PAKISTAN WATER & POWER DEVELOPMENT AUTHORITY
NEELUM JHELMUM HYDRO-POWER COMPANY

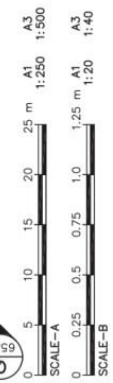
**POWER STATION
ROCK SUPPORT
SECTIONS**

DRAWN	M. SHARIF/NAV	CHECKED	ST/JKM	TENDER DWG. NO.
SUBMITTED	MBS/SRM	APPROVED	WES/JRS	PROJECT NO.
				11.07.11
				DWG. NO. NJC
				1005800
				REV
				C3-C-6531
				4

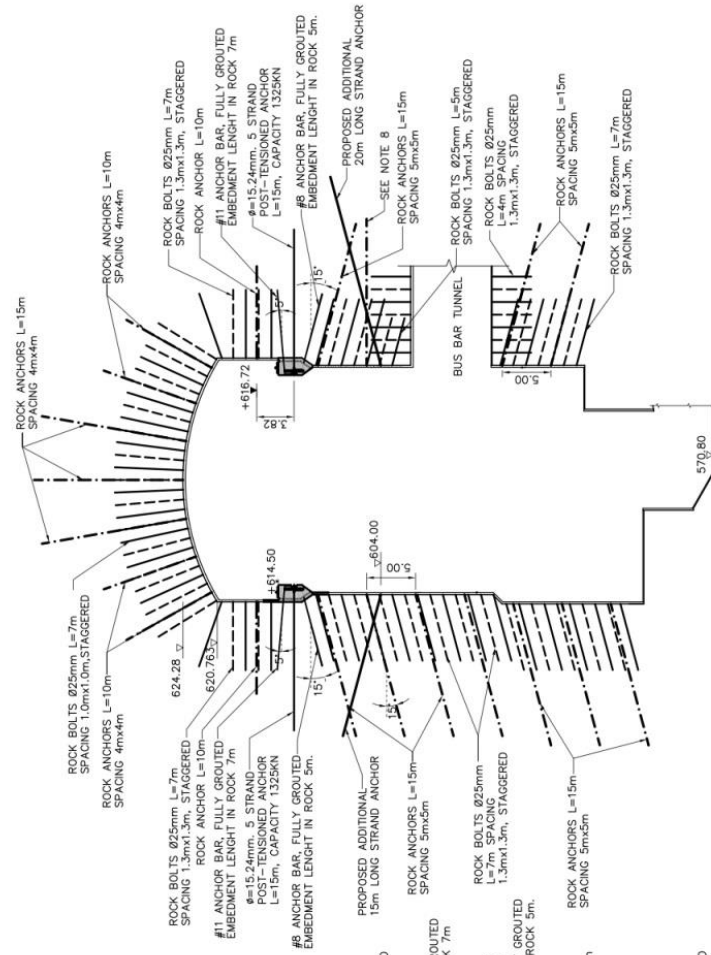
- NOTES**
- ALL DIMENSIONS AND ELEVATIONS ARE IN METERS UNLESS NOTED OTHERWISE.
 - ALL 15m ANCHORS ARE STRAND ANCHORS PRETENSIONED TO 30t IN ZONE 'A' AND 10t IN ZONE 'B'.
 - ALL 10m ANCHORS ARE BAR ANCHORS PRETENSIONED TO 15t IN ZONE 'A' 5t IN ZONE 'B'.
 - ANCHOR INSTALLATION SEQUENCE TO BE ADVISED BY ENGINEER.
 - ANCHOR PATTERNS CONSIST OF SQUARE GRIDS AND ARE NOT STAGGERED.
 - ZONE 'A' : SSI SANDSTONES PREDOMINATE--ANCHORS USUALLY INSTALLED ON 5mX2m GRID.
 - ZONE 'B' : MUD ROCKS PREDOMINATE--ANCHORS USUALLY INSTALLED ON 4mX4m GRID.
 - FOR DETAILS OF CRANE BEAM ANCHORS REFER DWGS C3-C-6313,6314
 - LONG ANCHORS LENGTH ON THE EASTERN END WALL VARIES FROM 15 TO 25m. STARTING FROM NORTH TO SOUTH SIDE.

LONGITUDINAL SECTION A
SCALE - A

DETAIL A
SCALE - B



ZONE A



SECTION A - A
SCALE - A

Rev	Description	Checked	Appr	Date
3	NOTE 7 ADDED, BAR ANCHORS BELOW EL.+592.0 REPLACED BY STRAND ANCHORS	JKM	JRS	12.08.11
2	ROCK SUPPORT UPDATED; NOTE 8 ADDED	JKM	JRS	11.07.11
1	ROCK SUPPORT AND SECTION REVISED	JKM	JRS	11.07.11

PAKISTAN WATER & POWER DEVELOPMENT AUTHORITY
NEELUM JHELUM HYDRO-POWER COMPANY

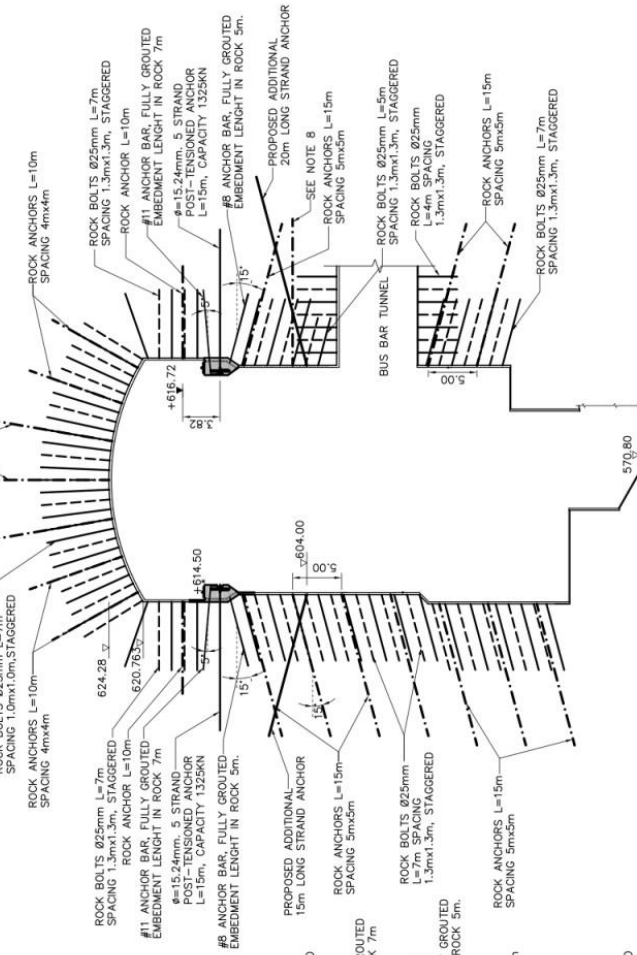
**NEELUM JHELUM HYDROELECTRIC PROJECT
POWER STATION
ROCK SUPPORT
SECTIONS**

DRAWN	M. SHARIF/NAV	CHECKED	JKM	TENDER DWG. NO.
SUBMITTED	MBS/SRM	APPROVED	JRS	PROJECT NO 1005800
				DATE 11.07.11
				DWG. NO. N/C C3-C-6532
				REV 3

NOTES

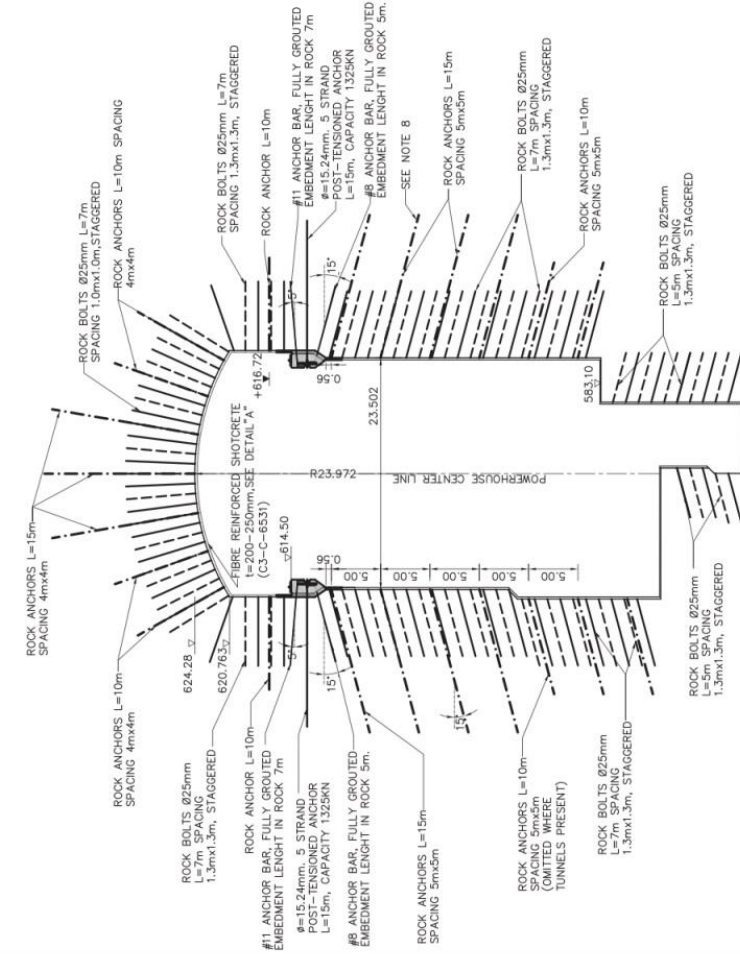
1. ALL DIMENSIONS AND ELEVATIONS ARE IN METERS UNLESS NOTED OTHERWISE.
2. ALL 15m ANCHORS ARE STRAND ANCHORS PRETENSIONED TO 30t IN ZONE 'A' AND 10t IN ZONE 'B'.
3. ALL 10m ANCHORS ARE BAR ANCHORS PRETENSIONED TO 15t IN ZONE 'A' & 5t IN ZONE 'B'.
4. ANCHOR INSTALLATION SEQUENCE TO BE ADVISED BY ENGINEER.
5. ANCHOR PATTERNS CONSIST OF SQUARE GRIDS AND ARE NOT STAGGERED EXCEPT WHERE SHOWN.
6. ZONE 'A' - SSI SANDSTONES PREDOMINATE--ANCHORS USUALLY INSTALLED ON 5mX5m GRID.
ZONE 'B' - MID ROCKS PREDOMINATE--ANCHORS USUALLY INSTALLED ON 4mX4m GRID.
7. FOR DETAILS OF CRANE BEAM ANCHORS REFER DWGS C3-C-6313,6314
15m ANCHORS INSTALLED HORIZONTALLY ABOVE GATE NICHES AND BUSBAR TUNNEL AND STAGGERED BY 2m WITH RESPECT TO ABOVE INSTALLED 15m ANCHORS TO AVOID CONFLICT.

ZONE A

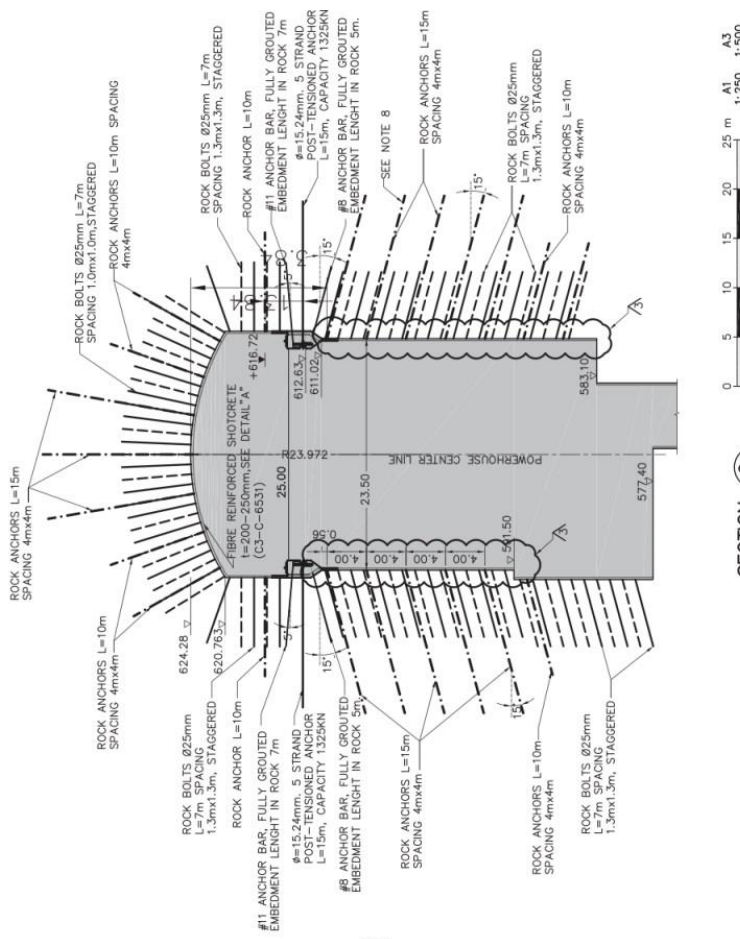


SECTION L - L
SCALE - L

ZONE A



ZONE B



SECTION Q
SCALE = A

SECTION P
SCALE = A

FOR CONSTRUCTION

3	ANCHORS ON UPSTREAM AND DOWNSTREAM WALL OF POWER STATION IN ZONE B ADJUSTED	JKM	JRS	12-08-11	ZB-11-11
2	NOTE B ADDED	JKM	JRS	11-07-11	
1	ROCK SUPPORT AND SECTION REVISED	JKM	JRS	11-07-11	
Rev	Description	Check	Appr	Date	

PAKISTAN WATER & POWER DEVELOPMENT AUTHORITY
NEELUM JHELUM HYDRO-POWER COMPANY

**NEELUM JHELUM HYDROELECTRIC PROJECT
POWER STATION
ROCK SUPPORT
SECTIONS**

DRAWN	M SHARIF/NAV	CHECKED	JKM	TENDER DWG. NO.	
SUBMITTED	MBS/SRM	APPROVED	JRS	DATE	11.07.11
				PROJECT NO	1005800
				DWG. NO. N/C	
				REV	
					C3-C-6533
					NEELUM JHELUM CONSULTANTS

- NOTES**
- ALL DIMENSIONS AND ELEVATIONS ARE IN METERS UNLESS NOTED OTHERWISE.
 - ALL 15m ANCHORS ARE STRAND ANCHORS PRETENSIONED TO 30t IN ZONE 'A' AND 10t IN ZONE 'B'.
 - ALL 10m ANCHORS ARE BAR ANCHORS PRETENSIONED TO 15t IN ZONE 'A' & 5t IN ZONE 'B'.
 - ANCHOR INSTALLATION SEQUENCE TO BE ADVISED BY ENGINEER.
 - ANCHOR PATTERNS CONSIST OF SQUARE GRIDS AND ARE NOT STAGGERED EXCEPT WHERE SHOWN.
 - ZONE 'A' : SSI SANDSTONES PREDOMINATE - ANCHORS USUALLY INSTALLED ON 5m x 5m GRID.
ZONE 'B' : MUD ROCKS PREDOMINATE - ANCHORS USUALLY INSTALLED ON 4m x 4m GRID.
 - FOR DETAILS OF CRANE BEAM ANCHORS REFER DWGS C3-C-6313, 6314
 - 15m ANCHORS INSTALLED HORIZONTALLY ABOVE GATE, NICHES AND BUSBAR TUNNEL AND STAGGERED BY 2m WITH RESPECT TO ABOVE INSTALLED 15m ANCHORS TO AVOID CONFLICT.

